

Sebastian Hoch
Studies of Post Combustion Carbon Dioxide Capture by Reactive Absorption
Scientific Report Series Volume 45
2024

Scientific Report Series
Laboratory of Engineering Thermodynamics (LTD)
RPTU Kaiserslautern
P.O. Box 3049
67663 Kaiserslautern
Germany

ISSN 2195-7606
ISBN 978-3-944433-44-8

© LTD all rights reserved

Studies of Post Combustion Carbon Dioxide Capture by Reactive Absorption

Vom Fachbereich Maschinenbau und Verfahrenstechnik
der Rheinland-Pfälzischen Technischen Universität
Kaiserslautern-Landau
zur Verleihung des akademischen Grades

Doktor-Ingenieur (Dr.-Ing.)

genehmigte

Dissertation

von

Sebastian Hoch

aus Emmereich am Rhein

Dekan: Prof. Dr. rer. nat. Roland Ulber

Berichterstatter: Prof. Dr.-Ing. Hans Hasse

Prof. Dr.-Ing. Erik von Harbou

Tag der mündlichen Prüfung: 19.01.2024

Danksagung

Diese Arbeit entstand während meiner Tätigkeit als wissenschaftlicher Mitarbeiter an den Lehrstühlen ITT an der Universität Stuttgart und LTD an der RPTU Kaiserslautern. Ich bedanke mich bei allen, die zum Gelingen dieser Arbeit beigetragen haben.

Mein besonderer Dank gilt Prof. Dr.-Ing. Hans Hasse für die hervorragende Betreuung und seine unglaubliche Unterstützung bis zum finalen Abschluss dieser Arbeit. Sowohl fachlich als auch persönlich habe ich bei ihm extrem viel gelernt. Ein großer Dank auch an Prof. Dr.-Ing. Erik von Harbou für die tollen Diskussionen und die Übernahme des Berichterstatters für diese Arbeit. Prof. Dr.-Ing. Eberhard Kerscher danke ich für die Übernahme des Promotionsvorsitzes.

Die wissenschaftlichen Mitarbeiter in Stuttgart und Kaiserslautern haben eine tolle Atmosphäre erzeugt, in der neben wissenschaftlichen und fachlichen Diskussionen auch das private Gespräch und die Freizeitgestaltung nie zu kurz kamen. Es war eine tolle Zeit und es sind viele Freundschaften daraus hervorgegangen, über dich ich äußerst glücklich bin.

Ohne die aktive Unterstützung aus Labor und Technik wäre diese Arbeit nicht möglich gewesen. Ein riesiges Dankeschön an alle technischen Mitarbeiter an den Lehrstühlen in Stuttgart und insbesondere Kaiserslautern, die mich tatkräftig unterstützt haben. Ein ebenfalls großes Dankeschön an die Sekretariate und die IT Unterstützung, die mir vieles an Arbeit abgenommen haben und somit eine große Hilfe gewesen sind.

Den vielen Kooperationspartnern dieser Arbeit sei gedankt für die wertvollen Beiträge sowohl in der Prozesssimulation als auch in der technischen Entwicklung des NMR Probenkopfes. Durch diese Beiträge wurde diese Arbeit erst ermöglicht und hat mir viele neue Einblicke in spannende Forschungseinrichtungen und Unternehmen gebracht.

Meinen Eltern danke ich für die Unterstützung während meiner Ausbildung. Mein grösster Dank gilt meiner Frau Wiebke, die mit ihrem Glauben an mich und dem nie endenden Rückhalt diesen Abschluss ermöglicht hat.

Freiburg, Januar 2024

Sebastian Hoch

Abstract

Reactive absorption with amines is the most important technique for the removal of CO₂ from gas streams, e.g. from flue gas, natural gas or off-gas from the cement industry. In this work a rigorous simulation model for the absorption and desorption of CO₂ with an amine-containing solvent is validated using data from pilot plants of various sizes. This model was then coupled with a detailed simulation of a coal-fired power plant. The power generation efficiency drop with CO₂ capture was determined and process parameters in the power plant and separation process were optimized. It was shown that the high energy demand of CO₂ separation significantly reduces power generation efficiencies, which underlines the need for improvements. This can be achieved by better solvents or by advanced process designs. In this work such improved CO₂ separation processes are described and evaluated by detailed simulation studies.

In order to develop detailed rigorous simulation models for reactive absorption with novel solvent systems, a precise knowledge of the liquid phase reaction kinetics is necessary. There are well established techniques for measuring species distributions in equilibrated aqueous amine solutions by NMR spectroscopy. However, the existing NMR techniques cannot be used for monitoring fast reactions in these solutions. Therefore, in this work a novel temperature-controlled micro-reactor NMR probe head was developed which enables studying reaction kinetics with time constants in the range of seconds.

On this basis, modern solvent systems for CO₂ absorption can be characterized and the scale-up of separation process for future plants can be accompanied using rigorous process simulation.

Kurzfassung

Die reaktive Absorption mit wässrigen Aminlösungen ist die wichtigste Technik zur Entfernung von CO₂ aus Gasströmen, z. B. aus Rauchgas, Erdgas oder Abgasen aus der Zementindustrie. In dieser Arbeit wird ein rigoroses Simulationsmodell für die Absorption und Desorption von CO₂ mit einem aminhaltigen Lösungsmittel anhand von Daten aus Pilotanlagen unterschiedlicher Größe validiert. Dieses Modell wurde dann mit einer detaillierten Simulation eines kohlebefeuerten Kraftwerks gekoppelt. Der Rückgang des Wirkungsgrads der Stromerzeugung durch Abscheidung von CO₂ wurde ermittelt und die Prozessparameter im Kraftwerk und Abtrennungsprozess wurden optimiert. Es zeigte sich, dass der hohe Energiebedarf der CO₂-Abtrennung den Wirkungsgrad der Stromerzeugung deutlich verringert, was die Notwendigkeit von Verbesserungen unterstreicht. Dies kann durch verbesserte Lösungsmittel oder durch ein optimiertes Prozessdesign erreicht werden. In dieser Arbeit werden optimierte Verfahren zur CO₂-Abtrennung beschrieben und durch detaillierte Simulationsstudien bewertet.

Um detaillierte, rigorose Simulationsmodelle für die reaktive Absorption mit neuartigen Lösungsmittelsystemen zu entwickeln, ist eine genaue Kenntnis der Reaktionskinetik in der Flüssigphase erforderlich. Es existieren gut etablierte Techniken zur Messung von Speziesverteilungen im Gleichgewicht von wässrigen Aminlösungen mittels NMR-Spektroskopie. Die vorhandenen NMR-Techniken können jedoch nicht zur Verfolgung schneller Reaktionen in diesen Lösungen eingesetzt werden. Daher wurde in dieser Arbeit ein neuartiger temperierter NMR Probenkopf mit Mikroreaktor entwickelt, der die Untersuchung der Reaktionskinetik mit Zeitkonstanten im Sekundenbereich ermöglicht.

Auf dieser Grundlage können moderne Lösungsmittelsysteme für die CO₂-Absorption charakterisiert und das Scale-up des Abtrennungsprozesses für künftige Anlagen durch rigorose Prozesssimulation begleitet werden.

Inhaltsverzeichnis

1 Einleitung	1
2 Rigoroses Simulationsmodell	5
2.1 Kolonnen- und Stoffdatenmodell	5
2.2 Anpassung an Absorptionsisothermen	6
2.3 Modellierung der Flüssigphasenreaktionen	7
2.4 Optimierung der Diskretisierung	8
3 Simulationsstudien zur CO₂ Abtrennung	11
3.1 Validierung des Simulationsmodells	11
3.2 Validierung eines Short-Cut Modells mittels rigoroser Prozesssimulation .	14
3.3 Simulation einer großtechnischen CO ₂ Abtrennung an einem Kraftwerk .	15
3.4 CO ₂ -Abtrennung aus Rauchgasen mittels einer Mischung aus MEA, Wasser und Ethanol	16
3.5 Verwendung von Seitenreaktoren bei der absorptiven Abtrennung von CO ₂	17
3.6 Erforschung neuer Lösungsmittelsysteme für die CO ₂ Abtrennung	19
4 Reaktionsmonitoring schneller Reaktionen mittels NMR Spektroskopie	21
4.1 Kopplung eines NMR Durchflusskopfes mit extern installierten Mikroreaktoren	22
4.2 Temperierter NMR Probenkopf mit integriertem Mikromischer	23
4.3 Untersuchungen am System MEA-H ₂ O-CO ₂	26
5 Einordnung und Ausblick	29
Literaturverzeichnis	31
Scientific Publications	43
Publication I	43
Pilot plant experimental studies of post combustion CO ₂ capture by reactive absorption with MEA and new solvents	43

Publication II	53
Comparison and validation of simulation codes against sixteen sets of data from four different pilot plants	53
Publication III	63
A short-cut method for assessing absorbents for post combustion carbon dioxide capture	63
Publication IV	75
Integration of a chemical process model in a power plant modelling tool for the simulation of an amine based CO ₂ scrubber	75
Publication V	85
Removal of carbon dioxide from flue gases with aqueous MEA solution containing ethanol	85
Publication VI	97
CO ₂ -Abtrennung aus Kraftwerksabgasen auf dem Weg von der Forschung und Entwicklung zur industriellen Anwendung	97
Publication VII	109
Quantitative online NMR spectroscopy in process analytics: coupling with mi- croreactors in studies of fast reactions	109
Publication VIII	115
Thermostatted micro-reactor NMR probe head for monitoring fast reactions .	115

*

*Die Publikationen in dieser kumulativen Dissertation sind hauptsächlich in Englisch verfasst. Deshalb wurde diese Dissertation in einem englischen Rahmendokument erstellt. Nur der Überblick über die Arbeiten wurde in Deutsch verfasst.

1 Einleitung

Die globale Erderwärmung durch Treibhausgase ist eines der größten Probleme der heutigen Zeit. Der weitere Anstieg der CO₂-Konzentration in der Atmosphäre soll mittels nationaler und internationaler Vereinbarungen zur Begrenzung des CO₂-Ausstoßes vermindert werden. Triebkraft dieser Anstrengungen zur Emissionsminderung sind neben ethischen und sozialen Gesichtspunkten auch die potentiellen Kosten zur Beseitigung der Auswirkungen von Wetterphänomenen [1].

Auf nationaler und internationaler Ebene wurden deshalb Reduktionsziele für die Emission von Treibhausgasen vereinbart. Durch den in der EU eingeführten CO₂ Zertifikathandel könnten Technologien zur CO₂-Emissionsminderung zukünftig wirtschaftlich werden [2]. Deshalb werden weltweit Konzepte und Technologien zur CO₂-Abtrennung und Speicherung (Carbon Capture and Storage, CCS) untersucht [3–6].

Die Abtrennung von CO₂ aus dem Rauchgas von Kraftwerken, auch Post Combustion Carbon Capture (PCC) genannt, ist ein hoch entwickeltes Verfahren. Es kann auch an bestehenden Kraftwerken nachgerüstet werden. Eingesetzt werden reaktive Wäschchen mit wässrigen aminhaltigen Lösungsmitteln. Solche Absorptions- / Desorptionsprozesse werden bereits in der Erdgasreinigung und in der chemischen Industrie zur Abtrennung von CO₂ aus Prozessströmen genutzt, während die Behandlung von Rauchgasen mit diesem Verfahren noch Gegenstand der Forschung ist [7].

Aufgrund der sehr hohen Rauchgasmassenströme in Kraftwerken ist allein die Größe der notwendigen Apparate eine technische Herausforderung. Deshalb wurde das Verfahren in zahlreichen nationalen und internationalen Projekten in unterschiedlichen Pilotanlagen untersucht.

Die Prozesssimulation ist eine wichtige Grundlage für das Scale-up und die Prozessoptimierung, da bei Parameterstudien und der Entwicklung von Auslegungsalternativen aufwendige experimentelle Arbeiten ersetzt werden können. Voraussetzung ist hier ein Simulationsmodell mit ausreichender Güte und Vorhersagekraft. Für die reaktive Absorption von CO₂ in aminhaltigen Lösungsmitteln wurde in dieser Arbeit ein Simulationsmodell verwendet, welches die auftretenden Wärme- und Stofftransportvorgänge explizit abbildet. Der Vorteil eines solchen Rate-based Modells ist die detaillierte Beschreibung der komplexen chemisch-physikalischen Vorgängen, die bei der reaktiven

Absorption von CO₂ auftreten [8–11]. Nachteil ist eine sehr hohe Anzahl an Modellparameter, die schwierig zu bestimmen sind.

Die Validierung des verwendeten Simulationsmodells durch Versuche in Pilotanlagen ist daher Gegenstand des ersten Teils dieser Arbeit. Hier wurde gezeigt, dass das verwendete Modell ausreichend genau und prädiktiv die Versuche in verschiedenen Pilotanlagen unterschiedlicher Baugröße und Konfiguration abbildet. In einer Studie, an der sich zahlreiche internationale Forschungsgruppen beteiligt haben, wurde die Vorhersagefähigkeit unterschiedlicher Modelle unter Verwendung einer einheitlichen experimentellen Datenbasis untersucht. Als Modellsystem dient in allen Studien die CO₂ Absorption mit einer wässrigen Lösung von Monoethanolamin (MEA) mit 0.3 g/g MEA.

Das so validierte Prozessmodell der CO₂-Abtrennung wurde mit einer detaillierten Simulation eines Kohlekraftwerks gekoppelt. Beide Einzelprozesse (konventioneller Kraftwerksprozess und absorptive CO₂ Abtrennung) wurde über separat validierte Modelle abgebildet, die Kopplung erfolgte über eine definierte Schnittstelle zum Prozessdatenaustausch. Mit Hilfe der so gekoppelten Simulationen konnte die Beeinflussung des Kraftwerksprozesses durch die nachgeschaltete CO₂ Abtrennung untersucht und auch die Erniedrigung des Gesamtwirkungsgrads bestimmt werden. Das Modell wurde zudem zur ganzheitlichen Prozessoptimierung genutzt.

Aufgrund der hohen Einbussen im Gesamtwirkungsgrad der Stromerzeugung durch die nachgeschaltete Abtrennung von CO₂ wird intensiv nach neuen Lösungsmittelsystemen gesucht, welche eine effizientere Entfernung von CO₂ aus Rauchgasen ermöglichen. In dieser Arbeit wurde die Zugabe von Ethanol zum System MEA-H₂O in Simulationsstudien untersucht. Dabei erfolgte eine Prozessoptimierung. Ferner wurden auch Maßnahmen zur Rückhaltung des Ethanols im Prozess evaluiert.

Da im verwendeten Modell die Kinetik der ablaufenden chemischen Reaktionen in der Flüssigphase explizit abgebildet wird, kann der Einfluss höherer Flüssigphasen-Verweilzeiten simulativ untersucht werden. Höhere Verweilzeiten in Absorptionskolonnen können über zugeschaltete Seitenreaktoren erreicht werden. Hierzu wurde eine Konzeptstudie durchgeführt, aus der auch ein Patent hervorgegangen ist.

Für das System MEA-H₂O-CO₂ konnten alle notwendigen Parameter für eine rigorose Simulation der Literatur entnommen werden. Bei neuen Lösungsmittelsystemen ist dies in der Regel nicht der Fall. Insbesondere Reaktionskinetiken müssen zunächst experimentell bestimmt werden. Die NMR Spektroskopie ist als berührungslose Messmethode mit hoher Dispersion eine sehr attraktive Methode für das Reaktionsmonitoring. In vorangegangenen Arbeiten wurde gezeigt, dass Flüssigphasenreaktionen in technischen Mischungen unter Verwendung von externen Reaktoren mit der NMR untersucht werden können. Die so untersuchten Reaktionen waren jedoch nur schwach exotherm und

hatten Halbwertszeiten im Bereich von Stunden [12]. In Mischungen aus CO₂, Wasser und Aminen treten jedoch schnelle exotherme Reaktionen auf. Die Reaktionszeit liegt hier im Minutenbereich. Um die Verweilzeit zwischen Reaktionsstart und Messung zu minimieren wurde in dieser Arbeit die Kopplung von Mikroreaktoren und der NMR Spektroskopie eingesetzt.

Die Entwicklung des Messsystems erfolgte in zwei Schritten. Zuerst wurde eine Machbarkeitsstudie durchgeführt, in der ein externer Mikromischer mit einem Standard-NMR-Durchflusskopf gekoppelt wurde. Hierdurch konnten Untersuchungen von Reaktionskinetiken mit Zeitkonstanten im Minutenbereich realisiert werden. Da das System nicht aktiv gekühlt werden konnte, wurde als Beispielsystem eine Veresterung gewählt, die nur eine schwache Wärmetönung aufweist.

Nach erfolgreichem Test des Messsystems wurde ein völlig neuer NMR Probenkopf entwickelt, der die Vermischung der Edukte mit einem im NMR-Probenkopf integrierten Mikromischer erlaubt. Das gesamte System wird mit Flüssigkeit temperiert und erlaubt somit auch die Untersuchung von Reaktionen mit starker Wärmetönung. Die Zeit zwischen Vermischung der Edukte und der Messung liegt hier im Sekundenbereich. In dieser Arbeit wird der entwickelte Probenkopf mit dem Modellsystem der zuvor gewählten Veresterung getestet. Zur Untersuchung der Kinetik von CO₂ beladenen Aminlösungen konnten in dieser Arbeit erste Stichversuche durchgeführt werden.

In den nachfolgenden Erläuterungen werden die durchgeführten Arbeiten als Überblick dargestellt und der Zusammenhang erläutert. Bezüglich der Einzelheiten wird auf die beigefügten Publikationen verwiesen.

2 Rigoroses Simulationsmodell

Für die weitgehende Abtrennung des im Rauchgas enthalten CO_2 ist die Chemiesorption besonders geeignet. Durch die ablaufenden chemischen Reaktionen wird der Stofftransport zwischen Gas- und Flüssigphase beschleunigt. Bei der Beschreibung von Chemiesorptionen muss berücksichtigt werden, dass stark gekoppelte Stoff- und Wärmetransportvorgänge vorliegen. Dies hat Auswirkungen auf die Wahl des Simulationsmodells für die CO_2 Abtrennung, insbesondere wenn eine prädiktive Simulation möglich sein soll [9, 10, 13]. In dieser Arbeit wird die Chemisorption von CO_2 in einer wässrigen Lösung von Monoethanolamin (MEA) mit 0.3 g/g MEA untersucht. Die physikalisch-chemischen Prozesse bei der Absorption von CO_2 in dieser Lösung sind in der Literatur gut beschrieben [11, 14–17]. Die komplexe Parametrierung eines rigorosen Simulationsmodells ist daher für dieses System möglich [10, 11, 18].

2.1 Kolonnen- und Stoffdatenmodell

Die Simulationen der CO_2 Abtrennung mittels reaktiver Absorption erfolgten mit einem Rate-Based Modell, das auf der rigorosen Beschreibung von Mengen- und Energiebilanzen und den zugehörigen Transportvorgängen beruht [19]. Das verwendete Modell zur Beschreibung der CO_2 Absorption im Gegenstrom beruht auf differentiellen Mengen- und Energiebilanzen in der Gas- und Flüssigphase für das Mehrkomponentensystem. Der Stoff- und Wärmeübergang zwischen Gas- und Flüssigphase wird mit einem Zweifilm-Modell abgebildet. Der Stofftransport wird über den Maxwell-Stefan Ansatz beschrieben [20]. Aufgrund der in der Flüssigphase vorliegenden ionischen Komponenten wird dieser Stofftransportansatz mit dem elektrostatischen Potential als Triebkraft ergänzt [10, 19].

Die ablaufenden Reaktionen in der flüssigen Phase werden explizit als Quellterme in den Bilanzgleichungen berücksichtigt. Neben CO_2 wird ebenfalls die Absorption von N_2 sowie die Verdampfung/Kondensation von H_2O und Monoethanolamin berücksichtigt.

Die Abbildung 1 verdeutlicht die zu berücksichtigen stofflichen Gleichgewichte bei der CO_2 -Absorption in einer wässrigen Monoethanolaminlösung. Das Phasengleichgewicht der nicht kondensierbaren Komponenten CO_2 und N_2 wird über das erweiterte Henry-

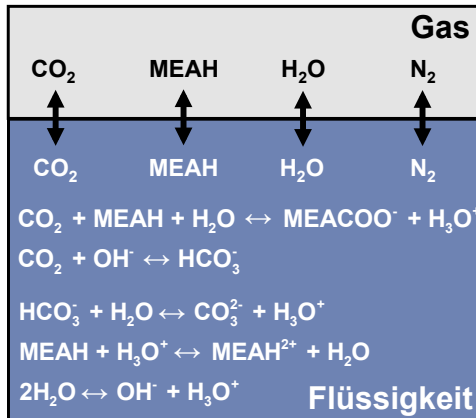


Abbildung 1: Phasengleichgewicht MEA-H₂O-CO₂ nach Veröffentlichung VI.

Gesetz beschrieben. Die Normierung erfolgt hier auf das Lösungsmittel Wasser. Die Beschreibung des Dampf-Flüssigkeits Gleichgewichts der kondensierbaren Komponenten MEA und H₂O erfolgt über das erweiterte Raoultsche Gesetz. Die Normierung erfolgt hier auf die reinen Komponenten. Die Reaktionsgleichgewichte der fünf Gleichgewichtsreaktionen in der flüssigen Phase werden über den aktivitätsbasierten Gleichgewichtsansatz beschrieben. Die zur Beschreibung der intermolekularen Wechselwirkungen notwendigen Aktivitätskoeffizienten werden über das Elektrolyt-NRTL-Modell beschrieben. Für die ersten beiden aufgeführten Reaktionen wird zudem die Reaktionskinetik berücksichtigt.

2.2 Anpassung an Absorptionsisothermen

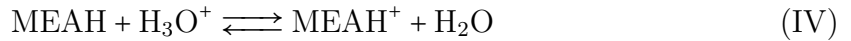
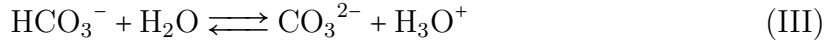
Eine möglichst genaue Abbildung des physikalischen Gleichgewichts zwischen Gas- und Flüssigphase ist für eine prädiktive Modellierung zwingend erforderlich. Im Modell wird für die Komponenten CO₂ und N₂ das erweiterte Henrygesetz verwendet:

$$H_{i,LM}(T) \exp\left(\frac{v_{i,LM}^\infty (p - p_{LM}^s)}{RT}\right) x_i \gamma_i^* = p y_i \phi_i'' \quad (1)$$

Die Aktivitätskoeffizienten γ_i^* werden über das Electrolyt-NRTL Modell bestimmt. Die Anpassung der Wechselwirkungsparameter erfolgt an experimentell bestimmte Absorptionsisothermen. Hier wurden für die Anpassung Daten bis zu einem CO₂-Partialdruck von 2 bar und Temperaturen zwischen 40 °C und 120 °C herangezogen. Die Absorptionsisothermen wurden nach Anpassung mit ausreichender Genauigkeit wiedergegeben. Insbesondere die experimentellen Ergebnisse bei niedrigen CO₂-Partialdrücken werden durch das Modell gut wiedergegeben.

2.3 Modellierung der Flüssigphasenreaktionen

Das Reaktionssystem in der Flüssigphase wird über 5 Schlüsselreaktionen abgebildet:



Dabei sind die Carbamatbildung (Reaktion I) und die Bicarbonatbildung (Reaktion II) kinetisch kontrolliert. Alle weiteren Reaktionen (Reaktionen III - V) sind Protoneentransferreaktionen. Für diese darf angenommen werden, dass aufgrund der hohen Reaktionsgeschwindigkeit stets das Gleichgewicht eingestellt ist.

Die Reaktionsgeschwindigkeit der kinetisch kontrollierten Reaktionen wird mit einem aktivitätsbasierten Ansatz beschrieben:

$$r_{r,j}^{lb} = k_{r,j,hin}^{lb} \prod (x_{e,j}^{lb} \gamma_{e,j}^{lb})^{\nu_{e,r}} - k_{r,j,rueck}^{lb} \prod (x_{p,j}^{lb} \gamma_{p,j}^{lb})^{\nu_{p,r}} \quad (2)$$

Die ermittelten Reaktionsraten in der Flüssigphase $r_{r,j}^{lb}$ hängen damit vom verwendeten Gleichgewichtsmodell und den Aktivitätskoeffizienten ab. Die Reaktionsgeschwindigkeit der Flüssigphasenreaktionen und das Phasengleichgewicht sind im Modell somit stets gekoppelt.

Die Temperaturabhängigkeit der Reaktionsgeschwindigkeit wird über den Arrhenius-Ansatz bestimmt:

$$k_{r,j,hin}^{lb} = k_{0,r}^{lb} \exp\left(\frac{-E_{A,r}}{RT_j^{lb}}\right) \quad (3)$$

Für die Modellierung der Reaktionsgeschwindigkeit der Carbamat- und Bicarbonatbildung wurden Stoßfaktor und Aktivierungsenergie aus der Literatur übernommen [11]. Für die möglichst gute Wiedergabe des Dampf-Flüssigkeits Gleichgewichts wurden in dieser Arbeit die Aktivitätskoeffizienten im verwendeten Elektrolyt-NRTL Modell wie oben beschrieben angepasst. Diese Anpassung hatte eine Veränderung der Reaktionskinetiken und der berechneten Stoffflüsse im Rate-Based Modell zur Folge, was weitere Änderungen im Modell erforderlich machte. Für die Flüssigphasenreaktionen im

vorliegenden Reaktionssystem lagen keine direkten kinetischen Daten vor. Publizierte Reaktionsgeschwindigkeitkonstanten wurden durch Absorptionsgeschwindigkeitsmessungen bestimmt [21–24]. Für eine zuverlässiger Bestimmung der Reaktionskinetik wäre eine Messung der reinen Flüssigphasenreaktionen wünschenswert. Ein Messsystem auf Basis der NMR Spektroskopie zur Bestimmung dieser Kinetik wurde in der vorliegenden Arbeit erst entwickelt. Daher wurden hier zur Anpassung der Reaktionsgeschwindigkeiten experimentell bestimmte Absorptionsraten in technischen Anlagen verwendet. Die verwendeten Pilotanlagendaten haben eine Vielzahl an Messstellen (Temperatur, Drücke, Konzentrationen) und bieten daher die Möglichkeit einer umfassenden Validierung des rigorosen Simulationsmodells. In dieser Arbeit wurde der Stoßfaktor der Carbamatbildung um den Faktor 2,7 erhöht, um eine möglichst gute Wiedergabe der Kolonnenprofile von Absorber und Desorber zu ermöglichen. Diese Anpassung wurde anhand von Daten aus mehreren Pilotanlagen überprüft, was in den Veröffentlichungen I und II näher beschrieben wird.

2.4 Optimierung der Diskretisierung

Die Modellierung des Wärme- und Stofftransportes führt zu einem System gekoppelter, nichtlinearer Differentialgleichungen. Zur Lösung wird dieses System diskretisiert. Aufgrund der stark gekrümmten Profile muss eine Diskretisierung sowohl über die Höhe der Kolonne als auch über den Film erfolgen. Die Transport- und Bilanzgleichungen müssen in jedem der so entstehenden diskreten Elementen unter Berücksichtigung der Kopplungen explizit gelöst werden, der numerische Aufwand und somit auch die benötigte Rechenleistung ist hoch.

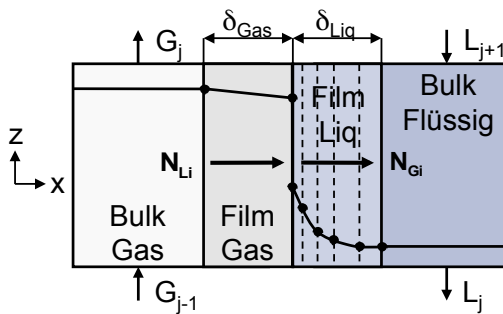


Abbildung 2: Darstellung eines Höhendiskrets des Kolonnenmodells.

Die Abbildung 2 zeigt ein Höhensegment. Die gewählte Diskretisierung hat dabei Einfluss auf die Genauigkeit des numerischen Simulationsergebnisses, andererseits aber auch auf die benötigte Rechenzeit. So nimmt die Qualität der Berechnung mit zunehmender Anzahl an diskreten Elementen zu. Allerdings muss für diese hohe Genauigkeit eine

teils deutlich längere Rechenzeit in Kauf genommen werden. Somit ist die Wahl der optimalen Diskretisierung ein Kompromiss zwischen diesen beiden Punkten.

Die Optimierung der Höhendiskretisierung im Ab- und Desorber wurde anhand von Kolonnenprofilen und den Konzentrationen in austretenden Strömen durchgeführt. Mit zunehmender Anzahl an Diskretisierungselementen werden die Profile in den Kolonnen immer genauer wiedergegeben. Verändert sich das Simulationsergebnis mit zunehmenden Diskretisierungselementen nicht mehr, ist eine ausreichende Diskretisierungstiefe erreicht. Im verwendeten Modell ist dies im Absorber bei etwa 50 Höhendiskreten und im Desorber bei etwa 40 Höhendiskreten der Fall.

Die Diskretisierung im Film muss für den Gas- und den Flüssigfilm getrennt festgelegt werden. Im Gasfilm liegt ein lineares Konzentrations- und Temperaturgefälle vor, da dort keine Reaktionen stattfinden und ein reiner Transportwiderstand vorliegt. Die linearen Profile können hier mit nur einem Diskretisierungselement abgebildet werden. Die im Flüssigfilm auftretenden, schnellen Reaktionen sorgen für hohe Gradienten in der Nähe der Phasengrenze, die möglichst genau wiedergegeben werden müssen. Daher ist es notwendig in der Nähe der Phasengrenze mit einem engen Gitter zu arbeiten. Ein äquidistantes Gitter würde zu einer nicht praktikablen hohen Zahl an diskreten Elementen führen. Die Positionierung der Stützstellenposition im Film erfolgt hier gemäß:

$$x_i = \delta \left(\frac{i}{n} \right)^{1/m} \quad (4)$$

Dabei ist x_i die Position der i-ten Stützstelle und n ist die Anzahl an Stützstellen. Der Parameter m steuert die Assymetrie. Für $m = 1$ erhält man eine lineare Verteilung, für steigendes m verschieben sich die Stützstellen mehr und mehr in Richtung der Phasengrenze. Parameterstudien zeigten, dass mit der Definition von $n = 15$ und $m = 30$ ein guter Kompromiss zwischen Genauigkeit und Rechenzeit vorliegt.

3 Simulationsstudien zur CO₂ Abtrennung

Mit dem zuvor beschriebenen Simulationsmodell zur CO₂-Absorption wurden in dieser Arbeit verschiedene Studien durchgeführt, über die im Folgenden ein Überblick gegeben wird. Das Modell und dessen Parametrierung wurde dabei nicht mehr verändert.

3.1 Validierung des Simulationsmodells

In dieser Arbeit konnte auf eine Vielzahl experimenteller Daten aus der am Lehrstuhl LTD installierten Pilotanlage zur CO₂-Absorption zurückgegriffen werden. In der Veröffentlichung I sind diese Pilotanlage und die damit durchgeföhrten experimentellen Studien mit dem Lösungsmittel MEA detailliert beschrieben.

Die Pilotanlage am LTD besteht aus einer Absorber- und einer Desorberkolonne. Die Kolonnen sind ausgestattet mit einer strukturierten, metallischen, Packung (Mellapak 250Y), Durchmesser 125 mm. Im Simulationsmodell werden zur Wiedergabe der Fluidodynamik in den Kolonnen Korrelationen aus der Literatur verwendet [25, 26].

Die experimentellen Daten aus der Pilotanlage wie Temperaturen, Massenströme, Drücke, Zusammensetzungen und Abtrennarten können für die Modellvalidierung herangezogen werden. Besonders aufschlussreich ist der Vergleich von Simulation und Experiment der durchgeföhrten Parametervariationen. Dabei ist insbesondere die Überprüfung der axialen Temperatur- und Konzentrationsprofile wichtig. Die Abbildung 3 zeigt exemplarisch simulierte Temperatur- und Konzentrationsprofile im Absorber und Desorber mit den jeweiligen experimentellen Daten für einen stationären Betriebspunkt. Man erkennt die sehr gute Übereinstimmung zwischen experimentellen Daten und den Simulationsergebnissen.

In der Abbildung 4 sind experimentell bestimmte und simulierte Regenerationsenergien für diverse Betriebspunkte der Pilotanlage am LTD mit dem Lösungsmittel MEA dargestellt. Die einzelnen Parametervariationen sind in der Veröffentlichung I detailliert

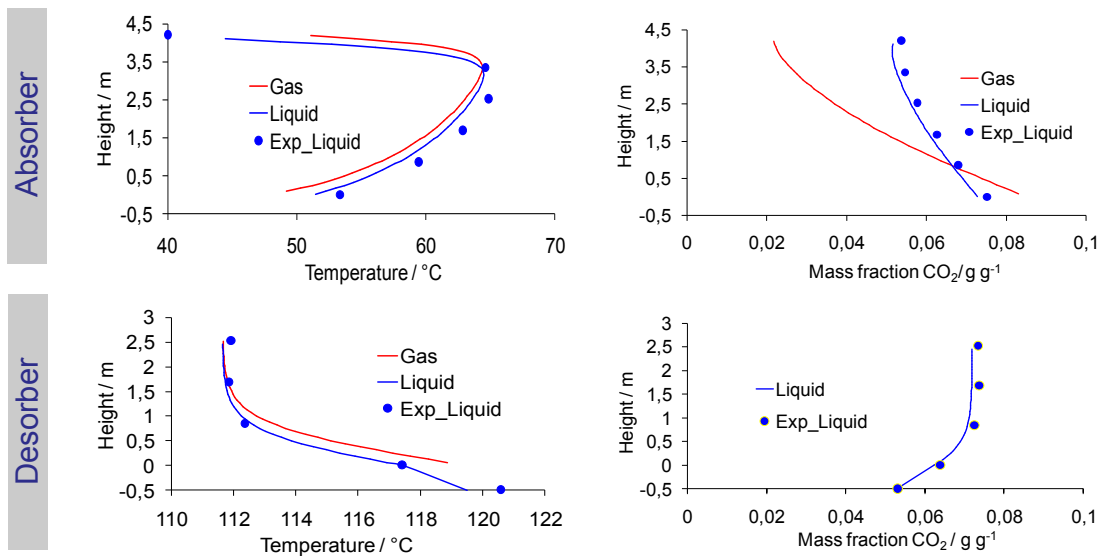


Abbildung 3: Temperatur- und Konzentrationsprofile für einen Betriebspunkt in der Pilotanlage am LTD: Simulation und Experiment gemäss Veröffentlichung I.

dargestellt. Eine Vielzahl von Betriebspunkten dieser Anlage kann mit einer Genauigkeit von -10% bis +10% wiedergegeben werden.

Alle Simulationen erfolgten mit einem festen Modellparametersatz, nur die Vorgabe der Betriebsbedingungen (Eintrittsbedingungen Gasstrom, Zirkulation Lösungsmittel, Temperaturen Desorber) wurde variiert. Das Modell hat somit bei dieser Pilotanlage eine sehr gute Vorhersagegüte, die markierten Punkte mit einer höheren Abweichung in der Abbildung 4 sind Betriebsbedingungen mit extrem niedrigen oder hohen Flüssigkeitsbelastungen zuzuschreiben. Hier treten in der Anlage, hervorgerufen durch Maldistribution respektive Anstauen, Abweichungen bezüglich Phasentrennfläche und Transportwiderständen auf. Diese Bedingungen werden durch die verwendete packungsspezifische Korrelation nicht mehr korrekt wiedergegeben.

Um auch die Vorhersagekraft des Simulationsmodells für ein Scale-up des CO₂ Abtrennprozesses zu untersuchen, wurde im Rahmen des EU Projektes CAPRICE zusammen mit internationalen Partnern eine Simulationsstudie mit Daten aus 4 verschiedenen Pilotanlagen durchgeführt. Ein Überblick über diese Studie gibt die Veröffentlichung II . Insgesamt standen 16 Betriebsdatenpunkte aus den verschiedenen Pilotanlagen in unterschiedlichen Skalen zur Verfügung. Alle Datenpunkte wurden, soweit möglich, auf Konsistenz geprüft und die Massenbilanz mit den gegebenen analytischen Daten untersucht. Daraufhin erfolgte mit unterschiedlichen Modellen die Simulation der ausgewählten Betriebspunkte. An den Ergebnissen erkennt man z.T. sehr deutliche Unterschiede in der Vorhersagekraft einzelner Simulationsmodelle. Insbesondere die verwendeten Gleichgewichtsstufenmodelle (z.B. Aspen Rad Frac) mussten auf jeden einzelnen Betriebsda-

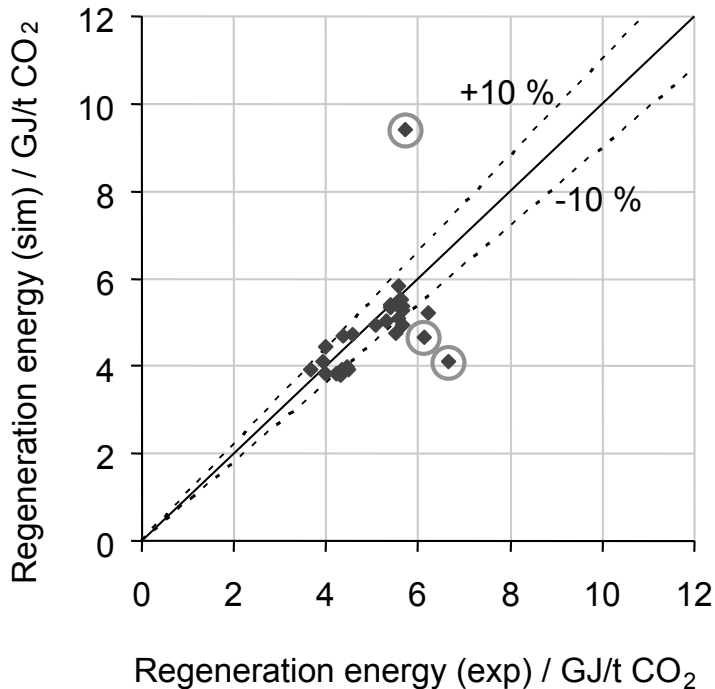


Abbildung 4: Vergleich von Simulationsergebnissen und experimentellen Daten für den spezifischen Wärmebedarf zur Lösungsmittelregeneration (Experimentelle Daten aus der Pilotanlage am LTD gemäss Veröffentlichung I). Kreise kennzeichnen Versuche bei extremen Betriebsbedingungen, für die die Fluidodynamik in der Kolonne vom Modell nicht richtig beschrieben wird.

tenpunkt separat angepasst werden (z.B. Gleichgewichtsstufenanzahl Absorber). Diese Modelle konnten dann zwar diesen Betriebspunkt mit ausreichender Genauigkeit wiedergeben, jedoch ist hier eine Prädiktion aufgrund der Parameteranpassung nicht gegeben.

Hier zeigt das in dieser Arbeit verwendete rigorose Simulationsmodell seine Vorteile, da hier mit einem einheitlichen Parametersatz alle Betriebsdaten in einer ausreichenden Genauigkeit wiedergegeben werden konnten. In Abbildung 5 ist als Beispiel der Vergleich von Simulationsergebnissen und experimentellen Daten für den Wärmebedarf zur Lösungsmittelregeneration aus der CASTOR Pilotanlage Esbjerg gemäss Veröffentlichung II dargestellt. Auch hier übersteigt die Abweichung zwischen Simulation und Experiment 10 % nicht. Absorber und Desorber haben in dieser Pilotanlage einen Durchmesser von über 1 m, was einem Scale-up Faktor von ca. 80 im Vergleich mit der LTD Pilotanlage entspricht.

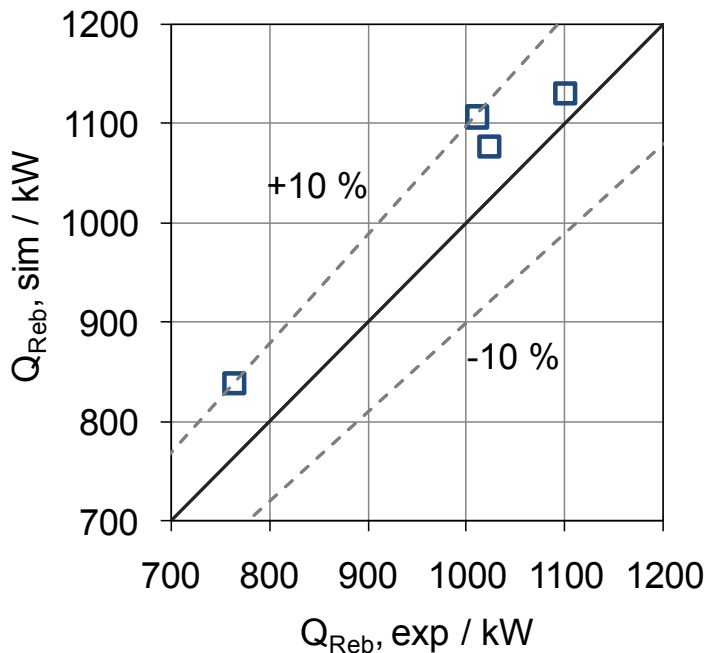


Abbildung 5: Vergleich von Simulationsergebnissen und experimentellen Daten für den Wärmebedarf zur Lösungsmittelregeneration (Experimentelle Daten aus der CASTOR Pilotanlage Esbjerg gemäss Veröffentlichung II).

3.2 Validierung eines Short-Cut Modells mittels rigoroser Prozesssimulation

Mit Hilfe des oben beschriebenen Simulationsmodells wurde ein durch Notz et. al. (Veröffentlichung III) entwickeltes Short-Cut Modell zur ersten Abschätzung des CO₂-Abtrennprozesses zusammen mit Pilotanlagendaten validiert. Ziel der Short-Cut Modellentwicklung ist es, ein Modell in einem frühen Stadium der Lösungsmittelentwicklung zur Verfügung zu haben, welches keine detaillierten Reaktions- und Transportparameter benötigt. Dennoch soll in diesem frühen Stadium der Absorptions- und Desorptionsprozess abgeschätzt und die Vorteile neuer Lösungsmittelsysteme für die CO₂-Abtrennung quantitativ bewertet werden. In der Veröffentlichung III wird diese Methodik auf zwei neue Lösungsmittel angewendet.

Das Short-Cut Modell beruht auf der Kremser Gleichung und ist nur für einen Vergleich von Lösungsmittelsystemen geeignet. Für Abschätzungen in einem frühen Stadium ist das Short-Cut Modell sehr hilfreich.

3.3 Simulation einer großtechnischen CO₂ Abtrennung an einem Kraftwerk

Das Simulationsmodell wurde verwendet, um einen Prozess zur Abtrennung von CO₂ aus Kraftwerksabgasen auszulegen und die wechselseitige Beeinflussung zwischen Energieerzeugung und CO₂ Abtrennung zu untersuchen. Dabei wurden zwei unterschiedliche Kraftwerke betrachtet: ein 600 MW Steinkohlekraftwerk und ein 1000 MW Braunkohlekraftwerk. Die Kraftwerksprozesse wurden in der Arbeitgruppe am IVD, Universität Stuttgart, in einer detaillierten Simulation im Tool EBSILON abgebildet und untersucht. Der Absorptions- / Desorptionsprozess für CO₂ wurde mit dem oben beschriebenen Simulationsmodell ausgelegt und untersucht.

Um die beiden Simulationen miteinander zu koppeln, wurde eine Schnittstelle geschaffen, die den Austausch der Prozessdaten zwischen beiden rigorosen Simulationen ermöglicht. Das Vorgehen wird in der Veröffentlichung IV beschrieben. Die für die Integration der CO₂-Abtrennung notwendigen Änderungen im Kraftwerksprozess sind ebenfalls dort erläutert. Zum einen muss der Dampf für die Lösungsmittelregeneration aus dem Dampfnetz des Kraftwerks bezogen werden. Zum anderen erfordert die Kompression des abgetrennten CO₂ elektrischer Energie und reduziert somit die Netto-Stromerzeugung des Kraftwerks. Die Modellierung der CO₂ Kompression erfolgt in EBSILON.

Für beide Kraftwerke wurde ein großtechnischer Absorptions- und Desorptionsprozess simulativ ausgelegt. Entscheidende Designparameter, wie z.B. die Absorber- und Desorberkolonnenhöhe, wurden in Parameterstudien variiert und deren Auswirkung auf den Kraftwerksprozess untersucht. Diverse Betriebsparameter im CO₂-Abtrennprozess, wie Zirkulationsrate, Desorberdruck und -temperatur wurden ebenfalls in der Simulation variiert und die Simulationsergebnisse des Abtrennprozesses über die Schnittstelle in die Kraftwerkssimulation implementiert.

In optimalen Betriebsbedingungen des Abtrennprozesses sinkt der Kraftwerkswirkungsgrad des Steinkohlekraftwerks von 45,0 % auf 31,0 % inklusive CO₂-Abtrennung und Kompression. Beim Braunkohlekraftwerk sinkt der Wirkungsgrad von 49,3 % auf 33,3 %. Durch die gezielte Optimierung des Gesamtprozesses bei leicht veränderten Betriebs- und Designparametern des Abtrennprozesses können nur wenig bessere Wirkungsgrade erzielt werden. Die veränderten Parameter liegen sehr nah am bereits bestimmten alleinigen Optimum des Abtrennprozesses. Die Verdampferleistung der Lösungsmittelregeneration bestimmt maßgeblich den Energiebedarf des gesamten Abtrennprozesses. Die errechneten Verluste im Kraftwerkswirkungsgrad würden zu deutlich gesteigerten Stromgestehungskosten in der Stromproduktion führen. Die Wirkungsgrade der Kraftwerke, in den letzten Jahrzehnten mühsam optimiert, würden mit der Implementierung

einer CO₂-Abtrennung mit MEA drastisch reduziert.

Die großen Einbußen im Kraftwerkswirkungsgrad lassen sich durch Verwendung anderer Lösungsmittel verringern, die eine hohe CO₂-Abtrennung mit einem geringen spezifischen Wärmebedarf in der Regeneration erlauben. In der durchgeföhrten Studie sind auch neue Lösungsmittelsysteme durch gekoppelte Simulationen untersucht worden. Es zeigt sich, dass mit geeigneten Lösungsmittelsystemen eine deutlich verringerte Einbuße im Kraftwirkungsgrad zu erreichen ist.

3.4 CO₂-Abtrennung aus Rauchgasen mittels einer Mischung aus MEA, Wasser und Ethanol

Eine bereits aus der Literatur bekannte Möglichkeit für neuartige Lösungsmittel mit optimierten Stoffeigenschaften ist die Zugabe polarer Lösungsmittel in wässrigen Aminlösungen [27–29]. Die Zugabe eines polaren Lösungsmittels beeinflusst die physikalisch-chemischen Eigenschaften des Lösungsmittelsystems positiv. Die zyklische Beladungsdifferenz von CO₂ steigt im Vergleich zum Standardlösungsmittel (0.3 g/g MEA) mit der Zugabe von Ethanol an. Zudem hat Ethanol einen positiven Effekt auf die ablaufenden kinetische limitierten Reaktionen in der Flüssigphase.

Die Veröffentlichung V beschreibt die zum Lösungsmittelsystem MEA-H₂O-Ethanol durchgeföhrten Studien. Neben experimentellen Untersuchungen zum Phasengleichgewicht und zur Makrokinetik wurden Simulationen zu Prozessdesign und -optimierung durchgeföhr. In dieser Arbeit wurden die Simulationen in Aspen Plus durchgeföhr.

Wird Ethanol zum Stoffsysteem MEA-H₂O hinzugegeben, wird insbesondere die Regeneration des Lösungsmittels durch das Vorhandensein einer Komponente mit geringerem Dampfdruck als Wasser positiv beeinflusst. Eine Stripping von CO₂ aus dem beladenen Lösungsmittel ist bei geringen Temperaturen und höheren Desorberdrücken möglich. Das ermöglicht eine Einsparung von Betriebskosten der Abtrennung durch geringere Regenerationsenergie und verringerte Kompressionsleistung für das abgetrennte CO₂. Da die Stoffübergangsgeschwindigkeit von CO₂ durch die Zugabe von Ethanol ebenfalls positiv beeinflusst wird, kann die Absorberkolonne mit geringerer Bauhöhe ausgeführt werden.

Diese energetischen und apparativen Vorteile stehen einem deutlich komplexeren Abtrennprozess gegenüber. Die Rückhaltung des Ethanols führt zu einem deutlich aufwändigerem Prozess, welcher auch zusätzliche Apparate beinhaltet. Sowohl Absorber als auch Desorber benötigen nachgeschaltete Wäscher, um das austretende Ethanol mit

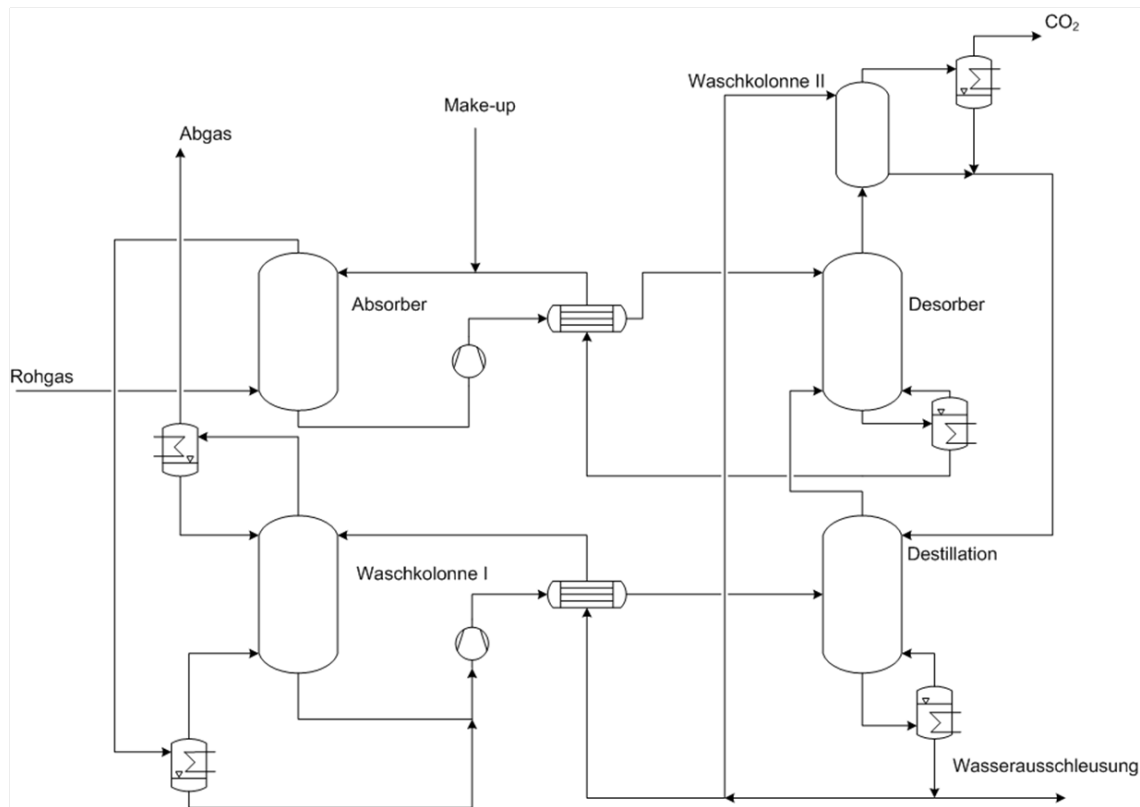


Abbildung 6: Schematische Darstellung der CO₂-Abtrennung inklusive Ethanol-Rückhaltung.

Waschwasser zu absorbieren. Für dieses Waschwasser wird eine weitere Regenerationseinheit benötigt. Hier sind zusätzlich ein Flüssig-Flüssig Wärmeübertrager, ein Verdampfer und eine Regenerationskolonne notwendig. Die Abbildung 6 zeigt schematisch den Gesamtprozess. Zusammen mit der BASF wurde dieses Prozesskonzept als Patent eingereicht [30].

Die Investitionskosten für diesen Prozess liegen deutlich über denen des Standard-Prozesses. Zudem ist die Prozessführung für diese Verfahrensvariante anspruchsvoll. Die Einhaltung der Massenbilanz für Wasser und Ethanol in diesem System sind kritische Größen für den Gesamtprozess und beeinflussen die CO₂-Abtrennung stark. Daher wird ein höherer Aufwand für das Regelkonzept des Gesamtverfahrens zu erwarten sein.

3.5 Verwendung von Seitenreaktoren bei der absorptiven Abtrennung von CO₂

Bei der Chemiesorption von CO₂ mit Alkanolaminen liegt in der Flüssigphase ein komplexes Reaktionsnetzwerk vor (vgl. Abbildung 1). Die Bildung von Carbamat und Bicarbonat sind dabei kinetisch kontrollierte Reaktionen. Die Bicarbonatbildung verläuft ins-

besondere bei niedrigen Temperaturen im Absorber langsam. Damit spielt die Verweilzeit hier eine wichtige Rolle für den Prozess. Zur Erreichung von hohen CO₂-Beladungen in der Flüssigphase wird die Bildung von Bicarbonat immer wichtiger. Um die Bedeutung der Bicarbonatbildung zu veranschaulichen, zeigt die Abbildung 7 die Speziesverteilung im System MEA-H₂O-CO₂ im Gleichgewicht bei 30 °C in Abhängigkeit der CO₂ Beladung bei 0.3 g/g MEA im unbeladenen Lösungsmittel. Möchte man Beladung über 0.5 mol CO₂ / mol Amin im Gleichgewicht erreichen, ist dies nur noch über eine vermehrte Bildung von Bicarbonat möglich.

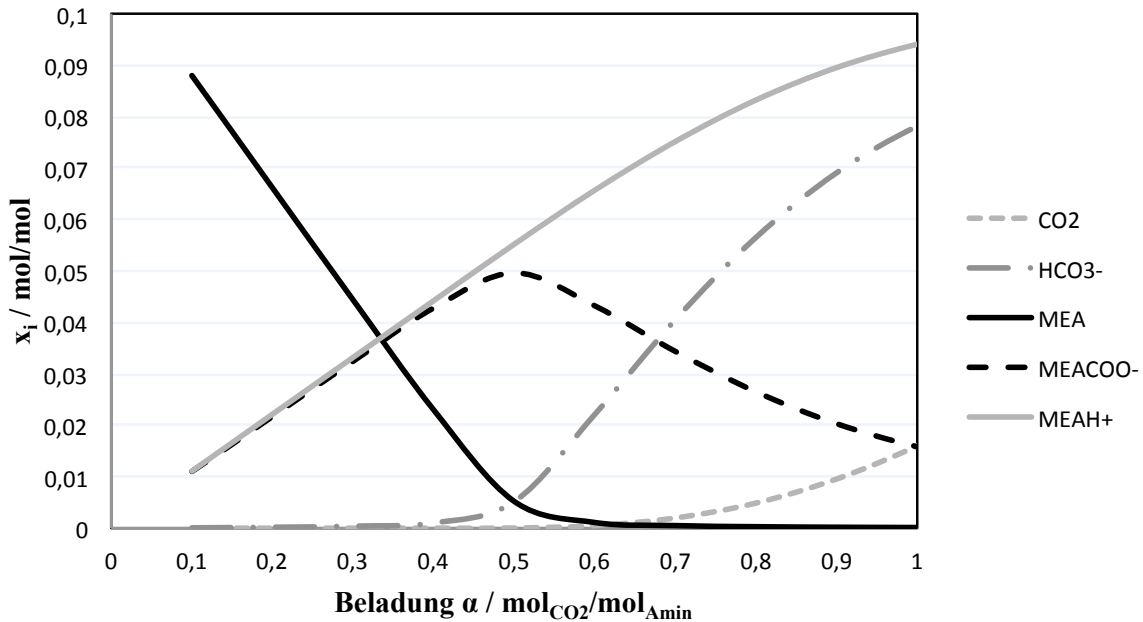


Abbildung 7: Speziesverteilung im System MEA-H₂O-CO₂ im Gleichgewicht bei 30°C in Abhängigkeit der CO₂ Beladung (0.3 g/g MEA im unbeladenen Lösungsmittel).

Die Bildung von Bicarbonat ist energetisch vorteilhaft. Die Reaktionsenthalpie ist im Vergleich zur Carbamat-Bildung gering, somit ist auch die Rückreaktion bei der Stripung des CO₂ aus dem Lösungsmittel nicht energieintensiv. Für die Reduktion des Gesamtenergiebedarfs der CO₂-Abtrennung ist eine hohe Bicarbonatbildung daher erstrebenswert. Limitierend ist hier die Verweilzeit in der Absorptionskolonne. Die technische Realisierung von längeren Verweilzeiten in Gas-Flüssig-Kontaktoren wie Absorbern ist ohne apparative Modifikationen nicht zu erreichen. Die Verweilzeit in Packungskolonnen ist typischerweise sehr gering [26]. Eine deutliche Erhöhung des Flüssigkeitsinhaltes (z.B. über Bodenkolonnen) würde zu einem hohen Druckverlust führen, was die Kompressionsenergie zur Förderung des Rauchgases erhöht.

Aus der Reaktivrektifikation ist das Konzept der Seitenreaktoren an Boden- und Packungskolonnen bekannt [31]. An definierten Stellen in der Kolonne wird entweder ein

Teilstrom oder der gesamte flüssige Strom aus der Kolonne entnommen und in einen Seitenreaktor geführt, bevor er von dort wieder in die Kolonne zurückgeführt wird.

Bei reaktiven Absorptionen wurde dieses Konzept bislang noch nicht umgesetzt. Für die reaktive Absorption von CO₂ aus Rauchgasen ist dieses Konzept jedoch interessant, da es die kinetisch kontrollierte Bildung von Bicarbonat bei geringen Druckverlusten in einer Absorptionskolonne ermöglicht. Die Seitenreaktoren sind hier einfache Verweilzeitbehälter.

Mit dem zuvor beschriebenen Simulationsmodell wurden in dieser Arbeit detaillierte Simulationsstudien zur Verwendung von Seitenreaktoren in der reaktiven Absorption untersucht. Die Auswirkungen von Anzahl an Seitenreaktoren, deren Volumen und die Lage der Abzugspunkte und Wiedereinspeisungen in der Kolonne wurden über Parameterstudien bestimmt.

Aus der Studie ist ein Patent hervorgegangen [32], das von Evonik Industries übernommen wurde. Mögliche apparative Ausführungen von Seitenreaktoren an Absorptionskolonnen werden im Patent genannt. Zudem sind zwei Beispiele aufgeführt, in denen die Auswirkung von Seitenreaktoren auf den Absorptionsprozess dargelegt wird. Für die Abtrennung von CO₂ aus dem Rauchgas eines 600 MW Steinkohlekraftwerk wurde die Prozessoptimierung mittels Seitenreaktoren untersucht. Bereits mit einem einzigen Seitenreaktor kann die spezifische Verdampferleistung in der Lösungsmittel-Regeneration um 1,2 % gesenkt werden. Die Details der Verfahrensvariante mit Seitenreaktoren sind im Patent [32] beschrieben.

3.6 Erforschung neuer Lösungsmittelsysteme für die CO₂ Abtrennung

Aufgrund des hohen energetischen Aufwands zur Abtrennung von CO₂ aus Kraftwerksabgasen mit bekannten Absorbentien wird intensiv nach neuen Lösungsmittelsystemen geforscht, die eine energetisch optimierte Abtrennung von CO₂ erlauben. Aufgrund der Größe der Apparate und der hohen Scale-Up Faktoren wird für die Prozessauslegung mit neuen Lösungsmittelsystemen eine Kombination von klassischem Anlagen Scale-up über Technikums- und Pilotanlagen und detaillierter prädiktiver Simulation erforderlich sein.

Dafür sind unterschiedliche Untersuchungen in den einzelnen Phasen der Prozessentwicklung erforderlich, die in der Veröffentlichung VI beschrieben sind. Die zur Prozessentwicklung notwendigen Studien in der Laborphase, Technikumsphase, Pilotanlagenphase und der Demonstration sind dargestellt.

4 Reaktionsmonitoring schneller Reaktionen mittels NMR Spektroskopie

Die direkte Bestimmung der Reaktionskinetik von CO₂ mit wässrigen Aminlösungen erfordert berührungsreie Messmethoden, die eine Bestimmung der Konzentrationsverläufe in der Flüssigphase ohne Störung der Prozessparameter wie Druck und Temperatur erlauben. Die NMR-Spektroskopie eignet sich hervorragend zur rückwirkungsfreien Untersuchung von komplexen Multikomponentenmischungen, auch unter technischen Bedingungen [12, 33–36]. Sie erlaubt neben detaillierten chemisch-strukturellen Aussagen eine zuverlässige quantitative Analyse, auch von nicht isolierbaren Zwischenprodukten.

Die Online-NMR-Spektroskopie ist damit hervorragend zum Reaktionsmonitoring der CO₂-Absorption in wässrigen Lösungsmittelsystemen geeignet. In anderen Arbeiten wurden bereits die Speziesverteilung in wässrigen aminhaltigen Lösungsmittelsystemen mit CO₂ untersucht [37–40].

Die ablaufenden Reaktionen sind teilweise sehr schnell, wie beispielsweise die Bildung von Carbamat. Die Untersuchung von Reaktionskinetiken mit Zeitkonstanten im Sekundenbereich ist durch die Kopplung von NMR-Spektroskopie und Mikroreaktionstechnik möglich. Dies erfordert jedoch eine Integration des Mikromischers in den Probenkopf und die Verwendung von solenoiden Messzellen mit sehr geringen internen Volumina [41–44].

Im Rahmen dieser Arbeit wurde ein NMR Probenkopf entwickelt, in dem ein Mikromischer mit einem Split-Recombine-Mischprinzip direkt in den NMR Probenkopf integriert ist. Durch diesen Aufbau sind Verweilzeiten von unter einer Sekunde zwischen Mischer und Messzelle realisierbar. Die Entwicklung dieses Probenkopfes und die durchgeführten Kinetikuntersuchungen werden im Folgenden beschrieben.

4.1 Kopplung eines NMR Durchflusskopfes mit extern installierten Mikroreaktoren

Für die Online-NMR-Spektroskopie bieten sich Durchflusszellen an, mit denen Reaktionsmischungen aus externen Reaktoren unter Beibehaltung der Reaktionsparameter wie Druck und Temperatur in einem Kreislauf durch den NMR Probenkopf gefördert werden können. NMR Probenköpfe mit Durchflusszellen wurden bereits in früheren Arbeiten für die Kopplung mit externen Reaktoren zum Reaktions- und Prozessmonitoring eingesetzt [45–48]. Bei der Verwendung externer Reaktoren ist der Durchfluss im Bypass durch das NMR Spektrometer aufgrund der Anforderungen an die Vormagnetisierung begrenzt. Aufgrund des Flüssigkeitsvolumens (Hold-Up) in Transferleitung und Standard-Durchflusszelle können mit dieser Technologie Reaktionen mit Halbwertszeiten über ungefähr 10 min untersucht werden [49, 50].

Die Mikroreaktionstechnik erlaubt eine direkte und effiziente Vermischung von aktiv gepumpten Reaktionspartnern in Apparaten mit sehr geringen Dimensionen und ohne weitere Einbauten (wie z.B. Rührer) [51]. Mikroreaktoren können verwendet werden, um den Ort des Reaktionsstarts (Vermischung der Reaktionspartner) nahe an den Punkt der Detektion zu verlagern [52–54]. Durch die örtliche Verlagerung ist bei gleichem Durchfluss der Reaktanden eine Verringerung der Totzeit zwischen Reaktionsstart und Konzentrationsmessung möglich. Für die Bestimmung von isothermen Reaktionskinetiken mit hoher Modellgüte ist es für das Reaktionsmonitoring unbedingt notwendig, Druck und Temperatur auf der Durchflusstrecke bis zum Ort der Messung konstant zu halten.

In dieser Arbeit wurde in einem ersten Aufbau ein externer Mikromischer direkt an den NMR Probenkopf unterhalb des Magneten montiert. Als Mikromischer wurde ein passiver Mikromischer mit Multilaminierung als Mischmethode (SIMM-V2, Edelstahl) von IMM, Mainz verwendet [55]. Der Mikromischer wurde in einem speziell entwickeltem Gehäuse installiert, welches kontinuierlich mit einer Temperierflüssigkeit durchströmt wurde. Der Mischer wurde mittels PEEK Kapillaren an den Standard-NMR Probenkopf mit Durchflusszelle angeschlossen. Die Zuleitung vom Mischer in den Probenkopf und die NMR Durchflusszelle selbst sind in diesem Aufbau nicht aktiv mit einer Flüssigkeit temperiert. Die Installation ist in der Veröffentlichung VII beschrieben. Der flüssige Hold-Up zwischen Mikromischer und NMR Durchflusszelle betrug 610 µl (verifiziert über Verweilzeitexperimente).

Mit diesem Aufbau wurde die Kinetik eines Modellsystems bestimmt. Als Modellsystem wurde die Veresterung von Methanol mit Ameisensäure gewählt, die nur eine schwache Wärmetönung aufweist. Über ^1H und ^{13}C Spektren bei variierter Temperatur und Kon-

zentration wurde die Kinetik mittels StopFlow- und Flow-Experimenten bestimmt. Ein aktivitätsbasiertes Kinetikmodell der Verestertungsreaktion wurde anhand der Messdaten parametrisiert und mit Literaturwerten verglichen. Bei geringen Temperaturen und Konzentrationen ergaben sich sehr gute Übereinstimmungen mit den Literaturwerten. Bei hohen Temperaturen und Konzentrationen der Reaktionspartner waren systematische Abweichungen ersichtlich, die auf die mangelnde Temperierung des beschriebenen Aufbaus zurückgeführt werden konnten.

Deshalb wurde im Rahmen dieser Arbeit ein vollständig neuer NMR Probenkopf entwickelt, in dem der Mikromischer direkt im Probenkopf integriert ist und der eine aktive Temperierung aller relevanten Reaktionsbereiche ermöglicht.

4.2 Temperierter NMR Probenkopf mit integriertem Mikromischer

Für die Neuentwicklung eines temperierten NMR Probenkopfes mit integriertem Mikromischer musste in einem ersten Schritt die Messzelle des NMR Probenkopfes modifiziert werden. In den bisherigen Studien zum Reaktionsmonitoring am Lehrstuhl wurden Standard Durchfluss-Probenköpfe (Varian Inc.) mit Zellvolumina von 90 -120 µl und einem Stattel-Spulendesign verwendet. Diese vertikal verbauten Durchflusszellen haben einen hohen Platzbedarf im NMR Probenkopf und besitzen einen großen flüssigen Hold-Up im Vergleich zu den Verbindungsleitungen.

Deshalb wurde in Zusammenarbeit mit der Arbeitsgruppe von Prof. Albert (Eberhard Karls Universität Tübingen) auf der Grundlage Ihrer Erfahrung im Messzellendesign [56] ein Prototyp eines Probenkopfes mit einer solenoide NMR-Messzelle entwickelt. Aufgrund des optimierten Spulendesigns können solenoide NMR Messzellen sehr klein ausgeführt und im NMR Probenkopf horizontal installiert werden. Sie besitzen aufgrund der direkt auf der Zelle aufgebrachten Messspule eine hohe Sensitivität trotz geringem Probevolumen [43, 57, 58]. In der Abbildung 8 ist eine solenoide Durchflusszelle schematisch dargestellt. Sie eignen sich daher insbesondere für Kopplungen mit chromatographischen Methoden (z.B. HPLC) [47, 59–61] und erlauben die NMR Analyse geringer Substanzmengen [62]. Aufgrund des geringen Hold-Ups eignen sich solenoide Messzellen hervorragend für das Reaktionsmonitoring und werden ebenfalls für Lab-on-the-Chip Systeme eingesetzt [52, 63, 64].

Im entwickelten Prototyp wird der Hohlraum um die solenoide Messzelle (aktives Volumen ca. 6 µl) mit einer vollständig perfluorierten Flüssigkeit (Perfluortributylamin / FC-43) gefüllt, um Suszeptibilitäteffekte um die Messpule zu vermindern. Eine Darstellung dieses Prototyps ist in der Veröffentlichung VII enthalten. Dieser NMR-Probenkopf

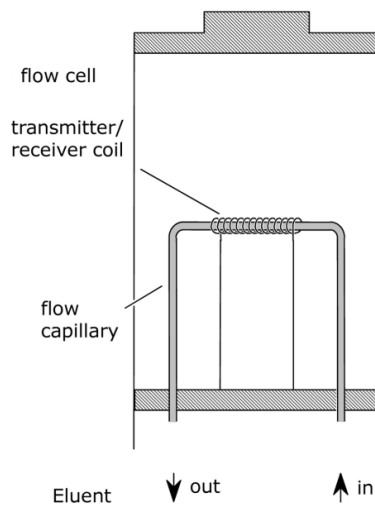


Abbildung 8: Schematische Darstellung einer solenoiden NMR Durchflusszelle.

mit solenoider Flusszelle dient in dieser Arbeit als Grundlage für die weiteren Entwicklungen.

In Zusammenarbeit mit dem Institut für Mikrotechnik Mainz GmbH (IMM) und der Arbeitsgruppe von Prof. Albert, Eberhard Karls Universität Tübingen, wurde ein vollständig neuer thermostatisierter NMR Probenkopf entwickelt, der einen Mikromischer direkt im Probenkopfbereich integriert hat. Die direkte Integration von Mikromischern in NMR Probenköpfe erlaubt ein gezieltes Reaktionsmonitoring direkt nach der Vermischung der Edukte und ermöglicht Strömungsanalysen mit bildgebenden Verfahren [65–67]. In dieser Arbeit wurde erstmalig ein vollständig flüssigtemperierter Probenkopf entwickelt, der den gesamten Bereich der Vermischung, der Verweilzeitstrecke und der NMR Messung thermostatisiert.

Der entwickelte Probenkopf ist aus modularen Einzelementen (Werkstoff PEEK) zusammengestellt, welche über Dichtungsebenen druckfest miteinander verpresst werden. Die Fluidführung von Edukten, Reaktant und Temperiermedium sind über vertikale Bohrungen in den Elementen des Probenkopfes ausgeführt. So können die unterschiedlichen Einheiten des Probenkopfes (Mikromischer, Verweilzeitstrecke, NMR Messzelle) ohne Schlauchverbindungen miteinander vereint werden. Zum Anschluss von Temperierleitungen und Edukt-/Produktleitungen wurde eine separate Anschlussdose außerhalb des NMR Magneten entwickelt.

Der Mikromischer im entwickelten Probenkopf ist als Raupenmischer mit einer Split- / Recombine Struktur ausgeführt, welcher am IMM entwickelt wurde [68]. Der im Probenkopf verbaute Mikromischer besitzt eine Länge von 11,7 mm und enthält 39 Split-/Recombine-Elemente. Er erlaubt Durchflüsse von 10 - 1000 µl/min. Die Abbildung 9 zeigt das Mischmodul des NMR Probenkopfes mit dem dort integrierten Raupenmischer.



Abbildung 9: Darstellung Mischmodul mit integriertem Raupenmischer (Split/Recombine).

Die NMR Messung des neu entwickelten Probenkopfes wird in einer Messzelle (Quarzglas) mit solenoider Spule durchgeführt, welche aktuell die Aufnahme von ^1H Spektren erlaubt. Die Abbildung 10 zeigt den Messzellaufbau. Das Volumen des aktiven Messbereichs beträgt 5 μl . Das äußere Volumen um die Messzelle wird mit FC-43 als Temperiermedium aktiv durchströmt. Von diesem Temperiermedium werden auch der Mikromischer und die Verweilzeitkapillare auf den Außenseiten umströmt, um möglichst isotherme Verhältnisse im gesamten Reaktions- und Messbereich sicher zu stellen. Das Temperiermedium FC-43 wird mittels eines externen Thermostaten temperiert und im Kreislauf gepumpt.

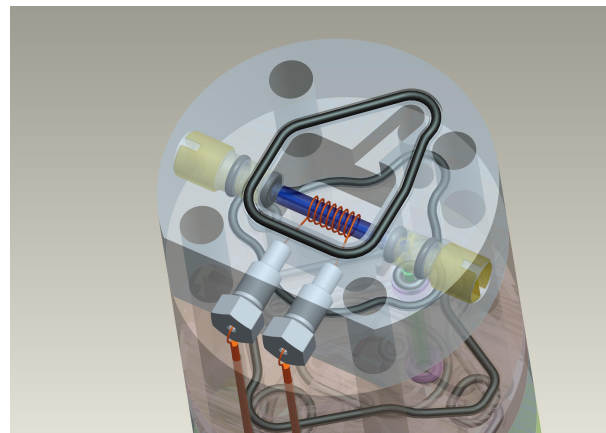


Abbildung 10: Darstellung NMR Messzelle mit solenoider Messspule.

Zunächst wurden mit dem neuen Probenkopf Untersuchungen der Kinetik an dem schon zuvor benutzten Modellsystem der Veresterung von Methanol mit Ameisensäure durchgeführt. Die ^1H Spektrenqualität ist vergleichbar mit NMR Standard-Durchflussköpfen und erlaubt ein gezieltes Reaktionsmonitoring durch die Aufnahme von Protonen-Spektren. Die ersten Messpunkte in Flow-Experimenten konnten nach 2 s Reaktionszeit genommen und die Zusammensetzung des Reaktionsgemisches quantifiziert wer-

den. Im Vergleich zur zuvor verwendeten Technologie (Externer Mischer, Standard-Durchflusskopf) sind nun für höher konzentrierte Mischungen und erhöhte Katalysatorkonzentrationen isotherme Kinetikmessungen möglich.

Die Veröffentlichung VIII beschreibt den entwickelten Probenkopf und die darin durchgeführten Messungen im Detail. Mit dem entwickelten System ist nun eine kinetische Untersuchung von schnell reagierenden Systemen unter isothermen Verhältnissen möglich. Da der entwickelte Probenkopf für höhere Drücke (bis zu 60 bar) ausgelegt ist, können nun auch Messungen unter Druck durchgeführt werden. Eine Aufnahme der Reaktionskinetik von CO₂ mit aminhaltigen Lösungsmitteln in der Flüssigphase wird mit diesem Probenkopf ermöglicht.

4.3 Untersuchungen am System MEA-H₂O-CO₂

Mit dem in dieser Arbeit entwickelten NMR Probenkopf wurden erste Kinetikmessungen zur Untersuchung der Flüssigphasenreaktionen bei der reaktiven Absorption von CO₂ durchgeführt.

Zur Untersuchung der ablaufenden Flüssigphasenreaktionen wurden Verdünnungsexperimente mit dem System MEA-H₂O-CO₂ durchgeführt. Dazu wurde eine mit CO₂ beladene Lösung (0.3 g/g MEA) unter Druck mit einer unbeladenen wässrigen MEA Lösung vermischt und die ablaufenden Reaktionen nach Verdünnung mit dem beschriebenen NMR Probenkopf verfolgt.

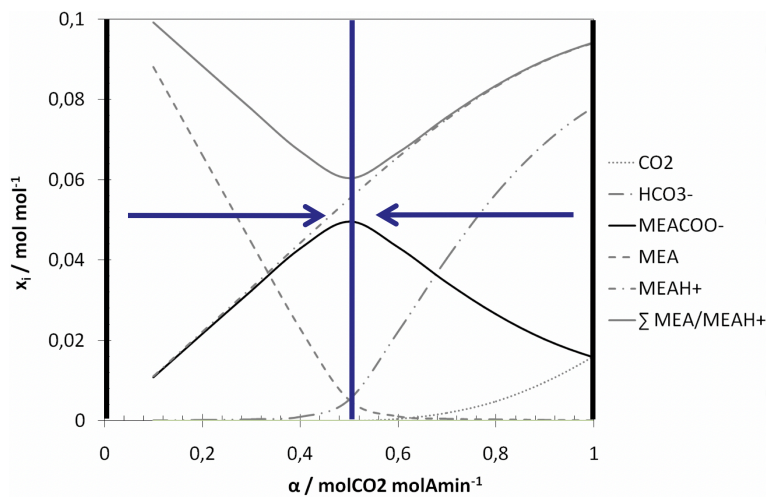


Abbildung 11: Schematische Darstellung des Verdünnungsexperiments mit einer beladenen und unbeladenen Aminlösung, dargestellt in der Speziesverteilung des System MEA-H₂O-CO₂ im Gleichgewicht.

Die Abbildung 11 illustriert das Verdünnungsexperiment an einer exemplarischen Darstellung der Speziesverteilungen im Gleichgewicht für das System MEA-H₂O-CO₂. Eine

unbeladene MEA-Lösung ($\alpha = 0$) wird mit einer beladenen Lösung (hier $\alpha = 1$) in gleichen Teilen (identische Gesamtmolmenge in beiden Lösungen) gemischt. Das bei hohen Beladungen gebildete Bicarbonat (HCO_3^-) reagiert in einer kinetisch kontrollierten Reaktion ab und es wird Carbamat (MEACOO^-) gebildet. Über die Verfolgung der Schlüsselkomponenten MEA/MEA H^+ und MEACOO $^-$ kann die Reaktionskinetik der beschriebenen Reaktion von Bicarbonat zu Carbamat verfolgt werden.

Die Herstellung der mit CO₂ beladenen Lösung erfolgte in einem speziellen Druckapparat mit Schauglas, welcher schon in vorangegangenen Arbeiten zur Untersuchung der Gleichgewichtszusammensetzung von beladenen Aminlösungen verwendet wurde [37, 69]. Die Aminlösung wurde bis zu einem Gesamtdruck von 30 bar mit CO₂ bei unterschiedlichen Temperaturen beladen. Es stellten sich CO₂-Beladungen von 0,85 - 0,99 mol CO₂ / mol Amin ein. Die beladene Aminlösung wurde unter Druckhaltung mit einer Spritzenpumpe in den NMR Probenkopf gepumpt und dort im Mikromischer mit der unbeladenen Aminlösung vermischt. Die Konzentrationsverläufe in der Reaktionsmischung konnte nun in StopFlow-Experimenten mittels ¹H Messungen untersucht werden. Der schematische Aufbau der Versuchsanlage ist in der Abbildung 12 dargestellt.

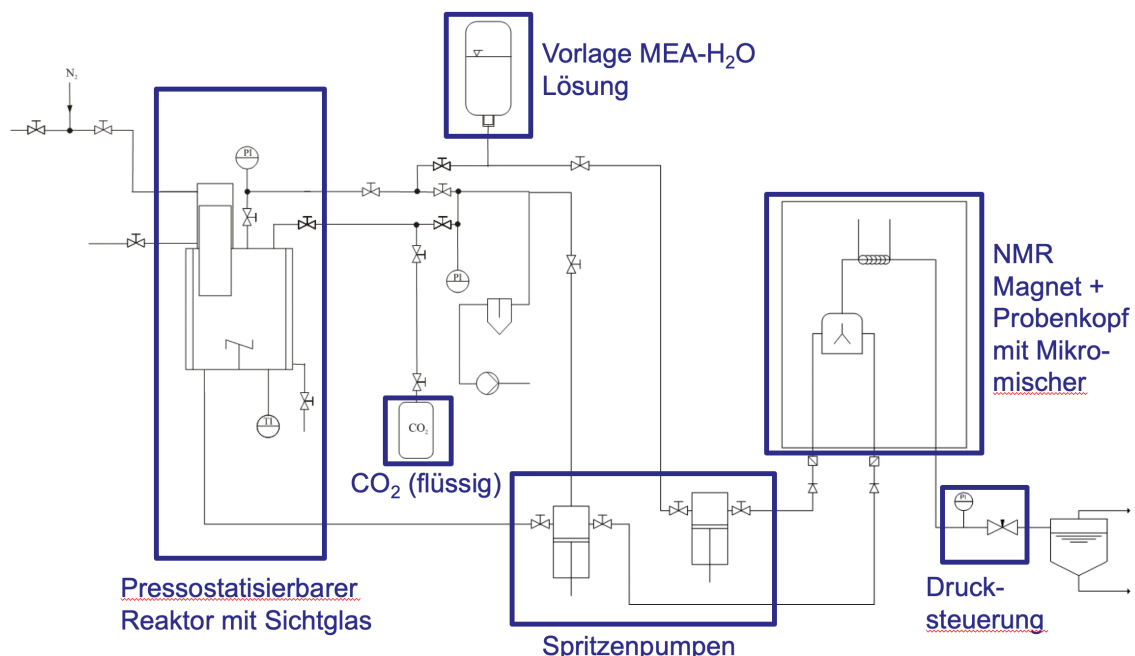


Abbildung 12: Versuchsaufbau zur Kinetikbestimmung der Flüssigphasenreaktionen am System MEA-H₂O-CO₂ mit dem entwickelten NMR Probenkopf.

Mit der beschriebenen Methode wurden Kinetiken der Flüssigphasenreaktionen bei isothermen Verhältnissen mittels ¹H Messungen bei vier verschiedenen Temperaturen aufgenommen. Mit dem neu entwickelten Probenkopf konnten die ersten Konzentrationsbestimmungen bereits wenige Sekunden nach der Vermischung unter Beibehaltung von Druck und Temperatur durchgeführt werden. Die Abbildung 13 zeigt die ermittelten

Konzentrationsverläufe für die Zielkomponenten MEA/MEA H^+ und MEACOO $^-$ bei vier unterschiedlichen Temperaturen.

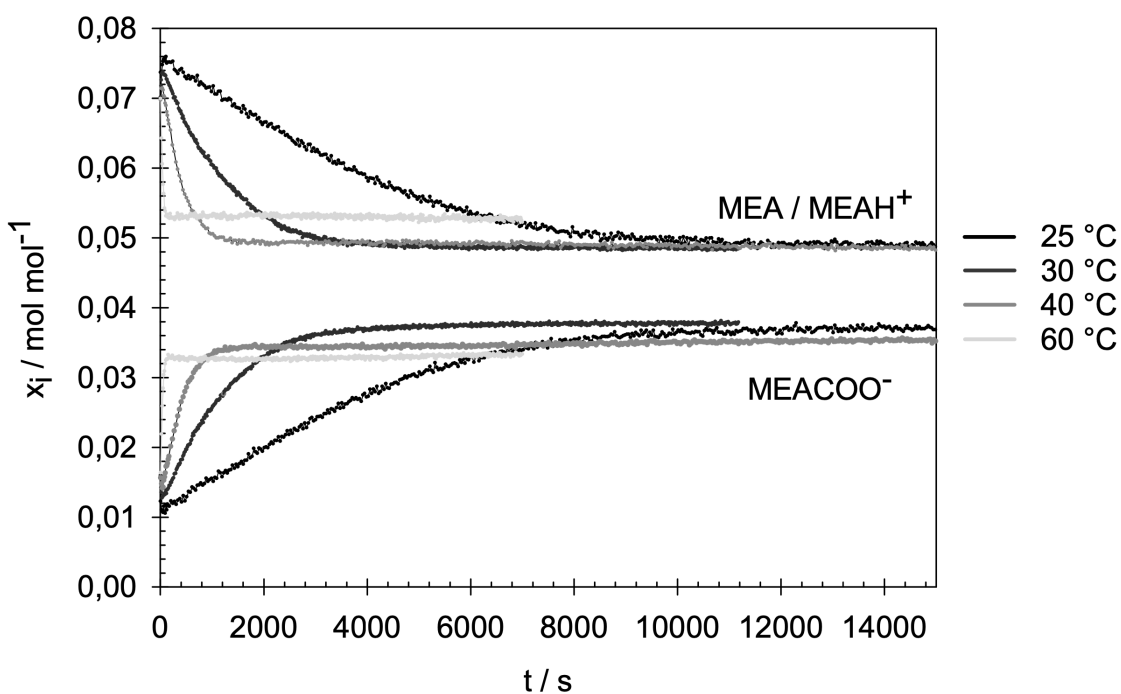


Abbildung 13: Konzentrationsverläufe Zielkomponenten der Flüssigphasenkinetik im isothermen Verdünnungsexperiment für das System MEA-H₂O-CO₂.

Die Quantifizierung des Reaktionsgemisches und die Bestimmung der Konzentrationsverläufe der Schlüsselkomponenten in der Flüssigphase ist mit dieser Methode möglich. Für alle 4 Temperaturen konnten Kinetiken bis zum Erreichen des chemischen Gleichgewichts aufgenommen werden. Bei 60 °C Reaktionstemperatur stellte sich das neue Gleichgewicht bereits nach 200 s Reaktionszeit ein, was den Einsatz der entwickelten Technologie zur Kinetikmessung verdeutlicht. In allen Experimenten ist eine Abnahme der protonierten Spezies MEAH $^+$ und ein Anstieg des Carbamats MEACOO $^-$ zu erkennen. Die Gleichgewichtszusammensetzung ist für alle durchgeführten Kinetiken aufgrund der unterschiedlichen Startbedingungen (CO₂-Beladung) und Reaktionstemperatur unterschiedlich. Der Einfluss der Reaktionstemperatur auf die Reaktionsgeschwindigkeit ist in den dargestellten Konzentrationsverläufen klar ersichtlich.

Die durchgeführten Experimente belegen die Möglichkeit, mit der entwickelten Technologie Reaktionskinetiken von CO₂ mit wässrigen Aminlösungen in der Flüssigphase unter Beibehaltung von Druck und Temperatur berührungslos zu analysieren. Für das System MEA-H₂O-CO₂ sind weitere Kinetikuntersuchungen mit ausführlichen Parametervariationen notwendig, um ein Kinetikmodell daran anzupassen.

5 Einordnung und Ausblick

Die hier vorgestellten Arbeiten wurde in den Jahren 2006 - 2011 während der Tätigkeit des Autors als wissenschaftlicher Mitarbeiter an den Lehrstühlen von Prof. Hasse in Stuttgart und Kaiserslautern durchgeführt. Die zugehörigen Publikationen erfolgten zeitnah. Sie bauen dementsprechend auf dem damaligen Stand des Wissens auf. Diese Arbeiten haben die Grundlage für Folgearbeiten gelegt, die nachfolgend eingeordnet werden.

Der in dieser Arbeit entwickelte NMR Probenkopf wurde von Brächer et.al. [70] verwendet, um eine Kinetikuntersuchung an schnell ablaufenden Veresterungen durchzuführen. Die Arbeit belegt, dass der hier entwickelte Probenkopf für den praktischen Einsatz geeignet ist. Er erweitert somit die Nutzung der NMR Spektroskopie zum Reaktionsmonitoring für schnell ablaufende Reaktionen. Friebel et.al. [71] untersuchten in einer detaillierten Studie, welche Einflüsse das Messzellendesign und die Ausführung der Vormagnetisierung für quantitative Analysen im Reaktionsmonitoring hat .

Die Online NMR Spektroskopie wurde in den letzten Jahren bezüglich Ihrer Einsatzfähigkeit im Prozessmonitoring sowie der qualitativen und quantitativen Analyse von Mischungen deutlich erweitert [72]. Insbesondere die Entwicklung von immer leistungsfähigeren Benchtop NMR ermöglichen den Einsatz der NMR Spektroskopie für das Reaktionsmonitoring und die Stoffdatenanalyse ohne die Notwendigkeit eines komplexen Kryo-Magneten [73–75]. Der Einsatz der NMR Spektroskopie im direkten Prozessumfeld wird dadurch erleichtert und die Möglichkeit zur Prozessanbindung deutlich weiter entwickelt [76]. Die Untersuchung von Hochtemperaturprozessen mit der NMR Spektroskopie wird durch die Weiterentwicklung von spezialisierten NMR Probenköpfen ermöglicht [77]. Neue Fertigungstechniken erlauben eine Entwicklung von immer kleineren Messzellen mit Volumina im Nanoliter Bereich, die den Bereich der NMR Spektroskopie mit verkleinerten Lab-on-the-chip Systemen zu neuen Analysemöglichkeiten in der Humanmedizin erweitern [78]. Mit diesen Entwicklungen wird der Einsatz der berührungslosen und quantitativen NMR Spektroskopie in der Zukunft in Forschung, Entwicklung und Produktion noch deutlich zunehmen.

Die in dieser Studie mit der NMR Spektroskopie untersuchte Flüssigphasenreaktion von CO₂ mit einer wässrigen MEA Lösung wurde durch Behrens et.al. [79] mit dem in die-

ser Arbeit entwickelten Probenkopf eingehend untersucht. Basierend auf den erhaltenen quantitativen Konzentrationsverläufen wurde das Simulationsmodell der CO₂ Absorption angepasst und die Genauigkeit der Vorhersage insbesondere für MEA-Lösungen mit hohen CO₂ Beladungen verbessert. Das so verbesserte rigorose Prozessmodell ermöglicht zuverlässige Vorhersagen von CO₂ Aminwäschen bei technischen Betriebsbedingungen. Dadurch werden die Risiken des Scale-Ups für neue CO₂-Abscheideverfahren mit diesem Lösungsmittel reduziert.

In den letzten 10 Jahren wurden große Anstrengungen unternommen, um neue Technologien zur Abscheidung von CO₂ aus Gasströmen zu entwickeln und die vorhandenen zu verbessern [80–82]. Insbesondere wurden zahlreiche neue Lösungsmittel für die Reaktivabsorption vorgeschlagen (siehe u.a. [83–86]). Aufgrund des immer noch hohen Energiebedarfs für CO₂ Abtrennprozesse wird weiterhin intensiv an neuen Technologien geforscht [87–89]. Die politischen Anstrengungen zur Reduktion von CO₂ Emissionen und zukünftig steigende Kosten für CO₂ Zertifikate lassen Technologien zum Carbon Capture and Storage (CCS) bei der Energieerzeugung, Zementherstellung und weiteren industriellen Herstellprozessen wirtschaftlich werden [90–93].

Für das Design zukünftiger Anlagen wird die rigorose Prozesssimulation eine wertvolle Unterstützung bieten, wofür detaillierte physiko-chemische Kenntnisse (z.B. über die ablaufende Reaktionskinetik) der optimierten Lösungsmittelsysteme notwendig sind. Hierfür hat die vorliegende Arbeit Grundlagen gelegt.

Literaturverzeichnis

- [1] R. Pachauri, L. Meyer (Eds.): IPCC: Climate Change 2014: Synthesis Report, IP-CC, Geneva, Switzerland, 2014.
- [2] E. Rubin, B. Anand: A Technical, Economic and Environmental Assessment of Amine-based CO₂ Capture Technology for Power Plant Greenhouse Gas Control, Annual Technical Progress Report, Carnegie Mellon University, Center for Energy and Environmental Studies, Pittsburgh, 2002.
- [3] R. Steeneveldt, B. Berger, T. A. Torp: CO₂ capture and storage - Closing the knowing-doing gap, Chemical Engineering Research & Design 84 (2006) 739–763.
- [4] S. Plasynski, Z.-Y. Chen: Review of CO₂ capture technologies and some improvement opportunities, ACS Division of Fuel Chemistry, Preprints 45 (2000) 644–649.
- [5] C. M. White, B. R. Strazisar, E. J. Granite, J. S. Hoffman, H. W. Pennline: Separation and capture of CO₂ from large stationary sources and sequestration in geological formations - Coalbeds and deep saline aquifers, Journal of the Air and Waste Management Association 53 (2003) 645–715.
- [6] J. Linssen, P. Markewitz, D. Martinsen, M. Walbeck: Technologies for the separation and storage of CO₂, BWK 58 (2006) 59–62.
- [7] M. Abu-Zahra, L. Schneiders, J. Niederer, P. Feron, G. Versteeg: CO₂ capture from power plants. Part I. A parametric study of the technical performance based on monoethanolamine, International Journal of Greenhouse Gas Control 1 (2007) 37–46.
- [8] E. Kenig: Advanced modeling of reactive separation units with structured packings, Chemical Product and Process Modeling 2 (2007) 1–30.
- [9] E. Kenig, P. Seferlis: Modeling Reactive Absorption, Chemical Engineering Progress 105 (2009) 65–73.
- [10] L. Kucka, I. Muller, E. Y. Kenig, A. Gorak: On the modelling and simulation of sour gas absorption by aqueous amine solutions, Chemical Engineering Science 58 (2003) 3571–3578.

- [11] S. Freguia, G. T. Rochelle: Modeling of CO₂ capture by aqueous monoethanolamine, *AICHE Journal* 49 (2003) 1676–1686.
- [12] M. Maiwald, H. Fischer, Y.-K. Kim, K. Albert, H. Hasse: Quantitative high-resolution on-line NMR spectroscopy in reaction and process monitoring, *Journal of Magnetic Resonance* 166 (2004) 135–146.
- [13] E. Y. Kenig, L. Kucka, A. Gorak: Rigorous modeling of reactive absorption processes, *Chemie Ingenieur Technik* 74 (2002) 745–764.
- [14] D. M. Austgen, G. T. Rochelle, X. Peng, C. C. Chen: Model of Vapor Liquid Equilibria for Aqueous Acid Gas Alkanolamine Systems using the Electrolyte NRTL Equation, *Industrial & Engineering Chemistry Research* 28 (1989) 1060–1073.
- [15] P. M. M. Blauwhoff, G. F. Versteeg, W. P. M. van Swaaij: A study on the reaction between CO₂ and alkanolamines in aqueous solutions, *Chemical Engineering Science* 39 (1984) 207–225.
- [16] H. Hikita, S. Asai, H. Ishikawa, M. Honda: The kinetics of reactions of carbon dioxide with monoethanolamine, diethanolamine and triethanolamine by a rapid mixing method, *Chemical Engineering Journal* 13 (1977) 7–12.
- [17] T. Pintola, P. Tontiwachwuthikul, A. Meisen: Simulation of pilot plant and industrial CO₂-MEA absorbers, *Gas Separation and Purification* 7 (1993) 47–52.
- [18] F. Tobiesen, H. Svendsen, O. Juliussen: Experimental validation of a rigorous absorber model for CO₂ postcombustion capture, *AICHE Journal* 53 (2007) 846–865.
- [19] N. Asprion: Nonequilibrium rate-based simulation of reactive systems: Simulation model, heat transfer, and influence of film discretization, *Industrial and Engineering Chemistry Research* 45 (2006) 2054–2069.
- [20] R. Krishna, J. Wesselingh: The Maxwell-Stefan Approach to Mass Transfer, *Chemical Engineering Science* 52 (1997) 861–911.
- [21] R. J. Littel, G. F. Versteeg, W. P. M. van Swaaij: Kinetics of CO₂ with Primary and Secondary-Amines in Aqueous-Solutions, *AICHE Journal* 38 (1992) 244–250.
- [22] P. Vaidya, E. Kenig: Gas-liquid reaction kinetics: A review of determination methods, *Chemical Engineering Communications* 194 (2007) 1543–1565.
- [23] A. Jamal, A. Meisen, C. J. Lim: Kinetics of carbon dioxide absorption and desorption in aqueous alkanolamine solutions using a novel hemispherical contactor. Part I: Experimental apparatus and mathematical modeling, *Chemical Engineering Science* 61 (2006) 6571–6589.

- [24] N. Ramachandran, A. Aboudheir, R. Idem, P. Tontiwachwuthikul: Kinetics of the absorption of CO₂ into mixed aqueous loaded solutions of monoethanolamine and methyldiethanolamine, *Industrial and Engineering Chemistry Research* 45 (2006) 2608–2616.
- [25] R. Billet, M. Schultes: Predicting mass transfer in packed columns, *Chemical Engineering and Technology* 16 (1993) 1–9.
- [26] P. Suess, L. Spiegel: Hold-up of Mellapak structured packings, *Chemical Engineering and Processing* 31 (1992) 119–124.
- [27] J. Jakobsen, E. da Silva, J. Krane, H. Svendsen: NMR study and quantum mechanical calculations on the 2-[(2-aminoethyl)amino]-ethanol-H₂O-CO₂ system, *Journal of Magnetic Resonance* 191 (2008) 304–314.
- [28] S.-W. Park, J.-W. Lee, B.-S. Choi, J.-W. Lee: Kinetics of absorption of carbon dioxide in monoethanolamine solutions of polar organic solvents, *Journal of Industrial and Engineering Chemistry* 11 (2005) 202–209.
- [29] A. Archane, L. Gicquel, E. Provost, W. Fuerst: Effect of methanol addition on water-CO₂-Diethanolamine system: Influence on CO₂ solubility and on liquid phase speciation, *Chemical Engineering Research and Design* 86 (2008) 592–599.
- [30] H. Garcia, R. Notz, G. Sieder, O. Spuhl, H. Hasse, I. Toennies, S. Hoch, H. Mangalapally: Removal of acid gases by means of an absorbent comprising a stripping aid, Patent WO2010/149599 A1 (2010).
- [31] R. Baur, R. Krishna: Distillation column with reactive pump arounds: an alternative to reactive distillation, *Catalysis Today* 79-80 (2003) 113–123.
- [32] H. Hasse, I. Toennies, S. Hoch: Method and device for separating off carbon dioxide from gas streams, Patent WO2012/163847 A1 (2012).
- [33] J. Bart, A. Kolkman, A. Oosthoek-de Vries, K. Koch, P. Nieuwland, H. Janssen, J. van Bentum, K. Ampt, F. Rutjes, S. Wijmenga, H. Gardeniers, A. Kentgens: A microfluidic high-resolution NMR flow probe, *Journal of the American Chemical Society* 131 (2009) 5014–5015.
- [34] J. A. Iggo, D. Shirley, N. C. Tong: High pressure NMR flow cell for the in situ study of homogeneous catalysis, *New Journal of Chemistry* 22 (1998) 1043–1045.
- [35] D. C. Roe, P. M. Kating, P. J. Krusic, B. E. Smart: High resolution NMR techniques in catalysis, *Topics in Catalysis* 5 (1998) 133–147.

- [36] S. I. Selivanov, B. A. Ershov: The application of high resolution Nuclear Magnetic Resonance in the study of fast non-equilibrium reactions, *Russian Chemical Reviews* 55 (1986) 395–410.
- [37] W. Boettinger, M. Maiwald, H. Hasse: Online NMR spectroscopic study of species distribution in MEA-H₂O-CO₂ and DEA-H₂O-CO₂, *Fluid Phase Equilibria* 263 (2008) 131–143.
- [38] P. Derkx, J. Hogendoorn, G. Versteeg: Experimental and theoretical study of the solubility of carbon dioxide in aqueous blends of piperazine and N-methyldiethanolamine, *Journal of Chemical Thermodynamics* 42 (2010) 151–163.
- [39] J. P. Jakobsen, J. Krane, H. F. Svendsen: Liquid-phase composition determination in CO₂-H₂O-alkanolamine systems: an NMR study, *Industrial and Engineering Chemistry Research* 44 (2005) 9894–9903.
- [40] F. Mani, M. Peruzzini, P. Stoppioni: CO₂ absorption by aqueous NH₃ solutions: speciation of ammonium carbamate, bicarbonate and carbonate by a ¹³C NMR, *Green Chemistry* 8 (2006) 995–1000.
- [41] A. M. Wolters, D. A. Jayawickrama, A. G. Webb, J. W. Sweedler: NMR detection with multiple solenoidal microcoils for continuous-flow capillary electrophoresis, *Analytical Chemistry* 74 (2002) 5550–5555.
- [42] E. McDonnell, S. Han, C. Hilty, K. Pierce, A. Pines: NMR analysis on microfluidic devices by remote detection, *Analytical Chemistry* 77 (2005) 8109–8114.
- [43] Y. Li, A. Wolters, P. Malawey, J. Sweedler, A. Webb: Multiple solenoidal microcoil probes for high-sensitivity, high-throughput nuclear magnetic resonance spectroscopy, *Analytical Chemistry* 71 (1999) 4815–4820.
- [44] A. Kentgens, J. Bart, P. Van Bentum, A. Brinkmann, E. Van Eck, J. Gardeniers, J. Janssen, P. Knijn, S. Vasa, M. Verkuijlen: High-resolution liquid- and solid-state nuclear magnetic resonance of nanoliter sample volumes using microcoil detectors, *Journal of Chemical Physics* 128 (2008) 1–17.
- [45] M. Lacey, J. Sweedler, C. Larive, A. Pipe, R. Farrant: ¹H NMR characterization of the product from single solid-phase resin beads using capillary NMR flow probes, *Journal of Magnetic Resonance* 153 (2001) 215–222.
- [46] S. Grob, H. Hasse: Reaction kinetics of the homogeneously catalyzed esterification of 1-butanol with acetic acid in a wide range of initial compositions, *Industrial and Engineering Chemistry Research* 45 (2006) 1869–1874.

- [47] A. G. Webb: Nuclear magnetic resonance coupled microseparations, *Magnetic Resonance in Chemistry* 43 (2005) 688–696.
- [48] O. Steinhof, E. J. Kibrik, G. Scherr, H. Hasse: Quantitative and qualitative ^1H , ^{13}C and ^{15}N NMR spectroscopic investigation of the urea-formaldehyde resin synthesis, *Magnetic Resonance in Chemistry* 52 (2014) 138–162.
- [49] M. Maiwald, H. Fischer, H. Hasse: Quantitative hochauflösende Online-NMR-Spektroskopie im Reaktions- und Prozessmonitoring, *Chemie Ingenieur Technik* 76 (2004) 965–969.
- [50] F. Dalitz, M. Maiwald, G. Guthausen: Considerations on the design of flow cells in by-pass systems for process analytical applications and its influence on the flow profile using NMR and CFD, *Chemical Engineering Science* 75 (2012) 318–326.
- [51] V. Hessel, H. Lowe, F. Schonfeld: Micromixers - a review on passive and active mixing principles, *Chemical Engineering Science* 60 (2005) 2479–2501.
- [52] H. Wensink, F. Benito-Lopez, D. C. Hermes, W. Verboom, H. J. G. E. Gardeniers, D. N. Reinhoudt, A. van den Berg: Measuring reaction kinetics in a lab-on-a-chip by microcoil NMR, *Lab on a Chip* 5 (2005) 280–284.
- [53] M. Brivio, W. Verboom, D. N. Reinhoudt: Miniaturized continuous flow reaction vessels: influence on chemical reactions, *Lab on a Chip* 6 (2006) 329–344.
- [54] W. Ferstl, T. Klahn, W. Schweikert, G. Billeb, M. Schwarzer, S. Loebbecke: In-line analysis in microreaction technology: A suitable tool for process screening and optimization, *Chemical Engineering and Technology* 30 (2007) 370–378.
- [55] W. Ehrfeld, K. Golbig, V. Hessel, H. Lowe, T. Richter: Characterization of mixing in micromixers by a test reaction: Single mixing units and mixer arrays, *Industrial and Engineering Chemistry Research* 38 (1999) 1075–1082.
- [56] J. Rehbein, B. Dietrich, M. D. Grynbaum, P. Hentschel, K. Holtin, M. Kuehnle, P. Schuler, M. Bayer, K. Albert: Characterization of bixin by LC-MS and LC-NMR, *Journal of Separation Science* 30 (2007) 2382–2390.
- [57] D. L. Olson, M. E. Lacey, J. V. Sweedler: High-resolution microcoil NMR for analysis of mass-limited, nanoliter samples, *Analytical Chemistry* 70 (1998) 645–650.
- [58] M. Macnaughtan, T. Hou, J. Xu, D. Raftery: High-throughput nuclear magnetic resonance analysis using a multiple coil flow probe, *Analytical Chemistry* 75 (2003) 5116–5123.

- [59] M. Lacey, R. Subramanian, D. Olson, A. Webb, J. Sweedler: High-resolution NMR Spectroscopy of sample volumes from 1 nL to 10 μl, *Chemical Reviews* 99 (1999) 3133–3152.
- [60] E. Rapp, A. Jakob, A. Schefer, E. Bayer, K. Albert: Splitless on-line coupling of capillary high-performance liquid chromatography, capillary electrochromatography and pressurized capillary electrochromatography with nuclear magnetic resonance spectroscopy, *Analytical and Bioanalytical Chemistry* 376 (2003) 1053–1061.
- [61] P. Keifer: Flow techniques in NMR spectroscopy, *Annual reports on NMR spectroscopy* 62 (2007) 1–47.
- [62] D. Olson, T. Peck, A. Webb, R. Magin, J. Sweedler: High-resolution microcoil 1H-NMR for mass-limited, nanoliter-volume samples, *Science* 270 (1995) 1967–1970.
- [63] L. Ciobanu, D. A. Jayawickrama, X. Z. Zhang, A. G. Webb, J. V. Sweedler: Measuring reaction kinetics by using multiple microcoil NMR spectroscopy, *Angewandte Chemie-International Edition* 42 (2003) 4669–4672.
- [64] C. Massin, F. Vincent, A. Homsy, K. Ehrmann, G. Boero, P. A. Besse, A. Daridon, E. Verpoorte, N. F. de Rooij, R. S. Popovic: Planar microcoil-based microfluidic NMR probes, *Journal of Magnetic Resonance* 164 (2003) 242–255.
- [65] R. Petkewich: Integrating micromixer and microcoils for time-resolved NMR, *Analytical Chemistry* 75 (2003) 94A–95A.
- [66] M. Kakuta, D. A. Jayawickrama, A. M. Wolters, A. Manz, J. V. Sweedler: Micromixer-based time-resolved NMR: Applications to ubiquitin protein conformation, *Analytical Chemistry* 75 (2003) 956–960.
- [67] S. Ahola, F. Casanova, J. Perlo, K. Munnemann, B. Blumich, S. Staph: Monitoring of fluid motion in a micromixer by dynamic NMR microscopy, *Lab on a Chip* 6 (2006) 90–95.
- [68] F. Schoenfeld, V. Hessel, C. Hofmann: An optimised split-and-recombine micromixer with uniform ‘chaotic’ mixing, *Lab on a Chip* 4 (2004) 65–69.
- [69] W. Boettinger, M. Maiwald, H. Hasse: Online NMR spectroscopic study of species distribution in MDEA-H₂O-CO₂ and MDEA-PIP-H₂O-CO₂, *Industrial and Engineering Chemistry Research* 47 (2008) 7917–7926.
- [70] A. Braecker, R. Behrens, E. von Harbou, H. Hasse: Application of a new micro-reactor 1H NMR probe head for quantitative analysis of fast esterification reactions, *Chemical Engineering Journal* 306 (2016) 413–421.

- [71] A. Friebel, T. Specht, E. von Harbou, K. Muennemann, H. Hasse: Prediction of flow effects in quantitative NMR measurements, *Journal of Magnetic Resonance* 312 (2020) 106683.
- [72] A. Saib, A. Bara-Estaun, O. Harper, D. Berry, I. Thomlinson, R. Broomfield-Tagg, J. Lowe, C. Lyall, U. Hintermair: Engineering aspects of FlowNMR spectroscopy setups for online analysis of solution-phase processes, *Reaction Chemistry and Engineering* 6 (2021) 1548–1573.
- [73] A. Friebel, E. von Harbou, K. Muennemann, H. Hasse: Online process monitoring of a batch distillation by medium field NMR spectroscopy, *Chemical Engineering Science* 219 (2020) 115561.
- [74] M. Grootveld, B. Percival, M. Gibson, Y. Osman, M. Edgar, M. Molinari, M. Mather, F. Casanova, P. Wilson: Progress in low-field benchtop NMR spectroscopy in chemical and biochemical analysis, *Analytica Chimica Acta* 1067 (2019) 11–30.
- [75] J. Giberson, J. Scicluna, N. Legge, J. Longstaffe: Chapter Three - Developments in benchtop NMR spectroscopy 2015–2020, *Annual reports on NMR spectroscopy* 102 (2021) 153–246.
- [76] T. Castaing-Cordier, D. Bouillaud, J. Farjon, P. Giraudeau: Chapter Four - Recent advances in benchtop NMR spectroscopy and its applications, *Annual reports on NMR spectroscopy* 103 (2021) 191–258.
- [77] M. Bornemann-Pfeiffer, K. Meyer, J. Lademann, M. Kraume, M. Maiwald: Contributions towards variable temperature shielding for compact NMR instruments, *Magnetic Resonance in Chemistry PrePrint* (2023) 1–10.
- [78] A. Dupre, K. Lei, P. Mak, R. Martins, W. Peng: Micro- and nanofabrication NMR technologies for point-of-care medical applications – A review, *Microelectronic Engineering* 209 (2019) 66–74.
- [79] R. Behrens, M. Dyga, G. Sieder, E. von Harbou, H. Hasse: NMR spectroscopic method for studying homogenous liquid phase reaction kinetics in systems used in reactive gas absorption and application to monoethanolamine–water–carbon dioxide, *Chemical Engineering Journal* 374 (2019) 1127–1137.
- [80] P. Moser, S. Schmidt, S. Wallus, T. Ginsberg, G. Sieder, I. Clausen, J. G. Palacios, T. Stoffregen, D. Mihailowitsch: Enhancement and Long-Term Testing of Optimised Post-Combustion Capture Technology - Results of the Second Phase of the Testing Programme at the Niederaussem Pilot Plant, *Energy Procedia* 37 (2013) 2377–2388.

- [81] R. Idem, T. Supap, H. Shi, D. Gelowitz, M. Ball, C. Campbell, P. Tontiwachwuthikul: Practical experience in post-combustion CO₂ capture using reactive solvents in large pilot and demonstration plants, *International Journal of Greenhouse Gas Control* 40 (2015) 6–25.
- [82] E. Adu, Y. Zhang, D. Liu, P. Tontiwachwuthikul: Parametric process design and economic analysis of post-combustion CO₂ capture and compression for coal- and natural gas-fired power plants, *Energies* 13 (2020) 2519.
- [83] D. Vasiliu, E. Kessler, E. von Harbou, H. Hasse: Short-cut method for assessing solvents for gas cleaning by reactive absorption, *Chemical Engineering Research and Design* 153 (2020) 757–767.
- [84] E. Kessler, L. Ninni, D. Vasiliu, A. Yazdani, B. Willy, R. Schneider, M. Irfan, J. Rolker, E. von Harbou, H. Hasse: Triacetoneamine-derivates (EvAs) for CO₂-absorption from process gases, *International Journal of Greenhouse Gas Control* 95 (2020) 102932.
- [85] P. H. Feron, A. Cousins, K. Jiang, R. Zhai, M. Garcia: An update of the benchmark post-combustion CO₂-capture technology, *Fuel* 273 (2020) 117776.
- [86] B. Aghel, S. Janati, S. Wongwises, M. S. Shadloo: Review on CO₂ capture by blended amine solutions, *International Journal of Greenhouse Gas Control* 119 (2022) 103715.
- [87] B. P. Spigarelli, S. K. Kawatra: Opportunities and challenges in carbon dioxide capture, *Journal of CO₂ Utilization* 1 (2013) 69–87.
- [88] L. Dubois, D. Thomas: Comparison of various configurations of the absorption-regeneration process using different solvents for the post-combustion CO₂ capture applied to cement plant flue gases, *International Journal of Greenhouse Gas Control* 69 (2018) 20–35.
- [89] C. Chao, Y. Deng, R. Dewil, J. Baeyens, X. Fan: Post-combustion carbon capture, *Renewable and Sustainable Energy Reviews* 138 (2021) 110490.
- [90] D. Leeson, N. Mac Dowell, N. Shah, C. Petit, P. Fennell: A techno-economic analysis and systematic review of carbon capture and storage (CCS) applied to the iron and steel, cement, oil refining and pulp and paper industries, as well as other high purity sources, *International Journal of Greenhouse Gas Control* 61 (2017) 71–84.
- [91] M. Bui, C. S. Adjiman, A. Bardow, E. J. Anthony, A. Boston, S. Brown, P. S. Fennell, S. Fuss, A. Galindo, L. A. Hackett, J. P. Hallett, H. J. Herzog, G. Jackson,

- J. Kemper, S. Krevor, G. C. Maitland, M. Matuszewski, I. S. Metcalfe, C. Petit, G. Puxty, J. Reimer, D. M. Reiner, E. S. Rubin, S. A. Scott, N. Shah, B. Smit, J. P. M. Trusler, P. Webley, J. Wilcox, N. Mac Dowell: Carbon capture and storage (CCS): the way forward, *Energy and Environmental Science* 11 (2018) 1062–1176.
- [92] S. O. Gardarsdottir, E. De Lena, M. Romano, S. Roussanaly, M. Voldsdund, J.-F. Pérez-Calvo, D. Berstad, C. Fu, R. Anantharaman, D. Sutter, M. Gazzani, M. Mazzotti, G. Cinti: Comparison of Technologies for CO₂ Capture from Cement Production—Part 2: Cost Analysis, *Energies* 12 (2019).
- [93] A. I. Osman, M. Hefny, M. I. A. A. Maksoud, A. M. Elgarahy, D. W. Rooney: Recent advances in carbon capture storage and utilisation technologies: a review, *Environmental Chemistry Letters* 19 (2020) 797–849.

Scientific Publications

Publication I

Pilot plant experimental studies of post combustion CO₂ capture by reactive absorption with MEA and new solvents

doi: 10.1016/j.egypro.2009.01.128

Available online at www.sciencedirect.com

Energy Procedia 1 (2009) 963–970

Energy
Procedia

www.elsevier.com/locate/procedia

GHGT-9

Pilot plant experimental studies of post combustion CO₂ capture by reactive absorption with MEA and new solvents

Hari Prasad Mangalapally^{a*}, Ralf Notz^{b,c}, Sebastian Hoch^a, Norbert Asprion^c, Georg Sieder^c, Hugo Garcia^c, Hans Hasse^a

^aLaboratory of Engineering Thermodynamics (LTD), Technische Universität Kaiserslautern, Germany

^bInstitute of Thermodynamics and Thermal Process Engineering (ITT), Universität Stuttgart, Germany

^cBASF SE, Ludwigshafen, Germany

Abstract

The main challenge for the CO₂ post combustion capture from power plant flue gases is the reduction of the energy requirement for solvent regeneration. The required reduction can only be achieved by application of new solvents. For the validation of new solvents in the absorption/desorption process, a pilot plant (column diameters 0.125 m, absorber packing height 4.2 m, flue gas flow 30–110 kg/h, CO₂ partial pressure 35–135 mbar) was built in the EU-project CASTOR. To obtain a baseline for testing of new solvents, first systematic studies were carried out with MEA in that plant. All important process parameters, i.e. CO₂ content in the flue gas, CO₂ removal rate Ψ_{CO_2} , fluid dynamic load, and solvent flow rate were varied. These studies allow detailed insight into the process, e.g., a quantification of the different contributions to the overall regeneration energy (namely: desorption enthalpy, stripping steam, heating up of solvent feed and condensate recycle) as a function of the chosen process parameters. A rate-based model of the process based on a detailed physico-chemical model was implemented in the process simulator CHEMASIM. It is shown that the model is able to predict the experimental results for MEA. Besides MEA, two new solvents were studied in the pilot plant. A direct comparison of different solvents in such pilot plant experiments is not trivial. The comparison of only a few operating points for the new solvents with seemingly corresponding results for MEA can lead to wrong conclusions, since for each solvent an optimisation of the operating conditions is necessary. Only systematical studies allow a meaningful comparison. The technique that was used in the present work for this purpose was measuring data sets at constant CO₂ removal rate (by adjustment of the regeneration energy in the desorber) and systematically varying the solvent flow rate. A minimal energy requirement for the given removal rate is found from these studies. Only the optima for different solvents should be compared. By this procedure, one solvent candidate was identified that shows an advantage compared to MEA.

© 2009 Elsevier Ltd. Open access under CC BY-NC-ND license.

Keywords: CO₂ capture; Reactive absorption; Desorption; Flue gas; Amines; Rate-based model; Simulations; New solvents

* Corresponding author. Tel.: +49-631-205-2761; fax: +49-631-205-3835.
E-mail address: hari.mangalap@mv.uni-kl.de

1. Introduction

Carbon dioxide is a greenhouse gas and substantially contributes to global warming and climate change. One of the options for reducing CO₂ emissions is the post combustion capture from power plant flue gases. Reactive absorption is the only technology that can be implemented quickly on a large scale at existing power plants for that purpose. The reference solvent for processes of this type is a 30 mass% aqueous solution of monoethanolamine (referred to simply as MEA in the following) which, however, has major drawback of high energy requirement for solvent regeneration, leading to an efficiency penalty up to 15 % points in fossil fuelled power plants. For better process economics it is essential to find more efficient solvents, tailored for post combustion capture. This was the task of the work that was carried out in the frame of the integrated European project CASTOR [1]. The paper reports on the achieved progress in this process.

Another major challenge for the carbon dioxide removal using post combustion capture is the amount of the flue gas. In typical applications flue gas flow rates are of the order of thousands of tons per hour corresponding to millions of cubic meters per hour, and hundreds of tons of carbon dioxide per hour [2]. At present there are several commercial processes available for CO₂ capture in post combustion systems. The maximum capacity of CO₂ capture of operational plants is not more than 32 tCO₂/h. So far, there is no application of full scale CO₂ capture in power plants, even though test facilities using flue gas slipstreams exist [1]. In most commercial processes an aqueous solution of MEA is used. Only Mitsubishi Heavy Industries together with Kansai Electric, employ other patented chemical solvents – sterically hindered amines called KS-1, KS-2 or KS-3. The regeneration heat of KS solvents is said to be ~ 3 GJ/t CO₂, i.e. 20 % lower than that of MEA with ~ 3.7 GJ/t CO₂ [3, 4].

To achieve progress in the development of low-cost post combustion CO₂ capture CASTOR aimed at developing and pilot plant testing of new solvents. For this purpose a gas-fired absorption/desorption pilot plant for removal of carbon dioxide from flue gases was built. It was initially operated at Universitaet Stuttgart, and has recently been transferred to TU Kaiserslautern, Germany. Before testing the new solvents, a base line with the standard solvent MEA had to be established. Therefore, systematic parameter studies were carried out with MEA. A rate-based model of the MEA process was developed, implemented in CHEMASIM and successfully tested. Finally two new solvents CASTOR1 and CASTOR2 were tested and compared to MEA.

2. Pilot plant

The basic scheme of the absorption/desorption process for CO₂ capture from flue gases and a picture of the pilot plant are shown in Figure 1. The flue gas is produced by a gas burner; SO₂ and other flue gas components can be added. The operation of this burner with two different stages as well as a CO₂ make-up from gas bottles and a CO₂ recycle from the plant allow a wide variation of the CO₂ partial pressure in the flue gas between 35 mbar and 135 mbar. The flue gas is fed into the pre-washer column by a blower. The flue gas flow rate can be set approximately between 30 kg/h and 150 kg/h. The maximum gas flow rate through the absorber is limited to approximately 110 kg/h (F-Factor $\approx 2.4 \sqrt{\text{Pa}}$) due to fluid dynamic limitations.

The pre-washer is built as a direct contact cooler to set the temperature of the flue gas at the absorber inlet and at the same time to make sure that the flue gas is saturated with water. The absorber is built of five sections, which are each equipped with four elements of the structured packing Mellapak 250.Y (Sulzer Chemtec). The total packing height is 4.2 m. To reduce solvent loss by flue gas, there is a washing section at the absorber top above the solvent inlet. The washing section is equipped with two elements of the structured packing Mellapak 250.Y. A low amount of fresh deionized water is added into the washing water recycle stream to avoid a prohibitive accumulation of amine in the washing water.

For steady state operation the liquid level in the absorber bottom is controlled by a pump. The rich solvent is pumped into the desorber through the rich lean heat exchanger. The desorber is built of three sections, which are each equipped with four elements of Mellapak 250.Y similar to the absorber. The total packing height in the desorber is 2.52 m. Both the absorber and desorber columns have a diameter of 0.125 m. The bottom of the desorber contains electrical heating elements for partial evaporation of the solvent. For aqueous amine solutions, mainly

water is evaporated. The vapor at the top of the desorber consists of water, CO₂ and some traces of amine. To retain the amine, also at the desorber top a washing section is installed. This washing section is equipped with two elements of the structured packing Mellapak 250.Y. The vapor at the desorber top is led into the condenser where most of the water is removed so that almost pure CO₂ is obtained. A part of the condensate is used in the washing section of the desorber and another part is withdrawn to fulfill the water balance of the absorption/desorption process.

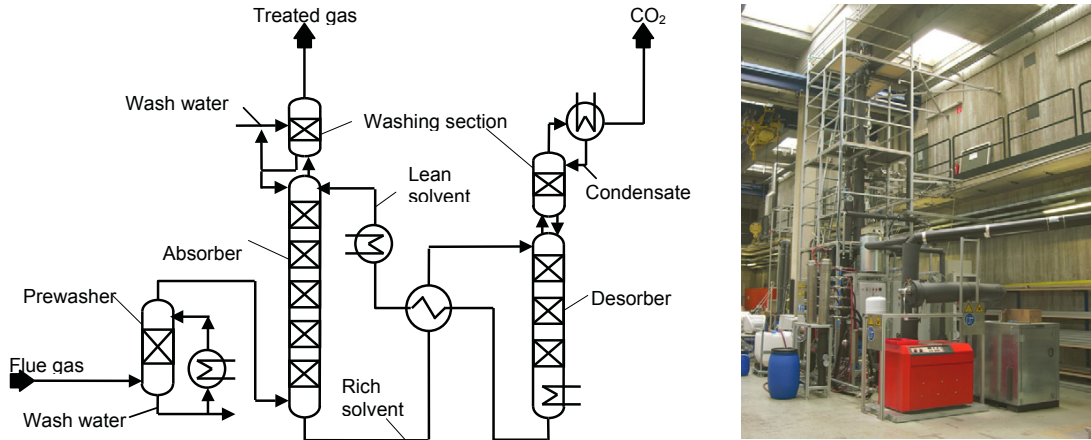


Figure 1: Basic scheme of the absorption/desorption process for post combustion carbon dioxide capture and picture of the pilot plant for CO₂ capture from flue gases by reactive absorption.

3. Pilot plant experiments with MEA

Parameter study

In this paper only some results of parameter studies carried out with MEA are reported. The full data set will be given in reference [5].

Table 1: Overview of process parameter studies that are discussed in the present work.

Varied parameter	Range of variation	Constant parameters
CO ₂ partial pressure	$p_{CO_2} = 35 - 135$ mbar	$\dot{Q}_{Evaporator}$, $\dot{m}_{Solvent}$, $\dot{m}_{Fluegas}$
CO ₂ removal rate	$\Psi_{CO_2} = 40 - 88$ %	p_{CO_2} , $\dot{m}_{Solvent}$, $\dot{m}_{Fluegas}$
Flue gas flow rate	$\dot{m}_{Fluegas} = 55 - 100$ kg/h	Ψ_{CO_2} , $\frac{\dot{m}_{Solvent}}{\dot{m}_{Fluegas}}$, p_{CO_2}
Solvent flow rate	$\dot{m}_{Solvent} = 100 - 350$ kg/h	Ψ_{CO_2} , p_{CO_2} , $\dot{m}_{Fluegas}$

3.1. Variation of CO₂ partial pressure

In order to study the influence of the CO₂ content on the process behavior, the CO₂ partial pressure in the flue gas was varied between 35 mbar and 135 mbar while maintaining the other parameters like solvent flow rate and evaporator energy constant, see Table 1. Figure 2a shows that with increasing CO₂ partial pressure the amount of

captured CO₂ increases asymptotically and finally reaches a constant value. Figure 2a also contains data on the total CO₂ flow in the flue gas, comparing both lines in Figure 2a therefore gives information on the capture rate. The increase of the captured CO₂ amount with increasing partial pressure of CO₂ is expected as the driving force for the mass transfer increase. However the amount cannot be increased above the saturation of the solvent, which explains the asymptotic behavior. Approaching the saturation limit leads to a decrease in the capture rate. This behavior can also be seen in Figure 2b. With the increase of driving force the loading difference between rich and lean solvent first increases and finally remains constant after reaching equilibrium.

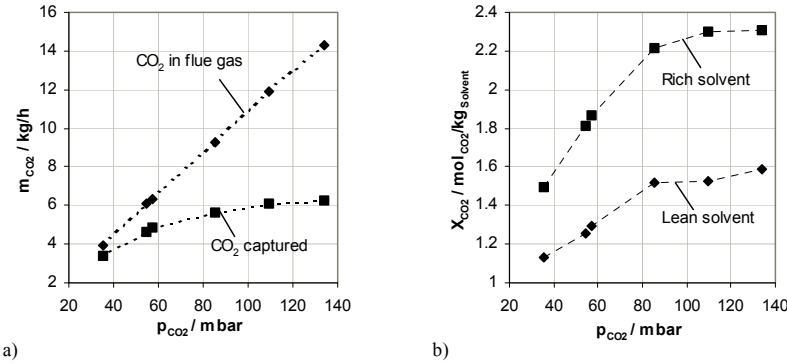


Figure 2: Influence of partial pressure of CO₂ on: a) CO₂ mass flow (total amount in the flue gas compared to captured amount), and b) CO₂ loading in rich and lean solvents. All other process parameters are kept constant see Table 1.

3.2. Variation of CO₂ removal rate

The CO₂ removal rate was varied by varying the evaporator energy while maintaining other parameters like the solvent flow rate and CO₂ partial pressure in the flue gas constant, see Table 1. Figure 3a shows that with an increase of the CO₂ removal rate, the regeneration energy requirement also increases. But after reaching a certain CO₂ removal rate there is a drastic increase in the regeneration energy requirement. This behavior can be explained by Figure 3b. With increasing CO₂ removal rate the loading difference between rich and lean solvent increases and for high removal rates the lean loading shifts to very low values such that CO₂ separation in the desorber for a particular packing height becomes difficult resulting in a very high regeneration energy requirement.

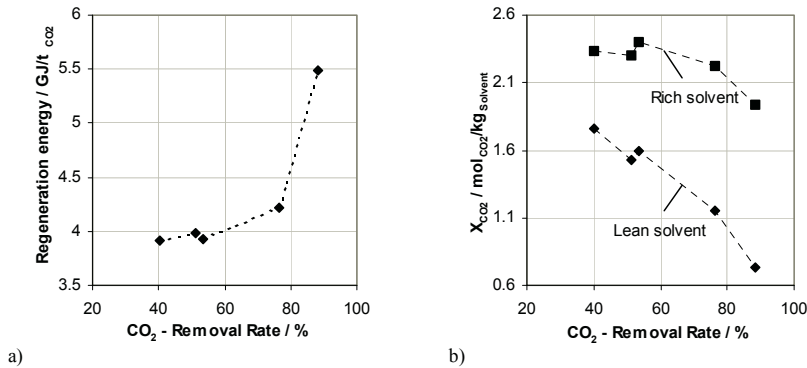


Figure 3: Influence of CO₂ removal rate on a) regeneration energy, and b) CO₂ loading in rich and lean solvents. All other process parameters are kept constant see Table 1.

For a given design of the absorption / desorption plant, a given solvent flow and for a given flue gas specification, there is a certain CO₂ removal rate that best fits the given plant design. In the case of the present pilot plant for MEA and p_{CO₂} = 110 mbar that removal rate is 54 %. Higher removal rates would require higher columns or more effective internals.

3.3. Variation of flue gas flow rate

To study the influence of the fluid dynamic load of the absorber on the regeneration energy, the flue gas flow rate (F-Factor) was varied while maintaining a constant removal rate and a constant liquid to gas ratio. If the process was equilibrium controlled, that variation should not have any influence on the regeneration energy. Figure 4a, however, shows that with the decrease of the flue gas flow rate also the regeneration energy demand decreases. At lower gas flow rates; the mass of CO₂ transferred between the phase's decreases, while the surface area remains almost constant. For kinetically controlled processes, this is favorable. Figure 4b gives more details. As the F-Factor decreases, the rich loading increases, and since the CO₂ removal rate and liquid to gas ratio are kept constant, also the lean loading increases. With the increase of the lean loading, the CO₂ separation in the desorber becomes easier, resulting in a decrease of the regeneration energy.

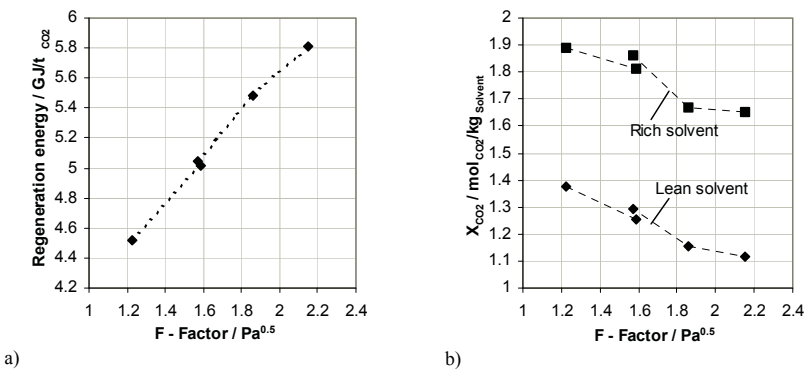


Figure 4: Influence of the gas-side fluid dynamic load of the absorber (F-factor) on a) regeneration energy, and b) CO₂ loading in rich and lean solvents. All other process parameters are kept constant see Table 1.

3.4. Variation of solvent flow rate

The solvent flow rate was varied maintaining a constant removal rate by adjusting the regeneration energy. Figure 5a shows the variation of the regeneration energy with the variation of the solvent flow rate for a constant removal rate and flue gas flow rate. For the shown operating conditions the optimum solvent flow rate at minimum regeneration energy was 200 kg/h. As shown in Figure 5b the increase in the regeneration energy to the left of the optimum solvent flow is related to the high amount of stripping steam needed to obtain the required low lean loading. The increase in the regeneration energy to the right of the optimum solvent flow can be explained by the energy requirement to heat up the higher solvent flows.

Figure 5b also shows that there are four major contributions to the regeneration energy, namely: desorption enthalpy, stripping steam, heating up of the solvent feed and the condensate reflux. The specific desorption enthalpy mainly depends on the temperature if the CO₂ loading is less than 0.5 mol_{CO₂}/mol_{MEA} [7] and thus is almost constant for the experimental conditions in this parameter study. In addition the reflux water flow at the top of the desorber is small, so that the optimum solvent flow rate depends mainly on the energy requirement for stripping steam and for heating up of the solvent. The four contributions to the regeneration energy shown in Figure 5b are mainly influenced by the heat of absorption and equilibrium data for the solubility of CO₂. For solvent selection these

physical properties have to be taken into account. Because of a coupling of the four energy parts and the mentioned properties, the solvent comparison has to be carried out carefully.

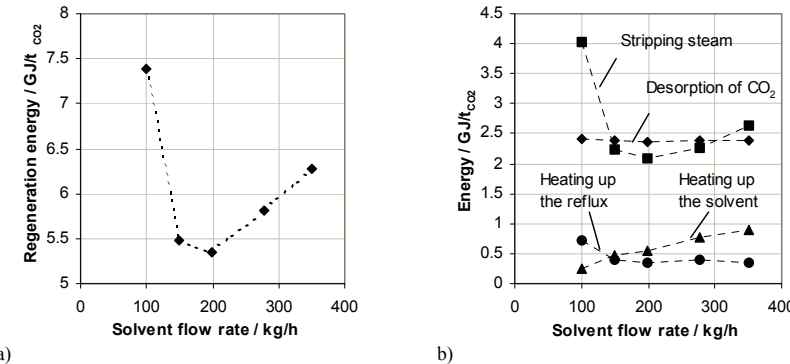


Figure 5: Influence of the solvent flow rate on a) regeneration energy, and b) four different contributions to the regeneration energy. All other process parameters are kept constant see Table 1.

4. Model

The experimental results were compared to simulations that are based on a rigorous rate-based model, which was developed by BASF [6] and was implemented in the process simulator CHEMASIM. In this model the column is divided vertically into segments and in each of these nonequilibrium segments, the gas and liquid are exchanging heat and mass. The two-film model is used to describe this process and it is assumed that the bulk phases are ideally mixed with uniform concentrations and temperatures. The mass-transfer resistance is assumed to lie in two film layers that are separated by the gas/liquid interface. At the interface, the vapor and the liquid are in equilibrium. The films are further divided into film segments. With this film discretization, it is possible to calculate more reliable concentration profiles in the film, which is essential for reactive systems, where as a consequence of the reaction the mass transfer can be enhanced. The simulation model allows the calculation of chemical reactions in the bulk phases, and also within the film. The diffusion of the different components in the film layers is described by the Stefan-Maxwell equations. The simulation results are discussed in the section 5.2.

5. New solvents

The research for new solvents for CO_2 capture in CASTOR was focused on amine solvents. Both pure amine and amine blends were studied. The present report covers two such blends, CASTOR1 and CASTOR2, which are compared to MEA as a reference. For solvent selection several criteria like equilibrium data for the CO_2 solubility, overall mass transfer kinetics, solvent degradation and corrosion behavior were analyzed. Among these criteria the equilibrium data are most important for determination of the regeneration energy of the process.

5.1. Methodology for solvent comparison in the pilot plant

For solvent comparison in the pilot plant, a consistent methodology has to be defined and applied to all solvents, here to MEA, CASTOR1 and CASTOR2. In the present work for that purpose experiments were carried out at constant CO_2 removal rate Ψ_{CO_2} but with varying solvent flow rates. This was achieved by adjusting the regeneration energy. The results of each of these sets of experiments are analyzed in plots of the regeneration energy versus the solvent flow rate, like the one shown in Figure 5a. This allows finding an optimum solvent flow rate. The optima for the different solvents are then compared. They basically only depend on the specified removal rate that has to be chosen suitably considering the design of the given pilot plant.

5.2. Comparison of new solvents with MEA

For CO₂ capture from power plant flue gas, the target is a CO₂ removal rate of 90 %. Although the total height of the pilot plant is approx. 8 m, especially the packing height of the absorber (4.2 m) is not sufficient to reach 90 % CO₂ removal with a reasonable energy. As consequence, experiments were carried out with a lower removal rate of ~54 % as already discussed above. Figure 6 shows the comparison of the regeneration energy for MEA, CASTOR1 and CASTOR2 solvents with the variation of the solvent flow rate. MEA experiments show a decrease of the regeneration energy with decreasing solvent flow rates down to the lowest flow rate of 150 kg/h. This was also confirmed by simulations with MEA that show a similar decrease of the regeneration energy with decreasing solvent flow rates down to 150 kg/h, but an increase of the regeneration energy at a lower solvent flow rates and an optimum at about 150 kg/h. The model predictions for MEA are reasonable, even though the model slightly overestimates the regeneration energy requirement especially at low solvent flow rates. One of the reasons for these deviations could be the inaccuracy of the mass transfer correlations.

At a first glance on Figure 6 CASTOR1 and CASTOR2 do not seem to have advantages compared to MEA. A detailed analysis, however, shows that the apparently unfavorable results for CASTOR1 and CASTOR2 are mainly due to kinetical effects. This can be seen from Figure 7, which shows absorber operating lines for CASTOR1, CASTOR2 and MEA compared to their equilibrium curves at 40°C (absorber conditions). The distance between the operating line and the equilibrium curve gives an indication of the driving force for the mass transfer. For CASTOR1 and CASTOR2 very high driving forces are needed, due to the slow reaction kinetics, which are also confirmed by independent kinetic studies carried out by other partners in the CASTOR project. Furthermore, experiments like those shown in Figure 4 (for the case of MEA) were also carried out for CASTOR1 and CASTOR2. They confirm the very strong influence of kinetics on the results for these solvents. For MEA, only low driving force was needed due to the fast reaction kinetics. If higher columns or more effective packings were used, it can be expected that the energy requirement would be considerably lower for CASTOR1 and CASTOR2 but not for MEA. Experiments on this are under the way. Figure 7 also contains equilibrium curves at 120°C (desorber conditions). The comparison of the equilibrium curves at 40°C and 120°C shows that very high cyclic capacities can be expected for CASTOR2. This should result in a minimum energy requirement at lower solvent flow rates that could not be reached in the present study due to limitations of the pumps (see Figure 6), so that further improvements can be expected also from this side.

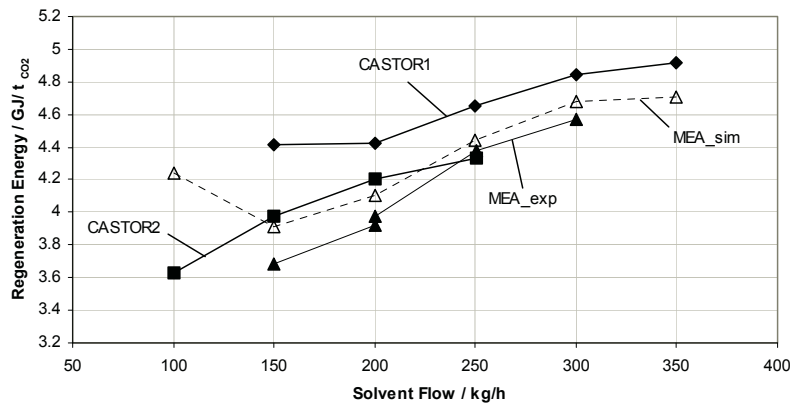


Figure 6: Regeneration energy comparison for MEA, CASTOR1 and CASTOR2 for a constant removal rate of 54 %.

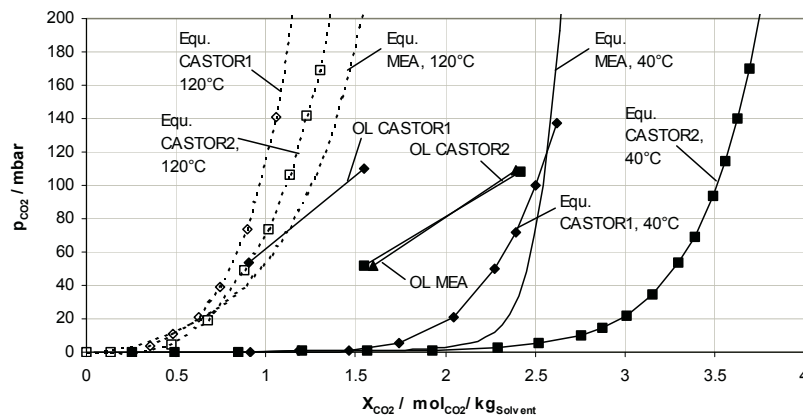


Figure 7: Comparison of absorber operating lines (OL) for MEA, CASTOR1 and CASTOR2 for a solvent flow rate of 150 kg/h and for a constant removal rate of 54 %.

6. Conclusions

Systematic parameter studies on CO₂ capture from flue gases were carried out with the standard solvent MEA in a pilot plant, to obtain a baseline for the new solvents. A rate based simulation model, which is implemented in the process simulator CHEMASIM, was able to predict the experimental results for MEA. A new methodology for comparison of new solvents with MEA has been developed and using this new methodology, two new solvents were tested in the pilot plant. Results from the pilot plant show that for lower solvent flows CASTOR2 show an advantage and for higher heights of the absorber column, CASTOR1 and CASTOR2 should allow lower regeneration energy compared to MEA.

Acknowledgment

This work was carried out within the CASTOR Integrated Project and supported by the European Commission (Contract n° SES6-CT-2004-502586).

References

- 1 CASTOR: CO₂ from Capture to Storage. Integrated Project partially funded by the European Commission under the 6th Framework Program (Contract n° SES6-CT-2004-502586). <https://www.co2castor.com>
- 2 R. Notz, N. Asprion, I. Clausen, H. Hasse: Selection and Pilot Plant Tests of New Absorbents for Post Combustion Carbon Dioxide Capture, Chemical Engineering Research and Design 85 (2007) 510-515
- 3 T. Mimura, S. Shimijo, T. Suda, M. Iijima, S. Mitsuoka: Research and Development on Energy Saving Technology for Flue Gas Carbon Dioxide Recovery and Steam System in Power Plant. Energy Convers. Mgmt 36 (1995) 397–400
- 4 T. Mimura, H. Simayoshi, T. Suda, M. Iijima, S. Mitsuoka: Developments of Energy Saving Technology for Flue gas Carbon Dioxide Recovery in Power Plant by Chemical Absorption Method and Steam System. Energy Conversion and Management 38 (1997) S57-S62
- 5 R. Notz: CO₂-Abtrennung aus Kraftwerkssabgasen mittels Reaktivabsorption. PhD Thesis- Universitaet Stuttgart, Germany (2009)
- 6 N. Asprion: Nonequilibrium Rate-Based Simulation of Reactive Systems: Simulation Model, Heat Transfer, and Influence of Film Discretization, Ind. Eng. Chem. Res. 45 (2006) 2054-2069
- 7 I. Kim, H.F. Svendsen: Heat of Absorption of Carbon Dioxide (CO₂) in Monoethanolamine (MEA) and 2-(Aminoethyl)ethanolamine (AEEA) Solutions. Ind. Eng. Chem. Res. 46 (2007) 5803-5809
- 8 M.R. Abu-Zahra, L.H.J. Schneiders, J.P.M. Niederer, P.H.M. Feron, G.F. Versteeg: CO₂ capture from power plants: Part I. A parametric study of the technical performance based on monoethanolamine. International Journal of Greenhouse Gas Control 1 (2007) 37-46

Publication II

**Comparison and validation of simulation codes
against sixteen sets of data from four different pilot
plants**

doi: 10.1016/j.egypro.2009.01.164

Available online at www.sciencedirect.com

Energy Procedia 1 (2009) 1249–1256

Energy
Procedia

www.elsevier.com/locate/procedia

GHGT-9

Comparison and validation of simulation codes against sixteen sets of data from four different pilot plants

X. Luo^a, J.N. Knudsen^b, D. de Montigny^c, Sanpasertparnich T.^c, R. Idem^c, D. Gelowitz^c, R. Notz^d, S. Hoch^e, H. Hasse^e, E. Lemaire^f, P. Alix^f, F.A. Tobiesen^g, O. Juliussen^g, M. Köpcke^h, H.F. Svendsen^{a*}

^aDepartment of Chemical Engineering, NTNU, Sem Sælands vei 4, N-7491 Trondheim, Norway

^bDONG Energy Power, A.C. Meyers Vænge 9, 2450 Copenhagen SV, Denmark

^cUniversity of Regina, Regina, Saskatchewan, Canada

^dInstitute of Thermodynamics and Thermal Process Engineering, University of Stuttgart, Stuttgart, Germany

^eLaboratory of Engineering Thermodynamics, University of Kaiserslautern, Kaiserslautern, Germany

^fIFP, Lyon, France

^gSINTEF Material and Chemistry, Sem Sælands vei 2, N-7491 Trondheim, Norway

^hVattenfall Research and Development AB, 16287 Stockholm, Sweden

Abstract

Sixteen data sets from four different pilot plant studies based on 30 wt% MEA solution as solvent have been simulated in four different commercial simulators and with two in-house codes. The simulations were performed on an as equal basis as possible given the constraints of the various simulators. Basically all the simulators are capable of giving reasonable predictions on overall performance, i.e. CO₂ absorption rate. The reboiler duties are less well predicted, as well as concentration and temperature profiles. For the reboiler temperature there is very much scatter.

© 2009 Elsevier Ltd. Open access under CC BY-NC-ND license.

Keywords: Type your keywords here, separated by semicolons ;

1. Introduction

To combat the global temperature increase by capture and storage of CO₂ (CCS), optimization and improvement of the currently most viable capture option, absorption processes, will be decisive for widespread deployment of this technology. One of the most important tools for achieving this is high quality process simulators. One objective of the EU FP6 CAPRICE project is to collect operational data from four different pilot plants, validate these data,

* Corresponding author. Tel.: +47 73 59 41 00; fax: +47 73 59 40 80.

E-mail address: hallvard.svendsen@chemeng.ntnu.no.

select a large set of runs based on data quality and their spread in conditions, and finally to validate a set of both commercial and in-house simulators against these data. The data sets are all for 30 wt% MEA operation and stem from the pilot plants at Esbjerg(CASTOR), the University of Stuttgart(now at the University of Keiserslautern), the University of Regina, and SINTEF/NTNU. These pilots range in CO₂ capture capacity from about 10-1000 kgCO₂/h.

The simulators that were tested were the commercial codes: Aspen Rad Frac, Protreat, Promax, Aspen Rate Sep., and the in-house codes CHEMASIM from BASF SE and CO2SIM from SINTEF/NTNU.

2. Description of pilot plants and experimental program

The four different pilot plants are shown in figures 1 and 2.

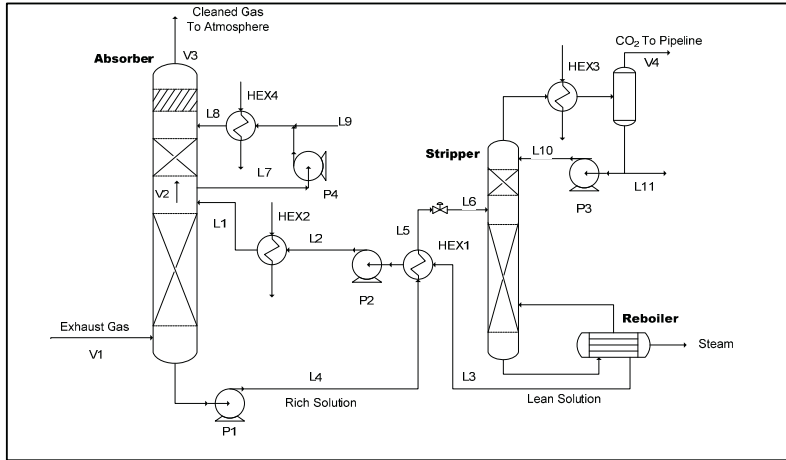


Figure 1 The Esbjerg CASTOR pilot plant, DONG Energy, the University of Kaiserslautern mini plant, and the ITC plant, University of Regina pilot

The Esbjerg CASTOR pilot plant

The flow sheet of the Esbjerg pilot plant is shown in Figure 1. The pilot plant operates on a slipstream of flue gas from the Esbjerg coal-fired power plant. The flue gas slip stream is taken downstream the wet FGD plant and does not undergo any pretreatment before supplied to the CO₂ absorption plant. The absorber consists of four consecutive packed beds with IMTP50 random packing. A water wash section is located on top of the absorber. A small stream (L9) of pure water is added to the wash section. The CO₂ concentration of the absorber inlet (V1) and outlet (V3) streams is continuously monitored by IR analyzers. The calibration of the analyzers is checked prior to each test and the analyzers are recalibrated if necessary. In addition, the flue gas flow to the absorber, the absorber temperature profile as well as the pressure drop are continuously measured. The stripper consists of two beds with IMTP50 random packing and a wash section on top. Condensate (L10) from the condenser is recycled to the wash section. The stripper pressure is controlled by an overhead regulation valve. The reboiler is driven by steam from the power plant. The flow of CO₂ from the condenser (V4) is continuously measured along with the stripper temperature and pressure at various positions. For all the tests conducted in CASTOR, the pilot plant was allowed at least three space times to reach steady state and each data point was an average of two hours steady state operation. During each test liquid samples of lean and rich MEA solution were collected at position L1 and L4, respectively. The liquid samples were analyzed for MEA and CO₂ by titration as outlined in (Ma'mun et al.[1]) and (Tobiesen et al.[2, 3]).

The ITC, University of Regina pilot plant

ITC pilot plant is operated to capture 1 tonne of CO₂ per day. Flue gas (V1) is generated by a natural gas boiler and micro turbine to supply a feed gas with CO₂ concentrations of 4% and 8% with a high oxygen concentration. A

booster fan is installed before the absorber to ensure a sufficient gas feed pressure into the absorber. The absorber is comprised of 3 sections packed with structured packing. On top of the top section is a wash water section to cool down the solution in order to minimize MEA loss. Each section is approximately 2.19 meter which includes packing support, packing material and liquid re-distribution. The packing material is Flexipac 700Y. Treated gas (V3) is released at the top of the absorber whereas the liquid solution flows downwards to the bottom of the absorber. A rich amine pump (P1) is integrated into a system to increase the liquid pressure to about 2 MPa before flowing through a rich-lean heat exchanger (HEX1) and then the desorber. The desorber is comprised of 3 sections packed with structured packing. The two bottom sections are approximately 3.22 meter while the top section is approximately 8.3 meter. The packing material is also Flexipak 700Y. At the top section of the desorber, it is integrated with a reflux process to separate the CO₂ product (V4) and the stream mainly containing water (L10) which flows back to the desorber. A reboiler is added at a bottom of the desorber to heat the liquid solution. The heat is supplied by a steam obtained from the natural gas boiler. The lean amine solution is cooled down to 40°C by a cooler (HEX2) while a makeup unit is integrated before HEX2 to compensate for any MEA loss and to control the MEA solution concentration.

The concentration of flue gas and corrosion rate are respectively monitored by gas analyzers and corrosometer probes while temperature, pressure and mass flow rate are respectively measured by temperature probes, pressure gauges and mass flow rate meters. All instruments are connected to a controller (Delta V) which also collects and records data in real time. The CO₂ loading in the amine solution is measured by a titration technique. Liquid samples for this purpose are taken while the process is at steady state.

The University of Keiserslautern mini plant

For testing the process behavior of new solvents for CO₂ capture a pilot plant was constructed at the University of Kasierslautern. The basic flow sheet is identical with the one shown in Figure 1, pictures of the plant are shown in Figure 2. The flue gas is produced by a gas burner, SO₂ and other flue gas components can be added. The flue gas flow rate can be set between approximately 70 kg h⁻¹ and 150 kg h⁻¹. The CO₂ partial pressure in the flue gas can be varied from 36 and 134 mbar by CO₂ recirculation. A solvent flow rate between about 50 kg h⁻¹ to 350 kg h⁻¹ can be established. Absorber and desorber, including the washing sections, are equipped with the structured packing Mellapak 250.Y (Sulzer Chemtec, Winterthur, Switzerland). The diameter of the columns is 125 mm. The packing height in the absorber is 4.2 m, arranged in five sections. The desorber has a packing height of 2.5 m in three sections. Despite these dimensions, which exceed those of typical laboratory set-ups, we use the term mini plant here, as compared to equipment in power plants, the size of our plant is small. (Notz et. al. [4])

The measurement and control equipment of the mini plant allows taking all data which are necessary for the process analysis. For all important gas and liquid streams the volume / mass flow, temperature, pressure and composition are detected. At the absorber and desorber column temperature and concentration profiles of the liquid and the pressure drop are measured. The CO₂ content in the dry flue gas at the absorber inlet and the absorber outlet is detected by infrared absorption, the O₂ content with by Para magnetism. The overall concentrations of CO₂, water and amine in the liquid samples are detected with different techniques. The amine content is analyzed by Gas Chromatography, the water content by Karl-Fischer titration and the CO₂ content by titration with KOH.

In different parameter studies, like the variation of the solvent flow rate, stripper pressure, flue gas flow rate and CO₂ content in flue gas, the process behavior with a 30 wt-% MEA solution was investigated. For all four selected operation points of this plant the component mass balances and the heat losses were calculated.

The SINTEF/NTNU pilot rig

At the time of performing the reported pilot campaign, the SINTEF-NTNU rig looked as depicted in Figure 3. The rig was based on recycle of the gas flow and also of CO₂ and did not have a water wash section on the absorber. Both absorber and desorber used a Mellapak 250Y packing. The recycle gas could be cooled before return to the absorber. The CO₂ from the condenser is recycled back to the gas circulation fan inlet. Sampling of the gas phase was done right after the absorber exit, (V2), and just before the inlet, (V1), as shown in the figure. The outlet gas sampling is placed at a distance from the recycle CO₂ inlet such that the analysis should not be influenced by recycle CO₂. These CO₂ analyses were online using a calibrated IR instrument. Online temperature and pressure measurements were performed at the same positions. The liquid phase in and out of the absorber were sampled at positions before the final lean amine cooling, (L1), and at the absorber outlet, (L4). It was also sampled before

entering the storage tank, (L2). For the stripper the CO₂ from the condenser passed through a mass flow meter and its flow rate recorded on-line. The desorber did also not have an upper water wash section and the condensate from the overhead condenser was piped directly back to the desorber reboiler. The liquid phase, (L6) into the stripper was taken to have the same total composition as (L4). The desorber lean outlet, (L3), was taken to have the same composition as (L2). However, both pressure and temperature were recorded independently for these two flows. The liquid flow between stripper column and reboiler was sampled. All liquid samples were analyzed for amine and CO₂ content by titration, (see Tobiesen et al.[2,3], Ma'mun et al.[1]).

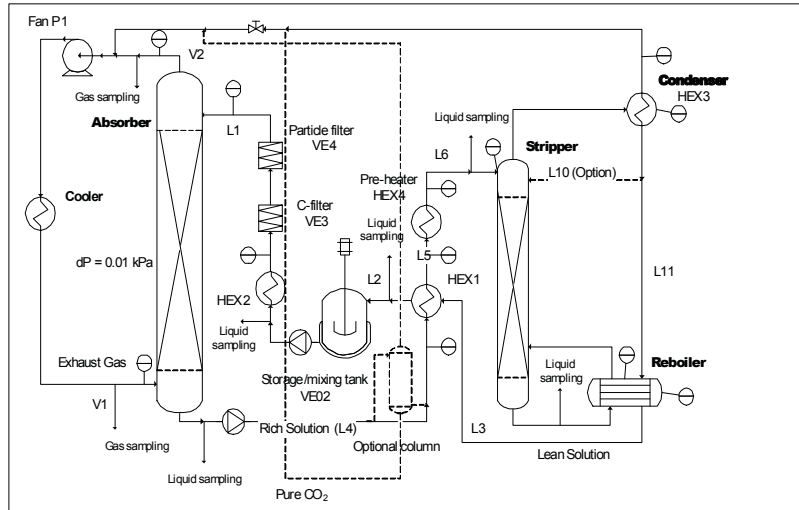


Figure 2 Pilot plant layout at SINTEF-NTNU

Table 1: Data for the 4 pilot plants

	Wash water section			Absorber			Stripper		
	Packing type	Diameter	Height	Packing type	Diameter	Height	Packing type	Diameter	Height
NTNU/SINTEF	N/A	N/A	N/A	Mellapak250Y	0.15m	4.36m	Mellapak250Y	0.1m	3.89m
DONG	Mellapak252Y	1.1m	3m	IMTP50	1.1m	17m	IMTP50	1.1m	10m
ITC, REGINA	Flexipac700Y	0.33m	2.93m	Flexipac700Y	0.33m	7.05m	Flexipac700Y	0.33m	9.97m
ITT, STUTTGART	Mellapak250Y	0,125	0.42m	Mellapak250Y	0.125m	4.2m	Mellapak250Y	0.125m	2.52m

3. Simulation software and common simulation basis

In the simulations we have tried as far as possible to adapt a common strategy. The whole flow-sheet was simulated for all cases and the basis was inlet gas and the lean amine entering the absorber, and as criterion for the desorber the lean amine outlet loading was set to the experimental one and the experimental total pressures were used.

Aspen Rad Frac: The four plant flowsheets were reproduced in Aspen Plus, v2006.5, using the equilibrium stage Radfrac modules to model absorber and stripper columns. With the focus on steady-state heat and mass balances around the columns tanks and pumps were neglected. Furthermore, disregarding the need for water and solvent make-up calculation, the lean solvent stream was teared and the balance of CO₂ and water (where positive) was externally converged by adapting the reboiler heat supply to match the lean loading entering the absorber as well as excess water removal from the stripper condensate reflux. A closed-loop simulation with water and solvent make-up stream calculation has initially been performed for one pilot experimental point (Dong, test 1) and confirmed equality of results to the faster converging teared flowsheet.

The methodology chosen to fit the absorber performance to the measured concentration and temperature profiles was to assume an abundant number of stages (25-35) and (a.) to adjust one constant stage efficiency for the CO₂ component in the entire column as well as (b.) the number of stages per packing section between the sampling

points. It was tried as an alternative to follow the recommendations given in the Aspen software documentation and keep the number of stages per packing section constant and calculate different absorption efficiencies in each section by specifying the measured gas concentrations along the column. This was not successful for convergence reasons.

The stripper was modelled with a constant number of stages and stage efficiencies of unity, including a wash section where applicable. The condenser section was modelled as an external flash block at the given pressure and temperature. The reboiler heat duty was iterated to reproduce the given absorber input lean loading. The solvent-solvent heat exchanger was adapted to the hot outlet/ cold inlet temperature approach given by the pilot stream data.

Promax: ProMax is a commercial process modeling software developed by Bryan Research & Engineering. The software has the capability to design and optimize chemical processes and refineries. It is combined with Microsoft Visio® for users who are not or little familiar with computer aided design to enable the easy implementation of schematic diagrams. It is also embedded with more than 50 thermodynamic packages (i.e. Electrolytic-ELR and NRTL) with the integration of TSWEET used to simulate the amine sweetening processes.

It needs to be recognized that a conventional CO₂ capture process uses amines (e.g. MEA, DEA, MDEA and AMP) as the chemical absorbent to capture CO₂. In addition, the CO₂ capture process requires the involvement of chemical reaction, CO₂ kinetic and solubility models. ProMax is equipped with all the necessary models. Thus, its simulation result can be used to represent an actual CO₂ capture process. Therefore, this then allows the user to validate an existing CO₂ capture process and/or simulate a new conceptual design.

The simulation has been performed under the current operating conditions of ITC's pilot plant at the University of Regina. Constraint parameters have been included to regulate the simulations. These consist of:

1. Mass and energy balance with a low tolerance in a recycle loop.
2. Removal efficiency by an equation solver put on the solvent recirculation flow rate.
3. Stripper column reflux condenser temperature of 40°C.
4. Temperature approach between rich amine solution inlet and lean amine solution outlet in HEX1 of 10°C.

CHEMASIM: A process model of the CO₂ absorption in a MEA solution is implemented into the in-house simulation environment CHEMASIM. CHEMASIM is a powerful tool for steady-state simulations of chemical processes and was developed by BASF SE. CHEMASIM contains a non-equilibrium absorber / desorber model, including the rigorous calculation of heat and mass transfer between gas and liquid phase, taking into account the complete chemical reaction system, as well.

The two-film theory is used for the description of heat and mass transfer over the gas-liquid interface. The resulting partial differential equation system is solved numerically by discretization of column height and fluid films. With a non-equidistant arrangement of discrete elements in the liquid film, an accurate calculation of heat and mass transfer under the strong influence of the fast reaction between CO₂ and amine is enabled. (Asprion [5])

An Electrolyte-NRTL model is used for calculation of the component activity coefficients in the strongly non-ideal solution. The parameters were adapted to gas-liquid equilibrium measurements. The reaction data were taken from literature and fitted to own experimental results. When possible, standard mass transfer correlations with parameters from literature for the calculation of effective interfacial area and mass / heat transfer coefficients were used. The simulations of the pilot plant experiments at the ITC, University of Regina, were carried out with a fixed interfacial area because of missing parameters for the used structured packing.

All simulations were carried out completely predictive without any fitting to experimental pilot plant data. The flue gas inlet stream, the solvent flow rate and the rich-solvent temperature at the desorber inlet were defined in simulation as measured in the experimental study. The lean-loading at the absorber were fixed in the simulation to the experimental measured value to calculate the CO₂ removal rate and the reboiler energy.

Aspen Rate Sep.: An Aspen RateSep absorber model was created by IFP to simulate absorber pilot plant data from Campaign 2 of the CASTOR project. The pilot plant campaign 2 experiments were conducted using a 5M (30 wt%) monoethanolamine (MEA) solvent[6]. The model required the adjustment of : property data, the installation of high amine concentration, high CO₂ loading kinetics, and the incorporation of hydrodynamic parameters.

The creation of the model required the modification of some property data within Aspen databanks. A heat of formation inconsistency was adjusted within the model. Heat capacity data was adjusted in the Aspen data banks to match VLE obtained heat of absorption data at temperatures other than 25C. The thermodynamic model used is

electrolyte NRTL. Also, parameters associated with density and viscosity were adjusted, especially for high MEA concentration and high loading.

Highly concentrated and highly loaded MEA rate data could match unloaded, dilute literature data when activity coefficient corrections were properly considered. This method is used to corrected the classical kinetic equation. The effect of ionic strength on the kinetics was quantified and implemented into the model.

CASTOR specific hydrodynamic and mass transfer properties were also implemented into the model. Correlations developed by IFP were used to calculate the liquid holdup, interfacial area and the liquid film mass transfer coefficient. The interfacial area correlation for the model was developed from experimental tests performed at IFP and for IMTP 50 random packing which equipped the Castor pilot plant. The liquid holdup was also correlated from experimental tests performed at IFP. The gas film mass transfer coefficient was calculated via Onda and the liquid film mass transfer coefficient was input into the model as a constant. The Aspen RateSep absorber model does not use any fitting parameters to match results to the pilot plant[7].

ProTreatTM: ProTreatTM is a commercial process rate based simulator specifically aimed at absorption processes made by Optimized Gas Treating Inc.. It uses a rate based approach to column modeling and several packing materials are included. All the packing materials used in these pilot studies could be simulated. It has two thermodynamic packages for the amine blends based on either a Kent-Eisenberg or a Lee-Mather approach. The Lee-Mather model was used for these simulations. The ProTreat model does not use any fitting parameters to match pilot plant results.

CO2SIM: CO2SIM is an in-house software package developed by NTNU and SINTEF. The simulator is restricted to absorption processes and has implemented a rate based approach. It is limited in number of packing materials and for this study the FlexiPack 700 had to be substituted with another packing with constant active interfacial area. For the IMTP 50 packing the correlations developed in CASTOR were used. As thermodynamic model a modified Deshmukh-Mather model was used for this study. The CO2SIM model does not use any fitting parameters to match pilot plant results [2,3].

4. Results

Validation of experimental data

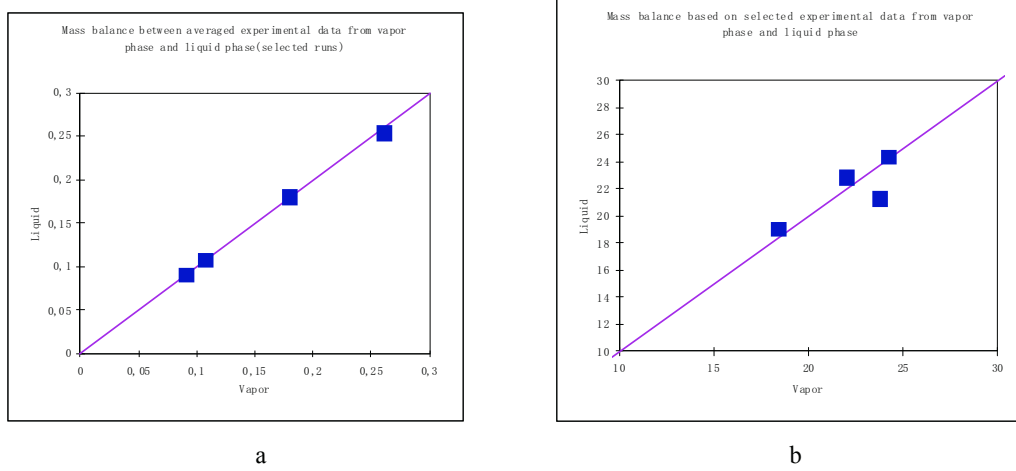


Figure 3. Examples of mass balance check on selected runs from the pilot plants, a) NTNU/SINTEF, b) DONG

The mass balance check on CO₂ was generally good in all runs, as illustrated by the results shown in Figure 3. This gave room for selection based on spread in rich and lean loading and in mass transfer rates.

Mass transfer rates

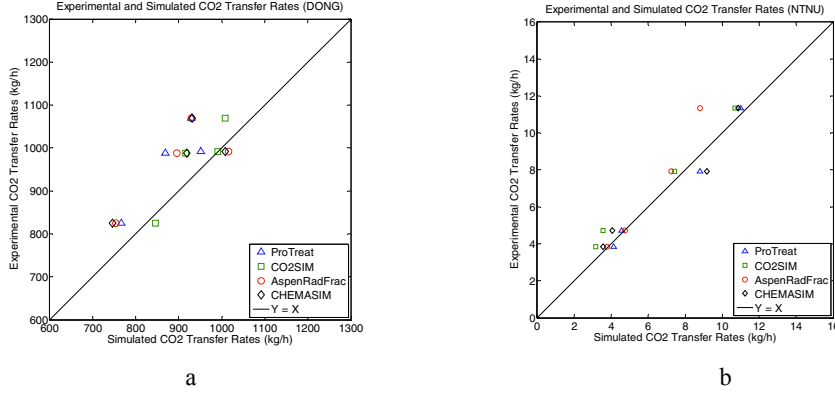


Figure 4. Experimental and simulated mass transfer rates, a) DONG, b) NTNU/SINTEF

The mass transfer rates are predicted within about 5-10% accuracy. It can be seen that there is a tendency to under-predict the transfer rate at Esbjerg(DONG) whereas for the NTNU/SINTEF plant it is evenly distributed. The deviations are about the same in the two columns so no clear effect of column size is seen. It is interesting to note that Aspen Rad Frac, in spite of being a stage based model, does predict changes in operating conditions quite well.

Reboiler heat duty

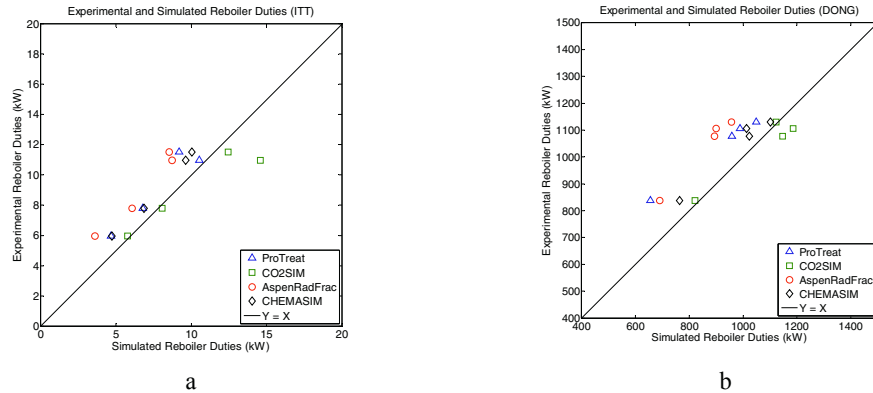


Figure 4. Examples of experimental and simulated reboiler duties, a) ITT Stuttgart, b) DONG

The basis for the simulated heat duties was the experimental lean loading. Generally more scatter is seen in the data than for mass transfer rates. This may not only be caused by less reliability in the simulations but also by higher uncertainty in the experimental data, e.g. caused by unaccounted for heat losses and uncertainties in the heat input.

Temperature profiles

Temperature profiles from the ITT Stuttgart stripper are shown in figure 5 a). This is a typical case and it can be seen that the simulators do not agree with each other and the departure from the experimental points is relatively large. The relative merits of the simulators varied from case to case and no one was better than the others. To predict temperature profiles in the desorber seem to be still very difficult. In figure 5b) profiles in the DONG absorber are used as an example. Here the agreement between the simulators is generally better and also the fit to experimental data. It should be noted that Aspen Rad Frac has been fitted to the actual experimental concentration profile in the case shown in figure 5b). This will also affect the temperature results of course. However it does show that if the mass transfer is well predicted then the temperatures follow.

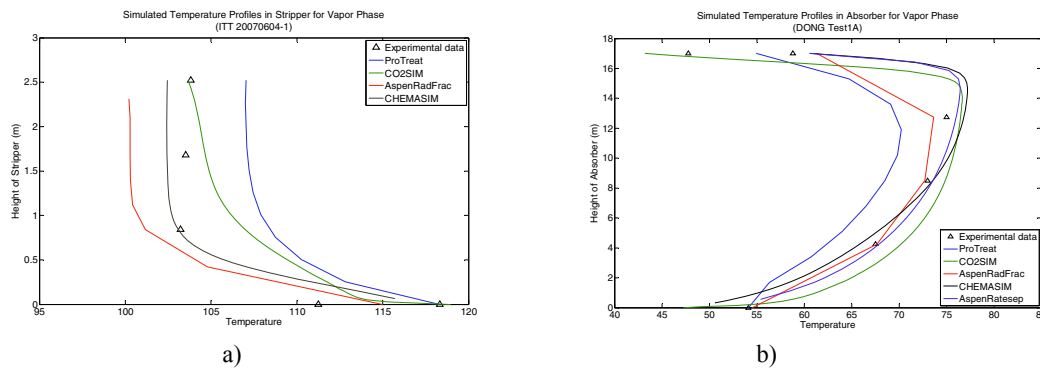


Figure 5 Temperature profiles in the stripper, ITT Stuttgart and in the absorber, DONG

Concentration profiles

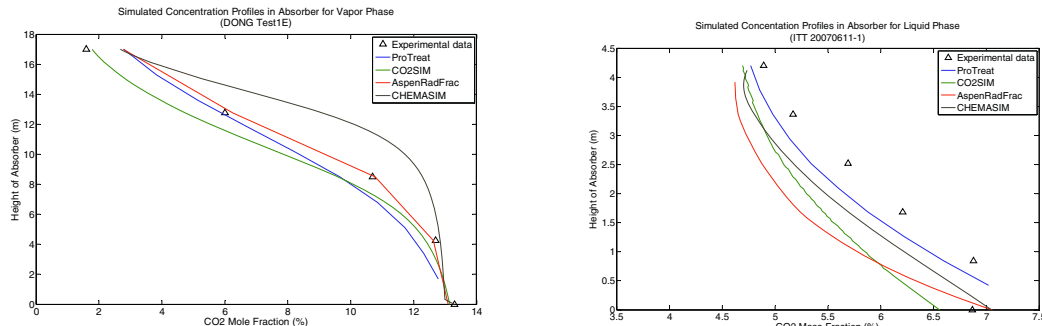


Figure 6 Gas and liquid phase concentration profiles from the DONG and ITT Stuttgart plants respectively. The absorber vapor phase profiles are in reasonable agreement with experimental data on the graph shown, but the variation from case to case was large. The liquid phase agreement is worse, and this was the trend for the liquid phase curves from ITT Stuttgart. This may reflect the added difficulty represented by the liquid phase analyses.

References

- [1] S. Ma'mun, V.Y. Dindore, and H.F. Svendsen, "Kinetics of the Reaction of Carbon Dioxide with Aqueous Solution of 2-((2-Amino(ethylamino)ethanol", Ind. Eng. Chem. Res., (2007), 46, 385-394
- [2] F.A. Tobiesen, O.Juliussen, and H.F. Svendsen, "Experimental Validation of a Rigorous Absorber Model for CO₂ Postcombustion Capture", AIChE Journal (2007), 53(4), 846-865
- [3] F.A. Tobiesen, O.Juliussen, and H.F. Svendsen, "Experimental validation of a rigorous desorber model for CO₂ post-combustion capture.", Chem Eng. Sci., 63(10), 2008, pp 2641-2656
- [4] R. Notz, N. Asprion, I. Clausen, H. Hasse: Selection and Pilot Plant Tests of New Absorbents for Post Combustion Carbon Dioxide Capture, Chem. Eng. Res. Des., 85 (2007) 510-515
- [5] N. Asprion, "Non-equilibrium rate-based simulation of reactive systems: simulation model, heat transfer, and influence of film discretization", Ind. Eng. Chem. Res., 45 (2006) 2054 - 2069
- [6] Dugas, R., P. Alix, et al. (2008). "Creation of an Aspen RateSep absorber model for the evaluation of castor pilot plant data." Preprint – American Chemical Society, Division of Petroleum Chemistry 53(1): 89-92.
- [7] Ross Dugas, Pascal Alix, Eric Lemaire, Paul Broutin, Gary Rochelle, "Absorber Model for CO₂ Capture by Monoethanolamine -Application to CASTOR Pilot Results", GHGT9, Washington Nov 2008, Oral presentation and proceeding of the congress

Publication III

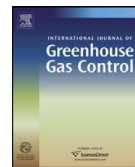
**A short-cut method for assessing absorbents for
post combustion carbon dioxide capture**

doi: 10.1016/j.ijggc.2010.03.008



Contents lists available at ScienceDirect

International Journal of Greenhouse Gas Control

journal homepage: www.elsevier.com/locate/ijggc

A short-cut method for assessing absorbents for post-combustion carbon dioxide capture

Ralf Notz^{a,1}, Inga Tönnies^b, Hari Prasad Mangalapally^b, Sebastian Hoch^b, Hans Hasse^{b,*}

^a Institute of Thermodynamics and Thermal Process Engineering, Universität Stuttgart, Pfaffenwaldring 9, 70569 Stuttgart, Germany

^b Laboratory of Engineering Thermodynamics, University of Kaiserslautern, Erwin-Schrödinger-Straße 44, 67663 Kaiserslautern, Germany

ARTICLE INFO

Article history:

Received 15 October 2009

Received in revised form 21 February 2010

Accepted 15 March 2010

Available online 15 April 2010

Keywords:

Short-cut method

CO₂ capture

Absorption

Kremser equation

New solvents

Equilibrium stage model

ABSTRACT

A short-cut method for the estimation of the minimum regeneration energy and optimum solvent flow rate in post-combustion carbon dioxide capture by absorption is presented. It is developed for comparing solvents of which only little thermo-physical data is known. The closed absorber-desorber cycle is described by an equilibrium stage model (modified Kremser equation with discretized equilibrium curves). The method can be implemented in any mathematical toolbox or as stand-alone solution. The only required input is the solubility data at absorber and desorber conditions, the heat of absorption and heat capacities. The calorific data may be estimated. The method was applied to monoethanolamine (MEA) and two solvents from the EU-project CASTOR. Comparisons with experimental results from pilot-plant studies with MEA show that the method, despite its simplicity, gives reasonable results. The method should also be useful in other applications where absorbents, of which only little data is available, need to be screened.

© 2010 Elsevier Ltd. All rights reserved.

1. Introduction

In order to mitigate climate change, methods to separate the greenhouse gas CO₂ from power plant flue gases and the subsequent geological storage are currently investigated. This concept is called carbon dioxide capture and storage (CCS). One promising technology for the capture of CO₂ from flue gases is the reactive absorption with aqueous amine solutions. The standard solvent that has been used in CO₂ absorption within the chemical industry is a 30 wt% solution of monoethanolamine (MEA).

In Fig. 1, a flowsheet of the typical absorption–desorption process for post-combustion CO₂ capture with aqueous amine solutions is shown. The flue gas enters the absorber with a temperature of approximately 40–60 °C. The regenerated solvent, also called lean solvent, is fed to the absorber top, typically at a temperature of 40 °C. Upon the CO₂ absorption into the liquid phase, absorption enthalpy is released, which leads to a temperature increase. The rich solvent at the absorber bottom is regenerated in the desorber at elevated temperature and pressure. For heat integration, the rich solvent passes through the rich-lean heat exchanger before entering the desorber column. Typically, the heat exchanger is designed such that a temperature difference of 10 K or less is achieved on

the hot side. The preheated rich solvent then enters the desorber where CO₂ is released from the solvent through a raise in temperature, leading to a shift of the equilibrium isotherm to lower loadings. At the bottom of the desorber, an evaporator generates steam, mainly consisting of water as amines have comparably low vapor pressures. This stripping steam is needed for the regeneration of the solvent. First of all, it reduces the partial pressure of CO₂ in the desorber and thus enhances the desorption. Through condensation, it provides the desorption enthalpy as well as the energy for heating the rich solvent and the reflux up to desorber temperature. A temperature of 120 °C is typically found in the desorber bottom, corresponding to a pressure of 2 bar. The steam at the top of the desorber column is passed through a condenser where water is separated from the CO₂ which is then compressed and sent for storage.

For the standard solvent MEA, the regeneration has a high energy demand which leads to a reduction of the power plant thermal efficiency of up to 10–15% points (Göttlicher, 2003). Thus, new solvent systems are being investigated at present that allow a less energy intensive regeneration. For MEA, a large amount of physical property data is available that allows an accurate prediction of the energy requirement with detailed models of the process. For new solvents, this database is not yet available. Therefore, in the screening process the prediction of the energy requirement has to be based on few simple measurements, e.g. absorption isotherms and calorimetric data. The ranking of new solvents in the literature has been based mainly on the cyclic capacity, that is the difference

* Corresponding author. Tel.: +49 631 205 3497; fax: +49 631 205 3835.

E-mail address: hans.hasse@mv.uni-kl.de (H. Hasse).

¹ Presently with BASF SE, Ludwigshafen, Germany.

Nomenclature

A	absorption factor
a	slope of the equilibrium isotherm
b	ordinate intercept of the equilibrium isotherm
c_p	isobaric heat capacity
D	desorption factor
Δh	enthalpy change
L/G	ratio of CO ₂ -free solvent mass flow to gas mass flow
M_i	molar mass of component i
\dot{m}	mass flow
\dot{n}	mole flow
N	total number of equilibrium stages
p	pressure
p_{CO_2}	CO ₂ partial pressure
T	temperature
X_{CO_2}	CO ₂ loading [mol CO ₂ /kg unloaded solvent]
x_i	mole fraction of component i

Greek letters

Ψ	CO ₂ removal rate
--------	------------------------------

Superscripts

Abs	absorber
Cond	condensate stream
Des	desorber
EQ	equilibrium
G	flue gas
in	inlet stream
L	liquid
lean	regenerated (lean) solvent
mix	mixture
out	outlet stream
reb	reboiler
rich	loaded (rich) solvent
S1, S2, S3	equilibrium segment 1, 2, 3
S*	unloaded solvent (H ₂ O and amines)
V	gas flow in desorber

Subscripts

abs	absorption
k	segment number of discretized absorption isotherm
n	current equilibrium stage counted from bottom to top
V	vaporization

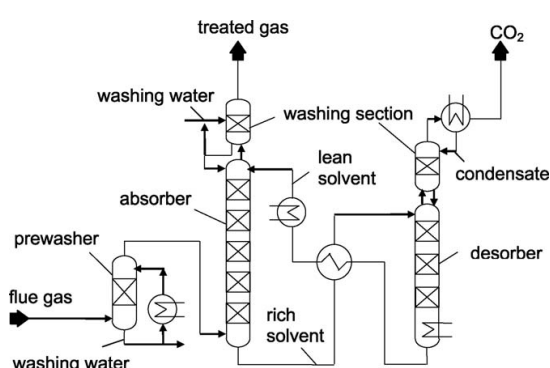


Fig. 1. Basic scheme of the absorption–desorption process for post-combustion CO₂ capture.

between the absorption isotherms at e.g. 40 °C and 120 °C at fixed partial pressures of CO₂ (Ma'mun et al., 2007; Tontiwachwuthikul, 1996). Using this method, however, the partial pressure of CO₂ in the desorber bottom is set and not calculated from the process conditions of the coupled absorber–desorber cycle. Because of that, the important influence of the solvent flow rate on the regeneration energy is not taken into account. Furthermore, when comparing new solvents solely on the basis of the cyclic capacity, only that part of the regeneration energy resulting from heating of the solvent can be directly compared. Thus, the dependence of the regeneration energy on the solvent flow rate cannot be described by existing screening methods. In the following, a short-cut method is presented which allows the estimation of the minimum regeneration energy at an optimum solvent flow rate only based on equilibrium data and calorimetric data.

The energy requirement consists of four parts:

1. desorption enthalpy
2. stripping steam
3. heating of the solvent
4. heating of the condensate reflux.

To estimate the energy requirement for new solvents, the desorption enthalpy can be obtained either from calorimetric measurements or from the temperature dependence of gas solubility data (Sherwood and Prausnitz, 1962). The energy required for heating up the solvent can be calculated when the heat capacities are known. To calculate the energy required for the stripping steam and the heating of the condensate reflux, the vapor flow in the desorber must be known. It depends on the equilibrium lines both at absorber and desorber temperature. In this work, the vapor flow is obtained through the short-cut method presented below. The method is based on the equilibrium stage concept. The short-cut assumption is on the one hand the use of a simplified model for the determination of the operating lines in the coupled absorption–desorption process and on the other hand a decoupling of the equations describing phase equilibrium and enthalpies. In this it differs from the standard equilibrium stage simulations in process simulators. The advantage of the present method is that only a minimum input is needed which can easily be specified, more specifically absorption isotherms at absorber and desorber temperature, heat capacity and absorption enthalpy. In more detailed equilibrium stage models, fluid property models need to be supplied that describe the temperature dependence of the phase equilibrium and caloric properties. It should be emphasized that the short-cut method which is presented here is not aimed at replacing a detailed process simulation. It should rather provide a tool for a simple but meaningful solvent screening with regard to the regeneration energy requirement.

2. Short-cut method

As the minimum energy requirement is obtained when equilibrium is reached in the absorber and desorber, an equilibrium stage model with a high number of stages is sufficient for a comparison between different solvents. In thermal process engineering, the Kremser equation is well known as a short-cut method establishing a relation between an operating line, an equilibrium line and the number of stages in an equilibrium stage model (Goedecke, 2006). In the method presented here, the gas flow rate \dot{n}^G and the CO₂-free solvent flow rate \dot{m}^{S*} are assumed to be constant over the whole column. Notz (2010) has shown by a comparison to experimental results that this assumption holds on the level of detail needed for a short-cut method. In order to apply the Kremser equation, also the

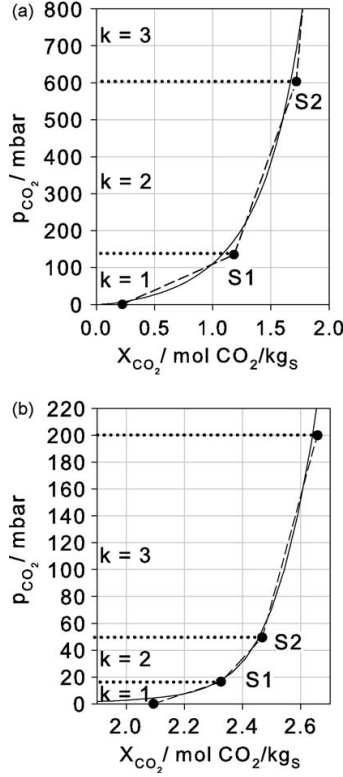


Fig. 2. Approximation of equilibrium isotherms with three linear segments for an aqueous solution of 30 wt% MEA: (a) $T = 120^\circ\text{C}$; (b) $T = 40^\circ\text{C}$.

equilibrium curve needs to be linear. Therefore, the equilibrium isotherms are discretized here into k linear segments as shown in Fig. 2 for the case of MEA (with $k = 3$). Based on the well-known Kremser equation, a modified Kremser equation was derived in the coordinates p_{CO_2} and X_{CO_2} . Of course the index could refer to any gas, but we prefer to use CO₂ as CO₂ absorption is our focus. The derivation is given in Appendix A for the case of one linear segment of the equilibrium isotherm k that is valid over the whole absorber column. The resulting modified Kremser equation (Eq. (1)) later can be applied for each discretization segment k of the equilibrium isotherm. The absorption factor A_k is defined in Eq. (2)

$$p_{\text{CO}_2}^{\text{Abs, out}} - p_{\text{CO}_2}^{\text{Abs, in}} = \left(a_k^{\text{Abs}} X_{\text{CO}_2}^{\text{Rich}} + b_k^{\text{Abs}} - p_{\text{CO}_2}^{\text{Abs, in}} \right) \times \begin{cases} N^{\text{Abs}} & \text{for } A_k = 1 \\ \frac{1 - (1/A_k)^{N^{\text{Abs}}}}{1 - (1/A_k)} & \text{for } A_k \neq 1 \end{cases} \quad (1)$$

$$A_k = \frac{\dot{m}_{\text{S}^*}^{\text{Abs}} p_{\text{CO}_2}^{\text{Abs}}}{\dot{n}^G a_k^{\text{Abs}}} \quad (2)$$

For modeling of absorber and desorber considering the discretized equilibrium curves, a case distinction is applied such that the calculation of the operating line in each segment k uses the corresponding equilibrium line. The intersection points of adjacent equilibrium lines are easily calculated. In addition, the boundary conditions of equal values for p_{CO_2} and X_{CO_2} of the operating lines at the intersection points between equilibrium segments must be fulfilled. The model uses a case distinction to determine which of

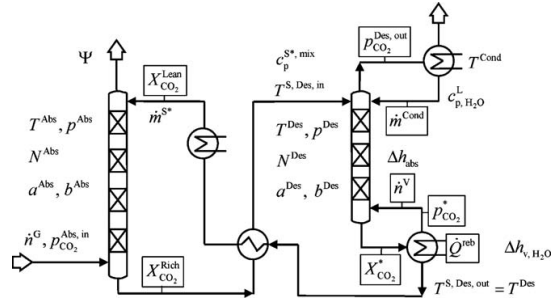


Fig. 3. Scheme of the absorption–desorption process with input data for the modified Kremser method and the resulting output data (depicted in boxes).

the equilibrium segments is valid and then the above equations are applied separately for each segment. For the calculation of Eq. (1) in all segments, an additional relation for the number of stages in each segment is required. This relation is that the summation of the number of stages in all segments must be equal to the specified number of stages in the column.

To calculate the coupled absorption–desorption process (see Fig. 3), the modified Kremser equation (Eq. (1)) is applied first for the absorber and is solved for the rich CO₂ loading $X_{\text{CO}_2}^{\text{Rich}}$, considering the three different segments. From the CO₂ mass balance of the absorber, the lean loading is calculated by Eq. (3)

$$X_{\text{CO}_2}^{\text{Lean}} = X_{\text{CO}_2}^{\text{Rich}} - \frac{\dot{n}^G}{\dot{m}_{\text{S}^*}^{\text{Abs}}} \left(p_{\text{CO}_2}^{\text{Abs, in}} - p_{\text{CO}_2}^{\text{Abs, out}} \right) \quad (3)$$

Before the modified Kremser equation is applied for the desorber, the evaporator at the desorber bottom is considered. The CO₂ partial pressure $p_{\text{CO}_2}^*$ at the gaseous outlet of the evaporator as well as the CO₂ loading $X_{\text{CO}_2}^*$ in the liquid flow from the desorber bottom to the evaporator (see Fig. 3) have to be determined. With the reasonable assumption of equilibrium in the reboiler of the desorber, the CO₂ partial pressure $p_{\text{CO}_2}^*$ can be calculated from the parameters of the equilibrium isotherm of the valid segment k (Eq. (4))

$$p_{\text{CO}_2}^* = a_k^{\text{Des}} X_{\text{CO}_2}^{\text{Lean}} + b_k^{\text{Des}} \quad (4)$$

Based on the assumption of constant vapor flow \dot{n}^V and constant solvent flow \dot{m}_{S^*} in the whole desorber including the evaporator, the CO₂ mass balance over the evaporator yields Eq. (5) containing the two unknowns $X_{\text{CO}_2}^*$ and \dot{n}^V

$$X_{\text{CO}_2}^* = X_{\text{CO}_2}^{\text{Lean}} + \frac{\dot{n}^V}{\dot{m}_{\text{S}^*}^{\text{Des}}} p_{\text{CO}_2}^* \quad (5)$$

Then, the modified Kremser equation is applied for the desorber (Eq. (6)) where the absorption factor A_k is exchanged with the desorption factor D_k (Eq. (7)). The three different segments for the discretization of the equilibrium curve again are considered via case distinctions. With the input of $X_{\text{CO}_2}^{\text{Lean}}$ and $X_{\text{CO}_2}^{\text{Rich}}$ from the absorber calculation, the CO₂ loading $X_{\text{CO}_2}^*$ and the vapor flow \dot{n}^V are determined by simultaneously solving the material balance around the reboiler (Eq. (5)) and the modified Kremser equation applied to the desorber (Eq. (6)). By application of the CO₂ mass balance over the whole desorber, the CO₂ partial pressure at the outlet of the desorber $p_{\text{CO}_2}^{\text{Des, out}}$ is calculated.

$$D_k a_k^{\text{Des}} (X_{\text{CO}_2}^{\text{Rich}} - X_{\text{CO}_2}^*) = (a_k^{\text{Des}} X_{\text{CO}_2}^* + b_k^{\text{Des}} - p_{\text{CO}_2}^*) \times \begin{cases} N^{\text{Des}} & \text{for } D_k = 1 \\ \frac{1 - (1/D_k)^{N^{\text{Des}}}}{1 - (1/D_k)} & \text{for } D_k \neq 1 \end{cases} \quad (6)$$

$$D_k = \frac{\dot{m}^{S*} p^{\text{Des}}}{\dot{n}^V a_k^{\text{Des}}} \quad (7)$$

A scheme of the simulation with input and output variables (depicted by boxes) is shown in Fig. 3.

Design input variables include the total number of equilibrium stages in the absorber and desorber (N^{Abs} , N^{Des}), the conditions of the flue gas at the absorber inlet ($p_{\text{CO}_2}^{\text{Abs}, \text{in}}$), the desired CO_2 removal rate Ψ and the temperature and pressure in the absorber and desorber. Main input data for differentiation of solvents are the equilibrium isotherms for typical absorber and desorber conditions. For the case of CO_2 absorption by aqueous amine solutions, the equilibrium isotherms at typical temperatures of 40 °C and 120 °C are used for the calculation. In principle, it is also possible to approximate the absorber temperature bulge by using an absorption isotherm at higher temperature in the middle segment of the absorber. The calorific data needed for the energy balance of the desorber are determined at temperatures typical for the absorption-desorption process as shown below.

Altogether, the model requires the following physical properties as an input:

- Two equilibrium isotherms at 40 °C (absorber) and 120 °C (desorber) in the relevant partial pressure range for CO_2 (approximately 5 mbar to 150 mbar at 40 °C, approximately 20 mbar to 2000 mbar at 120 °C).
- Constant value for the heat of vaporization of water at 100 °C (approximate temperature of gas stream at desorber top).
- Constant value for the absorption enthalpy of CO_2 in the solvent system at 100 °C (approximate temperature of gas stream at desorber top). Here the value for MEA is determined as an average value between a CO_2 -loading of 0.2 to 0.5 mol CO_2 / mol MEA based on measured data (Kim and Svendsen, 2007).
- Constant value for the heat capacity of the solvent in the desorber (average over desorber inlet and outlet temperature (110–120 °C) and composition).
- Constant value for the heat capacity of water averaged over reflux and desorber outlet temperature (20–120 °C).

In the simulation, the solvent flow rate \dot{m}^{S*} is varied to obtain the minimum energy requirement. As main results of the simulation, the CO_2 loadings $X_{\text{CO}_2}^{\text{Lean}}$ and $X_{\text{CO}_2}^{\text{Rich}}$ in the lean and rich solvent and the required vapor flow \dot{n}^V are obtained. From the total vapor flow \dot{n}^V , the water vapor flow in the desorber (equal to the condensate mass flow \dot{m}^{Cond}) is calculated from Eq. (8) which refers to the gas stream at the evaporator outlet. The amount of absorbed CO_2 is obtained through Eq. (9)

$$\dot{m}^{\text{Cond}} = \left(1 - \frac{p_{\text{CO}_2}^*}{p^{\text{Des}}} \right) \dot{n}^V M_{\text{H}_2\text{O}} \quad (8)$$

$$\dot{m}_{\text{CO}_2}^{\text{abs}} = \Psi \frac{p_{\text{CO}_2}^{\text{Abs}, \text{in}}}{p^{\text{Abs}}} \dot{n}^V M_{\text{CO}_2} \quad (9)$$

The specific energy consumption \dot{q}^{reb} of the reboiler can be calculated through a summation of the four different parts relevant to the reboiler energy (Eq. (10)) and division through the amount of absorbed CO_2 (Eq. (11)). As a simplification, the sensible heat of CO_2

Table 1
Boundary conditions for the calculations.

Model parameter	Value
$\Psi/\%$	90
$T^{\text{Abs}}/\text{°C}$	40
$p^{\text{Des}}/\text{mbar}$	2000
$T^{\text{S, Des, out}} = T^{\text{Des}}/\text{°C}$	120
$T^{\text{S, Des, in}}/\text{°C}$	110
$T^{\text{Cond}}/\text{°C}$	20
\dot{m}^{S*}	Varied
N^{Abs}	10
N^{Des}	15

Table 2
Flue gas conditions for power plant reference cases: brown coal (BC) and combined cycle power plant (CC).

	BC	CC
Mass flow/t/h	3568.7	2341.8
$p_{\text{CO}_2}/\text{mbar}$	141.8	46.6

is neglected in the calculations

$$\begin{aligned} \dot{Q}^{\text{reb}} = & \dot{m}^{S*} c_p^{S*, \text{mix}} (T^{\text{S, Des, out}} - T^{\text{S, Des, in}}) \\ & + \dot{m}^{\text{Cond}} c_{\text{p, H}_2\text{O}}^{\text{L}} (T^{\text{S, Des, in}} - T^{\text{Cond}}) + \dot{m}_{\text{CO}_2}^{\text{abs}} \Delta h_{\text{abs}} \\ & + \dot{m}^{\text{Cond}} \Delta h_{\text{v, H}_2\text{O}} \end{aligned} \quad (10)$$

$$\dot{q}^{\text{reb}} = \frac{\dot{Q}^{\text{reb}}}{\dot{m}_{\text{CO}_2}^{\text{abs}}} \quad (11)$$

The non-linear system of equations was programmed into gProms ModelBuilder 3.1.3 (Process Systems Enterprise Ltd.) and solved for different amine systems and conditions of the flue gas.

3. Results and discussion

The modified Kremser equation was applied to the standard solvent MEA (30 wt%) and to two new solvents which were tested in the EU-project CASTOR (CASTOR, 2008), denoted as CASTOR1 and CASTOR2. For the simulations which aimed at comparing the solvents, the boundary conditions as shown in Table 1 were used. A temperature difference of 10 K was set in the rich-lean heat exchanger. The number of equilibrium stages in the absorber and desorber is chosen so high that it can be assumed for practical purposes that the equilibrium limit is reached. Typical conditions of the flue gas of brown coal and gas power plants (combined cycle power plants) were used in the calculations according to Table 2. In Fig. 4, the measured equilibrium isotherms for the CASTOR solvents (CASTOR, 2008) are presented together with calculated equilibrium isotherms for MEA using extended Raoult's law and extended Henry's law together with the electrolyte NRTL-Model, see e.g. Austgen et al. (1989). CASTOR2 has a much larger cyclic capacity compared to MEA. The cyclic capacity of CASTOR1 is similar to that of MEA at moderate partial pressures of CO_2 and slightly larger for partial pressures above approximately 100 mbar. The calorific data used for the calculations in Eq. (10) is shown in Table 3. Here, the value for the absorption enthalpy into a 30 wt% MEA solution is determined as an average value between a CO_2 -loading of 0.2 and 0.5 mol CO_2 /mol MEA based on measured data (Kim and Svendsen, 2007). The same values are used for MEA, CASTOR1 and CASTOR2 as measurements in the CASTOR project (CASTOR, 2008) showed that the absorption enthalpies of CASTOR1 and CASTOR2 do not differ greatly from those of MEA.

The heat capacity for a 30 wt% MEA solution was calculated from the heat capacities of the pure components MEA and water (Rowley

Table 3
Caloric data for the calculations for MEA, CASTOR1 and CASTOR2.

Caloric data	Value
$\Delta h_{v, H_2O}/\text{kJ/kg}$	2211
$\Delta h_{abs}/\text{kJ/kg}$	2291
$c_p^S, \text{mix}/\text{kJ/(kg K)}$	4.048
$c_p^L, H_2O/\text{kJ/(kg K)}$	4.197

et al., 2007) and the excess heat capacity of MEA and water (Chiu and Li, 1999) and averaged between 110 °C and 120 °C. For the heat capacity of the aqueous solution of CASTOR1 and CASTOR2, no data was available and thus the heat capacity of the aqueous solution of MEA was used as an estimate.

In the following, the interaction between operating line and discretized equilibrium isotherms is discussed for the case of MEA as a solvent and brown coal (BC) flue gas conditions as an example. In Fig. 5, the operating lines and equilibrium isotherms are shown both for the absorber and the desorber for two different L/G ratios (\dot{m}^{S*}/\dot{n}^G). The roman numbers mark the intervals in which the different equilibrium isotherm segments are valid. In the absorber, the separated CO₂ stream is fixed since the flue gas mass flow, the inlet CO₂ partial pressure and the removal rate are fixed. For a fixed solvent flow rate, the difference between lean loading and rich loading is therefore fixed. With an infinite number of equilibrium stages corresponding to a minimum energy requirement, the operating line touches the equilibrium line. In the case considered here, this behavior is already observed for 10 equilibrium stages. In Fig. 5(a), the operating line touches the equilibrium isotherm in the absorber bottom. Only at very high L/G ratios, equilibrium is reached in the absorber top. The influence of the temperature bulge in a real absorber shifts the equilibrium curve to lower loadings which means that the operating line in a real absorber can touch the equilibrium curve in the middle of the column. Therefore, the real operating lines can be shifted to lower loadings when compared to the isothermal case considered here. This in turn leads to a higher energy requirement in the desorber. Thus, intercooling in the absorber can be favorable to achieve that the equilibrium curve is reached at the absorber bottom at a high loading.

Based on the results for the CO₂ loading in lean and rich solvent, the calculation of the desorber can be carried out. As results, the stripping steam \dot{m}^{Cond} and the CO₂ partial pressure at the desorber top $p_{CO_2}^{Des,out}$ are obtained and the operating lines can be drawn. The two operating lines shown in Fig. 5(b) touch the equilibrium isotherm at the intersection between segments I and II. For a higher L/G ratio, the required lean loading in the absorber inlet increases as shown in Fig. 6(a). With an increased lean loading, the consider-

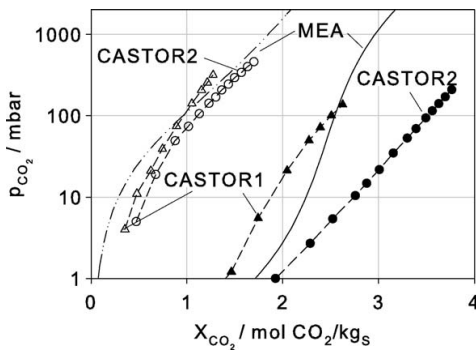


Fig. 4. Calculated equilibrium isotherms for MEA in comparison to experimental data for CASTOR1 and CASTOR2 at 40 °C and 120 °C (CASTOR, 2008).

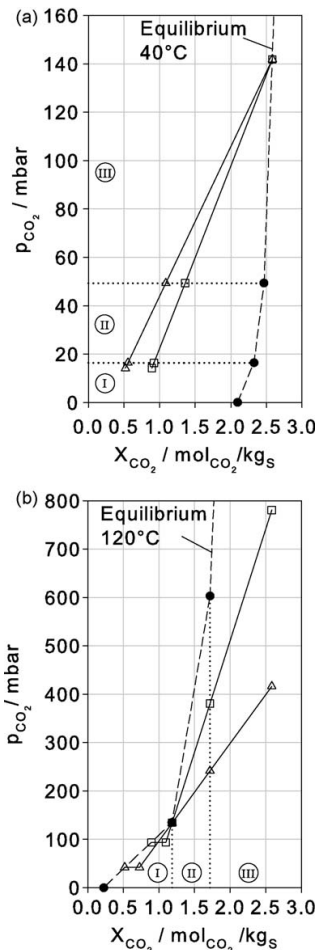


Fig. 5. Operating lines as a result of the modified Kremser method at two different L/G ratios (L/G : (Δ)=2.10; (□)=2.56) and discretized equilibrium isotherms for 30 wt% MEA for the case of a brown coal power plant: (a) absorber and (b) desorber.

ation of the reboiler as an equilibrium stage leads to an increase in $p_{CO_2}^*$ at the desorber bottom. This in turn results in a higher slope of the operating line and thus in a reduced steam flow and a higher CO₂ partial pressure at the desorber top. If, for this particular case, the lean loading increases further into the segment III, the operating line will reach the equilibrium isotherm at the desorber top. Then, $p_{CO_2}^{Des,out}$ can exceed the total pressure of the desorber. In reality, this is clearly not possible. The reason for this behavior mainly can be found in the assumption of an isothermal desorber. In a real desorber, the temperature decreases from bottom to top and thus the equilibrium isotherms are shifted towards higher loadings. Here, the vapor stream is set to zero in the model, if the CO₂ partial pressure $p_{CO_2}^*$ in the desorber bottom exceeds the total pressure. As an alternative, to avoid this problem, the pressure in the desorber bottom could be set free and could be calculated as the sum of the CO₂ equilibrium pressure $p_{CO_2}^*$ and the partial pressure of water ($p_{H_2O} = x_{H_2O}^L p_{H_2O}^S(T^{Des})$) instead of keeping it fixed at 2000 mbar. This was tested. The overall result showed only minor deviations between the two methods. The behavior explained above occurs at high L/G ratios, for which the energy requirement to provide the

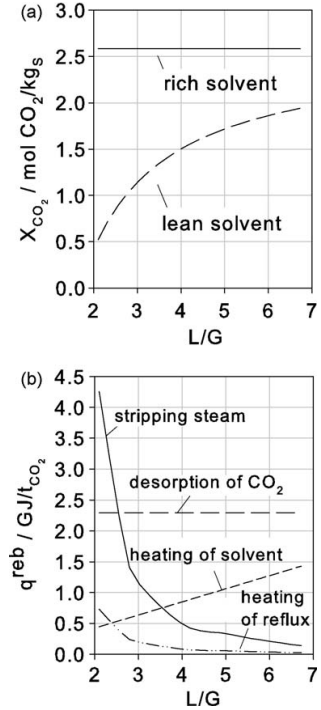


Fig. 6. Results of the modified Kremser method for the case of a brown coal power plant with an aqueous solution of 30 wt% MEA: (a) CO₂ loadings in the rich and lean solvent; (b) contributions to the reboiler energy requirement.

stripping steam is underestimated. The energy requirement to provide the desorption enthalpy as well as the energy to heat up the solvent are independent of that effect. Since the stripping steam requirement at low L/G ratios, which has an important influence on the minimum regeneration energy and the optimum solvent flow rate, is not influenced by that behavior, the modified Kremser method presented here can be applied for solvent comparison with regard to the minimum energy requirement.

As a result of the modified Kremser method, the four relevant contributions to the regeneration energy in dependence of the L/G ratio are determined, as the example in Fig. 6(b) shows. For illustration of the result, the specific energy requirement is plotted versus the L/G ratio. For the case shown in Fig. 6(b), the largest contribution is the desorption of CO₂. It is independent of the L/G ratio. The energy requirement for heating the solvent increases linearly with the L/G ratio as can be seen in Eq. (10). The energy contribution for the stripping steam and the heating of the condensate reflux are both related to the vapor flow rate in the desorber which itself depends on the required lean loading. At very low L/G ratios, the stripping steam requirement increases drastically as the separation task in the desorber becomes more difficult. At high L/G ratios, the stripping steam decreases to very low values which corresponds to the increasing slope of the operating line in Fig. 5(b). As already discussed, the model is less accurate at high L/G ratios due to the assumption of an isothermal desorber. In the real process, there will always be a vapor flow in the desorber due to water saturation of the CO₂ flow. Even though a very low stripping steam is required to fulfill the separation task at high L/G ratios, the vapor stream due to water saturation will contribute to the desorber energy through its vaporization and the heating of the corresponding reflux. Since this effect only occurs at high L/G ratios and it is similar for all

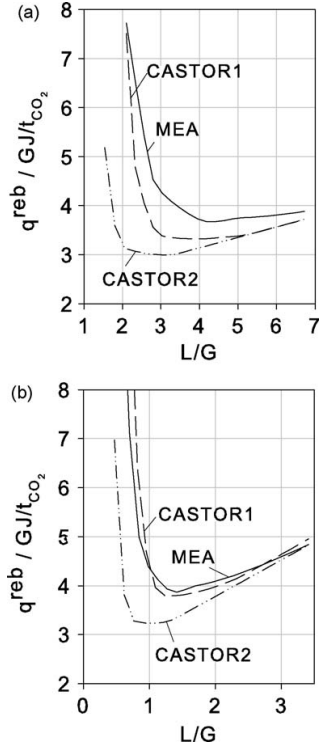


Fig. 7. Calculated specific energy requirement as a function of the L/G ratio at constant CO₂ removal rate for different flue gas compositions: (a) brown coal power plant and (b) combined cycle power plant.

solvents, the modified Kremser method can be applied for relative comparison of new solvents.

In Fig. 7, the calculated specific energy requirement is plotted over the L/G ratio for the brown coal power plant and the combined cycle power plant for the solvents MEA, CASTOR1 and CASTOR2.

For the case of the brown coal power plant shown in Fig. 7(a), the minimum regeneration energy increases in the order CASTOR2 < CASTOR1 < MEA. This is expected from the cyclic capacity. The L/G ratio at minimum regeneration energy is shifted to lower values with an increase in the distance of the absorption isotherms. Both CASTOR1 and CASTOR2 show a potential for an energy reduction. For the case of the combined cycle power plant shown in Fig. 7(b), CASTOR2 shows a significantly lower energy requirement than both MEA and CASTOR1. The difference between CASTOR1 and MEA is negligible. This can be explained by the fact that the cyclic capacity for CO₂ partial pressures below approximately 100 mbar is similar for MEA and CASTOR1 as Fig. 4 indicates.

Comparing both flue gas conditions, it can be seen that the optimum L/G ratio for the brown coal case is higher than for the combined cycle power plant case. This can be explained by the higher CO₂ partial pressure in the flue gas for the brown coal case. For $\Psi = 90\%$, the absorbed CO₂ mass flow in the brown coal power plant is much higher compared to the combined cycle power plant. To reach the same cyclic capacity, the solvent mass flow rate has to be higher for the brown coal case. Furthermore, the results show that the minimum regeneration energy is increased for the case of the combined cycle power plant. To explain this behavior, the different parts of the regeneration energy are shown in Table 4 for the optimum L/G ratio for the brown coal power plant (BC) and

Table 4

Comparison of the energy parts for the brown coal (BC) and the combined cycle (CC) power plant at optimized solvent flow rate for a 30 wt% MEA solution.

	BC	CC
Specific regeneration energy/GJ/t _{CO₂}	3.68	3.87
Desorption of CO ₂ /GJ/t _{CO₂}	2.29	2.29
Stripping steam/GJ/t _{CO₂}	0.38	0.45
Heating of solvent/GJ/t _{CO₂}	0.94	1.05
Heating of condensate reflux/GJ/t _{CO₂}	0.07	0.08

Table 5

Selected pilot-plant parameter studies for a 30 wt% MEA solution.

	P1	P2
p _{CO₂} /mbar	101	55
Ψ/%	90	90
\dot{m}^S	Varied	Varied

the combined cycle power plant (CC). The specific energy required for heating of the solvent is increased for the latter case as the ratio between solvent flow rate and absorbed CO₂ mass flow is increased for the combined cycle power plant. The stripping steam demand is increased because a lower lean loading is required for the combined cycle power plant as a result of the lower inlet CO₂ partial pressure.

To compare the results of the short-cut method with data from a pilot plant at the University of Kaiserslautern (Mangalapally et al., 2009), two experimental parameter studies P1 and P2 with 30 wt% MEA were chosen. For the boundary conditions in Table 5, the solvent flow rate was varied to study the behavior of the reboiler energy at constant CO₂ removal rate. The different contributions to the reboiler energy from the experimental data were obtained through energy balances as described in Notz (2010).

For the comparison between experiments and the short-cut method, it should be kept in mind that the short-cut method is not intended to be used for process design but for solvent screening. Fig. 8 shows the calculated and the experimental reboiler energy. Contrary to existing screening methods for solvent comparison (see Section 1), the new method is able to approximate the typical curve of the specific regeneration energy versus the L/G ratio with an accuracy which is sufficient for solvent screening. For low L/G ratios, the energy requirement is slightly underpredicted for parameter study P1 whereas it is slightly overpredicted for parameter study P2. Nevertheless the strong increase of the energy requirement by lowering the L/G ratio is shown in both cases. For high L/G ratios, the experimental value is always above the calculated value. The location of the experimental optimum L/G ratio for both parameter studies P1 and P2 agrees well with the opti-

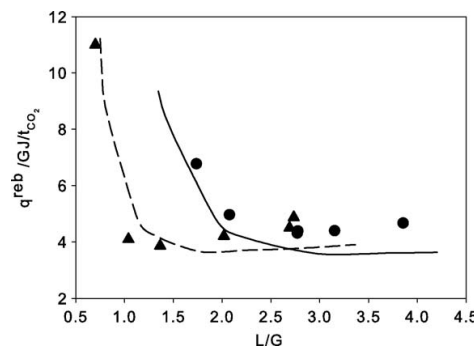


Fig. 8. Comparison of reboiler energy from experimental pilot-plant data with results from short-cut method for 30 wt% MEA (parameter studies ●=P1; ▲=P2).

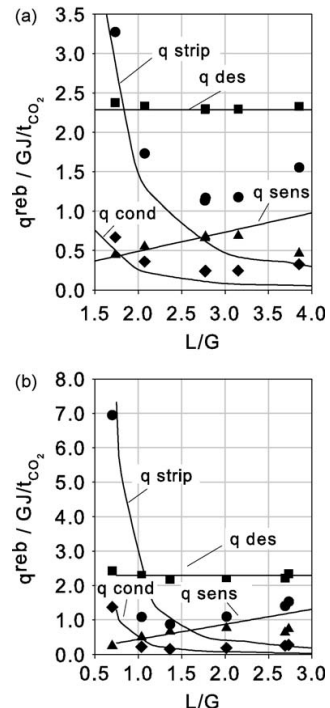


Fig. 9. Comparison of contributions to the reboiler energy from experimental pilot-plant data with results from short-cut method: (a) parameter study P1; (b) parameter study P2; q_{sens} (▲): sensible energy required for heating of the solvent; q_{des} (■): desorption enthalpy; q_{strip} (●): energy for stripping steam; q_{cond} (◆): energy for heating of the condensate reflux.

mum L/G ratio calculated by the short-cut method. This shows that the short-cut method is a suitable tool for solvent screening.

In Fig. 9, the four contributions to the reboiler energy calculated with the short-cut method and calculated from experimental data are compared for the parameter studies P1 and P2. In general there is a good agreement. It can be seen that the main difference between the calculated reboiler energy and the experimental reboiler energy especially for high L/G ratios results from a difference in the energy contribution of the stripping steam. This contribution is higher for the pilot-plant experiments compared to the short-cut method at high L/G. The difference between the calculated stripping stream energy contributions and the experimental values can be explained by various reasons.

Most importantly, a high number of equilibrium stages was used in the short-cut calculation so that the equilibrium limit is reached. In the pilot plant, the height of the columns is limited. This results in a kinetic limitation and a limited separation capacity which leads to a lower rich loading, especially at high L/G ratios, and consequently in a lower lean loading, as shown in Fig. 10. With a lower lean loading, the stripping steam demand increases as the difficulty of the separation task is increased. This makes clear that the developed short-cut method shows the potential for solvents only in sufficiently high columns.

Another reason for the discrepancies is that the distance between the operating line and the equilibrium line is not calculated accurately by the short-cut method due to the underlying short-cut assumptions. One assumption is that of an isothermal desorber. In a real desorber, the temperature decreases towards the desorber top and thus the equilibrium is shifted to higher load-

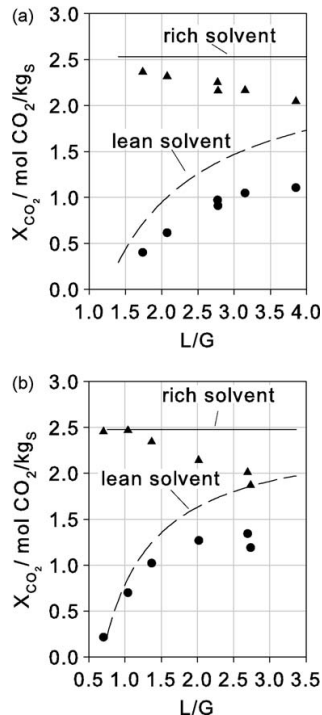


Fig. 10. Comparison of experimental and calculated lean and rich loading: (a) parameter study P1; (b) parameter study P2.

ings. Furthermore, the assumption of a constant vapor flow in the desorber leads to inaccuracies. In fact, for each mole of CO_2 that is released, approximately two moles of water will condense because the heat of absorption of CO_2 into a 30 wt% MEA solution is about twice the heat of evaporation of water. This results in a decrease in the vapor flow and thus in an increase in the slope of the operating line towards the top of the desorber. The operating line is thus shifted to lower loadings. These two effects both lead to a decrease in the distance between the operating line and the equilibrium line in the experiment. Thus, the separation task in the desorber is getting more difficult and a higher regeneration energy is required. Differences between the experiment and the short-cut method at high L/G ratio are also caused by the water saturation of the CO_2 flow at the desorber top. As discussed above, this water saturation implies that there will always be a vapor flow at the desorber top even if only minimal stripping steam is required for the separation task.

In Fig. 9, it can be seen that the experimental stripping steam demand increases again with higher L/G ratios. An explanation for this is that at higher L/G ratios, the temperature at the desorber inlet is higher due to a higher temperature in the absorber bottom. This temperature increase is due to a shift of the temperature bulge in the absorber towards the bottom. The resulting higher temperatures at the desorber top lead to a higher water vapor stream as discussed in detail in Notz (2010).

Furthermore, the energy requirement for heating the solvent does not increase linearly with the L/G ratio for the case of the pilot-plant experiments. This is because a better heat transfer is achieved with a higher solvent flow rate in the rich-lean heat exchanger, resulting in a smaller temperature difference between desorber inlet and outlet. Another possible reason for this behavior is the

increasing temperature in the absorber bottom with increasing L/G ratio as discussed above.

The modified Kremser method presented here is not suited for a detailed process description or for process design. Nevertheless, the influence of process parameters, especially of the solvent flow rate, on all important contributions to the regeneration energy are reasonably described for the closed absorber–desorber cycle. Overall, a good agreement between the results of the short-cut method and the experimental values is obtained. Comparisons that are carried out for different solvents based on the present method should yield a correct ranking of the solvents. Thus, this method should be a valuable tool for identifying new solvents that have the potential to reduce the energy demand for post-combustion CO_2 capture.

4. Conclusion

A short-cut method for the estimation of the minimum regeneration energy requirement of the absorption–desorption process for CO_2 capture is presented and discussed. In this method, absorber and desorber are described by a modified Kremser equation which is based on a simplified equilibrium stage model. Only equilibrium isotherms at absorber and desorber temperature and (estimated) caloric data are required as input to the method. The model allows the calculation of the four contributions to the energy requirement in the desorber. By variation of the solvent flow rate, the model predicts the minimum reboiler energy at an optimum solvent flow rate for given boundary conditions. The results can be used for comparing new solvents with regard to their potential for energy reduction.

Calculations were carried out for the two solvents CASTOR1 and CASTOR2 and compared to the standard solvent MEA. It was found that an advantage of CASTOR1 can only be expected at high CO_2 partial pressures in the flue gas since its cyclic capacity is only higher than that of MEA for high partial pressures. CASTOR2 always shows an advantage in terms of energy requirement. The results make clear that solvents with an increased cyclic capacity show a shift of the optimum L/G ratio towards lower values and as a consequence a decrease of the reboiler energy requirement, even if the absorption enthalpy is constant. On the other hand, a decrease of the absorption enthalpy at constant cyclic capacity would lead to a decrease of the minimum reboiler energy at a constant L/G ratio.

The short-cut method was compared to pilot-plant data for MEA. The experimental optimum lean loading is predicted fairly well. The absolute values of the desorber energy are slightly underestimated due to the underlying assumptions of the short-cut method. Especially for high L/G ratios, this results in a higher stripping steam demand in the experiment compared to the short-cut calculation. In conclusion, the short-cut method presented here allows to assess new solvents for CO_2 capture by evaluating the influence of equilibrium isotherms and the heat of absorption on the energy requirement under different boundary conditions. It is more generally applicable to solvent selection for absorption–desorption processes in cases where many new solvents have to be considered for which only a limited amount of data is available.

Acknowledgements

We gratefully acknowledge support of this work by the European Commission under the Integrated Project CASTOR (Contract n SES6-CT-2004-502586) and by BASF SE.

Appendix A. Derivation of model equations

The mass balance of CO₂ for each stage is given by Eq. (A.1), the linear equilibrium line by Eq. (A.2). Eq. (A.3), which gives the difference of the partial pressure of CO₂ over the stage, follows from Eqs. (A.1) and (A.2). The indices n , respectively $n+1$ refer to the gas and liquid flows below or above the equilibrium stage n . At the bottom of the considered column, n is equal to 1 and at the top, n is equal to N . Summation of Eq. (A.3) over all equilibrium stages yields Eq. (A.4), in which the finite series can be replaced by an analytical expression, cf. Eq. (A.5). Insertion of the equilibrium relation for the first equilibrium stage (A.6) yields the modified Kremser equation (Eq. (A.7)). For the absorber, this relation can be written as Eq. (A.8) by including the removal rate based on the assumption of constant gas flow rate \dot{n}^G in the absorber

$$\frac{p_{CO_2,n}}{p} \dot{n}^G + X_{CO_2,n+1} \dot{m}^{S*} = \frac{p_{CO_2,n+1}}{p} \dot{n}^G + X_{CO_2,n} \dot{m}^{S*} \quad (A.1)$$

$$p_{CO_2,n+1} = a_k X_{CO_2,n} + b_k \quad (A.2)$$

$$\underbrace{(p_{CO_2,n+1} - p_{CO_2,n})}_{\Delta p_{CO_2,n}} = \underbrace{\dot{m}^{S*} p}_{\dot{n}^G a_k} \underbrace{\left(p_{CO_2,n+2} - p_{CO_2,n+1} \right)}_{\Delta p_{CO_2,n+1}} \quad (A.3)$$

$$p_{CO_2}^{out} - p_{CO_2}^{in} = \Delta p_{CO_2,1} + \Delta p_{CO_2,2} + \dots + \Delta p_{CO_2,N} \\ = \Delta p_{CO_2,1} \left(1 + \frac{1}{A_k} + \frac{1}{A_k^2} + \dots + \frac{1}{A_k^{N-1}} \right) \quad (A.4)$$

$$p_{CO_2}^{out} - p_{CO_2}^{in} = (p_{CO_2,2} - p_{CO_2}^{in}) \begin{cases} N & \text{for } A_k = 1 \\ \frac{1 - (1/A_k)^N}{1 - (1/A_k)} & \text{for } A_k \neq 1 \end{cases} \quad (A.5)$$

$$p_{CO_2,2} = a_k X_{CO_2}^{out} + b_k \quad (A.6)$$

$$p_{CO_2}^{out} - p_{CO_2}^{in} = (a_k X_{CO_2}^{out} + b_k - p_{CO_2}^{in}) \begin{cases} N & \text{for } A_k = 1 \\ \frac{1 - (1/A_k)^N}{1 - (1/A_k)} & \text{for } A_k \neq 1 \end{cases} \quad (A.7)$$

$$-\psi p_{CO_2}^{Abs,in} \\ = \left(a_k^{Abs} X_{CO_2}^{Rich} + b_k^{Abs} - p_{CO_2}^{Abs,in} \right) \\ \times \begin{cases} N^{Abs} & \text{for } A_k = 1 \\ \frac{1 - (1/A_k)^{N^{Abs}}}{1 - (1/A_k)} & \text{for } A_k \neq 1 \end{cases} \quad (A.8)$$

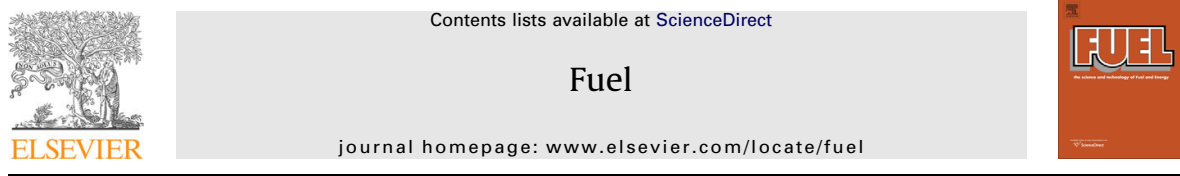
References

- Austgen, D.M., Rochelle, G.T., Peng, X., Chen, C.C., 1989. Model of vapor liquid equilibria for aqueous acid gas alkanolamine systems using the electrolyte NRTL equation. *Ind. Eng. Chem. Res.* 28 (7), 1060–1073.
- CASTOR, 2008. EU-Project CO₂ from Capture to Storage (CASTOR): Integrated research project under the 6th frame work programme of the European commission, contract nr. ses6-ct-2004-502586, project duration from 01.02.2004 to 31.01.2008, <http://www.co2castor.com>.
- Chiu, L.-F., Li, M.-H., 1999. Heat capacity of alkanolamine aqueous solutions. *J. Chem. Eng. Data* 44 (6), 1396–1401.
- Goedecke, R., 2006. Fluidverfahrenstechnik. WILEY-VCH Verlag GmbH & Co. KGaA, Weinheim.
- Göttlicher, G., 2003. Capture, transport and storage of CO₂ from fossil-fired power plants. VGB PowerTech 5, 96–101.
- Kim, I., Svendsen, H.F., 2007. Heat of absorption of carbon dioxide (CO₂) in monoethanolamine (MEA) and 2-(Aminoethyl)ethanolamine (AEEA) solutions. *Ind. Eng. Chem. Res.* 46 (August (17)), 5803–5809.
- Mamun, S., Svendsen, H., Hoff, K., Juliussen, O., 2007. Selection of new absorbents for carbon dioxide capture. *Energy Convers. Manage.* 48 (1), 251–258.
- Mangalapally, H.P., Notz, R., Hoch, S., Asprion, N., Sieder, G., Garcia, H., Hasse, H., 2009. Pilot plant experimental studies of post combustion CO₂ capture by reactive absorption with MEA and new solvents. *Energy Procedia* 1 (1), 963–970.
- Notz, R., 2010. CO₂-Abtrennung aus Kraftwerksabgasen mittels Reaktivabsorption. PhD Thesis, Universität Stuttgart, Logos Verlag Berlin GmbH.
- Rowley, R., Wilding, W., Oscarson, J., Yang, Y., Zundel, N., Daubert, T., Danner, R., 2007. DIPPR Data Compilation of Pure Compound Properties. Design Institute for Physical Properties AIChE, New York, NY.
- Sherwood, A.E., Prausnitz, J.M., 1962. The heat of solution of gases at high pressure. *AIChE J.* 8 (4), 519–521.
- Tontiwachwuthikul, P., 1996. Research and development activities on high efficiency separation process technologies for carbon dioxide removal from industrial sources at University of Regina, Canada. *Energy Convers. Manage.* 37 (6–8), 935–940.

Publication IV

Integration of a chemical process model in a power plant modelling tool for the simulation of an amine based CO₂ scrubber

doi: 10.1016/j.fuel.2009.01.031



Integration of a chemical process model in a power plant modelling tool for the simulation of an amine based CO₂ scrubber

P. Galindo Cifre^{a,*}, K. Brechtel^a, S. Hoch^b, H. García^c, N. Asprion^c, H. Hasse^b, G. Scheffknecht^a

^a Institute of Process Engineering and Power Plant Technology, Pfaffenwaldring 23, D-70569 Stuttgart (Vaihingen), Germany

^b Institute of Thermodynamics and Thermal Process Engineering, Pfaffenwaldring 9, D-70569 Stuttgart, Germany

^c BASF SE, Carl-Bosch-Strasse 38, D-67056 Ludwigshafen, Germany

ARTICLE INFO

Article history:

Received 29 September 2008

Received in revised form 19 January 2009

Accepted 23 January 2009

Available online 21 February 2009

Keywords:

Carbon dioxide removal

Amine scrubber

Process integration

Power plant

Energy penalty

ABSTRACT

Post-combustion is considered among the different options for CO₂ capture as the most mature available technology. All major components of the CO₂ absorption/desorption process are commercially available but at a smaller scale, and they are not integrated and optimized for the application in power plants. Therefore, it is still to be demonstrated that this process is a viable option for the capture of CO₂ at power plants. The amine scrubbing process with standard solvents is highly energy demanding due to solvent regeneration and CO₂ compression. This is a significant energy sink for the power plant and efficiency can be reduced up to 16%-points. In order to minimise the energy penalty, complete integration and optimization of the capture and the power plant processes are necessary.

Simulations of the power plant cycle and the amine scrubbing system have been performed with specialized software. The results of the integration are discussed.

© 2009 Elsevier Ltd. All rights reserved.

1. Introduction

Fossil fuel-fired power plants are nowadays the largest stationary emitting sources of CO₂, whose increasing atmospheric concentration is of great concern due to the consequences derived from the altered greenhouse effect. Fossil fuels provide most of the growing world's total energy demand and as it will continue increasing, the amount of CO₂ emitted is expected to keep on rising. Stabilizing the concentration of CO₂ in the atmosphere will likely require a variety of actions like increasing the efficiency of power plants and production processes, and decreasing the energy demand, together with a reduction of the CO₂ emissions. Carbon Capture and Sequestration (CCS) is also a promising method, in particular considering the possibility of retrofitting existing plants with capture, transport and storage of CO₂.

For many reasons post-combustion CO₂ capture with amine-based solvent systems is the most suitable technology for coal-fired power plants: for example, it can be used for dilute systems and low CO₂ concentrations, it is commercially available in small scale and can be retrofitted to existing power plants. The major disadvantage of this technology is the reduction of the power plant

efficiency, caused by the consumption of steam for solvent regeneration.

2. Post-combustion CO₂ capture in power plants

2.1. Basics of amine scrubbing

In a power plant the CO₂ scrubbing technology can be installed downstream the flue gas desulphurisation plant. It has two main elements: the absorption and the stripping column with random or structured packing as column internals. The process allows a continuous regeneration of the amine solution, which saves considerable amounts of solvent. Fig. 1 shows a schematic diagram of the scrubbing process.

Before entering the CO₂ absorption column, the flue gas is cooled down to a temperature of 40 to 50 °C and compressed in order to overcome the pressure losses in the column. The amine solution is contacted with the flue gas in a countercurrent column (absorber) and captures the CO₂ by chemical reaction. The CO₂-rich amine stream, leaving from the absorber bottom, is regenerated by thermal treatment at 100 °C up to 130 °C in the regeneration column (desorber), releasing the CO₂. The reboiler makes use of steam extracted from the water-steam cycle of the power plant. After regeneration the CO₂-lean amine solution is recycled back to the CO₂ absorption step after being cooled down in the rich/lean heat exchanger. The CO₂ stream leaving from the top of the desorber is finally dried and compressed.

* Corresponding author. Tel.: +49 711 685 63487; fax: +49 711 685 63491.

E-mail addresses: ivd@IVD.Uni-Stuttgart.DE, galindo-cifre@ivd.uni-stuttgart.de (P. Galindo Cifre), sekretariat@itt.uni-stuttgart.de (S. Hoch), global.info@basf.com (H. García).

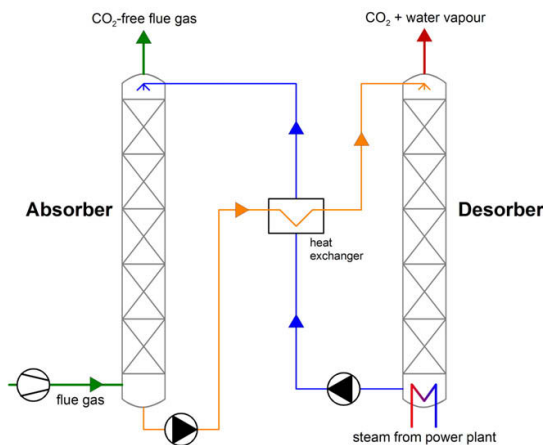


Fig. 1. Flowsheet of an amine scrubber.

At the moment an aqueous solution of monoethanolamine (MEA) is the standard solvent for gas streams with relatively low concentrations of CO₂ and essentially no minor contaminants such as SO₂. This is especially true, when the gas is treated at low pressures, and maximum removal of CO₂ is required, like in the case of coal-fired power plants. The main advantages in using MEA/water solutions are its high CO₂ reactivity, its high absorption capacity and its low molecular weight. Its main drawback is its high heat of reaction with CO₂, which leads to higher energy requirements for stripping in MEA systems [1].

2.2. Energy penalty

The regeneration of a CO₂-rich amine solution requires a high amount of energy. The related energy demand can be divided into three different proportions: first, to apply the desorption enthalpy, which is directly linked with the heat of absorption; second, to heat up the amine solution to the boiling point and third, to evaporate water as stripping steam. For MEA an energy demand between 3.9 and 4.2 MJ/kg captured CO₂ has been reported [2,3]. Furthermore, a significant amount of electricity is also needed to compress the captured CO₂ for pipeline transport to a storage site.

This energy requirement reduces the net efficiency of the power plant, if it is extracted internally by de-rating the last turbine stages of the steam cycle. This causes a decrease in the power plant energy efficiency up to 16%-points, excluding the compression of CO₂ which accounts for an additional loss of 3-4%-points [4].

Alternatively, a much bigger power plant needs to be built in order to achieve the same "net" power generation capacity, as it would have been without CO₂ capture [5]. Or else the fuel consumption needs to be increased, so that the power plant maintains its original output.

2.3. Changes on the steam power plant

In the integration of the capture process within the power plant, steam is taken from the crossover pipe between the intermediate pressure (IP) and low pressure (LP) cylinders of the steam turbine and used in the stripper reboiler. Since up to 2/3 of the LP steam mass flow (2-5 bar) of the turbine is consumed for this purpose, the LP turbine section must be adjusted accordingly [4].

Steam is extracted from the same point as the deaerating steam, and the condensate is sent back to the condensate system. This

causes a significant reduction of the steam flow rate in the condenser and in all the low pressure feed lines from the condenser to the deaerator (around 93 kg/s for a coal-fired plant). Smaller steam flow rates are, therefore, necessary in the low pressure feed-water heaters.

Another power plant process that needs to be modified in case of including an amine based CO₂ capture system is the desulphurisation plant. The amines also react with acidic flue gas compounds like SO₂, SO₃ and NO₂, forming stable byproducts, which can not react with CO₂ and reduce the CO₂ absorption capacity of the solvent. A high efficiency FGD plant will be required to meet the stringent SO_x level limits of the amine scrubber (10-30 mg/Nm³ with 6 vol% O₂ dry), which leads to levels lower than the limits imposed by current environmental regulations [6]. To prevent corrosion, the flue gas is treated so that NO₂ concentration is below 20 ppmv (dry) [7]. Other minor alterations would also be necessary regarding pipelines and auxiliary equipment.

Process simulation and evaluation are essential items to scale-up the scrubbing process, maximise its performance and investigate the effects of its integration within the power plant. The objective of this paper is to compare the power plant performance, with special attention to the power output and efficiency penalty, when a MEA scrubbing system and the necessary compression step are integrated with the steam cycle, and to find the scrubber operating conditions that minimise the impact on the power plant operation.

3. Process simulation and results

3.1. Power plant simulation

The modelling of the power plants was performed using the software EBSILON Professional. EBSILON is designed for the simulation of thermodynamic processes with emphasis on power plant technology. It is a mass and energy balance calculation program with a graphical user interface and a component library with more than 90 components such as turbines, condensers, heat exchangers, boilers, etc., that enable a very fast modelling and the convenient error analysis.

It allows modelling several processes connected by power or material lines. Therefore, it can be used to solve an optimization problem for the power cycle; that is, to find the operating conditions that minimise the energy penalty for the power plant, once the CO₂ capture system has been included.

A power plant model has been developed to provide a base case and essential information on coal consumption, thermal efficiency, net plant efficiency and electric output. Simulations also provide the quantity and quality of the steam through the power cycle as well as the emission rate, temperature and composition of the flue gas.

For this study two state-of-the-art power plant reference cases have been chosen, a 600 MW hard coal and a 1000 MW lignite power station. **Table 1** presents the main parameters used for the simulation [8]. Due to the fact that EBSILON is in principle not designed to simulate chemical processes, the integration of a sub-model for the CO₂ capture was necessary.

Table 1
Main simulation parameters for the power plants.

	600 MW hard coal	1000 MW lignite
Base plant gross generation (MW _e)	600	1000
Base plant net efficiency (LHV) (%)	45	49.3
Fuel calorific value (HHV) (MJ/kg)	26.2	10.8
CO ₂ emissions (g/kWh _e)	772	812

3.2. Simulation of the amine scrubber

The process model of the CO₂ absorption in a MEA solution is implemented into CHEMASIM. CHEMASIM is a powerful tool for steady-state simulations of chemical processes and was developed by BASF. CHEMASIM contains a non-equilibrium absorber model, including the rigorous calculation of heat and mass transfer between gas and liquid phase, taking into account chemical reactions, as well.

The two-film theory is used for the description of heat and mass transfer over the gas–liquid interface. The resulting partial differential equation system is solved numerically by discretization of column height and fluid films. With a non-equidistant arrangement of discrete elements in the liquid film, an accurate calculation of heat and mass transfer under the strong influence of the fast reaction between CO₂ and amine is enabled [9].

For the scrubbing process with the complex reaction system CO₂–MEA–H₂O, CHEMASIM achieves rather accurate results and shows an exceptionally good agreement with experimental data, obtained from various pilot plants of different sizes.

Initial conditions for the CO₂ scrubbing process simulation of both reference cases, using MEA as solvent, are as follows:

- 90% of CO₂ removal
- 30 wt.% MEA in aqueous solution
- Compression of captured CO₂ to 110 bar and 40 °C.

The optimal operating conditions for the CO₂ absorption/desorption process, calculated with CHEMASIM, are presented in Table 2.

3.3. Integration of power plant and CO₂ capture system

CHEMASIM and EBSILON were coupled to study the impact of post-combustion CO₂ capture on the power plant performance. In order to extrapolate the results from the chemical process simulation into EBSILON, a C++ code was developed. A new model was built that recreates the energy and mass balances in the CO₂ absorption/desorption system and was linked to the power plant model. The system was completed with the CO₂ compression stage (see Fig. 2).

An important consideration is the selection of the steam quality that will be fed to the stripper reboiler. Finding the optimum point to extract this steam is essential in order to minimise the energy penalty. It is significant whether the steam is extracted from the steam cycle at high or low pressure: high pressure steam can produce more electricity in the turbine and represents a more remarkable loss for the power plant than low pressure steam.

Simulations have been performed for the complete system with different steam extracting points at the LP stage of the turbine. Fig. 3 shows the resulting overall efficiency for the 600 MW hard coal power plant. The higher the pressure of the steam, the higher the efficiency loss, since steam of a better quality is taken away from the power cycle. On the other hand, the lower the pressure

of the steam and consequently, the lower its temperature, the less the plant will be affected. However, it will be necessary to take a higher steam flow rate to provide the energy required in the stripper, and the reboiler would require a much larger surface area. As a compromise steam at 3.4 bar and 233 °C was considered for the simulations.

The first results of the simulation for the complete system are summarized in Table 3. The 600 MW power plant fired with a 45% net efficiency losses 14%-points if the plant has an MEA-based CO₂ capture process and the subsequent compression. The 1000 MW lignite plant, in turn, experiences a 16%-points efficiency reduction. The efficiency loss in both cases comprise 2.7%-points due to the use of electrical power for the absorption process equipment (pumps, compressors, etc.), 3.4%-points caused by the compression work needed to prepare the CO₂ for transport conditions, and the remaining energy loss is due to the steam extracted for MEA regeneration.

4. Optimization

Some of the parameters affecting the energy requirement of the amine system were varied and their effects were studied in conjunction with the power plant. The following parameters were investigated:

- the stripper operating pressure
- the solvent circulation rate
- the height of absorber column packing.

This sensitivity analysis was performed with CHEMASIM and as mentioned before, the results were used as an input for the simulation of the integrated system in EBSILON. The optimization was carried out for both reference cases, showing similar results. Thus, in the following pages only the results for the 600 MW bituminous coal power plant are shown.

4.1. Desorber operating conditions

The effect of the stripper operating pressure, and therefore the operating temperature, was investigated. At a higher pressure the amine regeneration by means of releasing the CO₂ is likely to be favoured. Moreover, less compression work will be needed for the CO₂ product stream. The desorber pressure was varied in the range from 1 to 3 bar, with a constant pressure drop through the column of 40 mbar. As it can be seen in Fig. 4a, the reboiler duty is reduced with increasing pressure, as expected. Values drop from more than 5 to 3.81 and 3.77 GJ/t CO₂ captured, for the bituminous coal and the lignite plants, respectively.

Fig. 4b shows the effect on the net power plant efficiency. While the 1000 MW plant achieves an efficiency gain of 1.2%-points, the 600 MW plant experiences a raise of 3%-points in the net efficiency by changing the operating pressure from 1.25 to 2.1 bar. Thus, the optimal operating pressure lies between 1.9 and 2.1 bar.

It is important to note that after a certain pressure value the efficiency of the plant starts to decrease, although the energy required in the stripper continuously drops. Higher stripper pressures increase the boiling point of the rich solution, and the reboiler has to be fed with steam from the power plant either with a better quality or at a higher rate. At the same time, there is an increase in the amount of electric power necessary to reach the higher pressure in the desorber.

The impact of a higher pressure on the design and construction of the stripper has to be also taken into account. Furthermore, at elevated temperatures the loss of solvent by degradation and corrosion problems becomes significant.

Table 2
MEA system optimal operating point.

	600 MW hard coal	1000 MW lignite
Solvent mass flow (t/h)	8050	13,500
Absorber height (m)	18	18
Amine rich loading (mol _{CO₂} /mol _{MEA})	0.447	0.447
Amine lean loading (mol _{CO₂} /mol _{MEA})	0.217	0.217
Desorber temperature (°C)	120	120
Desorber pressure (bar)	2	2
Energy demand for regeneration (GJ/t CO ₂)	4.07	4.04

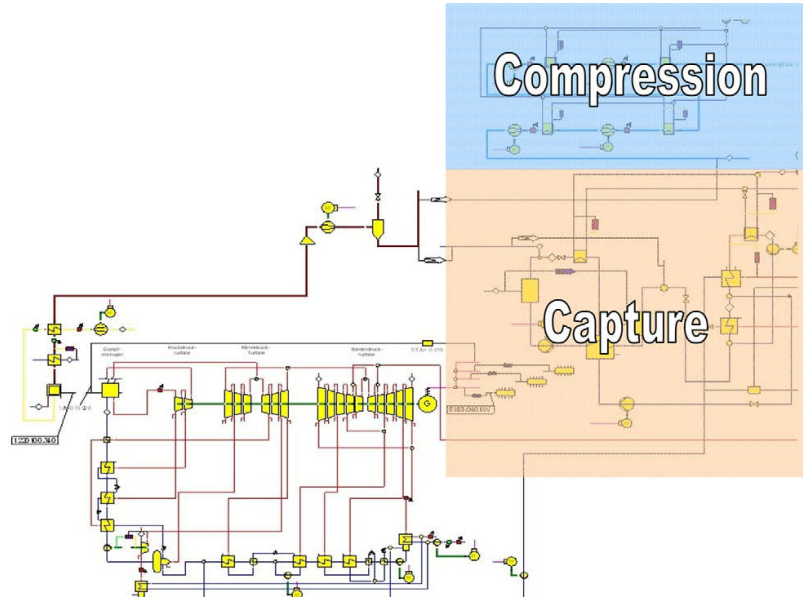


Fig. 2. EBSILON model for the power plant with CO₂ capture.

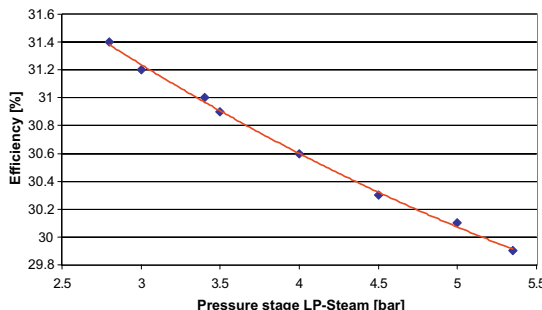


Fig. 3. Steam extraction pressure.

Table 3
First integration results.

	600 MW hard coal	1000 MW lignite
Base plant net efficiency (%)	45.0	49.3
With CO ₂ capture (%)	34.4	36.9
With CO ₂ capture and compression (%)	31.0	33.3
Efficiency loss (%-points)	14.0	16.0

4.2. Absorber column height

The height of the random packing IMTP50 in the absorber was varied from 14 to 22 m, resulting in a continuously decreasing energy requirement in the stripper (4.81–3.91 GJ/t CO₂ for the 600 MW hard coal plant and 4.6–3.9 GJ/t CO₂ for the 1000 MW lignite plant). With a higher packing, the mass transfer area is increased and this improves the absorption process. This turns out in an increase of efficiency in 1.4%-points for the 600 MW plant and in 1.2%-points increase for the lignite plant. The column design should be performed with a minimum height of 17 m, in order not

to be inefficient. However, for columns higher than 18 m, the efficiency of the plant is not significantly affected, as seen in Fig. 5.

The height of the absorber defines the energy required for the flue gas fan, since this has to overcome the pressure drop in the column. Thus, the higher the column the higher the pressure drop and consequently, the higher the fan energy requirement. Another problem of increasing the height of the column is that it implies higher capital costs. Thus, the selection of the design column has to take into account economic aspects.

The stripper height was also studied. Nevertheless, it affects the stripper heat requirement less dramatically than the absorber height does, and was not considered for the simulations of the power plants.

4.3. Amine solvent flow rate

As it can be seen in Fig. 6a, the reboiler duty is rather sensitive to the solvent flow rate. At low mass flow rates the reboiler duty is high; with the increase of the solvent flow, the energy required for the regeneration reduces until a minimum, and afterwards it starts to increase again. At low solvent ratio, it is necessary to use a low lean loading in order to maintain the CO₂ removal efficiency, which means that more stripping steam has to be produced to regenerate the solvent to a higher extent. At higher solvent flow rates, the required loading of the lean solvent increases. This reduces the energy required to regenerate the solvent in the stripper. At very high solvent flow rates, the energy which is necessary to heat up the solution to saturation temperature turns out to be dominant. Therefore, the reboiler duty becomes higher.

An optimum solvent mass flow rate was found for the CO₂ capture system (8050 t/h for the 600 MW hard coal power plant and 13,500 t/h in the case of a 1000 MW lignite plant), as shown in Fig. 6a. According to the simulation of the complete system, this optimal operating point does not coincide with the optimum for the power plant. The simulation of the 600 MW power plant shows better results with flow rates between 7600 and 7900 t/h. In the case of the 1000 MW power plant, a flow rate with values ranging

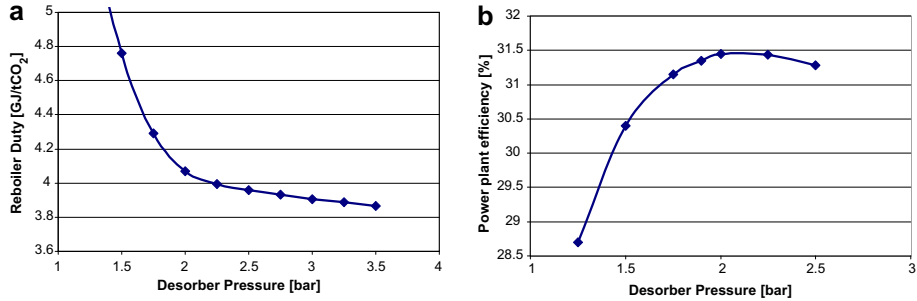


Fig. 4. Effect of stripping pressure: (a) on the reboiler duty; (b) on net power plant efficiency.

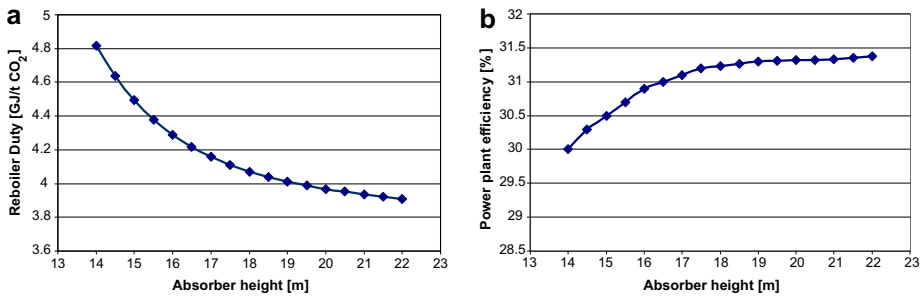


Fig. 5. Effect of absorber height: (a) on the reboiler duty; (b) on net power plant efficiency.

from 12,900 to 13,300 t/h would be preferred. In both cases, these values are significantly lower than the optimum solvent flow rate found just for the CO₂ scrubbing system. Lower mass flow rates require less pumping work and also involve a lower pressure drop in the absorption column, which reduces the energy demand for the flue gas blower.

The influence of the scrubbing process parameters such as column size, solvent mass flow rate, operating pressure and temperature on the power plant cycle has been pointed out. As a result, the energy penalty can be reduced, if the operating conditions of the CO₂ system are chosen according to their effects on the power plant performance.

4.4. Optimization results

The operating conditions for the amine system that minimise the energy penalty in the steam cycle have been selected. With

these optimized parameters, the simulation for the 600 MW plant shows 0.1%-points of efficiency gain, and for the lignite plant a gain of 0.4%-points is achieved. Table 4 summarizes the results derived from the optimization study.

The higher desorber pressure in the lignite plant generates most of the efficiency increase. Moreover, the lower solvent mass flow rate and the lower pressure drop in the absorber achieve a reduction of 5% in electricity consumption. In the 600 MW plant, the electricity requirement of pumps and the flue gas fan is almost 9% lower.

5. Options for further penalty reduction

The objective of an optimized process integration between the scrubbing system and the power plant is to minimise the impact of CO₂ capture on the power plant performance. Therefore, various

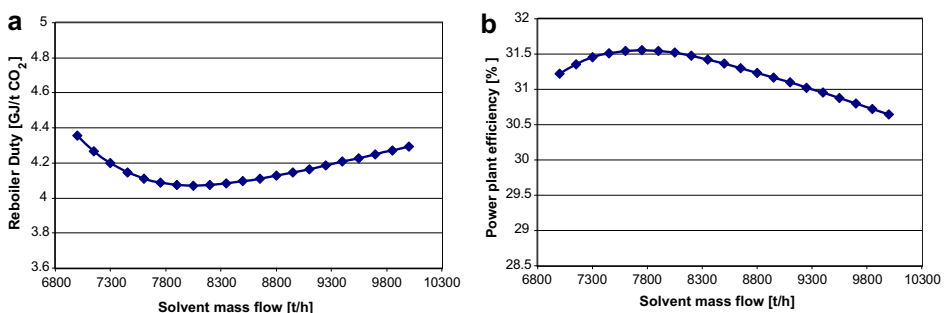


Fig. 6. Effect of solvent mass flow: (a) on the reboiler duty; (b) on net power plant efficiency.

Table 4
Optimization results summary.

	600 MW hard coal	1000 MW lignite
Desorber pressure (bar)	2	2.1
Solvent mass flow (t/h)	7700	13,100
Absorber height (m)	17	18
Net plant efficiency (%)	31.1	33.7

options for penalty reduction are proposed: to reduce the electric power demand, especially in the compression stage; to make use of the available sources of waste heat; and to lower the energy requirements in the reboiler. Some of these approaches were studied and simulated for the 600 MW bituminous plant, leading to the following energy saving opportunities.

Case 1: In order to improve cycle efficiency and thus, counteract the energy penalty due to the CO₂ capture, a modified compression process is proposed. The original design comprises four compression stages with intercooling, leading to a final CO₂ liquid stream at 110 bar and 40 °C. Taking the fluid to just above its critical pressure (73.9 bar at 31 °C), and replacing the final stage compressor by a more efficient and less energy demanding pump, reduces the compression power requirement by 6%. This leads to a reduction of 0.2%-points of efficiency loss. In addition, the cooling requirement and therefore, the amount of cooling water are reduced by approximately 4%. Fig. 7 shows the improved compression model.

Case 2: As the CO₂ stream reaches temperatures up to 160 °C during compression, it is possible to recover heat at the intercooler stages prior to the next compressor. Thermal energy from the second and third compressor discharge can be recovered to heat up the water after the turbine condenser in the power plant. This increases the plant efficiency by 0.1%-points, by reducing turbine bleed steam flow rates. In fact, with this configuration two low pressure pre-heaters can be eliminated from the boiler feed-water cycle.

Case 3: Steam is extracted from the LP turbine stage of the power plant due to the suitability of the steam pressure for reboiler use. Steam conditions at this point are 3.4 bar and 233 °C. Consequently, steam is superheated, since at 3.4 bar saturation temperature is 137 °C. Given that the reboiler temperature should not overcome 122 °C, above this value degradation of MEA and corrosion become significant, the quality of the extracted steam should

be then decreased to just above saturation before entering the reboiler.

This cooling can be accomplished by attemperation using part of the condensate at the reboiler exit or by pre-heating the boiler feed-water. Heating the condensate reduces steam flow to the high pressure feed-water heaters, as it is returned to the feed-water cycle at a higher temperature (in the base case its temperature is about 128 °C and with de-superheating it can increase up to 187 °C). Consequently, more steam passes to the low pressure turbine, thereby increasing the output. However, this approach raises the amount of steam supplied to the stripper reboiler. As a result, the net plant efficiency increases in 0.3 up to 0.4%-points. On the other hand, using the superheated steam to recover some heat in the boiler feed-water system accounts for just 0.1%-points increase.

Fig. 8 presents the power plant cycle with the adjustments described for Cases 2 and 3. The shaded area indicates the pre-heaters that can be saved by using the waste heat from CO₂ compression. The dashed line shows the change in the position of the reboiler condensate discharge indicated in Case 3.

Case 4: In order to assess the potential efficiency gain of a lower energy for regeneration, a hypothetical solvent was assumed which also achieves 90% of CO₂ removal. The idea was to define the characteristics that such a solvent should have with the aim of reducing as much as possible the energy penalty for the power cycle.

As mentioned before, the energy demand in the reboiler can be divided into three different energy sinks: the heat of CO₂ desorption, the sensible heat to bring the solution to reboiler temperature and the vaporization of water for stripping. They can be defined as follows [10]:

$$\begin{aligned} Q_{\text{reb}} &= Q_{\text{strip}} + Q_{\text{sens}} + Q_{\text{vap}} \\ &= -n_{\text{CO}_2} \Delta H_{\text{strip}} + L c_p (T_{\text{bottom}} - T_{\text{top}}) + m_v \Delta H_{\text{vap}} \end{aligned}$$

where Q_{reb} is the reboiler duty; n_{CO₂} is the amount of CO₂ removed from flue gas; ΔH_{strip} is the enthalpy of CO₂ desorption; L is the solvent mass flow rate; c_p is the specific heat of the solvent; m_v is the vapour flow rate in stripper; and ΔH_{vap} is the enthalpy of vaporization of water.

Simulations were run in EBSILON with hypothetical solvents that modify each one of the energy sinks. These are the potential solvents considered:

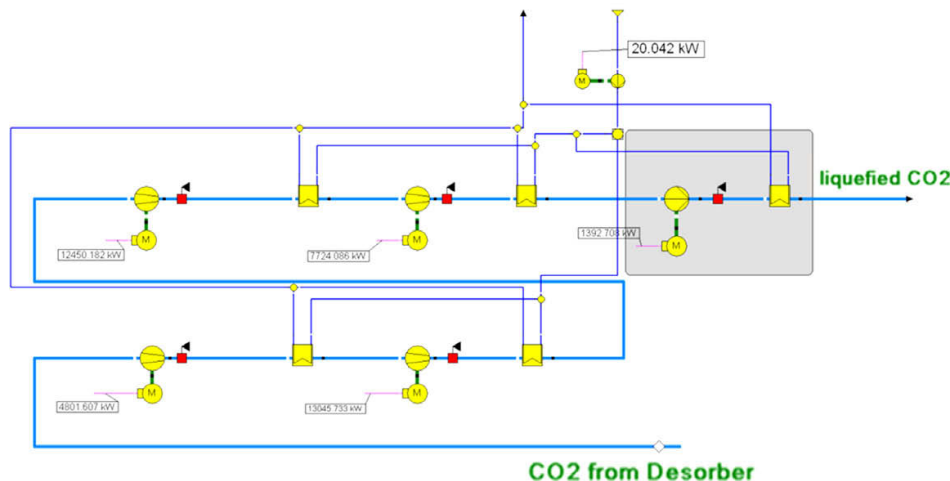


Fig. 7. Modified CO₂ compression process.

- Solvent A, requires a reduced circulating mass flow rate (L) to achieve the absorption. In this case the rich solvent loading is maximised while achieving a leaner amine after regeneration.

That is, the solvent has a better absorption capacity. It diminishes the amount of regenerating steam required, the sensible heat, as well as electrical work.

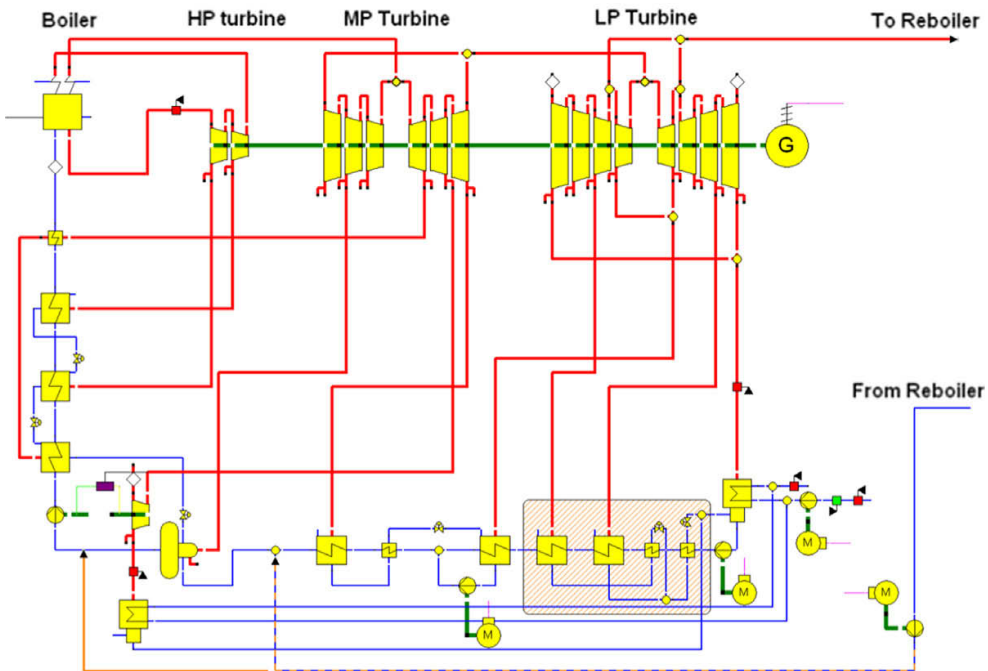


Fig. 8. Changes in the steam cycle with Cases 2 and 3.

Table 5
Results for enhanced solvents.

	MEA	Solvent A	Solvent B	Solvent C	Solvent D
Reboiler duty (MJ/kg CO ₂)	4	3.7	3.3	3.2	2
Plant net efficiency (%) 600 MW Bituminous plant with CO ₂ capture	31	32.5	32.6	32.8	36
Energy penalty (%-points)	14	12.7	12.4	12.2	9

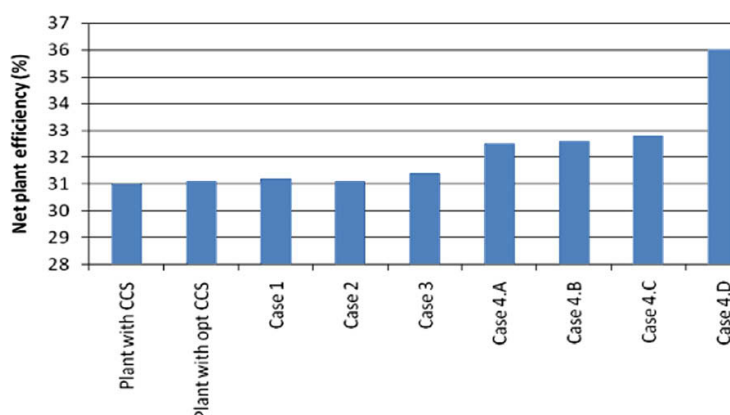


Fig. 9. Overview of efficiency improvement opportunities.

- Solvent B, its desorption enthalpy (ΔH_{strip}) is considered half of that of MEA. It reduces the energy needed for the stripping reaction.
- Solvent C, can be regenerated at a lower temperature. Then the amount of steam needed for regeneration (m_v) drops and thus, besides the reboiler duty, the stripper condenser duty decreases as well.
- Solvent D, is a combination of solvents A, B and C. This solvent has a higher CO₂ absorption capacity and consequently, solvent circulation rates are lower. This lower solvent flow rate combined with the lower heat of reaction results in a lower reboiler steam requirement. In addition, if the regeneration can be performed at lower temperatures, more energy can be saved.

Since all terms of the equation are strongly related, changing one of them would also affect the others. A new, improved formulated solvent would have a combined effect on all three components of the energy for regeneration. The results of the simulations are presented in Table 5.

Simulations of the process with MEA and with the best hypothetical solvent show a difference of 5 percentage points in the plant net efficiency. This optimal solvent should also have other properties, such as appropriate density and viscosity, vapour pressure, heat capacity, chemical and thermal stability, which are important parameters with regard to operational behaviour.

It is important to note that the efficiency gain through heat integration or lower compression work is far from the reduction in efficiency loss that a new solvent would generate, as seen in Fig. 9. The higher efficiency gain for heat integration accounts for up to 0.4%-points, whereas the smallest change in efficiency for a new solvent is already of almost 2%-points. According to these results, it seems to be more promising to search for improved solvents, since they produce a lower energy penalty and therefore, a lower cost of electricity.

6. Conclusions

The simulation of a power plant with an integrated amine based CO₂ capture system and compression step was carried out. The aim was to study the influence of the CO₂ capture process on the power plant performance. Results of the integration have been shown for two case studies: a 600 MW hard coal and a 1000 MW lignite power stations with nominal plant efficiencies of 45% and 49%, respectively. The energy penalty accounts for more than 30% of the power plant net efficiency when the optimal operating conditions for the amine system are considered.

It has been pointed out the influence of the scrubbing process parameters such as column size, solvent mass flow rate, operating pressure and temperature on the power plant cycle. As a result, the energy penalty can be reduced by 1 to 3%-points, if the operating

conditions of the CO₂ system are chosen by taking into account their effects on the power plant performance.

Among the parameters investigated, the operating pressure in the stripper proved to have the strongest influence on the power plant efficiency. However, each parameter affects not only the power plant efficiency but also other factors (pressure drop, energy requirements for auxiliary equipment, plant size...). This parameter interaction has to be taken into account in order to estimate the overall effect of the CO₂ capture process on the power plant. Definitely, economic aspects should always be considered in the selection of the design and operating conditions of the capture system.

In order to further improve the integration of the capture system in the power plant, the heat integration needs to be comprehensive. New optimized solvents with lower energy requirements for regeneration (~ 2 MJ/kg CO₂) could reduce the energy penalty up to 5%-points. Still, these new processes need to be integrated within the power plant and the process parameters have to be chosen according to their effect on the power plant performance.

Acknowledgements

This work was carried out within the project "Flue gas" in collaboration with BASF SE.

The BASF is gratefully acknowledged for their financial and scientific support.

References

- [1] Kohl A, Nielsen R. Gas purification. 5th ed. Gulf Publishing Company, Elsevier; 1997.
- [2] Tobiesen A, Mejell T, Svendsen HF. A comparative study of experimental and modelling performance results from the CASTOR Esbjerg pilot plant. In: Proceedings Eighth conference on greenhouse gas control technologies, Trondheim, Norway, June 19–22, 2006.
- [3] Chapel D, Mariz C, Ernest J. Recovery of CO₂ from flue gases: commercial trends. In: Canadian Society of Chemical Engineers annual meeting, Saskatoon, Saskatchewan, Canada, October 4–6, 1999.
- [4] Göttlicher G. The energetics of carbon dioxide capture in power plants. US Department of Energy (DOE), Office of Fossil Energy, NETL, February 2004.
- [5] Rubin ES, Rao AB. A technical, economic and environmental assessment of amine-based CO₂ capture technology for power plant greenhouse gas control. US Department of Energy (DOE), NETL, October 2002.
- [6] IEA GHG. CO₂ capture ready plants. IEA Greenhouse Gas R&D Programme, 2007/4, May 2007.
- [7] Nexant Inc. Environmental footprints and costs of coal-based integrated gasification combined cycle and pulverized coal technologies. US EPA-430/R-06/006, Environmental Protection Agency, July 2006.
- [8] Schwendig F, Biede O, Ekström C, Feraud A, Franco F, Haupt G, et al. Power systems evaluation and benchmarking. ENCAP WP 1.2, Deliverable D 1.2.4, Public version; February, 2008.
- [9] Asprion N. Non-equilibrium rate-based simulation of reactive systems: simulation model, heat transfer, and influence of film discretization. Ind Eng Chem Res 2006;45:2054–69.
- [10] Freguia, Rochelle. Modeling of CO₂ capture by aqueous monoethanolamine. AIChE J 2003;49(7):1676–86.

Publication V

Removal of carbon dioxide from flue gases with aqueous MEA solution containing ethanol

doi: 10.1016/j.cep.2013.11.004



Contents lists available at ScienceDirect

Chemical Engineering and Processing: Process Intensification

journal homepage: www.elsevier.com/locate/cep

Removal of carbon dioxide from flue gases with aqueous MEA solution containing ethanol



Inga von Harbou^{a,1}, Sebastian Hoch^{a,2}, Hari Prasad Mangalapally^{a,3}, Ralf Notz^b,
Georg Sieder^b, Hugo Garcia^b, Oliver Spuhl^b, Hans Hasse^{a,*}

^a Laboratory of Engineering Thermodynamics, University of Kaiserslautern, Germany^b BASF SE, Ludwigshafen, Germany

ARTICLE INFO

Article history:

Received 20 May 2013

Received in revised form 7 November 2013

Accepted 9 November 2013

Available online 19 November 2013

Keywords:

CO₂ capture

Reactive absorption

Novel solvents

Non-aqueous amine solvent

ABSTRACT

Adding ethanol to an aqueous amine solution offers several advantages for post-combustion CO₂ capture. The equilibrium isotherms at higher temperatures shift towards lower loadings, leading to an easier desorption. At constant temperature in the desorber bottom, the desorber pressure is increased, leading to energy savings in the CO₂ compression. Alternatively, at constant desorber pressure, the temperature in the desorber bottom is decreased, leading to a smaller efficiency drop of the power plant. Furthermore, the absorption rate of CO₂ is enhanced by adding ethanol. In the present work, the potential of using ethanol as a co-solvent for a 0.3 g/g aqueous monoethanolamine (MEA) solution is assessed based on simulations with an equilibrium stage model. A major drawback is the volatility of ethanol. The recovery of ethanol can be achieved using a water scrubber and subsequent stripping. The recovered ethanol vapor is sent directly to the desorber for heat integration. The process with ethanol recovery results in an increased complexity of the capture plant, difficulties in controlling the water balance and higher investment costs and offers, if any, only a moderate energetic advantage. The process concept could, however, be used for other co-solvents with similar properties as ethanol but lower vapor pressures.

© 2013 Elsevier B.V. All rights reserved.

1. Introduction

Carbon capture and storage (CCS) technologies are currently being developed that separate CO₂ from large point sources, e.g. power plants, and store it underground. For post-combustion capture (PCC), reactive absorption with aqueous amine solutions is state-of-the-art. The process with the standard solvent, an aqueous solution of monoethanolamine (MEA), has a high energy demand for regeneration which leads to a significant drop in the power plant efficiency.

Adding ethanol to an aqueous MEA solution shifts the equilibrium isotherms at high temperature to lower loadings, and thus facilitates the desorption of CO₂. The resulting increase of the cyclic capacity (distance between the equilibrium isotherms at absorber and desorber conditions) is expected to significantly reduce the

optimum solvent flow rate. Also, the regeneration energy demand is expected to drop.

The properties of non-aqueous solutions of amines have been discussed in the literature before [1–9]. Mixtures of a physical solvent and a chemical solvent, also called hybrid solvents, are already applied for CO₂ absorption in applications where the CO₂ partial pressure is higher than in PCC, especially in natural gas treatment. Hybrid solvents combine the advantages of physical solvents, that is a high physical solubility of the sour gas and low regeneration energies, with the advantages of chemical solvents, that is a high capacity. One example is Lurgis Amisol® process which uses a mixture of methanol and methyl diethanolamine (MDEA) or diethylamine (DEA) as solvent.

Henni and Mather [1] measured the solubility of CO₂ in aqueous solutions of methanol and MDEA at 40 °C and 120 °C and found a decrease in the solubility with increasing methanol content at low CO₂ partial pressures. This was attributed to the fact that the formation of ions, which are products of the reaction of CO₂ with the amine solution, is favored in solvents with high dielectric constants, that is a high polarity. Hamborg et al. [3] recently discussed the advantages of mixing alcohols to aqueous amine solutions used for PCC. They measured the dissociation constants (pK_a) of MDEA and MEA in aqueous solutions at different methanol, ethanol and *t*-butanol concentrations [10], and the effect of alcohol concentration

* Corresponding author at: Laboratory of Engineering Thermodynamics, Erwin-Schrödinger-Straße 44, 67663 Kaiserslautern, Germany. Tel.: +49 631 205 3497; fax: +49 631 205 3835.

E-mail address: hans.hasse@mv.uni-kl.de (H. Hasse).

¹ Present address: BASF SE, Ludwigshafen, Germany.

² Present address: Bayer Technology Services, Leverkusen, Germany.

³ Present address: Evonik Industries, Hanau, Germany.

on the initial mass transfer rates and the solubility of CO₂. It was found that the pK_a values were reduced significantly upon addition of the alcohol. The largest reduction was observed for methanol, the smallest for t-butanol. The initial mass transfer rates were found to increase upon addition of the alcohol. The solubility of CO₂ was only measured at 25 °C and was found to decrease upon addition of alcohol. In Patent WO 2010/113134 [11], it is suggested to add low polarity solvents to the absorber (to enhance the kinetics) and/or to the desorber (to enhance the desorption) or to apply an electrical field or electromagnetic waves, all with the purpose of changing the dielectric constant of the solvent. Sada et al. [4] studied the kinetics of the reaction of CO₂ with ethanalamines in non-aqueous solvents. Different apparent reaction orders with respect to MEA were found in different solvents. The reaction order was 1.0 for MEA in pure water, 1.7 for MEA in ethanol and 1.9 for MEA in 2-propanol. This variation of the reaction order was explained in terms of a reaction scheme via a zwitterion. Usubharatana and Tontiwachwuthikul [5] report on the increased overall mass transfer kinetics of CO₂ in a solution of MEA in methanol compared to MEA in water. They observed a lowered kinetic rate constant and a higher reaction order with increasing methanol fraction.

Besides the change in CO₂ solubility and kinetics, another advantage of replacing some of the water by a more volatile substance such as ethanol is that the boiling temperature of the system is lowered. Thus, the steam for heating the reboiler in the desorber can be extracted from the power plant at a lower pressure which will lead to a lower reduction of the overall efficiency of the power plant. Alternatively, at a fixed temperature in the desorber bottom, the pressure in the desorber increases. This higher pressure is an advantage because it lowers the energy required for CO₂ compression. Furthermore, ethanol has a lower enthalpy of vaporization than water (35.5 kJ/mol vs. 39.8 kJ/mol at 120 °C [12]) and thus stripping steam can be produced at a lower energetic cost.

A major and obvious drawback of using a volatile co-solvent like methanol or ethanol in the PCC process is its loss via off gas, especially in the absorber. For economical and environmental reasons, measures have to be taken to reduce this loss. Therefore, in the present work a concept for the recovery of the co-solvent is developed and a feasibility study for the resulting PCC process is carried out. Monoethanolamine (MEA) and ethanol are taken as examples for the amine and the co-solvent, respectively, but it is anticipated that similar effects will occur for combinations of other amines and other co-solvents with low polarity. The results of the present study have led to a patent application [13].

2. Solvent system MEA + ethanol + water

In order to estimate the performance of the absorption–desorption process using a mixture of monoethanolamine (MEA), ethanol and water as solvent, simulations are carried out with an equilibrium stage model in Aspen Plus™ (Version 7.3). For modeling the system MEA + water + CO₂, an existing model from the Aspen Plus example library [14] is used. In that model, the non-ideality of the liquid phase is described by the electrolyte-NRTL model with parameters from Austgen et al. [15] and the gas phase is described by the Redlich–Kwong equation of state. The Henry constant of CO₂ in pure water is used. For modeling the system MEA + ethanol + water + CO₂, binary NRTL-parameters between ethanol–water and ethanol–MEA and the Henry constant of CO₂ in ethanol from the Aspen databases VLE-RK and Henry-AP, respectively, are added to the existing model in the present work. The Henry constant of CO₂ in the solvent mixture is calculated from the Henry constants of CO₂ in the pure solvents (water and ethanol) by weighting with a factor containing the mole fractions in the (gas-free) solvent and the

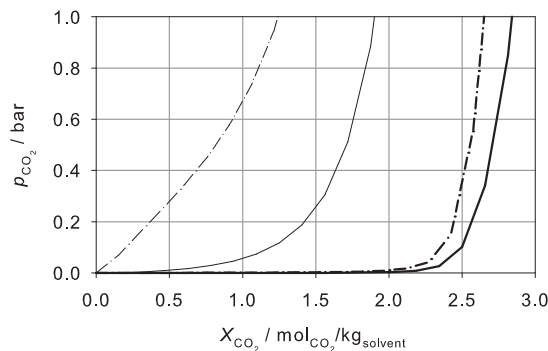


Fig. 1. Predicted solubility of CO₂ in an aqueous solution of 0.3 g/g MEA without ethanol (—) and with 0.35 g/g ethanol (---) at 40 °C (bold) and 120 °C (thin).

pure solvent critical volume.⁴ For details, see [16]. It is assumed that ethanol is an inert component that does not react with the other components and the autoprotolysis of ethanol is neglected. The reaction equilibrium constants remain unchanged, although it is known that the equilibrium constant of the MEA deprotonation changes upon addition of ethanol [10]. As the equilibrium isotherms are fairly well described by this preliminary model (see below), we did not undertake the major task of developing a validated physico-chemical model for the complex mixture studied here. Rather, we use the preliminary model for a process study that aims at an assessment of the possible benefits of adding ethanol to an aqueous MEA solution for PCC.

2.1. Equilibrium isotherms

Fig. 1 shows the solubility of CO₂ in aqueous solutions of MEA (0.3 g/g MEA) and in aqueous solutions of MEA containing ethanol (0.3 g/g MEA and 0.35 g/g ethanol) at 40 °C and 120 °C as predicted by the preliminary model described above. Upon addition of ethanol, the equilibrium isotherms shift to lower loadings, both at 40 °C and 120 °C. This shift is, however, much larger at 120 °C, leading to a larger distance between the equilibrium isotherms at absorber and desorber conditions, i.e. a larger cyclic capacity. This is expected to reduce the optimum circulated flow rate and thus the energy requirement in the desorber [17]. Gas solubility measurements at BASF SE verified the significant decrease of the CO₂ solubility upon ethanol addition at high temperatures. From the measurements, an estimate for the cyclic capacity ΔX_{CO_2} of the solvent was obtained using the difference between the equilibrium loading at 40 °C and a CO₂ partial pressure of 130 mbar (approximate rich loading) and the equilibrium loading at 120 °C and a CO₂ partial pressure of 100 mbar (approximate lean loading). In Table 1, the estimates for the cyclic capacity ΔX_{CO_2} are given both for the experiments at BASF SE and for the Aspen model. The relative deviations are of the order of 10% and hence acceptable for the purpose of the present study which focusses on conceptual process design.

2.2. Kinetics

Besides gas solubility, the kinetics of CO₂ absorption are also important for an economic operation of the absorption–desorption process since they determine the height of the columns and thus the investment costs. To study the effect of ethanol addition on the kinetics of the system, BASF SE carried out experiments in a double

⁴ The default exponent of 2/3 is used for the pure solvent critical volume.

Table 1

Estimates for the cyclic capacity ΔX_{CO_2} in an aqueous solution of 0.3 g/g MEA without ethanol (reference case) and with 0.35 g/g ethanol from the Aspen model compared to experimental data [22].

$x_{\text{EOH}}^{(m)}$ (g/g)	ΔX_{CO_2} experiment (mol $_{\text{CO}_2}$ /kg $_{\text{solvent}}$)	ΔX_{CO_2} model (mol $_{\text{CO}_2}$ /kg $_{\text{solvent}}$)	rel. dev. (%)
0.00	1.65	1.44	-13
0.35	2.35	2.18	-7

Table 2

Flue gas conditions for the reference brown coal power plant considered in the present study.

\dot{m}_G (t/h)	t (°C)	p (bar)	y_{CO_2} (mol/mol)	$y_{\text{H}_2\text{O}}$ (mol/mol)	y_{N_2} (mol/mol)
3600	40	1	0.140	0.073	0.787

stirred cell reactor. In the experiments, the overall absorption rate is measured which is the sum of the reaction kinetics and the physical mass transfer kinetics. The stirred cell was thermostatted at 50 °C and operated at a pressure of 50 hPa abs so that the partial pressure of CO₂ in the gas phase was almost constant. More details on the experimental set-up can be found in Garcia et al. [13]. The absorption rate was determined from the amount of CO₂ that had to be added to keep the pressure constant. At the beginning of the experiment, the liquid was unloaded. As expected, the absorption rate decreased with increasing loading of the liquid phase. An average absorption rate was calculated from the results corresponding to liquid loadings which are 75%, 50% and 20% of the equilibrium loading (for which the absorption rate would be zero). For an aqueous solution containing 0.3 g/g MEA, the absorption rate was 91% higher in the presence of 0.35 g/g ethanol than without ethanol. An increase in the absorption rate was also observed for other solvents [13]. This rate enhancing effect of alcohol addition is of special interest for slow amine solvents.

Based on the physico-chemical property data, adding a volatile co-solvent like ethanol to an aqueous amine solution seems very promising. The volatility is, however, a disadvantage and the loss of co-solvent needs to be controlled. Therefore, simulations were carried out with the preliminary model described above. Note again that the preliminary model describes the solvent system only crudely so that only qualitative conclusions are possible. In Section 3, results of simulations are described which were carried out to investigate the combined effects of ethanol addition on the energy performance of the absorption–desorption process. In Section 4, the recovery of ethanol from the absorber offgas using a water scrubber is discussed.

3. Absorption–desorption process with ethanol

For the simulation study, a 1000 MW brown coal power plant is taken as reference case. The flue gas conditions are shown in Table 2. An equilibrium stage model is used in this conceptual study to represent both absorber and desorber in order to determine the minimum regeneration energy, that is only very high columns are considered. The positive effect of the addition of ethanol on the overall absorption rate of the solvent is therefore not considered in the simulations. It should be kept in mind that the enhanced kinetics offer another important advantage of adding ethanol to amine solutions.

3.1. Desorber simulation

At first, only the desorber is considered. The flow sheet of the desorber simulation, consisting of a desorber column with a reboiler, a water scrubber and a condenser, is shown in Fig. 2. The condensate, consisting of ethanol and water, is recycled back to Scrubber I. The desorber pressure is adjusted so that the bottom temperature in the desorber is fixed to 120 °C (at

higher temperatures, the degradation rate of MEA significantly increases). The CO₂-free mass fraction of MEA in the rich solvent (S1) is $x_{\text{MEA}}^{(m)} = 0.3$ g/g and the CO₂-free mass fraction of ethanol is $x_{\text{EOH}}^{(m)} = 0.35$ g/g or zero for the reference case for which no ethanol is present in the solvent. The rich solvent (S1) is loaded with 0.5 mol CO₂/mol MEA (2.46 mol CO₂/kg solvent) which is close to the equilibrium loading at 40 °C and a partial pressure of CO₂ of $p_{\text{CO}_2} = 140$ mbar. The CO₂ mass flow at the desorber top (S3) is fixed to 90% of the CO₂ mass flow in the flue gas entering the absorber (see Table 2) by adjusting the reboiler duty (\dot{Q}_{des}). The solvent flow rate (S1) is varied in order to find the minimum reboiler duty. Further details on the desorber simulation are given in Appendix A.1.

In Fig. 3, the specific reboiler duty of the desorber q_{des} is shown as a function of the L/G ratio. The L/G ratio is the mass flow of the lean solvent (S2) divided by the mass flow of the flue gas, cf. Table 2. The specific reboiler duty q_{des} is the reboiler duty \dot{Q}_{des} divided by the mass flow of captured CO₂, i.e. here the CO₂ mass flow in the top stream leaving the condenser (S3). For the aqueous MEA solution without ethanol, the typical curve with a distinct optimum in the specific reboiler duty is observed, compare e.g. Mangalapally and Hasse [18]. The increase to the left of the minimum is related to the high amount of stripping steam required to fulfill the increasingly difficult separation task in the desorber. The almost linear increase in the specific reboiler duty to the right of the minimum is due to the

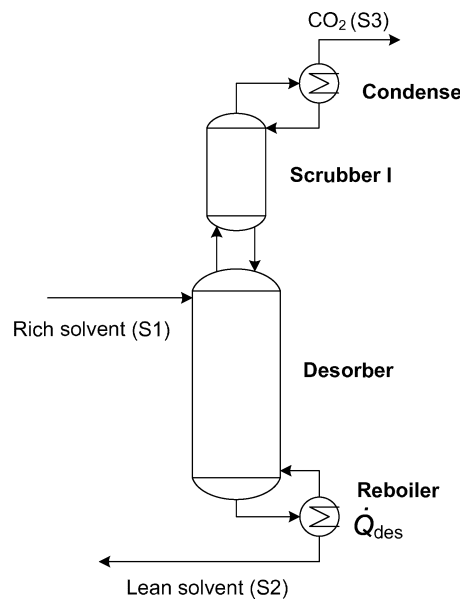


Fig. 2. Flow sheet of the desorber simulation.

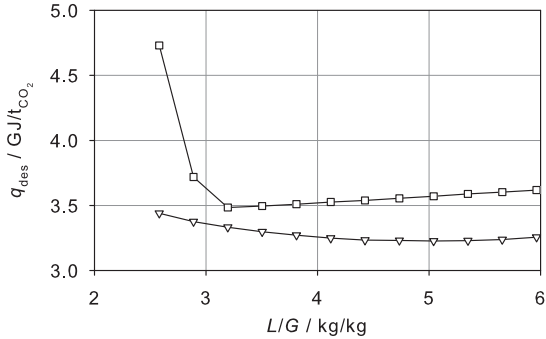


Fig. 3. Specific reboiler duty q_{des} from the desorber simulation as a function of L/G ratio for an aqueous solution of 0.3 g/g MEA without ethanol (□) and with 0.35 g/g ethanol (▽). The temperature at the desorber bottom is fixed to 120 °C. The lines are guides for the eye.

energy requirement to heat up the solvent to desorber temperature [18,17]. With a mass fraction of 0.35 g/g ethanol in the unloaded solvent, the specific reboiler duty decreases as expected compared to the aqueous solution without ethanol. Interestingly, the optimum in the reboiler duty is not so pronounced and the optimum solvent flow rate shifts towards higher values. From the estimates of the cyclic capacity based on the equilibrium curves, lower values for the optimum solvent flow rate were expected. The pressure in the desorber increases (at constant temperature in the desorber bottom) upon addition of the volatile co-solvent ethanol as shown in Fig. 4. This means that when estimating the cyclic capacity from the equilibrium isotherms, the 120 °C isotherm for the desorber has to be evaluated at a higher partial pressure of CO₂ and as it can be seen in Fig. 1, this leads to a reduction of the cyclic capacity. The increased pressure in the desorber is thus disadvantageous for the desorption of CO₂ but it reduces the energy for CO₂ compression significantly. The ethanol mass fraction in the separated CO₂ stream after the condenser (S3) is about 0.03 g/g. Measures to reduce the ethanol content might be necessary prior to compression.

3.2. Absorber–desorber simulation

In the next step, the absorber was considered as well. A flow sheet of the absorption–desorption process is shown in Fig. 5. The flue gas (S4) enters the absorber at the bottom. The lean

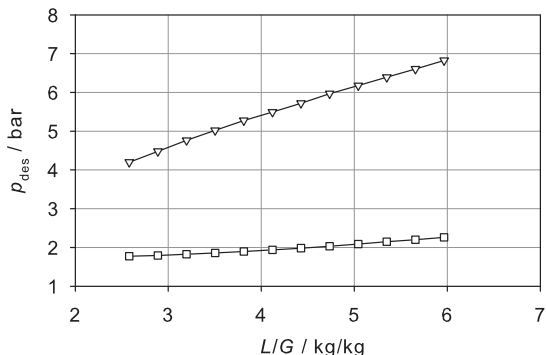


Fig. 4. Desorber pressure from the desorber simulation as a function of L/G ratio for an aqueous solution of 0.3 g/g MEA without ethanol (□) and with 0.35 g/g ethanol (▽). The temperature at the desorber bottom is fixed to 120 °C. The lines are guides for the eye.

solvent from the desorber bottom (S2) is cooled in the rich-lean heat exchanger HX-1 and the additional heat exchanger HX-2 and then introduced to the absorber top. The rich solvent at the absorber bottom (S1) is heated by the hot lean solvent (S2) in HX-1 before it is introduced to the desorber. The ethanol loss through the absorber offgas (S5) is significant and the ethanol has to be recovered and is reintroduced to the process. As ethanol losses in the absorber pose a problem, the make-up ethanol is supplied to the desorber. The make-up ethanol is supplied as a gas to the desorber bottom to enhance the stripping. The ethanol recovery described in Section 4 also yields gaseous ethanol. The energy needed for the evaporation of the ethanol \dot{Q}_{evap} is accounted for together with the reboiler duty \dot{Q}_{des} . For the absorber–desorber simulation, the ethanol make-up (S6) is simply reintroduced as liquid ethanol (at the same temperature as the rich solvent S1 at the desorber inlet) and evaporated at desorber pressure. The heat duty \dot{Q}_{evap} of the ethanol evaporator is a minimum estimate of the heat duty of the recovery process. Further details on the absorber–desorber simulation are given in Appendix A.2.

For the absorber–desorber simulation, two cases, Case A and Case B, were considered. In Case A, the bottom temperature in the desorber is fixed to 120 °C as for the desorber simulation, see Section 3.1. The fixed temperature leads to an increase in the desorber pressure upon ethanol addition. This results in a significant reduction of the energy needed for CO₂ compression. In Case B, the desorber pressure is fixed to 2 bar (typical desorber pressure), leading to a decrease in the bottom temperature in the desorber upon ethanol addition. This means that lower quality steam from the power plant is acceptable for heating the reboiler.

In order to evaluate the process taking into account the different pressure and temperature levels, the concept of specific lost work w_{lost} is used. The specific lost work w_{lost} of the power plant is calculated from the specific work that is required for compression w_{comp} and the loss of specific work in the power plant turbines due to steam extraction w_{steam} , see Eq. (1). For w_{comp} , correlations derived by Liebenthal et al. [19] are employed, for details see Appendix B. w_{steam} is estimated using the Carnot factor as suggested by Freguia and Rochelle [20] with a temperature difference in the reboiler of $\Delta T = 10$ K and a sink temperature of $T_{sink} = 313$ K, see Eq. (2). The obtained results for w_{steam} are similar to those using the correlation for w_{steam} of Liebenthal et al. [19] which was derived from detailed power plant models in EBSILON Professional™.

$$w_{lost} = w_{comp} + w_{steam} \quad (1)$$

$$w_{steam} = q_{des} \cdot \eta_{carnot} = q_{des} \cdot \left(1 - \frac{T_{sink}}{T_{des} + \Delta T} \right) \quad (2)$$

In Fig. 6(a) and (b), the specific lost work w_{lost} is shown as a function of the L/G ratio for Case A and Case B, respectively. For both cases, w_{lost} is reduced by about 10 % when ethanol is added. Case B is slightly more advantageous than Case A.

In Fig. 7, the absorber bottom temperature $t_{abs,bottom}$ is plotted over the L/G ratio for Case A with and without ethanol. The result for Case B is similar and not shown here. The evaporation of ethanol leads to a cooling of the absorber. This is advantageous because the equilibrium CO₂ loading at the absorber bottom increases with decreasing temperature. With ethanol, the rich/lean loading is 0.52/0.27 mol CO₂/mol MEA (2.55/1.33 mol CO₂/kg solvent) compared to 0.50/0.21 mol CO₂/mol MEA (2.46/1.03 mol CO₂/kg solvent) without ethanol. Thus, the slight shift of the equilibrium isotherms to lower loadings upon ethanol addition, cf. Fig. 1, is compensated by the temperature decrease through ethanol evaporation.

A further advantage of the reduced temperature in the absorber is that no additional cooler (HX-2) after the rich-lean heat exchanger (HX-1) is necessary, cf. Fig. 5. The slower kinetics at

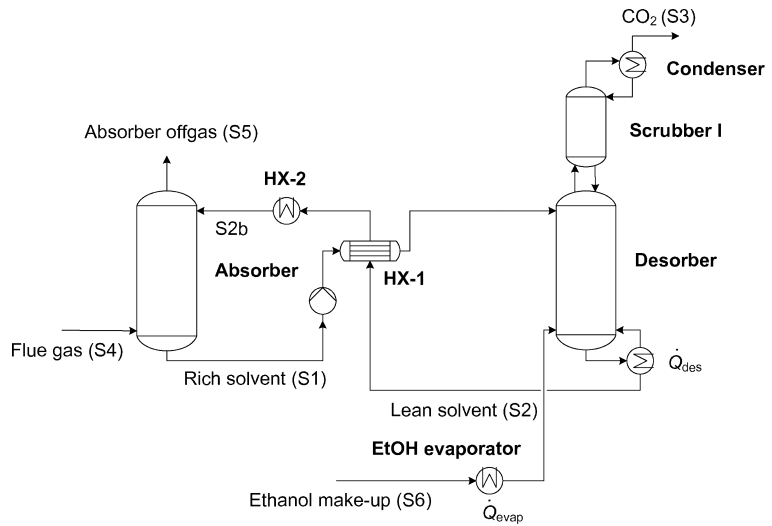
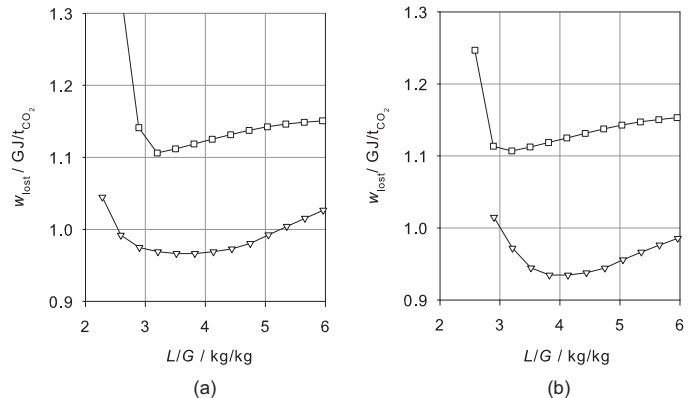
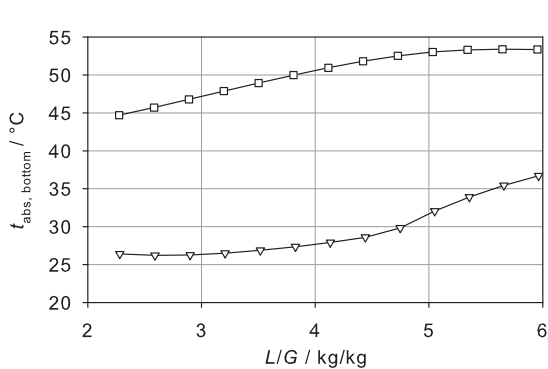
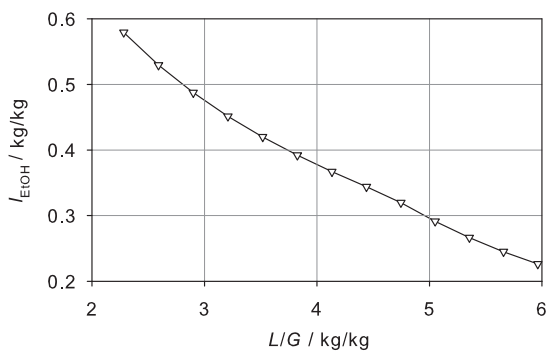


Fig. 5. Flow sheet of the absorption-desorption process.

Fig. 6. Specific lost work w_{lost} from the absorber-desorber simulation as a function of L/G ratio for an aqueous solution of 0.3 g/g MEA without ethanol (□) and with 0.35 g/g ethanol (▽); (a) Case A, (b) Case B. The lines are guides for the eye.Fig. 7. Temperature in absorber bottom $t_{abs,bottom}$ for Case A as a function of L/G ratio for an aqueous solution of 0.3 g/g MEA without ethanol (□) and with 0.35 g/g ethanol (▽). The lines are guides for the eye.Fig. 8. Specific ethanol loss l_{EtOH} (mass flow of ethanol through the absorber offgas (S5) related to the total ethanol mass flow at the absorber inlet (S2b)) as a function of L/G ratio for Case A with an aqueous solution of 0.3 g/g MEA and 0.35 g/g ethanol (▽). The line is a guide for the eye.

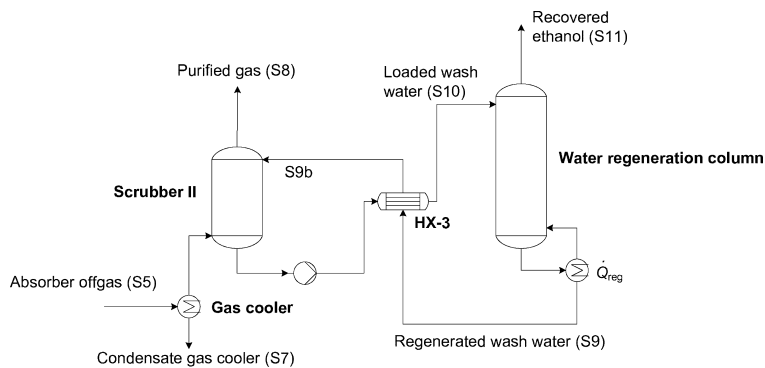


Fig. 9. Flow sheet of the ethanol recovery process.

lower temperatures are a potential disadvantage. Since the aqueous MEA solution with 0.35 g/g ethanol has a significantly faster overall absorption rate compared to the aqueous MEA solution without ethanol, cf. [Section 2.2](#), this is not considered to be a problem.

In [Fig. 8](#), the specific ethanol loss through the absorber offgas is shown as a function of the L/G ratio for Case A. Again, the results for Case B are similar and are not shown here. The specific ethanol loss l_{EtOH} is defined as the ratio of the ethanol mass flow through the absorber offgas (S5) related to the ethanol mass flow at the absorber inlet (S2b). The specific ethanol loss is very high, ranging from 20% to 60%. It decreases almost linearly with the L/G ratio. The absolute mass flow of ethanol through the absorber offgas is almost independent of the L/G ratio. The ethanol loss is problematic for two reasons. First, the outlet gases have to fulfill exhaust gas limits, e.g. the German air pollution control regulation TA Luft [\[21\]](#). Second, the lost ethanol has to be reintroduced into the desorber.

4. Ethanol recovery

Several possibilities exist to remove ethanol from a gaseous stream, e.g. condensation, absorption (with water or other solvents), adsorption or membrane separation. In the present work, only condensation and absorption are evaluated. The cooling temperature necessary to achieve TA Luft specifications⁵ only through condensation of the ethanol can be estimated from the vapor pressure curve of pure ethanol and is about -60°C which is economically unacceptable. A gas cooler can, however, be used in combination with absorption. Here, three cases are considered: absorption without cooling of the absorber offgas, and after cooling of the absorber offgas to 40°C and 30°C . Water is chosen as the absorbent. Preliminary simulations with another absorbent (monoethylene glycol) showed no improvement over the absorption with water which is already present in the process and is therefore the preferred solvent.

To avoid the losses in the absorber when using a volatile co-solvent, Hamborg et al. [\[3\]](#) suggested to separate the co-solvent (here ethanol) from the lean solvent behind the desorber (e.g. by distillation, pervaporation, liquid phase-split, or any other separation process) and directly reintroduce it to the desorber such that the solvent in the absorber contains no co-solvent. This concept was not evaluated in the present work. For the case of ethanol, however, a simple distillative separation of ethanol from the lean solvent is only possible up to the azeotropic concentration. Thus, either a

more complex separation would be required or additional measures to limit the ethanol loss through the absorber offgas would have to be taken.

A flow sheet of the ethanol recovery process considered in the present work is shown in [Fig. 9](#). Note that the recovery process resembles the absorption-desorption process shown in [Fig. 5](#). The absorber offgas (S5) from the optimum of Case A is used for the investigation of the ethanol recovery section. The absorber offgas from the optimum of Case B is similar. The absorber offgas is either introduced directly to Scrubber II or first cooled to 40°C or 30°C in a gas cooler. As an alternative to a gas cooler, interstage cooling in the absorber could be used. Ethanol is separated from the loaded wash water (S10) in a water regeneration column and reintroduced to the absorption-desorption process (S11). The regenerated wash water (S9) is returned back to Scrubber II. Stream S11, consisting of the recovered ethanol and water, is sent directly to the desorber without previous condensation. The vapor then serves as stripping steam in the desorber and reduces the reboiler duty \dot{Q}_{des} of the desorber. In the simulations, the concentration of ethanol in the purified gas (S8) is fixed to TA Luft specification [\[21\]](#) by adjusting the reboiler duty \dot{Q}_{reg} of the water regeneration column. Details on the simulation of the ethanol recovery section are given in [Appendix A.3](#).

In [Fig. 10](#), the specific reboiler duty for water regeneration \dot{q}_{reg} is shown as a function of the L_w/G ratio. The L_w/G ratio is the mass flow of wash water at the inlet of Scrubber II (S9b) divided by the mass flow of the flue gas (S4). The specific reboiler duty of the water

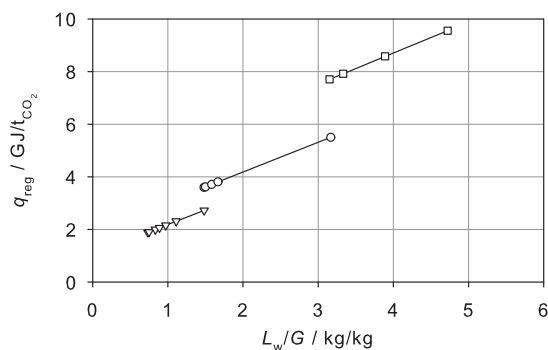


Fig. 10. Specific reboiler duty of the water regeneration column \dot{q}_{reg} (related to the CO_2 stream separated in the absorption-desorption process) as a function of L_w/G ratio (mass flow of wash water (S11) divided by flue gas flow (S4)) for the optimum of Case A with 0.35 g/g ethanol: no cooling of absorber offgas (\square), cooling to 40°C (\circ) and cooling to 30°C (\triangledown). The lines are guides for the eye.

⁵ According to the German air pollution control regulation TA Luft [\[21\]](#), the maximum allowable concentration for organic substances is 50 mg C/m³ dry gas at norm conditions ($T^0 = 273.15 \text{ K}$; $p^0 = 101.3 \text{ kPa}$), corresponding to 95.8 mg ethanol/m³.

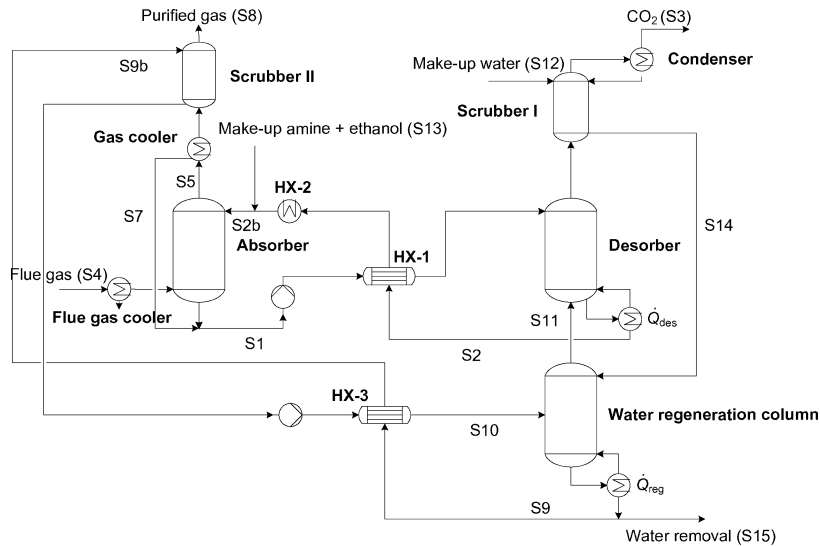


Fig. 11. Flow sheet of the absorption–desorption process with integrated ethanol recovery.

regeneration \dot{q}_{reg} is the reboiler duty \dot{Q}_{reg} of the water regeneration column divided by the mass flow of CO_2 separated in the absorption–desorption process (S3). Three cases are studied: without cooling of the absorber offgas, with cooling to 40 °C and with cooling to 30 °C. In all cases, \dot{q}_{reg} decreases linearly with decreasing L_w/G ratio until a lower bound in the L_w/G ratio is reached, corresponding to a minimum \dot{q}_{reg} . The ethanol concentration in the wash water (S9) is practically zero at this point. For lower L_w/G ratios, the emissions of ethanol are always above the target of TA Luft. For the case without gas cooling and cooling to 40 °C, the minimum for \dot{q}_{reg} is 7.7 GJ/t CO_2 and 3.6 GJ/t CO_2 , respectively, and, hence, above the specific reboiler duty \dot{q}_{des} of the absorption–desorption process without ethanol addition (3.4 GJ/t CO_2). For the case of cooling to 30 °C, the minimum for \dot{q}_{reg} is 1.9 GJ/t CO_2 and, hence, lower than the specific reboiler duty \dot{q}_{des} of the reference process. For this case, the minimum L_w/G ratio is 0.73 kg/kg and, hence, by a factor of 5 below the L/G ratio of the absorption–desorption process.

5. Integration of absorption–desorption process and ethanol recovery

A flow sheet of the complete process with ethanol recovery is given in Fig. 11. The water balances of the ethanol recovery section and the absorption–desorption process have to be controlled in order to achieve steady-state operation. In the absorption–desorption process without ethanol addition, the water balance is typically controlled by adjusting the temperature of the flue gas outlet, adjusting the temperature of the flue gas inlet, and/or adding fresh water or removing water from the condenser. In the process with ethanol, however, the degrees of freedom for controlling the water balance are reduced. The temperature of the flue gas outlet (S5) has to be kept to a minimum as otherwise the amount of wash water (S9) and thus the energy of the ethanol recovery process is greatly increased, as discussed in Section 4. Furthermore, the condensate at the desorber top contains mainly ethanol ($x_{\text{H}_2\text{O}}^{(\text{m})} \approx 0.1 \text{ g/g}$) and thus cannot be used for removing pure water. The water balance is further complicated as a large amount of water leaves the ethanol recovery section

together with the recovered ethanol (S11) and is introduced to the absorption–desorption process.

In order to close the water balance, the stream S14 from the bottom of Scrubber I in the absorption–desorption process is fed to the ethanol recovery section. All other liquid streams contain MEA and, hence, should not be introduced into the ethanol recovery section. In the flow sheet in Fig. 11, the stream S14 is supplied to the water regeneration column and used as reflux. A rectifying section is added to the water regeneration column. Compared to a simple stripping column, this leads to a higher ethanol concentration and a lower water concentration in stream S11.

The condensate from the gas cooler (S7) is rich in ethanol and should not be recycled to the absorber top. Instead, it is mixed with the rich solvent. Make-up water (S12) can, if necessary, be added to the process at the top of Scrubber I where it also serves for removing ethanol. At the bottom of the water regeneration column (S15), almost pure water can be withdrawn from the overall process if necessary.

For the simulation of the integrated process, the simulation of the absorption–desorption process and the simulation of the ethanol recovery section as described in Section 3.2 and Section 4 are coupled. Further details on the simulation of the integrated process are given in Appendix A.4.

The integrated process is simulated for Case A with a gas cooler temperature of 30 °C. No optimization of the integrated process is carried out. The specific lost work is increased to 1.19 GJ/t CO_2 compared to 0.97 GJ/t CO_2 in the absorber–desorber simulation. The specific lost work is, hence, higher than that of the reference process without ethanol (1.11 GJ/t CO_2). There are two main reasons for the energy penalty of the ethanol recovery process. First, the temperature at the bottom of the water regeneration column is higher than the temperature at the desorber bottom (157 °C versus 120 °C), leading to an increase in the specific lost work due to steam extraction w_{steam} . Second, a significant part of the energy of the water regeneration column \dot{Q}_{reg} is needed to heat the subcooled feed (S10) to the water regeneration column. This penalty could be reduced by increasing the area of heat exchanger HX-3 and further heat integration ($w_{\text{lost}} = 1.05 \text{ GJ/t CO}_2$ for the ideal case of $T_{10} = T_9$).

In the simulations, the water balance was not completely closed (cf. Appendix A.4). This is not only due to numerical problems but

also due to physical constraints. The water balance of the integrated process can only be closed for a narrow range of operating conditions (operation window). The operation window depends on many parameters, the most important of which are the temperatures of the flue gas and the gas cooler, the concentration of water in stream S11 at the top of the water regeneration column and the amount of water in stream S14 which is recycled to the ethanol recovery section. Furthermore, the window strongly depends on the chosen ethanol concentration in the solvent (here 0.35 g/g). The concentration at the top of the water regeneration column (S11) is limited by the azeotropic concentration. As the overall incentives for a realization of the process with ethanol are low, no attempt was made to close the simulation and discuss a design point.

From the discussions above, it is evident that the process with ethanol has a significantly increased complexity, especially regarding the control of the water balance. It has furthermore higher investment costs and a higher cooling duty and only a moderate, if any, energetic advantage. Through further energy integration and other optimizations, the energy performance could be improved, again with the disadvantage of increased investment costs. One possible optimization would be to operate the water regeneration column at a pressure lower than the desorber pressure and to compress the recovered ethanol (S11) to desorber pressure. This would have the advantage of lower temperatures in the bottom of the water regeneration column and thus lower quality steam could be used. The electric energy for the compression of the recovered ethanol, however, would have to be considered as well.

6. Conclusions

In the present work, a concept for a PCC process with an aqueous MEA solution containing ethanol as a co-solvent was developed. Adding ethanol to an aqueous MEA solution reduces the reboiler duty of the absorption–desorption process and offers the advantage of higher pressures or alternatively lower temperatures in the desorber, both leading to similar savings in the specific lost work. The absorption rate of CO₂ is also increased with the addition of ethanol, leading to smaller column heights. The loss of ethanol through the absorber top is, however, very large and the ethanol needs to be recovered. The recovery of ethanol is feasible using a simple water scrubber and a water regeneration column to regenerate the wash water and separate the ethanol. By introducing the recovered ethanol directly into the desorber bottom, the energy input of the recovery process is (partly) utilized in the desorber.

The complexity of the process with ethanol is greatly increased, especially regarding the control of the water balances during process operation. Additionally, the investment costs and the cooling duty of the process with ethanol are significantly increased. Overall, the process with ethanol shows only moderate, if any, energetic advantages over the reference case without ethanol. The suggested process seems thus unfavorable with ethanol as the co-solvent. The process concept could, however, be of interest for other water soluble organic compounds with a low dielectric constant and a lower boiling temperature than water. Possible compounds include higher alcohols, ethers and ketones.

Appendix A. Simulation details

A.1. Desorber simulation

The flow sheet of the desorber simulation is shown in Fig. 2. The CO₂-free mass fraction of MEA in the rich solvent (S1) is $x_{\text{MEA}}^{(m)} = 0.3 \text{ g/g}$ and the CO₂-free mass fraction of ethanol is $x_{\text{EtOH}}^{(m)} = 0.0 \text{ g/g}$ or $x_{\text{EtOH}}^{(m)} = 0.35 \text{ g/g}$. The rich solvent (S1) is loaded with 0.5 molCO₂/molMEA. The temperature difference between the rich

solvent (S1) and the lean solvent (S2) is 10 K. The pressure of S1 is set equal to the desorber pressure but flashing is inhibited. The desorber pressure is adjusted so that the bottom temperature in the desorber is fixed to 120 °C. The desorber is modeled with 15 equilibrium stages, Scrubber I with 2 equilibrium stages and the condenser with a flash at a temperature of 40 °C. The number of stages in the desorber is so high that a further increase does not significantly reduce the reboiler duty. The CO₂ mass flow at the desorber top (S3) is fixed to 90% of the CO₂ mass flow in the flue gas (see Table 2) by adjusting the reboiler duty (\dot{Q}_{des}).

A.2. Absorber–desorber simulation

The flow sheet of the absorption–desorption process is shown in Fig. 5. The CO₂-free mass fraction of MEA in the lean solvent entering the absorber (S2b) is $x_{\text{MEA}}^{(m)} = 0.3 \text{ g/g}$ and the CO₂-free mass fraction of ethanol is $x_{\text{EtOH}}^{(m)} = 0.0 \text{ g/g}$ or $x_{\text{EtOH}}^{(m)} = 0.35 \text{ g/g}$. The temperature of the solvent at the absorber inlet is 40 °C and the removal rate is fixed to 90% by adjusting the reboiler duty (\dot{Q}_{des}). The temperature difference between the rich solvent (S1) and the lean solvent (S2) is 10 K. The absorber and the desorber are modeled with 15 equilibrium stages, Scrubber I with 2 equilibrium stages and the condenser with a flash at a temperature of 40 °C. The number of stages in the absorber and desorber is so high that a further increase does not significantly reduce the reboiler duty. The ethanol make-up flow (S6) is equal to the ethanol flow in the absorber offgas (S5). The ethanol (S6) is introduced to the evaporator as a liquid at the same temperature as the rich solvent S1 at the desorber inlet. The pressures of the ethanol evaporator, the water scrubber I, the rich-lean heat exchanger HX-1 and the condenser are equal to the desorber pressure. The pressure of the absorber column is 1 bar. For reasons of convergence, the simulation is not completely closed but only the (apparent) CO₂ flow in the lean solvent (S2) is transferred to the solvent at the lean solvent at the absorber inlet (S2b).

A.3. Ethanol recovery simulation

The flow sheet of the ethanol recovery process is shown in Fig. 9. The absorber offgas (S5) from the optimum of Case A is used for the investigation of the ethanol recovery section. Both Scrubber II and the water regeneration column are modeled with 50 equilibrium stages. Above this number of stages, no change in the reboiler duty of the water regeneration column is observed. The minimum temperature difference in heat exchanger HX-3 is set to 10 K. The temperature of the wash water (S9b) is set to 30 °C. The pressure in the water regeneration column is equal to the pressure in the desorber and the pressure of Scrubber II is 1 bar. The concentration of ethanol in the purified gas (S8) is fixed to TA Luft specification [21] by adjusting the reboiler duty of the water regeneration column (\dot{Q}_{reg}). For reasons of convergence, the simulation is not completely closed but only the ethanol flow in the regenerated wash water (S9) is transferred to the wash water at the inlet of Scrubber II (S9b).

A.4. Integrated process simulation

The flow sheet of the integrated process is shown in Fig. 11. For the simulation, the absorber–desorber simulation and the ethanol recovery simulation as described in Appendices A.2 and A.3 are connected through the absorber offgas (S5), the recycle of the gas cooler condensate (S7), the recovered ethanol stream (S11) and the condensate from the desorber top (S14). A rectifying section with 50 stages is added to the water regeneration column and S14 is used as reflux. The optimum L/G ratio as determined in Section 3.2 and the minimum possible L_w/G ratio as determined in Section 4 are used. The simulation was not completely closed for reasons

of convergence. As in the absorber-desorber simulation, the lean solvent (S2) and the solvent at the absorber inlet (S2b) are not connected and only the (apparent) CO₂ flow in S2 is transferred to S2b. As in the simulation of the ethanol recovery section, the regenerated wash water (S9) and the wash water at the inlet of Scrubber II (S9b) are not connected and only the ethanol flow is transferred.

Appendix B. Correlations for the estimation of compression work

The correlation of Liebenthal et al. [19] is used to estimate the specific work required for CO₂ compression. They considered a radial compressor with six stages, intercooling to 40 °C and a polytropic efficiency of 85%. An outlet pressure of 110 bar was assumed which is considered a typical pressure for CO₂ pipeline transport. The resulting correlation for the specific lost work for compression w_{comp} as a function of desorber pressure p_{des} is shown in Eq. (B.1), where $a_{\text{el}} = 0.3948$, $b_{\text{el}} = -0.3893$ and $c_{\text{el}} = 0.0301$.

$$\frac{w_{\text{comp}}}{\text{GJ/t}_{\text{CO}_2}} = a_{\text{el}} \cdot \left(\frac{p_{\text{des}}}{\text{bar}} \right)^{b_{\text{el}}} + c_{\text{el}} \quad (\text{B.1})$$

Appendix C. Nomenclature

Latin letters

L	mass flow of lean solvent (S2b)
L/G	ratio of mass flow of lean solvent (S2b) to mass flow of flue gas (S4)
L_w/G	ratio of mass flow of wash water (S9b) to mass flow of flue gas (S4)
l_{EtOH}	specific ethanol loss, i.e. mass flow of ethanol through absorber offgas (S5) divided by mass flow of ethanol in lean solvent (S2b)
p_{CO_2}	partial pressure of CO ₂
\dot{Q}	reboiler duty
q	specific reboiler duty (related to separated CO ₂ mass flow)
t	temperature in °C
T	temperature in K
T_{sink}	sink temperature in K
w_{comp}	specific work required for compression
w_{lost}	total specific lost work
w_{steam}	specific lost work in power plant turbines due to steam extraction
ΔX_{CO_2}	cyclic capacity, i.e. difference between rich and lean CO ₂ -loading
$x_i^{(\text{m})}$	mass fraction of component i in liquid phase
y_i	mole fraction of component i in gas phase

Greek letters

η_{Carnot}	Carnot efficiency
------------------------	-------------------

Subscripts

abs	absorber
des	desorber
evap	evaporation (of ethanol)
G	flue gas
reg	water regeneration column

Abbreviations

HX	heat exchanger
MEA	monoethanolamine
PCC	post-combustion capture

References

- [1] A. Henni, A.E. Mather, Solubility of carbon dioxide in methyldiethanolamine+methanol+water, *J. Chem. Eng. Data* 40 (1995) 493–495.
- [2] A. Arcane, L. Gicquel, E. Provost, W. Fuerst, Effect of methanol addition on water-CO₂-diethanolamine system: influence on CO₂ solubility and on liquid phase speciation, *Chem. Eng. Res. Des.* 86 (2008) 592–599.
- [3] E.S. Hamborg, P.W. Derkx, E.P. van Elk, G.F. Versteeg, Carbon dioxide removal by alkanolamines in aqueous organic solvents. A method for enhancing the desorption process, *Energy Procedia* 4 (2011) 187–194.
- [4] E. Sada, H. Kumazawa, Z. Han, H. Matsuyama, Chemical kinetics of the reaction of carbon dioxide with ethanolamines in nonaqueous solvents, *AIChE J.* 31 (1985) 1297–1303.
- [5] P. Usubharatana, P. Tontiwachwuthikul, Enhancement factor and kinetics of CO₂ capture by MEA-methanol hybrid solvents, *Energy Procedia* 1 (2009) 95–102.
- [6] S.-W. Park, J.-W. Lee, B.-S. Choi, J.-W. Lee, Reaction kinetics of carbon dioxide with diethanolamine in polar organic solvents, *Sep. Sci. Technol.* 40 (2005) 1885–1898.
- [7] S.-W. Park, J.-W. Lee, B.-S. Choi, J.-W. Lee, Absorption of carbon dioxide into non-aqueous solutions of N-methyldiethanolamine, *Korean J. Chem. Eng.* 23 (2006) 806–811.
- [8] G. Versteeg, W. van Swaaij, On the kinetics between CO₂ and alkanolamines both in aqueous and non-aqueous solutions – I. Primary and secondary amines, *Chem. Eng. Sci.* 43 (1988) 573–585.
- [9] G. Versteeg, W. van Swaaij, On the kinetics between CO₂ and alkanolamines both in aqueous and non-aqueous solutions-II. Tertiary amines, *Chem. Eng. Sci.* 43 (1988) 587–591.
- [10] E.S. Hamborg, C. van Aken, G.F. Versteeg, The effect of aqueous organic solvents on the dissociation constants and thermodynamic properties of alkanolamines, *Fluid Phase Equilib.* 291 (2010) 32–39.
- [11] P.W. Derkx, E.S. Hamborg, P.G. Huttonhuis, S. van Loo, G.F. Versteeg, Method for enhancing performance of removal of acid gas e.g. carbon dioxide, involves adjusting dielectric constant of solvent used in acid gas removal process, Patent WO 2010/113134 (2010).
- [12] Design Institute for Physical Properties (DIPPR), DIADEM Professional Version 5.0.2, 2011.
- [13] H.R. Garcia, R. Notz, G.S.O. Spuhl, H. Hasse, I. Tönnies, S. Hoch, H. Mangalapally, Removal of acidic gases by means of an absorbent comprising a stripping aid, Patent application WO 2010/149599 A1 (2010).
- [14] Inc. Aspen Technology, Rate-Based Model of the CO₂ Capture Process by MEA Using Aspen Plus, Aspen Plus Example Library, 2008.
- [15] D.M. Austgen, G.T. Rochelle, X. Peng, C.C. Chen, Model of vapor liquid equilibria for aqueous acid gas alkanolamine systems using the electrolyte NRTL equation, *Ind. Eng. Chem. Res.* 28 (1989) 1060–1073.
- [16] Aspen Technology, Inc., Aspen Physical Property System: Physical Property Models, Aspen Plus Documentation, Version 7.3.2, 2012.
- [17] R. Notz, I. Tönnies, H.P. Mangalapally, S. Hoch, H. Hasse, A short-cut method for assessing absorbents for post-combustion carbon dioxide capture, *Int. J. Greenhouse Gas Control* 5 (2011) 413–421.
- [18] H.P. Mangalapally, H. Hasse, Pilot plant study of post-combustion carbon dioxide capture by reactive absorption: Methodology, comparison of different structured packings, and comprehensive results for monoethanolamine, *Chem. Eng. Res. Des.* 89 (2011) 1216–1228.
- [19] U. Liebenthal, S. Linnenberg, J. Oexmann, A. Kather, Derivation of correlations to evaluate the impact of retrofitted post-combustion CO₂ capture processes on steam power plant performance, *Int. J. Greenhouse Gas Control* 5 (2011) 1232–1239.
- [20] S. Freguia, G.T. Rochelle, Modeling of CO₂ capture by aqueous monoethanolamine, *AIChE J.* 49 (2003) 1676–1686.
- [21] Bundesministerium für Umwelt, Naturschutz und Reaktorsicherheit (engl: Federal Ministry for Environment, Nature Conservation and Nuclear Safety), Technische Anleitung zur Reinhalterung der Luft (TA Luft) (engl: Technical Instructions on Air Quality Control), 2002 <http://www.bmu.de/files/pdfs/allgemein/application/pdf/taluft.pdf>
- [22] G. Sieder, BASF SE. Personal communication, 2008.

Publication VI

**CO₂-Abtrennung aus Kraftwerksabgasen auf dem
Weg von der Forschung und Entwicklung zur
industriellen Anwendung**

doi: 10.1002/cite.201100015

Übersichtsbeitrag

CO₂-Abtrennung aus Kraftwerksabgasen auf dem Weg von der Forschung und Entwicklung zur industriellen Anwendung

Inga Tönnies¹, Hugo Garcia², Hari Prasad Mangalapally¹, Sebastian Hoch¹, Ralf Notz², Georg Sieder², Bernd Eck² und Hans Hasse^{1,3*}

DOI: 10.1002/cite.201100015

Die Entwicklung der Post-Combustion-Capture (PCC)-Verfahren vom Labormaßstab bis zur industriellen Anwendung wird vorgestellt. Der Weg führt von den physikalisch-chemischen Grundlagen bis zu Anlagen in bisher noch nicht erreichten Dimensionen. Die Entwicklung wird unterteilt in eine Laborphase, eine Technikumsphase, eine Pilotanlagenphase und eine Demonstrationsanlagenphase. Die Forschungsaktivitäten in den einzelnen Phasen und deren Ergebnisse werden detailliert diskutiert. Mit den bis heute durchgeführten Schritten konnte gegenüber dem Standardlösungsmittel Monoethanolamin eine Reduzierung des Energiebedarfs um 20 % erreicht werden. Durch die noch ausstehenden Schritte sind weitere Optimierungen sowohl im Bereich des Energiebedarfs als auch bei der Anlagentechnik zu erwarten.

Schlagwörter: Amine, CO₂-Abtrennung, Reaktivabsorption, Post-Combustion Capture

Eingegangen: 15. Februar 2011; *revidiert:* 10. März 2011; *akzeptiert:* 08. April 2011

CO₂ Capture Technology – from Research to Large Scale Industrial Operation

The development of post-combustion capture from laboratory scale up to large scale industrial operation is discussed. The technology development starts with the physico-chemical scientific basis and will lead to plants with dimensions larger than those currently in operation. It is separated into a laboratory phase, a mini plant phase, a pilot plant phase and a demonstration plant phase. The research activities and results are discussed in detail for each phase. With the steps taken until now, the energy demand was reduced by 20 % compared to the standard solvent monoethanolamine. Future improvements are expected through ongoing research both in terms of a reduced energy demand and in terms of an improved plant design.

Keywords: Amines, CO₂ capture, Post-combustion capture, Reactive absorption

1 Einleitung

Treibhausgase tragen in erheblichem Maße zum Klimawandel bei [1]. Kohlenstoffdioxid (CO₂) gilt neben Methan als eines der wichtigsten Treibhausgase und wird zu einem gro-

ßen Teil durch die Verbrennung von fossilen Energieträgern, wie z. B. Erdgas oder Kohle, freigesetzt. Um den Klimawandel zu begrenzen, müssen entweder Alternativen zu fossilen Energieträgern gefunden oder die CO₂-Emissionen der fossilen Stromerzeugung durch die Abtrennung und Speicherung des CO₂ (Carbon Capture and Storage (CCS)) gesenkt werden. Drei verschiedene Technologien stehen für die Abtrennung von CO₂ an den Kraftwerken zur Verfügung: Pre-Combustion Capture, Oxyfuel Combustion und Post-Combustion Capture. Im Folgenden wird nur die Post-Combustion Capture (PCC) betrachtet, bei der das CO₂ direkt aus dem Rauchgas abgetrennt wird. Da der CO₂-Partialdruck im Rauchgas gering ist, ist die chemische Absorption (Reaktivabsorption) zur CO₂-Abtrennung das am bes-

¹Inga Tönnies, Hari Prasad Mangalapally, Sebastian Hoch, Prof. Dr.-Ing. H. Hasse (hans.hasse@mv.uni-kl.de), Lehrstuhl für Thermodynamik, Technische Universität Kaiserslautern, Postfach 3049, 67653 Kaiserslautern, Germany, ²Hugo Garcia, Ralf Notz, Georg Sieder, Bernd Eck, BASF SE, 67056 Ludwigshafen, Germany.

³Vortragsveröffentlichung: ProcessNet Jahrestagung, Aachen, 23. September 2010.

ten geeignete Verfahren. Die verschiedenen Verfahren zur CO₂-Abtrennung mit Hilfe der Reaktivabsorption werden in [2] ausführlich diskutiert.

In diesem Artikel soll der Weg der CO₂-Abtrennung mittels Reaktivabsorption von den physikalisch-chemischen Grundlagen bis hin zur industriellen Anwendung aufgezeigt werden. Zur Entwicklung dieser Technologie tragen sowohl Hochschulen als auch die chemische Industrie, Energieversorger und Anlagenbauer bei. Ziel der Entwicklung ist eine kommerzielle Anlage zur CO₂-Abtrennung für ein großtechnisches Kraftwerk. Der Weg führt von einer Laborphase über eine Technikumsphase, eine Pilotanlagenphase und eine Demonstrationsanlagenphase bis hin zu der kommerziellen Großanlage (Tab. 1). Eine kommerzielle Anlage muss das gesamte Rauchgas eines kommerziellen

Großkraftwerks behandeln können. Bei einem 1100 MW_{el} Braunkohlekraftwerk bedeutet dies, dass pro Stunde aus einem Rauchgasstrom von ca. 3,6 Mio. Nm³ die Menge von 750 t CO₂ abgetrennt werden muss. Es werden heute bereits Erdgasanlagen zur Abtrennung von sauren Gasen im Maßstab von 1–2 Mio. Nm³ h⁻¹ betrieben. Der wesentliche Unterschied besteht allerdings darin, dass Erdgas bei ca. 70 bar und Rauchgas bei Umgebungsdruck behandelt wird, wodurch sich auf Basis der Betriebsvolumenströme ein erheblicher Skalierungsfaktor ergibt. Daher ist ein gesichertes Scale-up für die Entwicklung dieser Technologie unerlässlich. In der Laborphase werden geeignete Lösungsmittelkandidaten identifiziert und charakterisiert sowie Screeningmethoden entwickelt, um zu entscheiden, welche Lösungsmittel weiter in der Technikumsphase getestet wer-

Tabelle 1. Überblick über Entwicklungsphasen der CO₂-Abtrennung aus Kraftwerksabgasen mittels Reaktivabsorption.

Phase	Aktivitäten	Ergebnis
Laborphase	<ul style="list-style-type: none"> – Lösungsmittelcharakterisierung – Entwicklung von Screeningmethoden – Ermittlung von Stoffdaten zur Modellierung 	<ul style="list-style-type: none"> – Abschätzung für Energieverbrauch – Entscheidung über Lösungsmittel für Technikumsphase
Technikumsphase	<ul style="list-style-type: none"> – Lösungsmittelvergleich mittels Parameterstudien unter synthetischen Bedingungen und an höhenlimitierter Anlage – Erste Validierung vorhandener Modelle 	<ul style="list-style-type: none"> – relative Aussagen über Energiebedarf und Stoffübergangskinetik – erste Erkenntnisse über Betriebbarkeit, Degradation und Emission
Pilotanlagenphase	<ul style="list-style-type: none"> – Lösungsmitteltests mittels Parameterstudien unter realen Gasbedingungen ohne Höhenlimitierung – Langzeitverhalten 	<ul style="list-style-type: none"> – Absolute Aussagen über Energiebedarf und Stoffübergangskinetik – Gutes Verständnis über Betriebbarkeit, Degradation und Emission
Demonstrationsanlagenphase	<ul style="list-style-type: none"> – Erprobung der gesamten CCS-Kette (Abtrennung und Speicherung) – Klärung von Detailfragen 	<ul style="list-style-type: none"> – Detailplan – Absicherung des Scale-up Risikos für kommerzielle Anlagen

(ca. 0,01 t CO₂ h⁻¹, entspricht 0,015 MW_{el})

(ca. 0,3 t CO₂ h⁻¹, entspricht 0,45 MW_{el})

(ca. 140 t CO₂ h⁻¹, entspricht 200 MW_{el})

den. In der Technikumsphase wird der Prozess mit den vielversprechendsten Lösungsmitteln unter synthetischen Bedingungen, d. h. mit einer Gasmischung aus Gasflaschen oder mit dem Abgas eines Gasbrenners, betrieben. Als Beispiel werden hier Versuche an der Technikumsanlage des Lehrstuhls für Thermodynamik der TU Kaiserslautern gezeigt. Dort werden typischerweise $0,01 \text{ t CO}_2 \text{ h}^{-1}$ abgetrennt, was einem Kraftwerk mit einer elektrischen Leistung von nur $0,015 \text{ MW}_{\text{el}}$ entspricht. In der Technikumsphase kann ein relativer Vergleich zwischen verschiedenen Lösungsmitteln stattfinden und Prozessmodelle können, falls vorhanden, bereits validiert werden. Belastbare absolute Zahlen hinsichtlich des Energiebedarfs können allerdings erst in einer größeren Pilotanlage gewonnen werden. Hier wird als Beispiel die Pilotanlage am Innovationszentrum Kohle am RWE Standort Niederaußem betrachtet, die einen Teilstrom des dortigen Braunkohlekraftwerks behandelt. In der von RWE betriebenen Anlage werden die von Linde ausgearbeitete Anlagentechnik und die von BASF entwickelte CO_2 -Wäschetechnologie unter realen Bedingungen über einen längeren Zeitraum getestet. Zwischen der kommerziellen Anlage und der Pilotanlage liegt allerdings immer noch ein Scale-up-Faktor von ca. 2500. Daher wird ein weiterer Scale-up-Schritt auf eine sogenannte Demonstrationsanlage geplant, um die technischen und finanziellen Risiken beim Bau der kommerziellen Anlage zu minimieren. Ziel der Demonstrationsanlage ist die Umsetzung der gesamten CCS-Kette einschließlich der CO_2 -Kompression, des Transports und der Speicherung. Die Frage, ob die geschilderten Entwicklungen auch in der Praxis umgesetzt werden, wird nicht nur durch technische und wirtschaftliche Faktoren bestimmt, sondern auch durch politische. Hier spielt insbesondere die Akzeptanz der CO_2 -Speicherung und des -Transports eine zentrale Rolle.

2 Grundlagen zur Reaktivabsorption von CO_2

Absorptive Verfahren zur Abtrennung von CO_2 aus Gasströmen sind in der chemischen und erdgasfördernden Industrie bereits seit langem etabliert [3]. Die BASF verfügt bereits seit den 70er Jahren über Erfahrungen mit Aminwäschen zur Abtrennung saurer Gase aus Prozessströmen (z. B. Synthesegase und Erdgas) mit der sogenannten aMEA® Technologie, die heute in mehr als 250 Anlagen weltweit eingesetzt wird.

Ein Verfahrensschema zur Abtrennung von CO_2 aus Kraftwerksabgasen ist in Abb. 1 dargestellt. Der Prozess

ist ein klassischer Absorptions-Desorptionsprozess. Das Rauchgas tritt nach der konventionellen Rauchgasreinigung mit Temperaturen von $40\text{--}60^\circ\text{C}$ in den Absorbersumpf ein. Liegt die Temperatur des Rauchgases noch höher, wird dieses durch direkten Kontakt mit Waschwasser in einem Vorwässer gekühlt. Im Absorber wird im Gegenstrom zum Gas das unbeladene, ebenfalls gekühlte Lösungsmittel über die Kolonneneinbauten, üblicherweise Füllkörperschüttungen oder strukturierte Packungen, geführt. Dabei löst sich das CO_2 zuerst physikalisch im Lösungsmittel und reagiert dann in mehreren, zum Teil kinetisch kontrollierten, reversiblen Reaktionen mit dem Lösungsmittel. Es hat sich eine wässrige Lösung von $0,3 \text{ g g}^{-1}$ Monoethanolamin (MEA) als Standard für Anwendungen bei niedrigen CO_2 -Partialdrücken durchgesetzt. Am Kopf des Absorbers befindet sich eine Waschsektion zur Rückhaltung des Amins. Das mit CO_2 angereicherte Lösungsmittel im Sumpf des Absorbers muss im Desorber regeneriert werden. Vor Eintritt in den Desorber wird es mit dem heißen Lösungsmittel aus dem Desorbersumpf in einem Gegenstromwärmevertrager erwärmt. Im Desorber wird bei erhöhter Temperatur, und somit bei erhöhtem Druck, dem Lösungsmittel das CO_2 entzogen, da die Löslichkeit von CO_2 in der Aminlösung bei erhöhten Temperaturen stark reduziert ist. Der benötigte Strippdampf wird im Sumpf des Desorbers erzeugt, indem ein Teil des Lösungsmittels (hauptsächlich Wasser) verdampft wird. Am Kopf des Desorbers wird das Wasser kondensiert und zurückgeführt, während das gasförmige CO_2 für den Transport zu geeigneten Speicherstätten verdichtet wird.

Gegenüber der Anwendung des Prozesses zur Aufreinigung von CO_2 aus Prozessgasströmen ergeben sich bei der

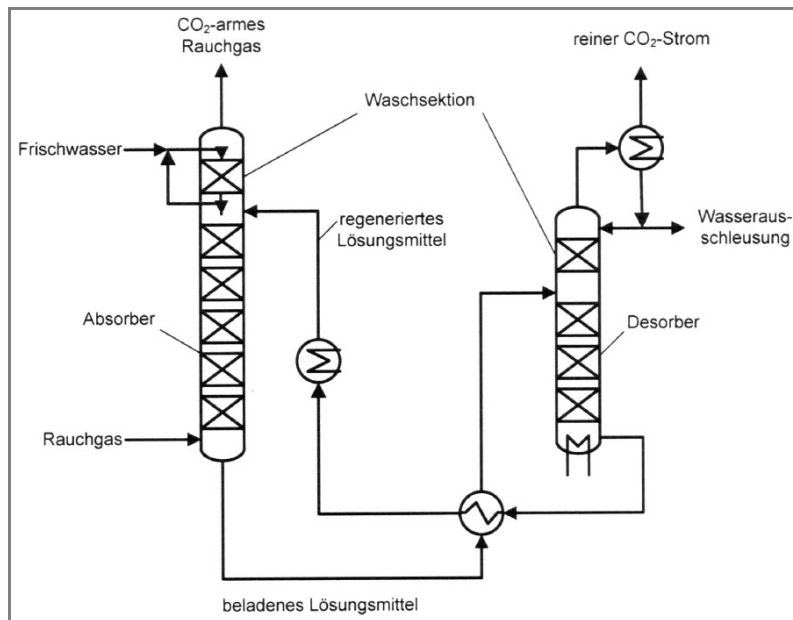


Abbildung 1. Verfahrensschema des CO_2 -Absorptions-Desorptionsprozesses.

Anwendung zur Abtrennung von CO₂ aus Rauchgasen einige Besonderheiten. Das Rauchgas enthält, anders als in den meisten Anwendungen in der chemischen Industrie, große Mengen an Sauerstoff und Spuren von Stickoxiden und Schwefeldioxid, die zu einer verstärkten Degradation der Amine führen. Der Partialdruck des CO₂ ist mit ca. 140 mbar bei Kohlekraftwerken bzw. 50 mbar bei Gaskraftwerken sehr gering. Eine weitere Herausforderung für die Anwendung zur CO₂-Abtrennung aus Rauchgasen sind die großen Rauchgasmengen bei niedrigen Drücken. Diese führen dazu, dass der Absorber bei einsträngiger Bauweise einen Durchmesser von ca. 30 m aufweisen würde. Die größte Herausforderung ist jedoch der Energiebedarf des Prozesses. So nimmt der Wirkungsgrad eines Kraftwerks mit CCS-Technologie signifikant ab. Um den durch die CCS-Technologie bedingten Wirkungsgradverlust zu reduzieren, gilt es neben Prozessmodifikationen neue Lösungsmittel mit einem reduzierten Energiebedarf im Vergleich zu MEA zu finden. Ein weiteres wichtiges Kriterium für die Wirtschaftlichkeit und Nachhaltigkeit eines PCC-Verfahrens ist eine niedrige Umweltbelastung. Die Identifizierung und Charakterisierung geeigneter Lösungsmittelkandidaten findet in der Laborphase statt.

Die physikalisch-chemische Beschreibung der Vorgänge bei der Rauchgaswäsche mit wässrigen Aminlösungen ist komplex (Abb. 2). Zum einen liegt ein komplexes Reaktionssystem vor, zum anderen werden bei den Reaktionen Ionen gebildet. Die Beschreibung der interessierenden physikalisch-chemischen Eigenschaften der reagierenden Elektrolytlösungen ist außerordentlich anspruchsvoll. Um ein voraussagefähiges, zuverlässiges Prozessmodell zu erhalten, müssen diese Vorgänge sinnvoll modelliert werden. Hinzu kommt, dass auch kinetische Vorgänge zuverlässig erfasst werden müssen, insbesondere bei der Modellierung des Absorbers. Auch dabei muss wieder der Zusammenhang zwischen physikalischen und chemischen Effekten erfasst werden.

3 Laborphase

Zunächst müssen die Anforderungen an ein gut geeignetes Lösungsmittel bestimmt werden. Neben einer hohen zyklischen Kapazität und einer niedrigen Absorptionsenthalpie ist auch eine ausreichend schnelle Absorptionskinetik wichtig. Eine hohe zyklische Kapazität bedeutet eine hohe Differenz der Gaslöslichkeit zwischen Absorber- und Desorberbedingungen. Dadurch wird die Umlaufrate des Lösungsmittels, die einen großen Einfluss auf den Energiebedarf im Desorber hat, gering gehalten. Eine niedrige Absorptionsenthalpie ist wünschenswert, da diese im Desorber zur Desorption des CO₂ wieder zugeführt werden muss. Eine ausreichend schnelle Absorptionskinetik ist wichtig, um die Kolonnenhöhen gering zu halten. Allerdings hängen beispielsweise die Absorptionsenthalpie und die CO₂-Löslichkeit über die Gibbs-Helmholtz-Beziehung zusammen. Dies führt dazu, dass eine niedrigere Absorptionsenthalpie nicht zwangsläufig zu einem geringeren Energiebedarf führt, da die zyklische Kapazität wiederum beeinflusst ist. Dieser Aspekt wird ausführlich in [4] diskutiert. Neben den oben genannten Anforderungen sollte ein Lösungsmittel außerdem umweltfreundlich, wenig flüchtig, nicht toxisch und nicht korrosiv sein. Für die Wirtschaftlichkeit des Prozesses ist zudem die Stabilität des Lösungsmittels wichtig, die in einfachen Screening-Apparaturen durch einen relativen Vergleich zu dem Standardlösungsmittel MEA ermittelt werden kann [5]. In der Screeningphase werden außerdem üblicherweise die Gaslöslichkeit (in einfachen Screening-Apparaturen) und die Stoffübergangskinetik gemessen. Genaue Gaslöslichkeitsdaten, die Reaktionskinetik sowie die Speziesverteilung und die kalorischen Daten werden in der Regel erst ermittelt, wenn aufgrund erfolgreicher Tests in der Technikumsanlage eine Modellierung des Lösungsmittels angestrebt wird. Im Folgenden werden die wichtigsten Größen für die Charakterisierung eines Lösungsmittels diskutiert.

3.1 Gaslöslichkeit

Die Gaslöslichkeit bestimmt die zyklische Kapazität eines Lösungsmittels und ist daher entscheidend für den Energiebedarf und die benötigte Umlaufrate. Für eine zuverlässige Modellierung des Prozesses sind genaue Gaslöslichkeitsdaten ebenfalls essentiell, da die Gaslöslichkeit einen großen Einfluss auf die Simulationsergebnisse hat [6]. Obwohl MEA das Standardlösungsmittel für diesen Prozess ist, streuen die Literaturwerte sehr stark. Genaue Gaslöslichkeitsdaten können beispielsweise mit einer Headspace-GC-Anlage für den für die industrielle Anwendung relevanten Niederdruckbereich bis 1 bar [7] und mit einer Hochdrucksichtzelle für den Hochdruckbereich ab 2 bar gemessen werden [8]. Auch wenn PCC-Verfahren bei sehr kleinen CO₂-Partialdrücken betrieben werden, sind Messungen bei erhöhten Drücken zur Entwicklung thermo-

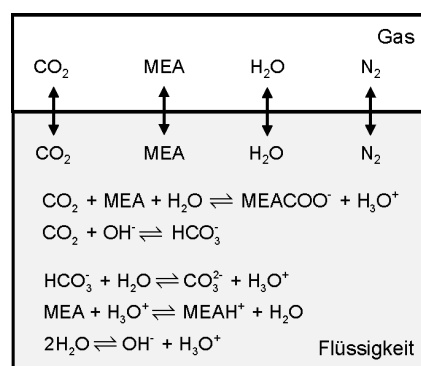


Abbildung 2. Schematische Darstellung der physikalisch-chemischen Vorgänge bei der Absorption von CO₂ in einer wässrigen Lösung von Monoethanolamin (MEA).

dynamischer Modelle hilfreich. Aufgrund der erhöhten Konzentrationen der relevanten Spezies bei erhöhtem Druck lassen sich die Wechselwirkungen zwischen den Spezies bei der Anpassung des Phasengleichgewichtsmodells besser bestimmen. Die Messung in zwei verschiedenen Apparaturen erhöht zudem die Verlässlichkeit der Messungen. In Abb. 3 ist die mit der Headspace-GC-Anlage gemessene Gaslöslichkeit für MEA zusammen mit den Literaturwerten gezeigt.

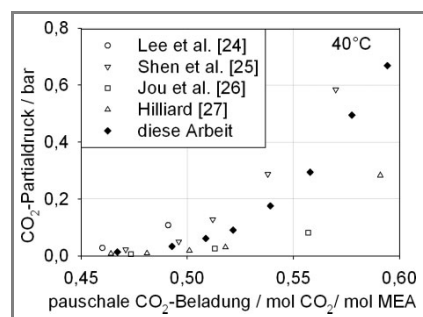


Abbildung 3. Gaslöslichkeit von CO_2 in MEA ($0,3 \text{ g g}^{-1}$ Monoethanolamin in Wasser) bei 40°C . Eigene Messungen und Vergleich mit Literaturwerten.

3.2 Speziesverteilung

Das gelöste CO_2 reagiert in der Flüssigphase mit dem Amin zu mehreren ionischen Spezies. Die Speziesverteilung, d.h. die Molenbrüche der verschiedenen Spezies im Gleichgewicht, kann mittels NMR-Spektroskopie gemessen werden. Messungen für MEA sind in Abb. 4 dargestellt [9, 10]. Die Speziesverteilung ist wichtig für das Verständnis der physikalisch-chemischen Vorgänge in der Lösung und für die Anpassung von G^E -Modellen zur Beschreibung der Nichtidealitäten in der Lösung, z.B. mit dem erweiterten Pitzer- oder dem Elektrolyt-NRTL-Modell. Zudem können chemische Gleichgewichtskonstanten, die nicht anders ermittelt werden können, an die Daten der Speziesverteilung angepasst werden [9].

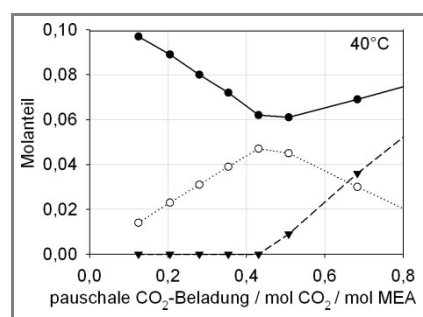


Abbildung 4. Speziesverteilung im System MEA-H₂O-CO₂, $x_{\text{MEA}}^0 = 0,3 \text{ g g}^{-1}$, $T = 40^\circ\text{C}$, MEA/MEA⁺ (● —), MEACOO⁻ (○ ····), HCO₃⁻ (▼ - -) [9].

3.3 Kalorische Messungen

Eine korrekte Abbildung der kalorischen Effekte bei der Absorption und Desorption von CO_2 in den Aminlösungen ist sehr wichtig, um bei der Modellierung die Energiebilanzen richtig darstellen zu können und dadurch insbesondere die Energie des Verdampfers im Desorbersumpf richtig wiederzugeben. Die Gesamtenthalpieänderung bei der Absorption von CO_2 in wässrigen Aminlösungen wird sowohl mit Batchkalorimetern [11] als auch mit Durchflusskalorimetern [12] bestimmt oder aus der Temperaturabhängigkeit der Gaslöslichkeit über die Gibbs-Helmholtz-Beziehung berechnet [13]. Des Weiteren ist die Wärmekapazität der Aminlösungen von großer Bedeutung, die am einfachsten durch Messungen mit einem dynamischen Differenzkalorimeter (DSC) bestimmt werden kann. Allerdings liegen kaum Daten zu den Wärmekapazitäten von CO_2 -beladenen Aminlösungen vor. Kürzlich ist es gelungen, mit einem isothermen Titrationskalorimeter die Reaktionswärmen aller auftretenden Reaktionen im Stoffsysteem zu ermitteln [14].

3.4 Kinetikmessungen

Die Kinetik der CO_2 -Absorption wird üblicherweise mit Laminarstrahlabsorbern, Fallfilmabsorbern oder Doppelrührzellen gemessen [15]. Die Stoffübergangskinetik bei der CO_2 -Absorption wird sowohl vom physikalischen Stofftransport als auch von der Kinetik der chemischen Reaktionen beeinflusst. In der Doppelrührzelle werden die Gasphase und die Flüssigphase mit Hilfe von Rührern gut durchmischt. Nachdem die Zelle mit Lösungsmittel gefüllt und thermostatisiert wurde, wird aus einem CO_2 -Vorratsbehälter über ein Dosierventil CO_2 eingeleitet, so dass der Druck in der Zelle während des gesamten Experiments konstant bleibt. Druck und Temperatur werden entsprechend typischer Absorberbedingungen gewählt. Während des Experiments nimmt der nachgeführte Strom an CO_2 kontinuierlich ab. Am Ende des Experiments ist das thermodynamische Gleichgewicht nahezu erreicht und der gemessene CO_2 -Strom wird folglich zu Null. Die Absorptionsrate entspricht dem gemessenen CO_2 -Strom bezogen auf die Flüssigkeitsmenge in der Zelle. Aus der Absorptionsrate kann bei bekannter Stofftransportkinetik die Reaktionskinetik ermittelt werden, was jedoch aufgrund der Unsicherheiten in der Stofftransportkinetik mit Fehlern behaftet ist.

Um die Reaktionskinetik direkt zu vermessen, kann das CO_2 unter erhöhtem Druck flüssig mit der Aminlösung vermischt werden, so dass der Phasenübergang vermieden wird. Da die Reaktionen jedoch sehr schnell ablaufen, ist eine Verfolgung der Reaktion direkt nach der Vermischung notwendig. Hierzu wurde in laufenden Arbeiten der Autoren ein thermostatisierter Mikromischer direkt in einen NMR-Probenkopf integriert. Unmittelbar nach der Vermischung von Aminlösung und flüssigem CO_2 können so die

Konzentrationen der Reaktanten mittels NMR-Spektroskopie erfasst werden. Mit Hilfe dieser Messdaten ist es möglich, die Reaktionsgeschwindigkeiten direkt zu bestimmen. Der NMR-Probenkopf befindet sich zurzeit noch in der Testphase.

3.6 Screeningmethode zur Abschätzung des Energiebedarfs

Die Auswahl der Lösungsmittel für die Technikumsphase erfolgt nach Berücksichtigung von Ausschlusskriterien, wie z. B. Toxizität, mit einer Screeningmethode zur Abschätzung des Energiebedarfs. Als Eingangsdaten werden nur die Gaslöslichkeiten bei Absorber- und Desorbertemperatur sowie Abschätzungen für die Absorptionsenthalpie und die Wärmekapazität benötigt. Als Ergebnis erhält man den minimalen Energiebedarf als Funktion des Lösungsmittel zu Gasstromverhältnisses (L/G) im Absorber. Der Energiebedarf wird hierbei aus einer Energiebilanz der Desorberkolonne berechnet. Aus der Bilanz erhält man vier Energiebeiträge, die durch den Verdampfer bereitgestellt werden müssen:

- Desorptionsenthalpie des CO₂
- Strippdampfbedarf
- Aufheizen des Lösungsmittels
- Aufheizen des Kondensatrücklaufs

Bis auf den Strippdampfbedarf lassen sich alle Anteile mit Messdaten bzw. sinnvollen Schätzungen hinsichtlich der Wärmekapazität und Absorptionsenthalpie direkt berechnen. Der Strippdampfbedarf wird über eine Gleichgewichtsstufenmethode aus den Gaslöslichkeiten bei Absorber- und Desorbertemperatur abgeschätzt [16]. In Abb. 5 werden die experimentellen Daten für die Lösungsmittel MEA, LM1, LM2 und LM3 mit den Ergebnissen der Screeningmethode verglichen. Man erkennt den typischen Verlauf mit einem Minimum des spezifischen Energiebedarfs über dem Lösungsmittelstrom bzw. dem L/G-Verhältnis. Links vom Optimum steigt der Strippdampfbedarf drastisch an, während

rechts vom Optimum der Energieanteil zum Aufheizen des Lösungsmittelstroms linear ansteigt. Die Screeningmethode ergibt für den Energiebedarf und das optimale L/G-Verhältnis die Reihenfolge LM1 < LM2, LM3 < MEA. Ein Vergleich mit den experimentellen Daten der Technikumsanlage bestätigt dieses Ranking. Die absoluten Werte der Screeningmethode liegen allerdings zu niedrig, da z. B. kinetische Effekte nicht berücksichtigt werden.

4 Technikumsphase

In der Laborphase werden einzelne Eigenschaften der Lösungsmittel untersucht. Das Zusammenspiel dieser Eigenschaften kann allerdings erst in einer Technikumsanlage abgebildet und untersucht werden. Zudem werden in der Technikumsanlage erste Erfahrungen zur Betreibbarkeit des Prozesses, Degradation und Emission gewonnen. Zur Auswahl der Lösungsmittel, die in der Technikumsphase getestet werden, spielen neben dem erwarteten Energiebedarf auch Flüchtigkeit, Stabilität, Kinetik und Sicherheitsaspekte eine Rolle [17].

Am Lehrstuhl für Thermodynamik der TU Kaiserslautern ist eine Technikumsanlage mit einem Durchmesser von 0,125 m und einer Packungshöhe in Absorber und Desorber von 4,25 m respektive 2,55 m vorhanden, die den geschlossenen Absorptions-Desorptionsprozess abbildet. Das Rauchgas wird über einen Erdgasbrenner erzeugt. Die CO₂-Konzentration im Rauchgas kann durch die Rückführung des abgetrennten CO₂ erhöht werden. Während der Versuche werden sowohl Konzentrations- als auch Temperaturprofile aufgenommen. Details über die Technikumsanlage und deren Betrieb sind in [5, 18] zu finden. Durch das große Oberflächen- zu Volumenverhältnis ist der Wärmeverlust der Anlage hoch. Die experimentellen Werte müssen daher vom Wärmeverlust bereinigt werden. Die Technikumsanlage ist in ihrer Höhe limitiert, so dass kinetische Effekte eine große Rolle spielen. Daher ist nur ein relativer Vergleich der Lösungsmittel untereinander möglich. Damit dieser Vergleich aussagekräftig ist, müssen geeignete Parameterstudien durchgeführt werden. Die gewünschte Abtrennrate wird bei allen Versuchen eingestellt, indem die Verdampferenergie variiert wird. Bei der Variation des Lösungsmittelstroms bei konstantem Abtrenngrad und konstantem Gasstrom erhält man als Ergebnis den Verlauf des Energiebedarfs über dem Lösungsmittelstrom bzw. dem L/G-Verhältnis, wie in Abb. 6a für das Standardlösungsmittel MEA gezeigt ist. Für verschiedene Lösungsmittel können das optimale L/G-Verhältnis und der minimale Energiebedarf aus dieser Parameterstudie verglichen werden.

Da die Technikumsanlage in ihrer Höhe limitiert ist, müssen kinetische Effekte untersucht werden, was mit einer Variation des Gasstroms, d. h. des *F*-Faktors, erreicht

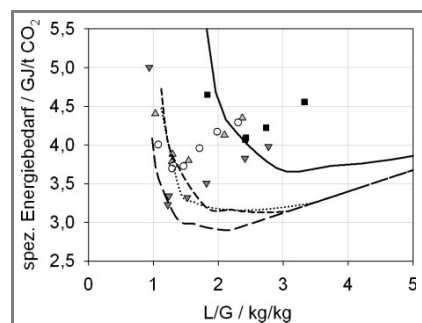


Abbildung 5. Experimentell bestimmter spezifischer Energiebedarf (Symbole) und Abschätzung mit der modifizierten Kremsergleichung (Linien) [16] für die Lösungsmittel MEA (■ —), LM1 (▼ —), LM2 (▲ —) und LM3 (○) bei 90 % CO₂-Abtrennung und einem CO₂-Partialdruck im Rauchgas von 100 mbar.

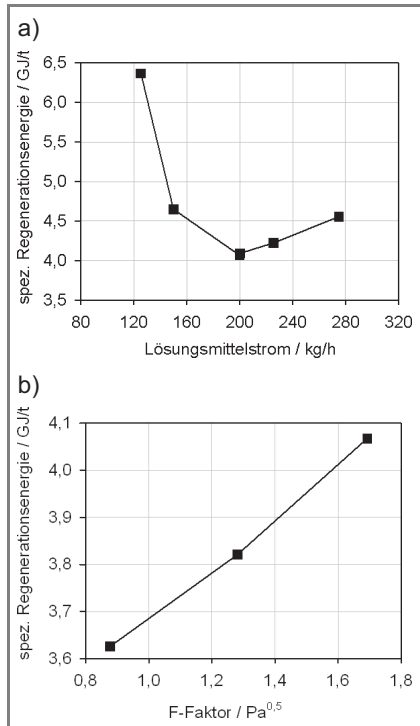


Abbildung 6. Experimentelle Ergebnisse der Technikumsanlage für die spezifische Regenerationsenergie von MEA ($0,3 \text{ g g}^{-1}$ Monoethanolamin in Wasser) bei 90 % CO_2 -Abtrennung und einem CO_2 -Partialdruck von 100 mbar. a) Lösungsmittelstrom-variation; b) Gasstromvariation bei konstantem L/G-Verhältnis.

wird. Bei einer Verringerung des Gasstroms muss bei konstantem Abtrenngrad weniger CO_2 pro Phasengrenzfläche (und damit pro Höhe) übertragen werden. Gleichzeitig wird bei dem Versuch ebenfalls der Lösungsmittelstrom verringert, so dass das L/G-Verhältnis konstant bleibt. Falls keine Höhenlimitierung vorhanden ist, sollte der Energiebedarf konstant bleiben, bei Höhenlimitierung jedoch absinken. In Abb. 6b ist zu sehen, dass die Technikumsanlage selbst für ein relativ schnell absorbierendes Lösungsmittel wie MEA nicht ausreichend hoch ist. Die CO_2 -Beladungen im Sumpf des Absorbers steigen mit Absenken des Gasstroms durch die geringere Höhenlimitierung an und führen zu dem geringeren Energiebedarf. Die Steigungen des Energiebedarfs über dem F-Faktor können für verschiedene Lösungsmittel verglichen werden, um relative Aussagen über deren Kinetik zu erhalten.

Vorhandene Prozessmodelle können bereits mit den in der Technikumsphase gewonnenen Daten validiert werden. Zur Modellierung des Prozesses müssen sogenannte Rate-Based-Modelle verwendet werden [19, 20]. Hierbei wird die Kolonne sowohl in vertikaler als auch in horizontaler Richtung diskretisiert. In jedem Diskret werden die Massen- und Energiebilanzen gelöst. An der Phasengrenze wird Phasengleichgewicht angenommen. Der Stofftransport wird mit dem

Zweifilmmodell beschrieben. Die Grenzschichtdicke und Phasengrenzfläche werden hierbei aus empirischen Korrelationen der Literatur entnommen. Die Mehrkomponentendiffusion in den Filmen wird durch die Maxwell-Stefan-Gleichung beschrieben. Die Reaktionen, die im flüssigseitigen Film auftreten, verursachen eine starke Krümmung des CO_2 -Konzentrationsprofils. Daher muss der flüssigseitige Film diskretisiert werden. Da das CO_2 -Konzentrationsprofil in der Nähe der Phasengrenze die größte Steigung aufweist, sollten die meisten Elemente in diesem Bereich liegen. Die Diskretisierung erfolgt daher in der Regel nicht äquidistant. Die Modelle sind numerisch aufwendig, dafür aber auch vorhersagefähig. Im Rahmen dieser Arbeit wurden sowohl mit dem kommerziell erhältlichen Simulationstool Aspen RateSep als auch mit dem Inhouse-Tool der BASF, CHEMASIM™, Simulationen durchgeführt. Beide Werkzeuge basieren auf einem Rate-Based-Modell. Es konnte für MEA gezeigt werden, dass der berechnete und der experimentell bestimmte Energiebedarf für die Technikumsanlage am Lehrstuhl für Thermodynamik um maximal 10 % voneinander abweichen (Abb. 7a). Insgesamt ist das Modell damit geeignet, um Prozessmodifikationen zu testen oder ein simulatives Scale-up durchzuführen.

In der Laborphase und der Technikumsphase wurden neue Lösungsmittel charakterisiert und ihr Potenzial abgeschätzt. Zum Erfolg der Technologie ist allerdings neben verbesserten Lösungsmitteln auch ein optimierter Prozess wichtig. Daher hat die BASF mit dem validierten Prozessmodell verschiedene Prozessparameter und Prozessmodifikationen untersucht.

- Eine Variation der Rauchgastemperatur zeigt, dass der Energiebedarf bis zu einer Rauchgastemperatur von 40 °C stark abfällt, bei geringeren Rauchgastemperaturen allerdings fast konstant bleibt.
- Ein erhöhter Desorberdruck führt zu erhöhten Temperaturen im Desorber und daher durch die ausgeprägte Temperaturabhängigkeit der CO_2 -Löslichkeit zu einer erhöhten zyklischen Kapazität. Allerdings wird mit steigender Desorbertemperatur auch höherwertiger Dampf benötigt, was zu einer Verminderung des Kraftwerkswirkungsgrads führt. Zudem steigt die Degradation des Lösungsmittels an. Die Simulationen ergeben, dass ab einem Desorberdruck von 1,8 bar der Energiebedarf für MEA kaum weiter absinkt.
- Die Eintrittstemperatur des regenerierten Amins in den Absorber hat den Simulationen zufolge keinen großen Einfluss auf den Energiebedarf.
- Für den Einbau eines Zwischenkühlers in den Absorber ergeben die Simulationen einen um 4 % niedrigeren Energiebedarf.

Alle bisher gewonnenen Erfahrungen aus der Laborphase, der Technikumsphase und den Simulationen sind in die Planung der Pilotanlage eingeflossen. Beispielsweise wurde auf Basis der Simulationen entschieden, die Pilotanlage in Niederaußem ebenfalls mit Zwischenkühlern und einem Rauchgaskühler auszustatten.

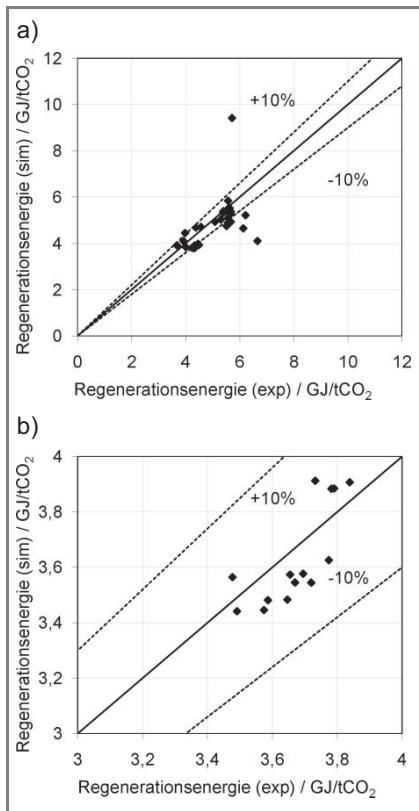


Abbildung 7. Vergleich von spezifischer Regenerationsenergie aus Simulation mit CHEMASIM und Experiment für MEA. a) Technikumsanlage des Lehrstuhls für Thermodynamik, b) Pilotanlage von BASF, RWE und Linde in Niederaußem.

5 Pilotanlagenphase

In der Pilotanlagenphase wird der Prozess unter realen Bedingungen, d.h. mit Rauchgas aus dem Kraftwerk, über einen längeren Zeitraum betrieben. Da die Pilotanlage im Gegensatz zu einer Technikumsanlage ausreichend Stoffaustauschfläche bietet, können absolute Werte für den Energiebedarf des Lösungsmittels gewonnen werden. Die Pilotanlage der RWE am Innovationszentrum Kohle in Niederaußem trennt mit $0,3 \text{ t CO}_2 \text{ h}^{-1}$ bereits einen 30-mal höheren CO₂-Strom als die Technikumsanlage ab. Dennoch werden nur ca. 0,05 % vom Abgasstrom des 1-GW-Braunkohlekraftwerks der Wäsche zugeführt. Da die Anlage Forschungszwecken dient, ist sie mit einer hohen Anzahl an Messstellen, insgesamt 250, ausgestattet. So kann beispielsweise jeder Wärmetauscher einzeln bilanziert werden, da neben Durchfluss und Temperatur des Lösungsmittels auch alle Kühlwasserflüsse und Temperaturen aufgezeichnet werden. Die Anlage verfügt neben der standardmäßigen Onlinemessung der O₂- und CO₂-Konzentration in allen ein- und austretenden Gasströmen über eine Online-Mes-

sung von Total Organic Carbon (TOC) im CO₂-armen Rauchgas und im CO₂-Produktstrom.

Für ein neues Lösungsmittel wird zur Ermittlung des Energieoptimums eine umfassende Versuchsmatrix durchgeführt [21]. Es wird beispielsweise eine Desorberdruckvariation, eine Variation der Rauchgastemperatur und des Abtrenngrads für verschiedene Umlaufraten durchgeführt. In Abb. 8 ist der Energiebedarf über dem Lösungsmittelstrom für das Standardlösungsmittel MEA und ein neu entwickeltes Lösungsmittel der BASF mit dem Arbeitsnamen GUSTAV 200 dargestellt. Mit GUSTAV 200 wurde eine Energiereduzierung von 20 % gegenüber MEA erreicht. Des Weiteren zeigt die Variation des Desorberdrucks, dass der Energiebedarf im Optimum bei GUSTAV 200 bei Absenken des Drucks von 1,75 bar auf 1,5 bar nicht ansteigt, während bei MEA ein Anstieg von ca. 4,5 % zu verzeichnen ist (Tab. 2). Dies ist ein Vorteil, da bei niedrigem Desorberdruck und damit niedriger Desorbertemperatur niederwertiger Dampf zum Beheizen des Verdampfers verwendet werden kann, was zu einem geringeren Wirkungsgradverlust des Kraftwerks führt.

Tabelle 2. Desorberdruckvariation für MEA und GUSTAV 200 an der Pilotanlage in Niederaußem bei 90 % CO₂-Abtrennung.

Druck [bar]	Energiebedarf im Optimum [GJ t ⁻¹ CO ₂]	
	MEA	GUSTAV 200
1,50	3,64	2,76
1,75	3,48	2,77
2,00	3,52	2,79

Mit dem umfangreichen Testprogramm der Pilotanlagenphase können im Gegensatz zur Technikumsphase verlässliche absolute Werte für den Energiebedarf des Lösungsmittels bei Betrieb unter realen Bedingungen gewonnen werden. Jedes Lösungsmittel wird nach ausführlichen Parameterstudien 500 h im Dauerbetrieb bei optimalen Betriebsparametern getestet. Durch die lange Betriebsdauer von insgesamt ca. 6 Monaten pro Lösungsmittel werden aussagekräftige Daten zur Emission, Degradation und Korrosion erhalten.

Das bereits an der Technikumsanlage validierte Prozessmodell für MEA kann die Daten der Pilotanlage sehr gut wiedergeben. Die Abweichungen zwischen berechnetem und experimentell bestimmtem Energiebedarf betragen maximal 6 % (Abb. 7b). Der mittels Simulationen ermittelte Effekt der Zwischenkühlung konnte in der Pilotanlage bestätigt werden. Für MEA konnte der Energiebedarf durch den Zwischenkühler um max. 3 % und für GUSTAV 200 um ca. 4 % gesenkt werden. Durch eine Kostenrechnung konnte gezeigt werden, dass die Zwischenkühlung sich wirtschaftlich rechnet. In der Pilotanlage werden ebenfalls verschiedene Werkstoffe hinsichtlich ihrer Beständigkeit gegenüber den Aminlösungen und den Gasen getestet. Diese Informationen sind bei der Wahl der Konstruktionswerkstoffe für eine Demonstrationsanlage von großer Bedeutung.

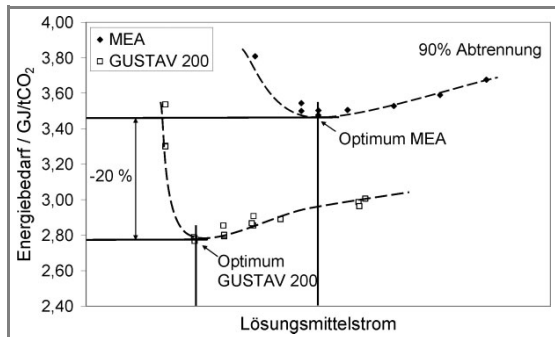


Abbildung 8. Experimentelle Ergebnisse der Pilotanlage von BASF, RWE und Linde am Standort Niederaußem für die spezifische Regenerationsenergie von MEA und dem neu entwickelten Lösungsmittel GUSTAV 200 bei 90 % CO₂-Abtrennung.

6 Demonstrationsanlagenphase

Mit der Demonstrationsanlage soll das finanzielle und technische Risiko beim Bau der kommerziellen Anlage gemindert werden. Dafür müssen zunächst die Risiken und Unbekannten bei der Planung einer kommerziellen Anlage sorgfältig evaluiert und auch Detailfragen geklärt werden, die beim Bau der kleineren Pilotanlage keine Rolle spielen. Zudem wird bei der Demonstrationsanlage der Gesamtprozess inklusive CO₂-Kompression abgebildet. Für die Planung sind das Wissen und die Erfahrungen eines Chemieunternehmens, eines Anlagebauers und eines Energieversorgers wichtig. Daher haben Experten von BASF, Linde und RWE in einer interdisziplinären Arbeitsgruppe aus Ingenieuren, Chemikern und Werkstofftechnikern gemeinsam eine Konzeptstudie für einen kosteneffizienten Post-Combustion-Capture-Prozess für ein 1,1-GW_{el}-Kraftwerk durchgeführt. Hierbei wurde u. a. die beste Kopplung des Abtrennprozesses mit dem Kraftwerksprozess untersucht. Auch wurde mittels Simulationen untersucht, inwieweit durch Prozessmodifikationen der Energiebedarf weiter gesenkt werden kann. Bei der kommerziellen Anlage spielt der Druckverlust im Absorber eine große Rolle, da die Energie des Zusatzgebläses zum Wirkungsgradverlust des Kraftwerks beiträgt. Daher ist die Auswahl von Kolonneneinbauten mit möglichst geringem Druckverlust und dennoch möglichst hoher Phasengrenzfläche sehr wichtig. Auch die Position des Gebläses spielt für den Energiebedarf eine Rolle. Als günstigste Variante hat sich hierbei die Anordnung hinter dem Absorber herausgestellt. Bei einer Gasmenge von 1,1 t s⁻¹ und dem niedrigen Druck werden die benötigten Apparate sehr groß. Daher kommen neuartige, in der chemischen Industrie bisher nicht übliche Bauweisen, beispielsweise des Absorbers, in Betracht. Möglich ist z. B. eine quaderförmige statt einer zylindrischen Bauweise. Als Werkstoffe kommen neben Stahl für einige Bauteile auch glasfaserverstärkte Kunststoffe (GFK) und Beton mit Polypropylen (PP)-Inliner in Betracht. Bei den Werkstoffuntersuchungen in der Pilotanlage werden die neuen Werk-

stoffe entsprechend berücksichtigt und in Form von Coupons, Passstücken und Modulen getestet [22]. Bei der Planung der kommerziellen Anlage ist ebenfalls eine möglichst platzsparende Anordnung der Bauteile zu berücksichtigen. Dabei ist die Frage zu klären, aus wie vielen Strängen die Anlage bestehen soll. Mehrere Stränge erhöhen die Flexibilität und verringern die Dimensionen der einzelnen Kolonnen, führen aber zu einem höheren Platzbedarf und zu höheren Investitionskosten. Eine zweisträngige Bauweise hat sich bei der Studie sowohl von den Investitionskosten als auch vom Platzbedarf her als optimal erwiesen. Die CO₂-Kompression ist aufgrund der erhöhten Flexibilität hierbei viersträngig geplant. Um das anschließende Scale-up-Risiko auf eine kommerzielle Anlage möglichst gering zu halten, sollte die Demonstrationsanlage in der Größenordnung von 150 – 250 MW_{el} gebaut werden. Von der EU werden derzeit in diesem Maßstab mehrere größere PCC-Demonstrationsprojekte gefördert. Diese Förderung ist Bestandteil der Programme „European Energy Programme for Recovery“ (EEPR) und NER-300 [23].

7 Zusammenfassung

In diesem Beitrag wurde der Weg der CO₂-Abtrennung mittels Reaktivabsorption von den komplexen physikalisch-chemischen Grundlagen bis zu Anlagen in bisher noch nicht erreichten Dimensionen dargestellt. Die Entwicklung wurde in eine Laborphase, eine Technikumsphase, eine Pilotanlagenphase und eine Demonstrationsanlagenphase unterteilt (Tab. 1). In der Laborphase werden die Lösungsmittel charakterisiert. Durch eine geeignete Screening-Methode ist bereits mit wenigen Stoffdaten ein Ranking der Lösungsmittel hinsichtlich ihres Energiebedarfs möglich. In der Technikumsphase werden die vielversprechenden Kandidaten unter synthetischen Bedingungen getestet. Als Ergebnis erhält man aufgrund der Höhenlimitierung einer Technikumsanlage nur relative Aussagen bezüglich des Energiebedarfs und des Stoffübergangs. In der Pilotanlage werden die Lösungsmittel unter realen Bedingungen, d. h. direkt mit Kraftwerkstrauchgas, und ohne Höhenlimitierung getestet, so dass absolute Daten zum Energiebedarf des Lösungsmittels ermittelt werden können. Zudem können aufgrund der langen Betriebsdauer Aussagen zu Degradation, Korrosion und Emissionen getroffen werden. In der Demonstrationsanlagenphase wird die gesamte CCS-Kette abgebildet werden, um alle Detailfragen klären zu können und somit das Scale-Up-Risiko für eine kommerzielle Anlage zu reduzieren.

Das Bundesministerium für Wirtschaft und Technologie, BMWI, fördert dankenswerterweise das CO₂-Wäsche-Pilotprojekt Niederaußem von RWE Power, BASF und Linde (Förderkennzeichen: 0327793).

Literatur

- [1] *Climate Change 2007: The Physical Science Basis. Contribution of Working Group I to the Fourth Assessment Report of the Intergovernmental Panel on Climate Change* (Eds: S. Solomon, D. Qin, M. Manning, Z. Chen et al.), Cambridge University Press, Cambridge 2007.
- [2] R. Notz, I. Tönnies, G. Scheffknecht, H. Hasse, *Chem. Ing. Tech.* **2010**, *82* (10), 1639. DOI: 10.1002/cite.201000006
- [3] A. Kohl, R. Nielsen, *Gas Purification*, 5th ed., Gulf Professional Publishing, Houston, TX 1997.
- [4] J. Oexmann, A. Kather, *Int. J. Greenhouse Gas Control* **2010**, *4* (1), 36. DOI: 10.1016/j.ijggc.2009.09.010
- [5] R. Notz, *Dissertation*, Universität Stuttgart 2009.
- [6] I. Tönnies, H. P. Mangalapally, H. Hasse, *Energy Procedia* **2011**, *4*, 533. DOI: 10.1016/j.egypro.2011.01.085
- [7] V. Ermatchkov, A. P. S. Kamps, G. Maurer, *Ind. Eng. Chem. Res.* **2006**, *45* (17), 6081. DOI: 10.1021/ie0604270
- [8] A. Böttger, V. Ermatchkov, G. Maurer, *J. Chem. Eng. Data* **2009**, *54* (6), 1905. DOI: 10.1021/je900083k
- [9] W. Böttlinger, M. Maiwald, H. Hasse, *Fluid Phase Equilib.* **2008**, *263* (2), 131. DOI: 10.1016/j.fluid.2007.09.017
- [10] W. Böttlinger, *Dissertation*, Universität Stuttgart 2005.
- [11] I. Kim, H. F. Svendsen, *Ind. Eng. Chem. Res.* **2007**, *46* (17), 5803. DOI: 10.1021/ie0616489
- [12] C. Mathonat, V. Majer, A. E. Mather, J. P. E. Grolier, *Ind. Eng. Chem. Res.* **1998**, *37* (10), 4136.
- [13] C. Mathonat, V. Majer, A. E. Mather, J. P. E. Grolier, *Fluid Phase Equilib.* **1997**, *140*, 171.
- [14] N. McCann, M. Maeder, H. Hasse, *J. Chem. Thermodyn.* **2011**, *43* (5), 664. DOI: 10.1016/j.jct.2010.12.001
- [15] A. Aboudheir, P. Tontiwachwuthikul, A. Chakma, R. Idem, *Chem. Eng. Sci.* **2003**, *58*, 5195. DOI: 10.1016/j.ces.2003.08.014
- [16] R. Notz et al., *Int. J. Greenhouse Gas Control* **2011**, *5* (3), 419. DOI: 10.1016/j.ijggc.2010.03.008
- [17] O. Spuhl, H. Garcia, G. Sieder, R. Notz, *Energy Procedia* **2011**, *4*, 51. DOI: 10.1016/j.egypro.2011.01.022
- [18] H. Mangalapally, H. Hasse, *Chem. Eng. Res. Des.* **2011**, in press. DOI: 0.1016/j.cherd.2011.01.013
- [19] L. Kucka, I. Müller, E. Y. Kenig, A. Gorak, *Chem. Eng. Sci.* **2003**, *58* (16), 3571. DOI: 10.1016/S0009-2509(03)00255-0
- [20] N. Asprion, *Ind. Eng. Chem. Res.* **2006**, *45* (6), 2054. DOI: 10.1021/ie050608m
- [21] P. Moser, S. Schmid, G. Sieder et al., *Energy Procedia* **2011**, *4*, 1310. DOI: 10.1016/j.egypro.2011.01.188
- [22] P. Moser, S. Schmid, R. Uerlings et al., *Energy Procedia* **2011**, *4*, 1317. DOI: 10.1016/j.egypro.2011.01.189
- [23] ZEP, EU CCS demonstration projects, <http://www.zeroemissionsplatform.eu/projects/eu-projects>, accessed 14.01.2011.
- [24] J. I. Lee, F. D. Otto, A. E. Mather, *Can. J. Chem. Eng.* **1974**, *52*, 803.
- [25] K.-P. Shen, M.-H. Li, *J. Chem. Eng. Data* **1992**, *37*, 96.
- [26] F.-Y. Jou, A. E. Mather, F. D. Otto, *Can. J. Chem. Eng.* **1995**, *73*, 140.
- [27] M. D. Hilliard, *Dissertation*, University of Texas at Austin 2008.

Publication VII

Quantitative online NMR spectroscopy in process analytics: coupling with microreactors in studies of fast feactions

Extended Abstract: International Symposium on Micro Chemical Process and Synthesis (MiPS), Kyoto, Japan, 2008, September 11-13

Quantitative Online NMR Spectroscopy in Process Analytics: Coupling with Microreactors for Kinetic Studies of Fast Reactions

Sebastian Hoch^{1*}, Klaus Albert² and Hans Hasse¹

¹*Laboratory of Engineering Thermodynamics, University of Kaiserslautern, Germany*

²*Institute of Organic Chemistry, Eberhard-Karls University of Tübingen, Germany*

**E-Mail: sebastian.hoch@mv.uni-kl.de*

Keywords: Online analysis, NMR spectroscopy, Microreactors, Reaction kinetics, Process engineering

INTRODUCTION

NMR spectroscopy is one of the most powerful analytical techniques, and has the potential to play an important role in designing and improving processes in the chemical and pharmaceutical industry [1-9]. In many technical processes complex multicomponent mixtures have to be handled. High-resolution NMR spectroscopy is an excellent tool to study these mixtures and gain insight into their behavior in the reaction or separation processes. For online studies under process conditions NMR flow probes can be used in a wide range of temperature and pressure. This has been used for reaction monitoring [1-8] as well as for process monitoring [9]. One of the drawbacks of this technique when using external reactors is that only kinetics of relatively slow reactions can be monitored. To make progress here, the delay time of the sample transport from the reactor to the NMR probe must be reduced. This can be achieved by coupling microreaction technology with NMR flow probes, namely with capillary probes.

QUANTITATIVE ONLINE NMR SPECTROSCOPY

The most important information obtained from NMR spectroscopy in studies of reacting multicomponent mixtures is that on the concentrations of the individual species. Even chemically very similar components can normally be distinguished in the NMR spectrum due to the high spectral dispersion. Quantification is much easier for NMR spectra than, for example, for optical spectroscopy (UV, NIR, IR) as calibration is not needed in most cases [5]. All peak fractions are directly proportional to the number of nuclei contributing to the signals. This is a remarkable advantage which makes NMR spectroscopy especially attractive, in particular if compounds that are not available as pure substances have to be monitored, as demonstrated in the examples. The sensitivity of NMR spectroscopy is sufficient for most engineering applications, as a reliable quantification of peak area fractions down to 0.05% is often possible. Furthermore, valuable qualitative information can be obtained from the NMR spectra, for example on the side reactions and byproducts or the clarification of reaction pathways.

The development of online techniques has increased the value of NMR spectroscopy for engineering applications. For process monitoring non-invasive methods which work at the system temperature and pressure are particularly attractive, as these allow obtaining almost undisturbed information. Online NMR spectroscopy can meet these demands when flow probes are directly coupled to process equipment like reactors or separators from laboratory size up to industrial scale. Flow probes are offered commercially in a wide temperature (up to 400 K) and pressure range (up to 35 MPa). A further extension of the pressure and temperature range is technically possible. Even in cases in which a direct coupling is not mandatory, NMR flow techniques offer advantages over conventional NMR spectroscopy with sample tubes, as the samples can be transferred much faster to the place of detection. Different economically important reaction networks of parallel and sequential reactions from industrial organic chemistry were successfully studied in this way [5,6,8]. However, the experimental set-up with external conventional reactors allows studies of reactions with time constants down to several minutes only.

COUPLING MICROREACTORS WITH ONLINE NMR SPECTROSCOPY

Novel types of mixers with miniaturized channel structures (micromixers) are now available that allow efficient mixing with mixing times down to a few milliseconds. The internal volume and hence the hold-up of micromixers is extremely reduced compared to standard laboratory reactors. The hyphenation of such mixers with NMR probes allows studying kinetics of fast chemical reactions with NMR spectroscopy. For that purpose setups made from glass have been described in literature [10,11]. These setups are non-thermostated and suffer from low sensitivity due to the use of planar coils for NMR detection. In the present work two different setups for hyphenation of micromixers with NMR spectrometers were developed and tested. A static micromixer was mounted directly below the NMR magnet for the first setup (Fig. 1). A pulsation free continuous flow of the reactants is provided by syringe pumps. This new development allows monitoring of reaction kinetics with time constants of less than one minute. The residence time between the mixing and the detection can be adjusted by the flow rates of reactants. A large number of transients can be accumulated for any state of the reaction, as the composition in the NMR probe cell is constant. That opens up, among others, the possibility to monitor fast reactions by ^1H - and ^{13}C -spectroscopy and allows kinetic studies by non-invasive quantitative measurements. Even faster reactions can be monitored with a second setup, in which the micromixer is directly integrated in the NMR probe head.

KINETIC STUDIES WITH TEST SYSTEM

The feasibility of this analytical method was proven using the simple but fast esterification reaction of methanol with formic acid as an example. A commercial micromixer with an inner volume of 8 μl (SIMM-V2, IMM, Mainz, Germany), using multi-lamination mixing principle, was installed in a housing for tempering with liquids. This installation was connected directly with a standard NMR-probe head (Varian Inc., Palo Alto, USA) under the NMR magnet, which is equipped with a 120 μl flow cell (Fig. 2). The volume of tubing and liquid connectors between micromixer and measurement cell was about 500 μl .

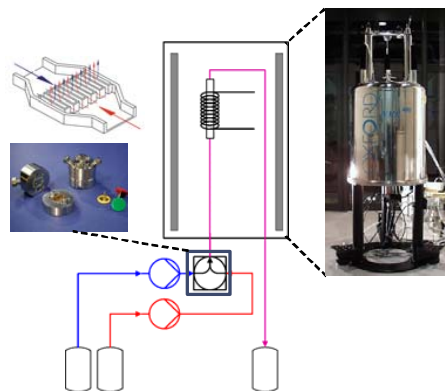


Figure 1: Principle of coupling micromixing device with NMR spectrometer



Figure 2: Left: Micro mixer from IMM, Mainz, Germany; Middle: Micro mixer with housing for thermostatization; Right: Complete installation of micro mixer with NMR probe under the NMR magnet

After determination of the residence time characteristics kinetic measurements were carried out with the test system. Methanol and formic acid were used as educts in different molar ratios. Hydrochloric acid was used as homogeneous catalyst in different concentrations (x_{HCl} up to $1.8 \cdot 10^{-3} \text{ mol} \cdot \text{mol}^{-1}$). The temperature was varied between 25°C and 40°C. The total flow rate was adjusted between 0.1 ml/min and 10 ml/min. In the reaction

kinetic studies proton and carbon spectra were acquired at predefined time intervals during the entire reaction time using both flow- and stop-flow-techniques (Fig. 3). After deconvolution and integration of the signals quantitative information on the composition is obtained (Fig. 4).

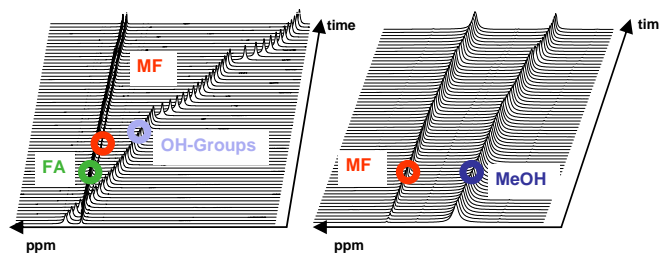


Figure 3: Staggered ^1H NMR spectra acquired during reaction monitoring of esterification in stopped flow after micro mixing

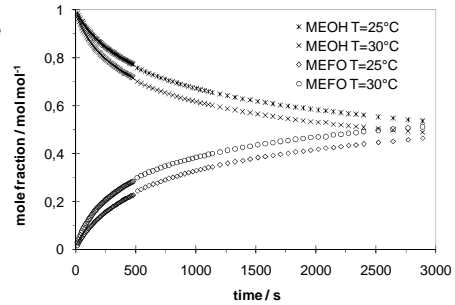


Figure 4: Reaction kinetics of esterification (equimolar feed) at two different temperatures measured using ^1H NMR spectroscopy (flow probe coupled with micro mixer)

The data was used to develop a kinetic model of the technical reacting mixture, which is not described here in detail. The comparison of the results with data from literature [12,13], obtained with other methods, shows good agreement. This demonstrates the applicability of the developed technique for kinetic studies of fast reactions.

For studying reactions that show strong caloric effects, improvements of the thermostatisation are needed. The external microreactor is tempered with a liquid as described above. The PEEK tubing, which connects mixer and NMR cell, as well as the NMR probe itself are thermostated with air. Furthermore, liquid thermostatisation of all components of the experimental setup (mixer, tubing and NMR cell) would be desirable. These developments are in progress.

CAPILLARY MICROCOIL FLOW NMR WITH INTEGRATED MICROMIXER

Capillary flow probes allow NMR measurements with extremely small active volumes by using a very small probe cell, made from a glass capillary (internal volume of only 4–6 μl), and a solenoidal microcoil [14]. The combination of solenoidal microcoil flow probes with micromixers allows a further significant reduction of the time needed for the transport of the reactants from the mixing zone to the detection zone. Figure 5 shows a NMR probe head with such a solenoidal microcoil cell, developed in the present work. Despite of the small active volume in the cell, quantitative concentration measurements with similar sensitivity to that of commercial NMR flow probes with active volumes of about 100 μl were obtained. Such small NMR probes must be coupled with micromixers that allow flow rates in the range of about 0.1 – 100 $\mu\text{l}/\text{min}$. Figure 6 shows such a micromixer that is commercial available. A prototype of a NMR probe head with integrated micromixer and microcoil cell was built. Together with IMM (Mainz, Germany) a liquid thermostated version of that probe head is presently being developed.



Figure 5: Solenoidal micro flow probe head.



Figure 6: Nano-Mixer (Upchurch Scientific)

This novel probe head, which is suited for monitoring very fast reactions, will allow obtaining reliable quantitative data on complex reacting mixtures with time constants of only some seconds. Kinetics studies of fast and complex reaction networks with NMR spectroscopy for process development will then become possible.

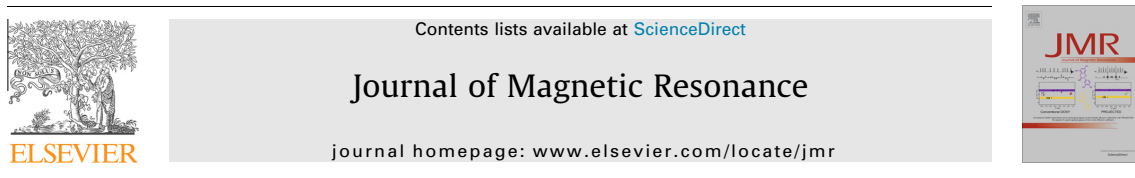
REFERENCES

- [1]: R. Neudert, E. Strofer and W. Bremser, *Magn. Res. Chem.* 24, 1089–1092, 1986.
- [2]: S.I. Selivanov and B.A. Ershov, *Russ. Chem. Rev.* 55, 395–410, 1986.
- [3]: C. Sarazin, F. Ergan, J.P. Seguin, G. Goethals, M.D. Legoy and J.N. Barbotin, *Biotechnol. Bioeng.* 51, 636–644, 1996.
- [4]: M. Maiwald, H. Fischer, Y.-K. Kim and H. Hasse, *Anal. Bioanal. Chem.* 375, 1111-1115, 2003.
- [5]: M. Maiwald, H. Fischer, Y. K. Kim, K. Albert and H. Hasse, *J. Magn. Res.* 166, 135-146, 2004.
- [6]: M. Maiwald, T. Gruetzner, E. Ströfer and H. Hasse, *Anal. Bioanal. Chem.* 385, 910-917, 2006.
- [7]: M. Maiwald, H. Li, T. Schnabel, K. Braun and H. Hasse, *Journal of Supercritical Fluids* 43, 267-275, 2007.
- [8]: W. Böttinger, M. Maiwald and H. Hasse, *Fluid Phase Equilibria* 263, 131-143, 2008.
- [9]: K. Schilling, M. Sohn, E. Ströfer, H. Hasse, Conference Proceedings, AIChE Spring National Meeting, New Orleans, 2003.
- [10]: M. Kakuta, D.A. Jayawickrama, A.M. Wolters, A. Manz and J.V. Sweedler, *Anal. Chem.* 75, 956-960, 2003.
- [11]: H. Wensink, F. Benito-Lopez, D.C. Hermes, W. Verboom, H.J.G.E. Gardeniers, D.N. Reinhoudt and A. van den Berg, *Lab on a Chip* 5, 280–284, 2005.
- [12]: B. Indu, W. Ernst and L. Gelbaum, *Ind. Eng. Chem. Res.* 39, 981 – 985, 1993.
- [13]: H. Goldschmidt and R. Melbey, *Zeitschrift fuer Physikalische Chemie*, 4, 139–156, 1929.
- [14]: D.L. Olson, T.L. Peck, A.G. Webb, R.L. Magin and J.V. Sweedler, *Science* 270, 1967-1970, 1995.

Publication VIII

Thermostatted micro-reactor NMR probe head for monitoring fast reactions

doi: 10.1016/j.jmr.2014.02.013



Thermostatted micro-reactor NMR probe head for monitoring fast reactions



A. Brächer^a, S. Hoch^{a,1}, K. Albert^b, H.J. Kost^c, B. Werner^{c,2}, E. von Harbou^{a,*}, H. Hasse^a

^a University of Kaiserslautern, Kaiserslautern, Germany

^b Eberhard Karls University, Tübingen, Germany

^c Institut für Mikrotechnik Mainz GmbH, Mainz, Germany

ARTICLE INFO

Article history:

Received 18 December 2013

Revised 10 February 2014

Available online 1 March 2014

Keywords:

Online NMR spectroscopy

Micro-reaction technology

Capillary flow NMR

Reaction kinetics

Reaction monitoring

Thermostatted micro-reactor

ABSTRACT

A novel nuclear magnetic resonance (NMR) probe head for monitoring fast chemical reactions is described. It combines micro-reaction technology with capillary flow NMR spectroscopy. Two reactants are fed separately into the probe head where they are effectively mixed in a micro-mixer. The mixed reactants then pass through a capillary NMR flow cell that is equipped with a solenoidal radiofrequency coil where the NMR signal is acquired. The whole flow path of the reactants is thermostatted using the liquid FC-43 (perfluorotributylamine) so that exothermic and endothermic reactions can be studied under almost isothermal conditions. The set-up enables kinetic investigation of reactions with time constants of only a few seconds. Non-reactive mixing experiments carried out with the new probe head demonstrate that it facilitates the acquisition of constant highly resolved NMR signals suitable for quantification of different species in technical mixtures. Reaction kinetic measurements on a test system are presented that prove the applicability of the novel NMR probe head for monitoring fast reactions.

© 2014 Elsevier Inc. All rights reserved.

1. Introduction

NMR spectroscopy is a powerful tool as it facilitates non-invasive *in situ* analysis of complex fluid mixtures without sample preparation. The method has a high resolution and enables resolving species that are chemically similar. Contrary to most optical spectroscopy methods, no prior calibration is needed for quantitative analysis. Thus, even unstable intermediates can be quantified by NMR spectroscopy [1–3]. Furthermore, NMR spectroscopy is an excellent tool for identifying unknown components such as side products [4,5]. Online NMR techniques have the advantage that the liquid compositions during reactions or in equilibria are not disturbed by sampling and that the temperature and pressure can be maintained [2,6–8]. Thus, when complex reaction systems with unknown and/or unstable intermediates have to be monitored, online NMR spectroscopy is often not only the best choice but also the sole analytical method that will yield the desired detailed quantitative data, see e.g. [2,9–11].

Often, NMR tubes are used to monitor chemical reactions by NMR spectroscopy. This simple set-up, however, has many drawbacks, for example the long delay between external mixing of the reactants, inserting the tube into the NMR and starting the acquisition of the spectra. Furthermore, it is difficult to control the pressure and temperature within the NMR tube.

To overcome these disadvantages, conventional reactors have been coupled to NMR flow probes, for details; see e.g. Maiwald et al. [11,12]. The reaction mixture is pumped from the external reactor, typically a stirred tank reactor, through a sample loop to the NMR flow probe head, where the composition of the reacting mixtures is analyzed. Numerous studies using similar flow set-ups have been carried out by several groups; see e.g. [13–18]. Furthermore, this type of set-up was used for pharmaceutical research [14,19] and to investigate complex reaction networks from industrial organic chemistry [10,11,20,21,3].

The characteristics of flowing samples, e.g. the signal intensity and the resolution as a function of the flow rate were investigated for example by Sudmeier et al. [22] and Haner et al. [23]. As the quality of the NMR signal (e.g. signal-to-noise ratio, resolution of the spectra) is strongly influenced by the geometry of the radio frequency (RF) coil, e.g. planar, solenoidal or stripline design, and the diameter of the RF coil, these parameters were investigated and optimized in several studies [24–26]. As discussed by Webb [27] and Fratila and Velders [28] the miniaturization of the RF coils

* Corresponding author. Address: Laboratory of Engineering Thermodynamics, P.O. Box 3049, 67653 Kaiserslautern, Germany.

E-mail address: erik.vonharbou@mv.uni-kl.de (E. von Harbou).

¹ Present address: Bayer Technology Service GmbH, Leverkusen, Germany.

² Present address: Boehringer Ingelheim GmbH, Ingelheim, Germany.

can have several advantages such as increasing sensitivity and decreasing mass limitations for detection.

The set-ups consisting of a combination of external reactors with NMR flow cells, however, have considerable disadvantages. For quantitative analysis, a certain residence time of the sample in the permanent magnetic field of the spectrometer (B_0 field) is required. Thus, the maximum flow rate in the sample loop is limited and thus there is a time delay between the moment when the sample leaves the external reactor and it is analyzed in the NMR probe head. Hence, the set-up with external reactors is difficult to apply for kinetic studies of reactions with time constants below approximately 10 min [11,12,29]. In order to enable investigations of fast reactions with online NMR spectroscopy, a novel NMR probe head was developed in the present work. Several groups have applied micro-reaction technology either in combination with conventional NMR cells (volume 60–120 μl) or with miniaturised NMR flow cells (volume from 50 μl down to picoliters) [30–39]. Because of differences in the quality of the micro-mixer, in the reactor volume, in the RF coil geometry, in the pressure and temperature range, and in the applied thermal management, the set-ups differ significantly in their performance. In many publications, however, no specifications are given concerning these parameters. Often, the temperature is controlled with air as cooling or heating medium, which is common for standard NMR probe heads. Even for studies of mildly exo- or endothermic reactions, this temperature control turns out to be insufficient in maintaining isothermal conditions. To our knowledge, the present work describes for the first time a design of a NMR probe head in which the whole flow path of the reactants is liquid thermostatted to ensure efficient thermostatisation of the reactants.

In this NMR probe head, a liquid thermostatted micro-mixer is coupled with a capillary NMR flow cell and mounted directly in the probe head. Hence, the residence time between mixing of the reactants and analysis in the NMR flow cell is significantly reduced compared to the set-up with external reactor. At the same time, the residence time within the B_0 field is sufficiently long so that quantitative studies of fast reactions in technical mixtures (highly concentrated solutions relevant to industrial applications) with time constants of only seconds can be studied. The focus of this work was to develop a robust measurement method, and an easy to use set-up and probe head which can be applied without long preparations and large adjustments in different laboratories and different spectrometers.

In this work, the design of the novel NMR probe head is presented in detail. After assessing the quality of the NMR measurements (signal-to-noise ratio, limit of detection, RF homogeneity), the novel NMR probe head was tested in two different studies. In the first study, measurements with a non-reacting mixture of acetone and ethanol were carried out to determine the resolution of acquired spectra and the accuracy of the probe head for quantitative concentration measurements in the flow mode. In the second study, the kinetics of the homogeneously catalyzed esterification of methanol with acetic acid were measured with the probe head both in the stopped flow and in the flow mode.

2. Micro-reactor probe head

2.1. Design

The basic units of the new probe head are the micro-mixer, the dwell unit, and the NMR flow cell. These units are mounted in a cylindrical block made of PEEK (poly(etheretherketone)). The probe head (i.e. the PEEK block) has a height of 80 mm and an outer diameter of 38 mm. PEEK was chosen as it is inert regarding most chemicals, it has good mechanical properties in a wide

temperature range, and, in addition, is non-magnetic. The probe head is assembled together with the supply tubes in a housing (made of brass). Fig. 1 gives an overview of the assembled probe.

The probe head consists of five segments, which are shown in Fig. 2: bottom plate (I), micro-mixer (II), dwell unit (III), NMR flow cell (IV), and top plate (V). The bottom plate (I) is the connection between the feed tubes and the PEEK block. Screws reaching from the bottom plate (I) to the top plate (V) give stability to the whole block and apply the pressure needed for a proper sealing of the reactants and the thermostating liquid. The two feed tubes of the reactants (both made of PEEK) are connected to passage channels, which are milled into the bottom plate (I) of the probe head, so that they enter the micro-mixer (II) separately. The micro-mixer is a crawler-type mixer developed by the Institut für Mikrotechnik Mainz (IMM, Germany) [40]. A special design was tailored by the IMM for this probe head to meet the given requirements (flow rates, density, surface tension, etc. of the reactants). The micro-mixer consists of two PEEK plates with mixing channels on the micro-scale, which are fabricated via laser ablation. While passing through the micro-mixer, the two incoming flows are split and recombined 39 times to achieve an efficient mixing. The total volume of the micro-mixer is only 0.27 μl . The mixed fluid flows through a short capillary made of PEEK (outer diameter 1/16 in., length 23 mm), the dwell unit (see Fig. 3, III, vertical line). By using capillaries of different inner diameters (from 0.025 mm to 1.3 mm), it is possible to adjust the volume of the dwell unit and therefore the volume between mixer and NMR flow cell in a range of 18 μl to 48 μl . After having passed the dwell unit, the reactants enter the NMR flow cell (see Fig. 3, IV, horizontal line), which is oriented perpendicular to the B_0 field. It consists of a capillary made of silica glass (inner diameter 1 mm) with a total volume of 12 μl . A solenoidal micro-RF coil made of copper is wrapped around the

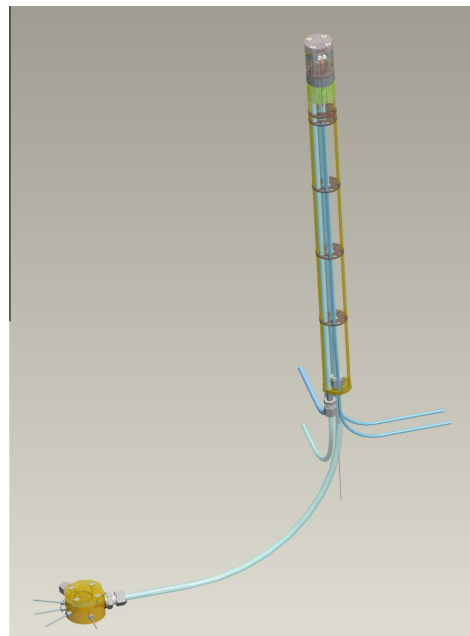


Fig. 1. Overview of the NMR probe including the micro-reactor probe head (top), supply lines (blue) and connection box for the feed and product lines (bottom left). (For interpretation of the references to color in this figure legend, the reader is referred to the web version of this article.)

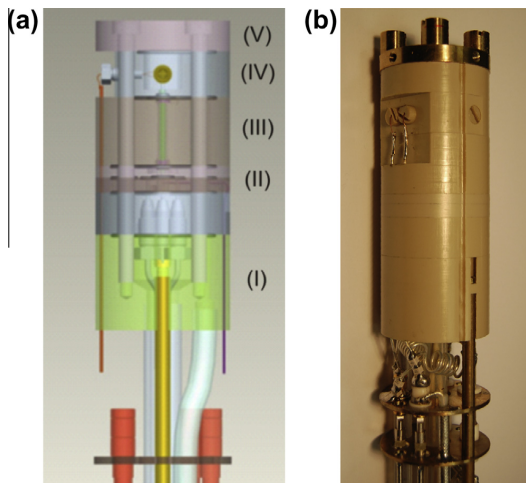


Fig. 2. (a) Drawing of the micro-reactor probe head (PEEK block) including bottom plate (I), micro-mixer plate (II), dwell unit (III), NMR flow cell (IV), and top plate (V). (b) Photograph of the micro-reactor probe head.

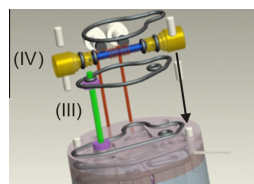


Fig. 3. Dwell unit (III) and NMR flow cell (IV) of the micro-reactor probe head visualized without the surrounding PEEK. The gray loops show the sealings. The arrow indicates the direction of the reactants leaving the NMR flow cell. The same numbering as in Fig. 2 is used.

capillary, resulting in a NMR active volume of approximately 5 μl . In the present set-up, only a ^1H NMR RF circuit is installed. An upgrade for the observation of ^{13}C nuclei is in preparation.

After passing the NMR flow cell, the fluid mixture leaves the probe head through the bottom plate (I) via milled channels in the PEEK block. Finally, the reactants leave the NMR probe through the connected lines (see Fig. 2).

The new probe head is designed in a way that the whole flow path of the reactants including the feed tubes, the micro-mixer plates, the dwell unit, and the NMR flow cell is thermostatted. Liquid perfluorotributylamine (FC-43) was chosen as thermostating fluid. FC-43 is a favorable choice for NMR applications because of several reasons. First, FC-43 is fully fluorinated so that it causes no ^1H NMR signals, which would interfere with the measurements, and, in addition, the signals of FC-43 in the ^{13}C spectrum are shifted far from the regions commonly investigated in NMR spectroscopy. Second, the magnetic susceptibility of the RF coil, the glass and FC-43 is very different from that of air. Thus by replacing air with FC-43 the differences in magnetic susceptibility of the materials surrounding the sample are smaller and therefore the spectral resolution is improved as shown by Subramanian et al. [33]. Additionally, it is well suited as thermostating liquid because of its low melting and high boiling point (operating range at ambient pressure about -40°C to 120°C). The temperature of the reactants is monitored by means of a calibrated thermocouple, which is

installed in the PEEK block directly underneath the micro-mixer. The temperature of the FC-43 is controlled by a cryostat. The standard air-based temperature control of the NMR spectrometer is employed for cooling the electronic components in the probe head, which are mounted below the PEEK block. The probe head is designed for pressures up to 60 bar. The range of the operating temperature is limited both by the properties of the FC-43 as well as the fact that an efficient cooling of the electronics must be guaranteed. It is approximately -20°C to 100°C .

2.2. Operating modes

The micro-mixer probe head can be used in two different operating modes: the stationary flow mode and the stopped flow (non-steady) mode. In the stationary flow mode, the probe head is operated as a continuous tubular reactor with the two feeds being set to constant flow rates. After the reactor has reached steady-state, the NMR measurements are started and spectra are acquired which yield information on the composition of the liquid in the NMR active volume (volume of the capillary which is wrapped by the RF coil, see above). As the operation is stationary, in principle any time is available for collecting the spectra so that using ^{13}C NMR with long acquisition times poses no problem. By adjusting the flow rates of the reactants, both the inlet composition and the residence time within the reactor can be varied so that reaction kinetics can be measured at different conversion rates and compositions. Shifting the reference frame and moving it with the sample, a mean time can be assigned to each experiment which elapses between the mixing and the analysis in the flow cell. This assignment is not trivial and involves determining residence and flow characteristics of the studied system by measurements of residence time distributions. This work is in progress. For the purposes of the present study, a simple first estimate is used: it is assumed that the acquired NMR signal corresponds to the position in the middle of the active volume of the NMR flow cell (1), that the mixing takes place instantaneously in the micro-mixer (2) and that the flow pattern corresponds to plug flow. Thus, the corresponding residence time is found by dividing the volume between (1) and (2) by the volumetric flow rate.

In the stopped flow mode, the reactants are fed into the reactor at high flow rates so as to minimize the time that elapses between the mixing and the filling of the NMR flow cell with the reacting mixture. After the NMR flow cell is filled with the reacting mixture, the flow is stopped abruptly and the signal acquisition is started. Thus, the NMR flow cell is operated as a batch reactor, i.e. the operation is non-steady and the composition of the reacting mixture is obtained as function of time. By means of this composition profile, the reaction kinetics can be calculated.

Both operating modes have advantages and disadvantages. In the stationary flow mode, as stated above, the composition of the sample in the active volume of the NMR flow cell is constant. Thus, multiple scans and time-consuming measurements such as ^{13}C NMR or two-dimensional methods with high resolution can be applied to obtain qualitative or quantitative data. In the stopped flow mode, however, these time-consuming measurements are only possible for slow reactions. But as ^1H NMR spectroscopy enables obtaining spectra that yield good quantitative data at intervals of about 1 s, also the stopped flow mode is suited for kinetic studies of comparatively fast reactions. Furthermore, it is easier to control the temperature of exo- and endothermic reactions in the stationary flow mode than in the stopped flow mode, as in the stopped flow mode hardly any convection occurs inside the cell and as the cryostat has a limited control response time.

The stopped flow mode has the advantage that reactions can be monitored within one experiment over a long period of time starting from the first acquisition after the flow was stopped (typically

after a few seconds) and ending after several hours. In the stationary flow mode, the window of the feasible residence times in the reactor is limited. At low flow rates of the reactants, the accuracy and stability of the pumps may cause problems and/or the micro-mixer may be outside its operating range, so that the reactants are not well mixed. In contrast, at high flow rates of the reactants, the resolution of the spectrum deteriorates for several reasons. First, the residence time in the NMR flow cell is short and the excited nuclei are rapidly flushed out of the NMR active volume during acquisition. This rapid flushing results in a faster decay of the NMR signal and it leads to a line broadening in the spectrum compared to low flow rates [41,22]. The line broadening caused by flushing out excited nuclei can be easily estimated assuming plug flow in the probe head [29,12]. The resulting difference of the peak widths for flow and stopped flow is less than about 3.5 Hz for the volume flow rates applicable in the probe head presented in this work. Second, the mixing of two reactants with different magnetic susceptibilities can cause local inhomogeneities in the B_0 field that in turn results in a faster decay of the signal and hence in a line broadening of the peaks. Furthermore, if the residence time of the nuclei in the premagnetisation volume is too short, the nuclei are not fully Boltzmann equilibrated before their excitation in the RF coil. This can imply that the spectral information is not quantitative any longer without prior calibration [12]. Finally, the pressure drop over the probe head increases significantly with high flow rates. Regarding the mentioned constraints, the probe head design used in this work facilitates residence times of the reactants in the reactor volume from 2 s to approximately 5 min.

3. Experimental section

3.1. Experimental set-up

The experiments were carried out using a 400 MHz NMR spectrometer (Unity Inova 400, Varian, Palo Alto, USA), which was equipped with the new micro-mixer probe as described in Section 2. The measured spectra were processed with the MestReNova 6.0 software package (Mestrelab Research, Santiago de Compostela, Spain) including phasing, baseline correction and integration.

Fig. 4 shows the set-up used for the NMR experiments. Two syringe pumps (pump A and pump B; Dual 260D, Teledyne Isco, Lincoln, USA, accuracy 0.5% of setpoint) are used to feed two mixtures or two pure liquids (here called A and B) pulsation-free, via PEEK capillaries (inner diameter 0.8 mm) into the NMR probe. In the present work, a capillary with a diameter of 0.75 mm is installed in the dwell unit resulting in a total volume of the micro-reactor of 34 μ L. To prevent plugging of the capillaries or the micro-mixer structure by impurities (e.g. dust, precipitated solids), 0.5 μ m filters (stainless steel frits, type number A-103, Upchurch Scientific Inc., Oak Harbor, USA) are installed in the feed lines of NMR probe. The purge tube leaving the NMR probe is connected to a vessel that is pressurized with nitrogen to apply a back-pressure. This vessel is important for the stopped flow mode. In that mode, unavoidable small fluctuations of the temperature would lead to large pressure changes if dilatation of the liquid volume were not enabled. Hence, a constant pressure can be applied in the micro-reactor both in the flow mode and in the stopped flow mode. The pressure is measured in the two feed tubes and in the purge tube. Valves (V1-V4, cf. **Fig. 4**) are used to switch between the different operating modes (stationary flow mode and stopped flow mode, see Section 2.2).

The feed and the purge lines are embedded in silicon tubes (outer diameter 8 mm). This silicon tube is filled with water outside of the NMR and it is connected to a cryostat (F12-ED, Julabo GmbH, Seelbach, Germany) to control the temperature of the reactants. In a second circuit, the silicon tube is filled with the thermostating liquid FC-43 (see **Fig. 4**) and it is connected via the connection box with the NMR probe (see **Fig. 1**) and a second cryostat (Petite Fleur, Two to Tango, Huber Kältemaschinenbau GmbH, Offenburg, Germany, temperature range -40 °C to 200 °C, accuracy ± 0.01 °C), so that the whole flow path of the reactants in the probe, including the feed lines, the micro-mixer, the dwell unit, the NMR flow cell, and the purge lines are surrounded by a constant flow of the thermostating liquid FC-43 to assure a good thermostatisation. The thermocouple, which is installed directly beneath the micro-mixer and which is used as control variable for the cryostat, was calibrated on the temperature of the reactants within the NMR flow cell prior to the experiments. The temperature of the reactants was measured by means of the temperature dependence of the proton resonance frequency shift between the two peaks of

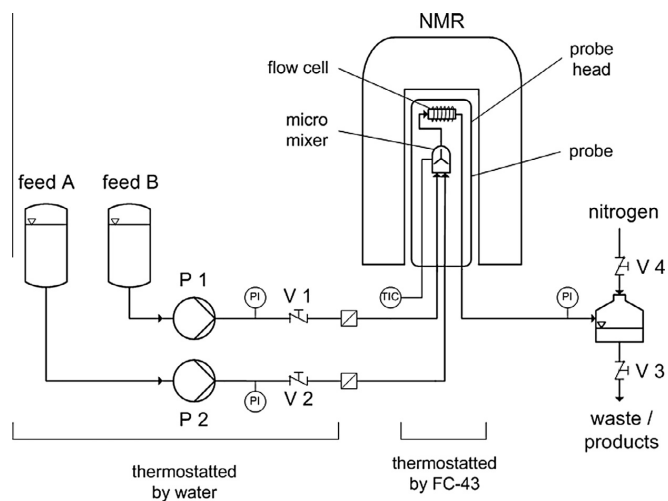


Fig. 4. Flow diagram of the experimental set-up for online NMR measurements with the micro-reactor probe head.

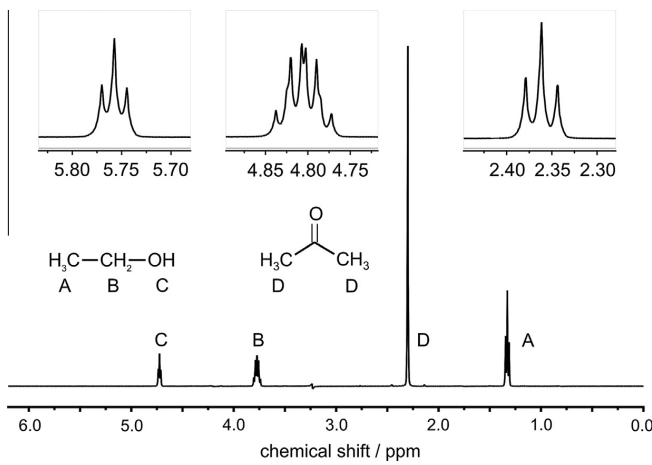


Fig. 5. ^1H NMR spectrum of an ethanol/acetone mixture ($x_{\text{ethanol}} = 0.5 \text{ mol/mol}$, $T = 20^\circ\text{C}$) acquired in stopped flow mode (single scan, acquisition time 1 s, flip angle 45°).

ethane-1,2-diol [42]. The measurement showed that the calibration of the thermocouple on the temperature of the reactants depends only weakly on the flow rate of the reactants. Thus, the temperature of the reactants can be measured by the thermocouple within an accuracy of $\pm 0.5^\circ\text{C}$.

Methanol, acetone, ethanol, acetic acid, sulfuric acid (all analytical grade) were purchased from Sigma Aldrich (St. Louis, Missouri, USA) and were used as received. Water was taken from a Milli-Q water purification system from Millipore (Bedford, Massachusetts, USA). The thermostating liquid FC-43 was from 3M (St. Paul, Minnesota, USA).

3.2. Non-reactive measurements

First, sensitivity measurements were carried out with a solution of sucrose in D_2O (10 mM) [36]. Single scan spectra with an acquisition time (AT) of 2 s, a relaxation delay (RD) of 59 s and a pulse width of 10 μs (RF power of 58 dB) were acquired, yielding a SNR (signal-to-noise ratio) of 70. For the micro-reactor probe head a $n\text{LOD}_m$ of 0.1 μmol was determined using the method described by Kojanski et al. [36]. The peak area ratio A_{810}/A_{900} , which is a measure for the RF homogeneity of the coil, was 68%.

The non-reactive measurements were carried out as follows. First, the probe head was filled with a mixture of acetone and ethanol and measurements in the stopped flow mode were carried out. 60 single scans were acquired with an AT of 1 s, a RD of 59 s and a pulse width of 14 μs , which corresponds to a flip angle (β) of 45° (RF power of 50 dB). Second, a mixture of acetone and ethanol was fed into the probe head at a constant flow rate of 100 $\mu\text{l}/\text{min}$. ^1H NMR spectra (60 signal scans, AT 1 s, RD 59 s, $\beta = 45^\circ$) were taken every minute to test the long term stability of the acquisition in the stationary flow mode. As a premixed feed was used, there was no influence of mixing effects on the spectra. Last, pump A was filled with acetone and pump B with ethanol so that both species were fed separately into the probe head and first mixed in the micro-mixer (non-premixed feeds). The flow rate of each pump was set to 50 $\mu\text{l}/\text{min}$ resulting in a total flow rate of 100 $\mu\text{l}/\text{min}$ and ^1H NMR spectra (60 signal scans, AT 1 s, RD 59 s, $\beta = 45^\circ$) were taken every minute. By comparing the results of the experiments with premixed feeds and the results of the experiments with two non-premixed feeds insight in the stability and accuracy of the pumps and the micro-mixer were gained. The mole

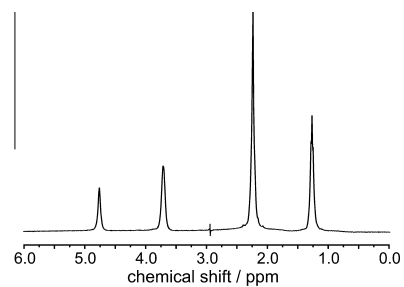


Fig. 6. ^1H NMR spectrum acquired in the stationary flow mode with two non-premixed feeds of ethanol (flow rate 50 $\mu\text{l}/\text{min}$) and acetone (flow rate 50 $\mu\text{l}/\text{min}$) ($x_{\text{ethanol}} = 0.56 \text{ mol/mol}$, $T = 20^\circ\text{C}$). Acquisition parameters: single scan, acquisition time 1 s, flip angle 45° . The FWHM is approximately 12 Hz.

fraction of acetone was calculated for all experiments from the peak areas of the CH_3 groups of acetone and ethanol. The values shown here are the means of the repeated scans.

Fig. 5 depicts the ^1H NMR spectrum of the mixture of acetone and ethanol acquired in the stopped flow mode. The single scan measurements yield a well resolved fine structure of ethanol with a full width at half maximum (FWHM) of approximately 2 Hz. Fig. 6 shows the ^1H NMR spectrum in the flow mode experiment with acetone and ethanol being fed separately into the probe head. The resulting peaks are broader (FWHM of 12 Hz) than in the stopped flow experiments (cf. Fig. 5). This line broadening is expected. As mentioned above, the line broadening is mainly caused by two effects. First, the excited nuclei are flushed out of the NMR active volume during acquisition which causes a faster decay of the NMR signal and thus a line broadening of the peaks compared to the spectra acquired in the stopped flow mode [41,22]. Second, the mixing of two species with different magnetic susceptibilities introduces local inhomogeneities of the B_0 field that causes line broadening. In the present case, the contribution to the broadening of the spectra by flushing out nuclei is less than 2 Hz thus the dominating effect is the mixing of the species with different susceptibilities.

Table 1 gives an overview of the non-reactive measurements. The measured mole fraction of acetone is in good agreement with

Table 1

Comparison of measured and the expected mole fractions of acetone for the non-reactive experiments in different operation modes. The ranges given for the measure mole fractions are the 95% confidence interval of the repeated measurements.

Experiment	Mole fraction of acetone		
	Expected	Measured	Rel. error (%)
Stopped flow mode	0.499	0.500 ± 0.0004	0.2
Flow mode: premixed feeds	0.443	0.442 ± 0.0004	0.2
Flow mode: non-premixed feeds	0.443	0.436 ± 0.0013	1.6

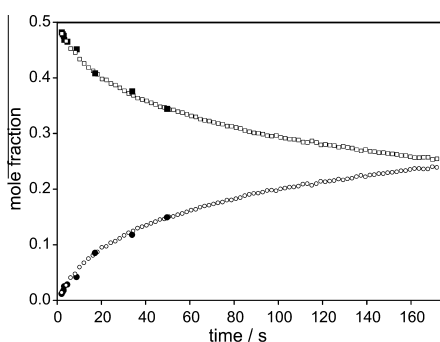


Fig. 7. Comparison of experimental reaction kinetic data for the esterification of methanol and acetic acid carried out in the stationary flow mode (filled symbols) and in the stopped flow mode (open symbols) at 50 °C (equimolar feed with 0.04 g/g sulfuric acid). (■/□) mole fraction of methanol. (●/○) mole fraction of methyl acetate.

the expected mole fraction of acetone. The relative error is approximately 0.2% for the stopped flow mode and for the flow mode with premixed feeds, and 1.6% for the flow mode with non-premixed feeds, cf. Table 1. The small variance of the measurements (indicated by the small 95% confidence interval of 4×10^{-4} mol/mol) both in the stopped flow mode and in the flow mode with pre-mixed feeds demonstrates that stable spectra can be acquired over a long period of time and that the flow of thermostating liquid around the NMR coil has no adverse effects on the spectra. The only minor increase of the variance for the measurements in the flow mode with the non-premixed feeds (the 95% confidence interval is 1.3×10^{-3} mol/mol) shows that the pumps and the mixer introduce hardly any fluctuation. To conclude, the results of this study prove that the probe head facilitates the acquisition of constant, high-resolved, and quantitative NMR signals.

3.3. Reactive measurements

To demonstrate that the probe head is suited for the investigation of fast reactions, the homogeneously catalyzed esterification of methanol with acetic acid was studied in this work at 50 °C using both the stationary flow mode and the stopped flow mode.

The experiments were carried out as follows. One pump was filled with methanol and the other pump was filled with a mixture of acetic acid and the catalyst sulfuric acid. The ratio of the flow rates of the two pumps was set so that an equimolar feed ratio was achieved. The concentration of sulfuric acid in the reacting mixture was 0.04 g/g. Before the acquisition was started, the setup was thermostatted for at least 1 h to ensure that the temperature was in steady-state. During the stopped flow measurements, a large number of ^1H NMR spectra were acquired at intervals of 2 s (AT 1 s, RD 1 s, $\beta = 45^\circ$) to follow the reaction and obtain the composition of the reactants as a function of time. The experiments

in the stationary flow mode were carried out at seven different flow rates (35 $\mu\text{l}/\text{min}$ to 800 $\mu\text{l}/\text{min}$), i.e. with seven different residence times (2–47 s). For each flow rate, an array of 30 single scan ^1H NMR spectra was acquired (AT 1 s, RD 59 s, $\beta = 45^\circ$) and the peak areas were averaged. During all measurements (stationary flow and stopped flow mode), fluctuations in the temperature were less than ± 0.5 °C.

Fig. 7 depicts the results for the reaction kinetics measurements carried out both in the stationary flow mode and in the stopped flow mode. The concentration profiles of methanol and methyl acetate are plotted as function of time (stopped flow mode) and as function of the residence time (stationary flow mode), respectively. Both concentration profiles agree well, hence, both operating modes yield consistent results. The first data points were taken only 2 s after the reaction had started (cf. Fig. 7). This shows that the probe head facilitates quantitative measurements and kinetic studies of fast reactions.

4. Conclusion

A novel NMR probe head design for non-invasive investigation of fast reactions is presented. The probe head combines a micro-mixer with a solenoidal capillary NMR flow cell. The total volume of the micro-reactor used in the present work is 34 μl . The temperature of the whole flow path of the reactants is controlled by a thermostating liquid, so that also exo- and endothermic reactions can be studied under isothermal conditions. Non-reactive mixing experiments with the new probe head demonstrate that highly resolved spectra can be acquired and that the concentration of different species in technical mixtures can be measured accurately with a relative error less than 2%. Using the esterification of methanol with acetic acid as test system, the applicability of the probe head for measurements of reaction kinetics under isothermal conditions was demonstrated. The two possible operating modes of the probe head (stationary flow mode and non-steady stopped flow mode) yield consistent results. First data points were obtained 2 s after the reaction had started. The novel micro-mixer probe head is a useful device for online monitoring of fast reactions with NMR spectroscopy under industrially relevant conditions.

Acknowledgments

We gratefully acknowledge financial support of this project by DFG. We thank Berthold Mrawek, University of Kaiserslautern and Paul Schuler, Eberhard Karls University, Tübingen, for technical support.

References

- [1] I. Hahnstein, M. Albert, H. Hasse, C.G. Kreiter, G. Maurer, NMR spectroscopic and densimetric study of reaction kinetics of formaldehyde polymer formation in water, deuterium oxide, and methanol, *Ind. Eng. Chem. Res.* 34 (1995) 440–450.
- [2] M. Maiwald, H.H. Fischer, M. Ott, R. Peschla, C. Kuhnert, C.G. Kreiter, G. Maurer, H. Hasse, Quantitative NMR spectroscopy of complex liquid mixtures: methods and results for chemical equilibria in formaldehyde–water–methanol at temperatures up to 383 K, *Ind. Eng. Chem. Res.* 42 (2003) 259–266.
- [3] M. Maiwald, T. Grützner, E. Ströfer, H. Hasse, Quantitative NMR spectroscopy of complex technical mixtures using a virtual reference: chemical equilibria and reaction kinetics of formaldehyde–water–1,3,5-trioxane, *Anal. Bioanal. Chem.* 385 (2006) 910–917.
- [4] W. Böttiger, M. Maiwald, H. Hasse, Online NMR spectroscopic study of species distribution in MEA-H₂O-CO₂ and DEA-H₂O-CO₂, *Fluid Phase Equilib.* 263 (2008) 131–143.
- [5] C.A. Fyfe, L. Vanveen, Flow nuclear magnetic resonance investigation of the intermediates formed during the bromination of phenols in acetic acid, *J. Am. Chem. Soc.* 99 (1977) 3366–3371.
- [6] C.A. Fyfe, M. Cocivera, S.W.H. Damji, T.A. Hostetter, D. Sproat, J. O'Brien, Apparatus for the measurement of transient species and effects in flowing systems with high-resolution nuclear magnetic resonance spectroscopy, *J. Magn. Reson.* 23 (1976) 377–384.

- [7] M. Maiwald, H. Li, T. Schnabel, K. Braun, H. Hasse, On-line ^1H NMR spectroscopic investigation of hydrogen bonding in supercritical and near critical CO₂-methanol up to 35 MPa and 403 K, *J. Supercrit. Fluids* 43 (2007) 267–275.
- [8] W. Böttninger, M. Maiwald, H. Hasse, Online NMR spectroscopic study of species distribution in MDEA-H₂O-CO₂ and MDEA-PIP-H₂O-CO₂, *Ind. Eng. Chem. Res.* 47 (2008) 7917–7926.
- [9] O. Steinhof, NMR-spektroskopische Aufklärung des bei der Umsetzung von Harnstoff mit Formaldehyd auftretenden Reaktionsnetzwerks, Ph.D. thesis, University Stuttgart, 2010.
- [10] E.J. Kibrik, O. Steinhof, G. Scherr, W.R. Thiel, H. Hasse, Proof of ether-bridged condensation products in UF resins by 2D NMR spectroscopy, *J. Polym. Res.* 20 (79) (2013) 1–10.
- [11] M. Maiwald, H.H. Fischer, Y. Kim, K. Albert, H. Hasse, Quantitative high-resolution on-line NMR spectroscopy in reaction and process monitoring, *J. Magn. Reson.* 166 (2004) 135–146.
- [12] M. Maiwald, Hochauflösende Online NMR-Spektroskopie für das Reaktions- und Prozessmonitoring, Civillier Verlag, Göttingen, 2012.
- [13] M. Ott, H.H. Fischer, M. Maiwald, K. Albert, H. Hasse, Kinetics of oligomerization reactions in formaldehyde solutions: NMR experiments up to 373 K and thermodynamically consistent model, *Chem. Eng. Process.* 44 (2005) 653–660.
- [14] M.A. Bernstein, M. Stefinovic, C.J. Sleigh, Optimising reaction performance in the pharmaceutical industry by monitoring with NMR, *Magn. Reson. Chem.* 45 (2007) 564–571.
- [15] H. Weber, L. Brecker, Online NMR for monitoring biocatalysed reactions, *Curr. Opin. Biotechnol.* 11 (2000) 572–578.
- [16] D.W. Jones, T. Child, *Advances in Magnetic Resonance*, Academic Press, New York, 1976.
- [17] P.A. Keifer, Flow techniques in NMR spectroscopy, *Annu. Rep. NMR Spectrosc.* 62 (2007) 1–47.
- [18] H. Fischer, K. Albert, *Online LC NMR and Related Techniques*, John Wiley & Sons, New York, 2003, pp. 195–218.
- [19] U. Holzgrabe, I. Wawer, B. Diehl, *NMR Spectroscopy in Pharmaceutical Analysis*, Elsevier, Amsterdam, 2008.
- [20] M. Maiwald, H.H. Fischer, Y.-K. Kim, H. Hasse, Quantitative on-line high-resolution NMR spectroscopy in process engineering applications, *Anal. Bioanal. Chem.* 375 (2003) 1111–1115.
- [21] W. Neudert, E. Ströfer, On-line NMR in process engineering, *Magn. Reson. Chem.* 24 (1986) 1089–1092.
- [22] J.L. Sudmeijer, U.I. Günther, K. Albert, W.W. Bachovchin, Sensitivity optimization in continuous-flow FTNMR, *J. Magn. Reson. Series A* 118 (1996) 145–156.
- [23] R.L. Haner, W. Llanos, L. Mueller, Small volume flow probe for automated direct-injection NMR analysis: design and performance, *J. Magn. Reson.* 143 (2000) 69–78.
- [24] K.R. Minard, R.A. Wind, Solenoidal microcoil design. Part I: optimizing RF homogeneity and coil dimensions, *Concepts Magn. Reson.* 13 (2001) 128–142.
- [25] A.P.M. Kentgens, J. Bart, P.J.M. van Bentum, A. Brinkmann, E.R.H. van Eck, J.G.E. Gardeniers, J.W.G. Janssen, P. Knijn, S. Vasa, M.H.W. Verkuijlen, High-resolution liquid- and solid-state nuclear magnetic resonance of nanoliter sample volumes using microcoil detectors, *J. Chem. Phys.* 128 (052202) (2008) 1–17.
- [26] A.G. Webb, Radiofrequency microcoils for magnetic resonance imaging and spectroscopy, *J. Magn. Reson.* 229 (2013) 55–66.
- [27] A.G. Webb, Radiofrequency microcoils in magnetic resonance, *Prog. Nucl. Magn. Reson. Spectrosc.* 31 (1997) 1–42.
- [28] R.M. Fratila, A.H. Velders, Small-volume nuclear magnetic resonance spectroscopy, *Annu. Rev. Anal. Chem.* 4 (2011) 227–249.
- [29] F. Dalitz, M. Maiwald, G. Guthausen, Considerations on the design of flow cells in by-pass systems for process analytical applications and its influence on the flow profile using NMR and CFD, *Chem. Eng. Sci.* 75 (2012) 318–326.
- [30] D.L. Olson, J.A. Norcross, M. O’Neil-Johnson, P.F. Molitor, D.J. Detlefson, A.G. Wilson, T.L. Peck, Microflow NMR: concepts and capabilities, *Anal. Chem.* 76 (2004) 2966–2974.
- [31] H. Wensink, F. Benito-Lopez, D.C. Hermes, W. Verboom, H.J.G.E. Gardeniers, D.N. Reinoudt, A. van den Berg, Measuring reaction kinetics in a lab-on-a-chip by microcoil NMR, *Lab Chip* 5 (2005) 280–284.
- [32] M. Kakuta, D.A. Jayawickrama, A.M. Wolters, A. Manz, J.V. Sweedler, Micromixer-based time-resolved NMR: applications to ubiquitin protein conformation, *Anal. Chem.* 75 (2003) 956–960.
- [33] R. Subramanian, W.P. Kelley, P.D. Floyd, Z.J. Tan, A.G. Webb, J.V. Sweedler, A microcoil NMR probe for coupling microscale HPLC with on-line NMR spectroscopy, *Anal. Chem.* 71 (1999) 5335–5339.
- [34] K. Ehrmann, K. Pataky, M. Stettler, F.M. Wurm, J. Brugger, P.A. Besse, R. Popovic, NMR spectroscopy and perfusion of mammalian cells using surface microprobes, *Lab Chip* 7 (2007) 381–383.
- [35] J. Bart, A.J. Kolkman, A.J. Oosthoek-de Vries, K. Koch, P.J. Nieuwland, H.J.W.G. Janssen, J.P.J.M. van Bentum, K.A.M. Ampt, F.P.J.T. Rutjes, S.S. Wijmenga, H.J.G.E. Gardeniers, A.P.M. Kentgens, A microfluidic high-resolution NMR flow probe, *J. Am. Chem. Soc.* 131 (2009) 5014–5015.
- [36] H.G. Krojanski, J. Lambert, Y. Gerikalan, D. Suter, R. Hergenröder, Microslot NMR probe for metabolomics studies, *Anal. Chem.* 80 (2008) 8668–8672.
- [37] O. Gökay, K. Albert, From single to multiple microcoil flow probe NMR and related capillary techniques: a review, *Anal. Bioanal. Chem.* 402 (2012) 647–669.
- [38] M. Gal, M. Mishkovsky, L. Frydman, Real-time monitoring of chemical transformations by ultrafast 2D NMR spectroscopy, *J. Am. Chem. Soc.* 128 (2006) 951–956.
- [39] E. Harel, A. Pines, Spectrally resolved flow imaging of fluids inside a microfluidic chip with ultrahigh time resolution, *J. Magn. Reson.* 193 (2008) 199–206.
- [40] F. Schönfeld, V. Hessel, C. Hofmann, An optimised split-and-recombine micro-mixer with uniform ‘chaotic’ mixing, *Lab Chip* 4 (2004) 65–69.
- [41] D.A. Laude, C.L. Wilkins, Direct-linked analytical scale high-performance liquid chromatography/nuclear magnetic resonance spectrometry, *Anal. Chem.* 56 (1984) 2471–2475.
- [42] C. Ammann, P. Meier, A. Merbach, A simple multi-nuclear NMR thermometer, *J. Magn. Reson.* 46 (1982) 319–321.

Declaration

In the following list the contributions of the author to the individual publications that form the basis of this cumulative doctoral thesis are specified.

- H. P. Mangalapally, R. Notz, S. Hoch, N. Asprion, G. Sieder, H. Garcia, H. Hasse: Pilot Plant Experimental Studies of Post Combustion CO₂ Capture by Reactive Absorption with MEA and new Solvents, Energy Procedia 1 (2009) 963-970.

The author carried out the model validation and the process simulation studies and wrote the corresponding parts of the manuscript.

- X. Luo, J. N. Knudsen, D. de Montigny, T. Sanpasertparnich, R. Idem, D. Gelowitz, R. Notz, S. Hoch, H. Hasse, E. Lemaire, P. Alix, F. A. Tobiesen, O. Juliussen, M. Kopcke, H. F. Svendsen: Comparison and Validation of Simulation Codes against Sixteen Sets of Data from Four Different Pilot Plants, Energy Procedia 1 (2009) 1249-1256.

The author performed the simulation studies with CHEMASIM and wrote the corresponding parts of the manuscript.

- R. Notz, I. Tönnies, H. P. Mangalapally, S. Hoch, H. Hasse: A Short-cut Method for Assessing Absorbents for Post Combustion Carbon Dioxide Capture, Int. J. Greenhouse Gas Control 5 (2011) 413-421.

The author carried out the simulation with the rate-based model for shortcut model validation and wrote the corresponding parts of the manuscript.

- P. G. Cifre, K. Brechtel, S. Hoch, H. Garcia, N. Asprion, H. Hasse, G. Scheffknecht: Integration of a Chemical Process Model in a Power Plant Modeling Tool for the Simulation of an Amine based CO₂ Scrubber, Fuel 88 (2009) 2481-2488.

The author performed the simulation studies for the CO₂ capture process and wrote the corresponding parts of the manuscript.

- I. von Harbou, S. Hoch, H. Mangalapally, R. Notz, G. Sieder, H. Garcia, O. Spuhl, H. Hasse: Removal of Carbon Dioxide from Flue Gases with Aqueous MEA Solution Containing Ethanol, Chemical Engineering and Processing: Process Intensification 75 (2014) 81-89.

The author developed the first process concept together with R. Notz and H. Mangalapally and made first calculations with a simplified model. He contributed to the corresponding parts of the manuscript.

- I. Tönnies, H. Garcia, H. Mangalapally, S. Hoch, R. Notz, G. Sieder, B. Eck, H. Hasse: CO₂-Abtrennung aus Kraftwerksabgasen auf dem Weg von der Forschung und Entwicklung zur industriellen Anwendung, Chem. Ing. Tech. 83 (2011) 1005-1015.

The author carried out the NMR measurements of the intrinsic reactions kinetics and performed the process simulations within CHEMASIM. He wrote the corresponding parts of the manuscript.

- S. Hoch, K. Albert, H. Hasse: Quantitative Online NMR-Spectroscopy in Process Analytics: Coupling with Microreactors in Studies of Fast Reaction Networks, International Symposium on Micro Chemical Process and Synthesis, Kyoto, Japan, 11.-13.09.2008.

The author carried out the kinetic studies with the test system and developed the NMR probe head together with the group of K. Albert, University of Tübingen. He wrote the manuscript.

- A. Brächer, S. Hoch, K. Albert, H. J. Kost, B. Werner, E. von Harbou, H. Hasse: Thermostatted Micro-reactor NMR Probe Head for Monitoring Fast Reactions, J. Magn. Reson. 242 (2014) 155-161.

The author developed the probe head together with IMM and the group of K. Albert. He carried out the tests and performed the flow and stop-flow measurements with the reactive system. He wrote the corresponding parts of the manuscript.

Student theses

The following student theses were prepared under the supervision of the author of the present doctoral thesis in the frame of her research:

- Ahmad, D.: Evaluation and Validation of Rate-Based Simulation Model for Reactive Absorption of CO₂ with Monoethanolamine, Master Thesis, Institute of Thermodynamics and Thermal Process Engineering (ITT), University of Stuttgart (2007).
- Braininger, D.: Reaktionskinetische Untersuchung der Veresterung von Methanol und Ameisensäure mittels Kopplung von Mikroreaktionstechnik und Durchfluss-NMR-Spektroskopie, Bachelor Thesis, Institute of Thermodynamics and Thermal Process Engineering (ITT), University of Stuttgart (2008).
- Schäfer, M.: Simulation der absorptiven CO₂-Abtrennung aus Rauchgasen in verschiedenen Skalen: Modellvalidierung und -optimierung, Diploma thesis, Institute of Thermodynamics and Thermal Process Engineering (ITT), University of Stuttgart (2008).
- Linsmayer, S.: Scale-up und Optimierung einer absorptiven CO₂-Abtrennung aus Rauchgasen anhand eines rigorosen Simulationsmodells, Bachelor thesis, Laboratory of Engineering Thermodynamics (LTD), University of Kaiserslautern (2009).
- Seiberth, D.: Scale-Up einer absorptiven CO₂-Abtrennung aus Rauchgasen anhand eines rigorosen Simulationsmodells und Prozessoptimierung mittels Seitenreaktoren, Bachelor thesis, Laboratory of Engineering Thermodynamics (LTD), University of Kaiserslautern (2010).

Curriculum vitae

Personal information

Name Sebastian Hoch
Place of Birth Emmerich am Rhein

Education

1986 - 1990	St. Michael Grundschule, Emmerich-Praest
1990 - 1999	Städt. Willibrord Gymnasium, Emmerich
	Final degree: Allgemeine Hochschulreife
2000 - 2006	University of Dortmund
	Course: Chemical Engineering
	Final degree: Dipl.-Ing.
2006 - 2008	Research Assistant
	Institute of Thermodynamics and Thermal Process Engineering
	University of Stuttgart
	Prof. Dr.-Ing. H. Hasse
2008 - 2011	Research Assistant
	Laboratory of Engineering Thermodynamics
	University of Kaiserslautern
	Prof. Dr.-Ing. H. Hasse

Professional Experience

2011 - 2014	Bayer Technology Services, Leverkusen
2014 - 2018	Bayer CropScience Schweiz AG, Muttenz, Schweiz
2018 - 2020	F. Hoffmann-La Roche AG, Basel, Schweiz
2020 - today	Bayer CropScience Schweiz AG, Muttenz, Schweiz